Subsurface microbial ecosystems and the origin of methane in serpentinites of the Samail Ophiolite, Oman

by

Daniel Blake Nothaft

B.A., Institut d'études politiques de Paris, 2015

B.A., Columbia University in the City of New York, 2015

A thesis submitted to the faculty of the Graduate School of the

University of Colorado in partial fulfillment of the requirements for the degree of

Doctor of Philosophy, Department of Geological Sciences

Committee Members:

Boswell Wing, chair

Alexis Templeton, faculty advisor

Sebastian Kopf

Noah Fierer

Peter Kelemen

Tom McCollom

Daniel Blake Nothaft (Ph.D., Geological Sciences)

Subsurface microbial ecosystems and the origin of methane in serpentinites of the Samail Ophiolite, Oman

Thesis directed by Professor Alexis S. Templeton

Abstract

Serpentinization of ultramafic rocks can produce hydrogen (H_2), a strong electron donor that microbes can react with electron acceptors such as carbon dioxide (CO_2) to produce methane (CH_4) and yield energy. This type of chemosynthetic process is relevant to life on Earth and potentially on other silicate bodies of the Solar System. However, serpentinization results in high-pH (> 11), low-CO_2 conditions that can be challenging to life. This dissertation assesses relationships between hydrogeochemical parameters and subsurface microbial communities at a site of low-temperature serpentinization in the Samail Ophiolite, Oman. We pumped groundwaters from deep wells, determined fluid chemical compositions, analyzed taxonomic profiles of microbial communities, and measured isotopic compositions of hydrocarbon gases. For some work, we used a packer system to pump discrete intervals as deep as 108 m to 132 m from two 400 m-deep wells, isolating multiple aquifers ranging in pH from 8 to 11. 16S rRNA gene sequencing of deep groundwaters revealed the presence of an ecosystem dominated by microbial sulfate reduction coupled to oxidation of H_2 and small organic acids. In shallower, oxidized groundwaters, heterotrophic aerobes or denitrifiers were more prevalent. However, the majority of this dissertation focused on the origin of CH_4 in hyperalkaline fluids. Although it has been argued that CH_4 in the ophiolite is abiotic due to its ^{13}C-enriched composition (δ^{13}C commonly -10 ‰ to $+5$ ‰ VPDB), we found that 16S rRNA gene sequences affiliated with methanogens were widespread and in high relative abundance in some samples. Further, we measured clumped isotopologue ($^{13}CH_3D$

and $^{12}CH_2D_2$) relative abundances less than equilibrium, consistent with microbial CH_4 production. Relationships between CO_2 concentrations and $\delta^{13}C_{CH_4}$ suggest that the C isotope effect of microbial CH_4 production is modulated by C availability, and strongly suppressed at pH $>$ 11. CH_4 samples from two wells had ^{14}C contents significantly above analytical blanks, and one well had CH_4 of up to 0.304 fraction modern. This is the first proof of active ($<$ 10 ka) conversion of atmospheric CO_2 to CH_4 in a serpentinizing setting. Although we do infer a second abiotic source of CH_4 from high $\delta^{13}C$ values of co-occurring ethane and propane, we attribute substantial CH_4 production to microbial activity despite high pH and C limitation.

Acknowledgments

I am thankful to the entire Templeton lab group for their support. I am particularly grateful for Alexis Templeton for believing in me and making a scientist out of me. I respect and admire her not only for her scientific rigor and integrity, but also her inspiring vision and management abilities. As her lab group's fearless leader, she has fostered an environment of teamwork and friendly willingness to intellectually challenge each other. This will be a model to which I will aspire in future collaborative environments. I am also thankful for the continued support of Peter Kelemen, who has been looking out for me ever since I wandered into his office as a wide-eyed undergrad. I am deeply appreciative of all of my committee members. I feel so fortunate to be guided by world experts in my area of study. I am further grateful for the entire community of Earth and life scientists at CU-Boulder, particularly the members of the Geobio Supergroup for their support and interdisciplinary discussions. I thank all the PI's and lab managers (especially Katie Snell, Sebastian Kopf, Julio Sepúlveda, Scott Lehman, Brett Davidheiser-Kroll, Nadia Dildar, and Steve Morgan) who welcomed me into their labs, provided me with ample precious instrument time, and never got mad at me for breaking things. I cannot express enough gratitude towards the people and government of the Sultanate of Oman for their heartwarming hospitality and openness to international scientific collaboration. I am grateful that I was fully funded, both by NASA and the Department of Geological Sciences to pursue basic research. Last but not least, I thank my bandmates, The New Family Recipe, for 5 epic years of music and camaraderie.

For my loving and supportive family

Contents

List of Tables

List of Figures

Chapter 1

Introduction

وَأَنْزَلْنَا مِنَ السَّمَاءِ مَاءً بِقَدَرٍ فَأَسْكَنَّاهُ فِي الْأَرْضِ وَإِنَّا عَلَى ذَهَابٍ بِهِ لَقَادِرُونَ

And We send down from the sky water in due measure, and We lodge it in the earth. But, behold, We are able to withdraw it.

Quran 23:18

1.1 Motivations and background

1.1.1 Water-carbon-peridotite interactions: important for microbial and human life

Hydration and oxidation of peridotite and other ultramafic rocks, i.e. "serpentinization" and related processes, can produce labile reduced compounds such as molecular hydrogen (H_2) at temperatures at least as low as 55 °C (Mayhew et al., 2013; Miller et al., 2017b). Abiotic generation of these compounds well below the temperature maximum of known microbial cell proliferation (122 °C; Takai et al., 2008) has garnered interest across disciplines due to its potential to fuel subsurface ecosystems that function without photosynthesis or its products

(Nealson et al., 2005). That is, microbes can catalyze reactions between electron donors such as H_2 derived from serpentinization and electron acceptors such as carbon dioxide (CO_2), sulfate (SO_4^{2-}), or nitrate (NO_3^-) to yield energy and grow. An example of such a process is microbial methane (CH_4) production via hydrogenotrophic methanogenesis, which can be represented as

$$CO_2 + 4H_2 = CH_4 + 2H_2O. \tag{1.1}$$

This niche is likely to have existed on early Earth and may exist today on other silicate bodies of the Solar System, including Enceladus, Europa, and Mars (McCollom, 1999; Hand et al., 2007; Mumma et al., 2009; Etiope et al., 2011; Waite et al., 2017). In serpentinizing settings, microbial CO_2 reduction as in Equation 1.1 competes for inorganic C with abiotic C reduction as well as precipitation of carbonate minerals, which results from the consumption of protons and release of Ca^{2+}, Mg^{2+}, and Fe^{2+} during the alteration of primary minerals (Sleep et al., 2004; Leong and Shock, 2020). Thus, the question of how autotrophs contend with abiotic processes to obtain C is central to understanding the deepest, earliest, and furthest reaches of life.

There are large uncertainties regarding the reservoirs and fluxes of C in settings of peridotite alteration, and even less is known concerning the mechanisms of C transformations. However, a growing body of studies quantifying the fluxes of C into and out of peridotite-hosted systems has succeeded in demonstrating the planetary-scale importance of these systems. On geologic scales of time and mass transfer, the impact of peridotites as reservoirs of volatiles such as water and CO_2 in crustal and upper mantle settings is immense. Water and CO_2 are loaded into subseafloor peridotites through serpentinization and carbonation reactions near spreading centers and at the outer rise of subduction zones. However, these serpentinites dehydrate in downgoing slabs in subduction zones, and the liberated water may dissolve and mobilize most of the C previously loaded into the serpentinites as well as CO_2 present as carbonates in overlying, altered igneous rocks and sediments in the slab ($14\,\mathrm{Mt\,C\,yr^{-1}}$ to $66\,\mathrm{Mt\,C\,yr^{-1}}$ transfer from downgoing slab to hanging wall of subduction

zone; Kelemen and Manning, 2015). Some of this C returns to the atmosphere via arc volcanism ($18\,\mathrm{Mt\,C\,yr^{-1}}$ to $43\,\mathrm{Mt\,C\,yr^{-1}}$) and diffuse outgassing ($4\,\mathrm{Mt\,C\,yr^{-1}}$ to $12\,\mathrm{Mt\,C\,yr^{-1}}$), but it has been proposed that relatively more of the C removed from the slab may precipitate as carbonate minerals in the lithospheric mantle beneath the crust (up to $47\,\mathrm{Mt\,C\,yr^{-1}}$), implying net transfer of C from the convecting mantle to the lithosphere, ocean, and atmosphere, collectively, if the subduction zone C cycle is nearly closed on time scales of 5 Myr to 10 Myr (Kelemen and Manning, 2015). Alternatively, C recycling to the convecting mantle may be more efficient, as indicated by low CO_2/Ba of the Earth's fluid envelopes, surficial deposits, and the continental and oceanic crust (Hirschmann, 2018). In any case, the function of lithospheric mantle rocks as carriers and repositories of volatiles is integral to the global C cycle.

Compared to peridotites in the lithospheric mantle, peridotites exposed at Earth's surface are associated with smaller C fluxes, but these fluxes have some more immediate impacts to society due to their direct contact with the atmosphere, hydrosphere, and biosphere. The largest, best-exposed, and most-studied peridotite body at Earth's surface is the Samail "Ophiolite"—a thrust-bounded slice of oceanic crust and upper mantle—in the Sultanate of Oman and the United Arab Emirates. Radiocarbon (^{14}C)-dating of carbonate minerals and reconnaissance mapping show that $10^4\,\mathrm{t\,yr^{-1}}$ to $10^5\,\mathrm{t\,yr^{-1}}$ of atmospheric CO_2 are converted to solid carbonate minerals via peridotite weathering in the Samail Ophiolite (Kelemen and Matter, 2008; Kelemen et al., 2011; Mervine et al., 2014; Streit et al., 2012). Although peridotite weathering sequesters CO_2, peridotite weathering can release CH_4 to the atmosphere. CH_4 fluxes from subaerial weathering peridotites may be similar to macroseepage and diffuse seepage in conventional biogenic gas in sedimentary basins (Etiope et al., 2016). The Chimaera seep of the Tekirova Ophiolite in Turkey has the largest known area-normalized CH_4 flux of an on-land peridotite exposure ($150\,\mathrm{t\,CH_4\,yr^{-1}}$ to $190\,\mathrm{t\,CH_4\,yr^{-1}}$ over a $5000\,\mathrm{m^2}$ outcrop, or $3.0\times10^5\,\mathrm{t\,CH_4\,yr^{-1}\,km^{-2}}$ to $3.8\times10^5\,\mathrm{t\,CH_4\,yr^{-1}\,km^{-2}}$; Etiope et al., 2011). There has been some study of H_2 flux from the Samail Ophiolite (Neal and Stanger, 1983; Zgonnik

et al., 2019), which suggests that CH_4 flux may be less per unit area than Chimaera, but a systematic study of CH_4 flux over a representative area has not been reported for the Samail Ophiolite at the time of writing. While the fluxes associated with these individual sites of continental peridotite weathering are minor compared to global emissions of CO_2 ($42.5 \pm 3.3\,\mathrm{Gt\,CO_2\,yr^{-1}}$ anthropogenic, the vast majority of CO_2 emissions; data for year 2018; Friedlingstein et al., 2019) and CH_4 ($550\,\mathrm{Mt\,CH_4\,yr^{-1}}$ to $881\,\mathrm{Mt\,CH_4\,yr^{-1}}$; average from 2000 to 2017; Saunois et al., 2020), $\approx 3\,\%$ of Earth's surface is composed of ultramafic rocks (Guillot and Hattori, 2013) and their cumulative CO_2 and CH_4 fluxes are not well known.

Although natural CO_2 and CH_4 fluxes associated with continental exposures of peridotites are likely minor (albeit poorly-constrained) components of global C cycle, it has been proposed that these peridotite-hosted systems could be engineered to store massive amounts of atmospheric CO_2 in order to counteract global warming trends. Kelemen and Matter (2008) estimated that a factor of 10^5 increase in natural carbonation rates could be achieved by injecting CO_2 into the subsurface of the Samail Ophiolite at elevated temperatures (185 °C), which could consume $4\,\mathrm{Gt\,CO_2\,yr^{-1}}$. CO_2 storage via mineral carbonation has advantages over alternatives such as storage in deep saline sedimentary rock formations because carbonate minerals are solids and thermodynamically stable, in contrast to the more labile aqueous or supercritical forms of CO_2 associated with storage in sedimentary rocks. However, the potential effects of CO_2 injections in mafic to ultramafic rocks on CH_4 release and subsurface microbial ecosystems has only begun to be addressed (Trias et al., 2017). These are important considerations because, due to differences in infrared absorbance band saturations of CH_4 and CO_2 (Archer, 2011; Myhre et al., 2013), if 1 unit mass of CH_4 were released to the atmosphere for every 30 unit mass of CO_2 injected and stored as subsurface carbonate minerals, the decrease in global warming potential resulting from mineral carbonation would be negated (over a 100-year period). The necessity of investigating these potential feedbacks is supported by growing recognition of the presence of considerable quantities of CH_4, mainly

formed at temperatures of 300 °C to 400 °C, stored in fluid inclusions in olivine-rich mantle and crustal rocks. This CH_4 can be stored over millions of years and transported along with these rocks during their tectonic emplacement onto continents (Kelley, 1996; Kelley and Früh-Green, 1999; Sachan et al., 2007; Klein et al., 2019; Grozeva et al., 2020). Thus, drilling, fracturing, and engineered alteration of peridotite could unintentionally release CH_4 stored in fluid inclusions, and CO_2 injected into peridotites could be partially converted to CH_4 via microbial or abiotic processes that normally function in C-limited conditions. In sum, C-peridotite interactions have profound consequences for habitability on scales ranging from microbial cells to gigatons.

1.1.2 Biogeochemistry of ultrabasic materials: the basics

While the biogeochemistry of serpentinizing settings will be discussed in greater detail in subsequent chapters of this dissertation, a brief overview is provided here. In environments of surface recharge of peridotite aquifers, as occurs in ophiolites (Figure 1.1), serpentinization and carbonation proceeds in three steps (Barnes and O'Neil, 1969; Barnes et al., 1978; Bruni et al., 2002; Cipolli et al., 2004; Kelemen et al., 2011; Paukert et al., 2012; Falk et al., 2016; Leong and Shock, 2020). First, shallow infiltration of water in an open system with atmospheric CO_2 dissolves primary minerals such as olivine and orthopyroxene and secondary minerals such as serpentines, resulting in $Mg^{2+} - HCO_3^-$ waters with a pH of 8 to 9. Second, as waters percolate deeper into the subsurface, they enter a closed system, without communication with the atmosphere. This results in continued dissolution of Mg^{2+}, as well as Ca^{2+} from clinopyroxene (Ca-rich end member cpx, diopside, $CaMgSi_2O_6$), with no subsequent additions of inorganic carbon. Mg^{2+} is incorporated into serpentine, clay minerals, and carbonates precipitated along the reaction path, whereas Ca^{2+} is largely excluded from secondary silicate minerals. Thus, the precipitation of Ca-Mg carbonates such as dolomite and magnesite proceeds until most of the initial dissolved inorganic carbon ($\sum CO_2$) is exhausted. Primary mineral dissolution proceeds until chrysotile-brucite-diopside-calcite equilibrium is

reached, resulting in $Ca^{2+} - OH^-$ "hyperalkaline" waters with pH from 11 to 13, depending on factors including temperature and mineralogy. Third, $Ca^{2+} - OH^-$ waters resurface and mix with shallow subsurface waters rich in $\sum CO_2$ or directly contact atmospheric CO_2 (g). This mixing causes rapid precipitation of $CaCO_3$ in travertines and shallow veins, and neutralizes fluid pH. Collectively, hydration (serpentinization) together with a small amount of carbonation of peridotite can be expressed in simplified form as:

$$\begin{aligned} &Mg_2SiO_4\,\text{(forsterite "Fo" olivine)} + CaMgSi_2O_6\,\text{(diopside clinopyroxene)} + 6H_2O \\ &+ CO_2 = 3Mg_3Si_2O_5\,(OH)_4\ \text{(serpentine, e.g. chrysotile)} + CaCO_3\,\text{(calcite)} \end{aligned} \tag{1.2}$$

where the release of Mg/Ca cations from primary minerals and their reaction with CO_2 to precipitate carbonates may be separated in space and time as described above.

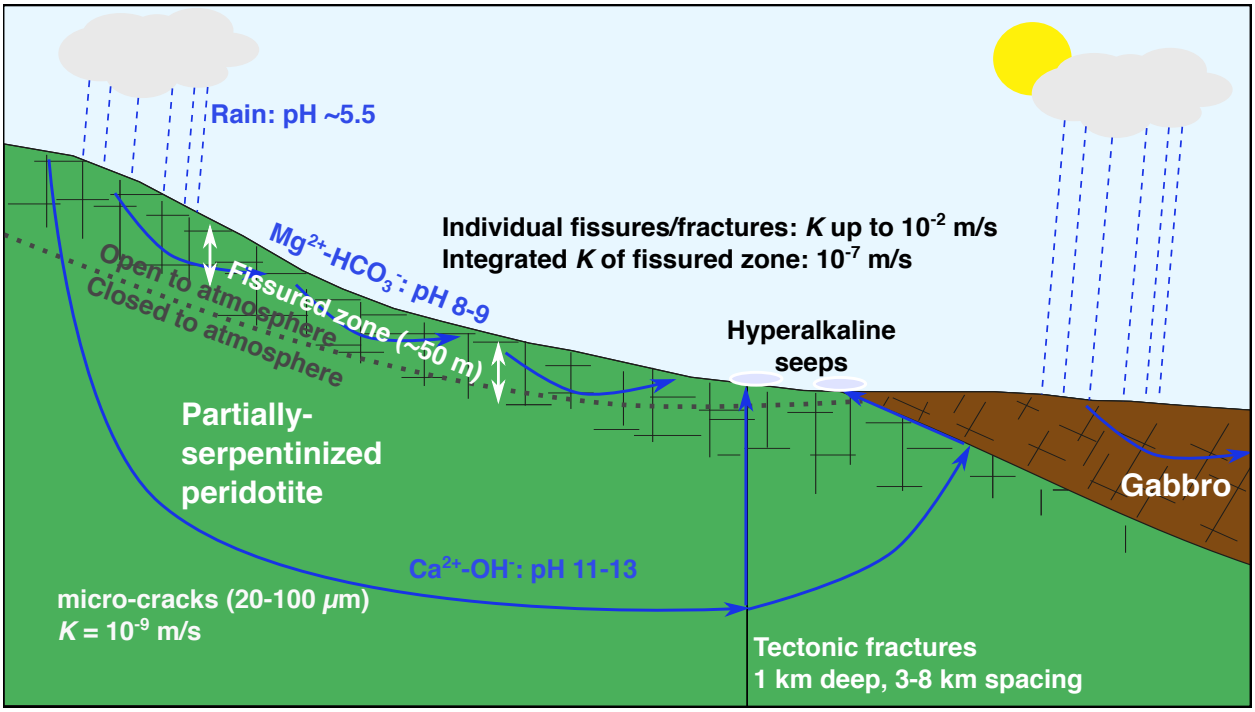

Figure 1.1: Cross-section conceptual model of ophiolite aquifers, adapted from Neal and Stanger (1985) and Rempfert et al. (2017). Hydraulic conductivities (K) of different regions of the subsurface from Dewandel et al. (2005) and Lods et al. (2020).

Another important geochemical consequence of serpentinization is the production of labile, reduced compounds such as H_2 and organic acids. As Fe^{2+} in primary peridotite

minerals is oxidized and incorporated into secondary minerals, water can be reduced to H_2 as

$$\begin{aligned} \mathrm{Mg_{1.8}Fe_{0.2}SiO_4\,(olivine,\ Fo90)} + 1.37\mathrm{H_2O} = {} & 0.5\mathrm{Mg_3Si_2O_5\,(OH)_4\ (serpentine)} \\ & + 0.3\mathrm{Mg\,(OH)_2\ (brucite)} \\ & + 0.067\mathrm{Fe_3O_4(magnetite)} + 0.067\mathrm{H_2} \end{aligned} \tag{1.3}$$

(Frost, 1985; Sleep et al., 2004; McCollom and Bach, 2009). Fluids become more reduced as the water/rock ratio decreases, and can sometimes reach H_2 fugacities at which Fe-Ni alloys are stable. While Equation 1.3 applies conceptually to serpentinization occurring above $\approx$ 150 °C, additional complexities arise regarding how electrons are transferred to various secondary minerals and volatiles over the course of temperature and reaction histories experienced by serpentinites altering at near-Earth-surface conditions. For example, Fe^{2+} can partition into brucite in earlier stages of serpentinization, and then Fe^{2+}-bearing brucite can act as a particularly labile reservoir of electrons at low-temperatures, facilitating rapid H_2 production in subaerial peridotites via oxidation of brucite-hosted Fe^{2+} (Miller et al., 2016; Templeton and Ellison, 2020). Reduced conditions resulting from serpentinization can also lead to abiotic reduction of $\sum CO_2$ to organic compounds such as small organic acids. For example, formate ($HCOO^-$) rapidly forms from the reduction of CO_2 in the presence of olivine at 300 °C in laboratory experiments (McCollom and Seewald, 2003), and formate production has been documented during experimental hydration of partially-serpentinized dunite at 100 °C (Miller et al., 2017b). Formate has also been shown to be produced through reduction of seawater $\sum CO_2$ in sediment-poor seafloor hydrothermal vent systems influenced by serpentinization (McDermott et al., 2015; Lang et al., 2018).

H_2 and simple organic compounds formed through serpentinization and related reactions can fuel subsurface microbial ecosystems. In a study of the Samail Ophiolite, Oman, Rempfert et al. (2017) presented aqueous geochemical data and taxonomic information inferred from 16S rRNA gene sequencing, which indicated that microbial metabolisms including methanogenesis, acetogenesis, and fermentation, as well as oxidation of CH_4, H_2 and

small organic acids using (SO_4^{2-}) or nitrate (NO_3^-) as electron acceptors may proceed in subsurface fluids impacted by serpentinization. Further, Rempfert et al. (2017) found that microbial community compositions correlated with the chemical compositions of fluids from which biomass was sampled. Of the metabolisms that may occur in the Samail Ophiolite (Miller et al., 2016; Rempfert et al., 2017), methanogenesis will be a primary focus of this dissertation. Methanogenesis is performed primarily by archaea that reduce dissolved CO_2, CO and/or formate with H_2 as an electron donor (i.e. Equation 1.1), or ferment a variety of methylated substrates such as acetate, methanol, and dimethylsulfide (Whiticar, 1999).

1.2 Research program design

1.2.1 Entering a discussion

Around the time of my matriculation at CU-Boulder in August, 2015, several studies were published concerning the origin of CH_4 in serpentinizing environments that influenced the trajectory of my dissertation. One of these was McCollom (2016), which employed a ^{13}C-labeled source of inorganic C in experiments on olivine serpentinization and found no measurable reduction of inorganic C to CH_4 in aqueous conditions at temperatures $\leq 300\,^{\circ}C$ in experiments lasting up to 9287 h and using 17 g to 31 g olivine. This added constraints to a long-standing debate on this subject, which stemmed in part from the lack of isotopically-labeled inorganic C sources in earlier experiments, in which CH_4 accumulation was observed during serpentinization (Jones et al., 2010; Neubeck et al., 2011; Oze et al., 2012; Okland et al., 2014). These were then shown by McCollom (2016) to have been sourced exclusively from reduced C already present in the mineral reactants or in the reaction vessels. However, McCollom (2016) did observe more extensive CH_4 production in an experiment performed under conditions that allowed a H_2-rich vapor phase to form, suggesting that serpentinizing environments where a separate gas phase is present may be more favorable for abiotic synthesis of CH_4. Thus, while serpentinization creates a thermodynamic drive to reduce

inorganic C to CH_4, McCollom (2016) proposed that kinetic inhibitions limit the production of abiotic CH_4, particularly under aqueous conditions. In a perspective article addressing the McCollom (2016) study, Bradley (2016) noted that kinetic inhibition to abiotic reactions are a boon to microbial activity, and that methanogenic microbes may "finish what peridotite started."

In a contemporaneous set of abiotic methanation experiments, Etiope and Ionescu (2015) used synthetic ruthenium (Ru) catalysts in water-free reactors and observed reaction of $H_2\,(g)$ and $CO_2\,(g)$ to form CH_4 at temperatures as low as 20 °C at considerable rates ($0.003\,mg\,CH_4\ (g\,Ru)^{-1}\ d^{-1}$ at 20 °C to 25 °C and $2.9\,mg\,CH_4\ (g\,Ru)^{-1}\ d^{-1}$ at 90 °C) in both ^{13}C-labelled and unlabelled experiments. In control experiments where the only transition metals provided were Ni and Fe, which are more abundant than Ru in serpentinizing environments, CH_4 production was not observed. This finding is consistent with chemical engineering literature, in which ruthenium and rhodium have been documented as effective catalysts for methanation < 100 °C (Thampi et al., 1987; Jacquemin et al., 2010). While rhodium is scarce in ultramafic rocks, Ru can reach $\mu g\,g^{-1}$ concentrations in chromitite lenses in igneous complexes and ophiolites (Economou-Eliopoulos, 1996; Garuti and Zaccarini, 1997; Page et al., 1982; Prichard and Brough, 2009). Based on these data, Etiope and Ionescu (2015) proposed that $H_2\,(g)$ and $CO_2\,(g)$ react in water-unsaturated conditions on Ru catalysts in chromite-rich rocks to produce the majority of CH_4 found in low-temperature serpentinizing environments.

It was within the context of these experimental findings that a field-based study of fluids, rocks, and biomass sampled from wells in the Samail Ophiolite was conducted by Miller et al. (2016), who found 16S rRNA gene sequences related to methanotrophs (CH_4 oxidizers) and methanogens co-occuring with dissolved CH_4 with a bulk stable isotopic composition of 3 ‰ VPDB $\delta^{13}C$ and -232 ‰ VSMOW δD. Such ^{13}C enrichment and D depletion in CH_4 is rarely observed outside of low-temperature serpentinizing environments (Etiope and Whiticar, 2019). From these data, Miller et al. (2016) proposed that both abiotic and micro-

bial contributions to the total CH_4 pool were plausible, noting that C isotope fractionation in microbial methanogenesis could have been suppressed due to the low-C conditions resulting from serpentinization and that CH_4 could have been subsequently enriched in ^{13}C and D by methanotrophy. In a comment on the Miller et al. (2016) study, Etiope (2017b) argued that any appreciable microbial contribution to CH_4 in the Miller et al. (2016) samples was implausible due to its ^{13}C-enriched isotopic composition, which contrasts with relatively ^{13}C-depleted microbial CH_4 in sedimentary settings, and the prior detection of ethane (C_2H_6), which is not typically produced by microbes, elsewhere in the ophiolite (Fritz et al., 1992; Etiope et al., 2015) (C_{2+} alkanes were not measured by Miller et al. (2016)).

1.2.2 Research approach

In light of the studies summarized in Section 1.2.1, I identified several key gaps in research on subsurface microbial ecosystems and the origin of CH_4 in low-temperature serpentinizing settings that needed to be filled in order to advance the understanding of these subjects. While McCollom (2016) and Etiope and Ionescu (2015) differed in their emphasis, their work converged on questions that were fundamentally hydrogeological: to what extent do H_2 (g) and CO_2 (g) come into contact in low-temperature serpentinizing settings, and in what geologic contexts might this occur? These questions beckoned for field-based study integrating precise aqueous and gas chemical analyses across a diverse array of lithologic settings with a specific focus on the hydrogeology of the system.

The Miller et al. (2016, 2017a) and Etiope (2017b) debates were inconclusive because the dimensions of CH_4-related data gathered by Miller et al. (2016), which were limited to 16S rRNA gene sequences obtained from rather shallow and low-flow pumping (22 m depth and 0.5 L min^{-1} flow maximum) and CH_4 bulk stable isotopic compositions, were insufficient to resolve the CH_4 dynamics of such a complex system. Thus, I embarked on a deep literature review to plan a extensive study of CH_4 biogeochemistry in the Samail Ophiolite leveraging state-the-art analytical techniques. From my assessments of the liter-

ature, I set out to contribute dimensions of data including the concentrations and C and H stable isotopic compositions of $C_2 - C_6$ alkanes, the radiocarbon (^{14}C) content of CH_4, and multiply-substituted "clumped" isopologue compositions of CH_4 ($^{13}CH_3D$ and $^{12}CH_2D_2$). The rationale for measuring $^{14}CH_4$ was to test whether the C in CH_4 was derived from atmospheric CO_2 in less than 50 000 years. These data would be complemented by CH_4 clumped isotopologue analyses, which are well-suited for the study CH_4 in serpentinizing settings, where source effects (C limitation) have been proposed to result in unusally ^{13}C-enriched microbial CH_4 (Miller et al., 2016). This is because bulk isotopic composition is, by definition, normalized out in the clumped isotopologue relative abundance metrics $\Delta^{13}CH_3D$ and $\Delta^{12}CH_2D_2$. As such, $\Delta^{13}CH_3D$ and $\Delta^{12}CH_2D_2$ circumvent source effect biases and highlight functional/mechanistic isotope effects (Young, 2020). In addition, I endeavored to assess potential effects of C limitation on microbial processes by measuring concentrations and $\delta^{13}C$ of $\sum CO_2$ and sequencing amplified 16S rRNA genes of DNA extracted from biomass filter-concentrated from subsurface groundwaters. Moreover, the question of changes in C availability as a function of mixing of $Ca^{2+} - OH^-$ waters and $Mg^{2+} - HCO_3^-$ waters (which differ in $\sum CO_2$ concentrations by a factor of 10^3) would be addressed through the use of advanced groundwater sampling techniques and the analysis of mixing extents through the lens of recently proposed mixing tracers applicable to on-land serpentinizing environments ($\sum$Si vs. pH; Leong et al., 2020).

The Samail Ophiolite has many advantages as a study area for the investigation of low-temperature serpentinization and related processes, including its large size, excellent exposure, relatively intact geologic structure, deep base of supporting literature, and an arid environment that limits input of exogenous organic C from soils. Further, and perhaps most crucially, the opportunities to sample fluids within this ophiolite are unparalleled. The Ministry of Municipalities and Water Resource of the Sultanate of Oman installed a series of groundwater monitoring wells ranging in depth from ≈ 70 m to 300 m throughout the Ophiolite from the 1980s to early 2000s, which have afforded access to samples of deeply-sourced

groundwaters (Miller et al., 2016; Rempfert et al., 2017; Vankeuren et al., 2019). Adding to these, the Oman Drilling Project of the International Scientific Continental Drilling Program drilled 15 new wells of up to 400 m depth into gabbro, harzburgite, and dunite rocks from 2016 to 2018. This included the creation of a multi-borehole observatory that is well-suited to hydrogeologic tests. For the purpose of hydrogeologic testing, the Oman Drilling Project acquired a packer system (SolExperts), which is essentially a system of inflatable rubber bladders ("packers") that can be installed at depth in a well to isolate and pump waters from discrete intervals in the subsurface. This affords hydrogeologic testing possibilities that surpass other techniques, which for a biogeochemist working in a fractured-rock system, makes a crucial parameter attainable: actually knowing where one's water samples come from. Additional details of the geological setting of the ophiolite and details of the packer system are provided in Section 2.2.

1.3 Outline and dissemination of work

This thesis contains three chapters (Chapters 2, 3 and 4) that are intended to be submitted for peer-review and publication. Chapter 2, "Geochemical, biological and clumped isotopologue evidence for substantial microbial methane production under carbon limitation in serpentinites of the Samail Ophiolite, Oman", investigates CH_4 cycling in the ophiolite on a system-wide scale. Fluids and biomass from ten wells across a diverse range of geologic settings in the ophiolite were studied. 16S rRNA gene sequences related to methanogens affiliated with the genus *Methanobacterium* were found to be widespread in the system. Concentrations and stable C and H isotopic compositions of CH_4, C_2H_6, and C_3H_8 were quantitated in samples obtained over a four-year period. CH_4 was found to range widely in $\delta^{13}C$ (by 90 ‰) in the system and exhibit an apparent inverse relationship with the concentration of $\sum CO_2$, suggesting a link between C availability and expressed isotopic fractionation of microbial methanogenesis. State-of-the-art measurements of multiply-substituted

"clumped" isopologue compositions of CH_4 ($^{13}CH_3D$ and $^{12}CH_2D_2$) revealed intramolecular isotopic disequilibrium in CH_4, suggesting that microbial CH_4 is quantitatively important in the system, in addition to abiotic CH_4. This work has been submitted to the *Journal of Geophysical Research - Biogeosciences* in the special issue, "Ophiolites and Oceanic Lithosphere, with a focus on the Samail ophiolite in Oman" (Nothaft et al., 2020).

Chapter 3, "Active conversion of atmospheric CO_2 to CH_4 in serpentinites of the Samail ophiolite, Oman", adds a temporal component to my isotopic analyses of CH_4 via the measurement of the radiocarbon (^{14}C) content of CH_4. This study more than doubled the number of ^{14}C measurements of CH_4 from ophiolites reported in the literature. CH_4 in the Samail Ophiolite was characterized by up to 0.304 fraction modern, which equates to a radiocarbon age of 9570 ± 45 years. This is the first report of active production of substantial quantities of CH_4 from atmospheric CO_2 in an ophiolite. The sample with the highest ^{14}C content of CH_4 also had the highest relative abundance of 16S rRNA gene reads affiliated with methanogens in the ophiolite ($\approx 25\,\%$ of reads), suggesting that the recently-produced CH_4 is microbial in origin. These observations were made in a hyperalkaline well with pH 11.4, indicating that biological adaptations to extreme energy and carbon limitation must exist. While this study is presented in a long format in this dissertation, we plan to distill and streamline it for submission to a shorter-format, higher-impact journal such as *Proceedings of the National Academy of Sciences, USA*.

Chapter 4, "Aqueous geochemical and microbial variation across discrete depth intervals in a peridotite aquifer assessed using a packer system in the Samail Ophiolite, Oman", deployed a packer system in two 400 m-deep, peridotite-hosted wells 15 m apart in the Oman Drilling Project multi-borehole observatory in an effort to understand the interconnections of hydrogeology and biogeochemistry of peridotite-hosted aquifers more deeply (literally and figuratively) than ever before. Multiple discrete intervals were isolated at depths reaching 108 m to 132 m. Different intervals had distinct microbial communities and chemical states. The most purely hyperalkaline, reduced waters were dominated by relatives of putative sul-

fate reducers of the class Thermodesulfovibrionia (up to 92 % of 16S rRNA gene reads), while shallower, more mixed, and oxidized waters had greater abundances of aerobic or denitrifying bacteria. Thus, in contrast to the preceding chapters, the data led us to broaden our focus from the C cycle to other microbial ecological systematics where methanogenesis is not dominant. We put into practice a recently-proposed mixing tracer for on-land serpentinizing environments ($\sum$Si vs. pH; Leong et al., 2020) to deconvolve mixing between $Mg^{2+} - HCO_3^-$ waters and $Ca^{2+} - OH^-$ waters, thereby adding interpretative power to physical hydrologic interpretations of the same aquifers (Lods et al., 2020).

Chapter 5 synthesizes overall conclusions from the dissertation and offers suggestions on exciting avenues of future research. Appendices A, B, and C contain supporting information for Chapters 2, 3, and 4, respectively. Appendix D documents selected additional contributions I have made in analytical method development and data analysis/curation over the course of my dissertation.

The work presented in this dissertation has been deeply collaborative. I have shared my efforts with those of many talented and dedicated scientists, for whom I am very grateful, and who are credited in subsequent chapters, where appropriate. In turn, I have contributed to the work of several other studies that have been published or are in preparation or review. These include Rempfert et al. (2017), a pioneering analysis of geochemical and microbial community interrelations in the Samail Ophiolite, Kraus et al. (in press), which used shotgun metagenomic and metatranscriptomic techniques to demonstrate the activity of CH_4-cycling microbes in the Samail Ophiolite, Fones et al. (2019), which used ^{14}C-labeled microbial rate assays, shotgun metagenomics, and cell counts, to investigate microbial C cycling and adaptations to high pH in the Samail Ophiolite, Rempfert et al. (in prep.), a study using intact polar lipids to assess the living microbiological communities in fluids circulating within the Samail Ophiolite, their biomarker preservation potentials, and their cell membrane adaptions, Templeton et al. (in prep.), an overview of efforts to integrate mineralogy, geochemistry and microbiology in the serpentinite cores recovered in the Oman Drilling

Project "Active Alteration" sites, and Cheng et al. (2019), an inter-laboratory round-robin experiment that assessed best practices in $\delta^{13}C_{\sum CO_2}$ analyses and proposed the use of an aqueous reference material for $\delta^{13}C_{\sum CO_2}$ calibration (which has traditionally be calibrated to solid carbonate isotope standards, despite the difference in phase of the analytes).

Chapter 2

Geochemical, biological and clumped isotopologue evidence for substantial microbial methane production under carbon limitation in serpentinites of the Samail Ophiolite, Oman

Daniel B. Nothaft, Alexis S. Templeton, Jeemin H. Rhim, David T. Wang, Jabrane Labidi, Hannah M. Miller, Eric S. Boyd, Juerg M. Matter, Shuhei Ono, Edward D. Young, Sebastian H. Kopf, Peter B. Kelemen, Mark E. Conrad, and The Oman Drilling Project Science Team

Abstract

In high-pH (pH > 10) fluids that have participated in low-temperature (< 150 °C) serpentinization, the dominant form of C is often methane (CH_4), but the origin of this CH_4 is uncertain. To assess CH_4 origin during low-temperature serpentinization, we pumped fluids from aquifers within the Samail Ophiolite, Oman. We determined fluid chemical compositions, analyzed taxonomic profiles of fluid-hosted microbial communities, and measured isotopic compositions of hydrocarbon gases. We found that 16S rRNA gene sequences affiliated with methanogens were widespread in the aquifer. We measured clumped isotopologue ($^{13}CH_3D$ and $^{12}CH_2D_2$) relative abundances less than equilibrium, consistent with substantial microbial CH_4 production. Further, we observed an inverse relationship between dissolved inorganic C concentrations and $\delta^{13}C_{CH_4}$ across fluids bearing microbiological evidence of methanogenic activity, suggesting that the apparent C isotope effect of microbial methanogenesis is modulated by C availability. A second source of CH_4 is evidenced by the presence of CH_4-bearing fluid inclusions in the Samail Ophiolite and our measurement of high $\delta^{13}C$ values of ethane and propane, which are similar to those reported in studies of CH_4-rich inclusions in rocks from the oceanic lithosphere. In addition, we observed 16S rRNA gene sequences affiliated with aerobic methanotrophs and, in lower abundance, anaerobic methanotrophs, indicating that microbial consumption of CH_4 in the ophiolite may further enrich CH_4 in ^{13}C. We conclude that substantial microbial CH_4 is produced under varying degrees of C limitation and mixes with abiotic CH_4 released from fluid inclusions. This study lends insight into the functioning of microbial ecosystems supported by water/rock reactions.

2.1 Introduction

At temperatures and pressures near the Earth's surface (< 400 °C, < 100 MPa), ultramafic rocks such as peridotite in contact with water are thermodynamically driven to hydrate and oxidize, forming variable amounts of serpentine, magnetite, brucite, hydrogen (H_2),

and other phases (Evans, 1977; Frost, 1985; McCollom and Bach, 2009; Klein and Bach, 2009; Klein et al., 2009, 2019). This process, often called "serpentinization", can produce H_2 at temperatures at least as low as 55 °C (Miller et al., 2017b). The resultant H_2 can be thermodynamically favored to reduce carbon dioxide (CO_2) to methane (CH_4) (Shock, 1992). The reduction of CO_2 by H_2 to form CH_4 can be catalyzed on mineral surfaces as in the Sabatier reaction (Etiope and Ionescu, 2015; Klein et al., 2019), or enzymatically through microbial methanogenesis (Whiticar, 1999).

In continental settings undergoing serpentinization, where fluid-rock reactions typically occur at low temperatures (< 150 °C), there is disagreement regarding the origin of CH_4. Three key potential CH_4 sources have been identified in these environments. One potential source is the abiotic reduction of CO_2 to CH_4 at warmer-than-present temperatures in fluid inclusions within crystals that can store CH_4 and subsequently release it. Another potential source is the abiotic, mineral-catalyzed reduction of CO_2 to CH_4 at the low temperatures that prevail in the present-day weathering environment. A third potential source is microbial methanogenesis.

Storage of CH_4 produced at temperatures of 270 °C to 800 °C in fluid inclusions in minerals such as olivine and the release of this CH_4 through subsequent chemical/physical alteration are the dominant processes contributing to CH_4 fluxes from sediment-poor seafloor hydrothermal vents (Kelley, 1996; Kelley and Früh-Green, 1999; McDermott et al., 2015; Wang et al., 2018). Debate continues, however, regarding whether fluid inclusions sustain CH_4 fluxes from continental, low-temperature serpentinizing settings (Etiope and Whiticar, 2019; Grozeva et al., 2020).

Abiotic reduction of CO_2 to CH_4 can occur at temperatures at least as low as 20 °C when catalyzed by the transition metal ruthenium (Ru) (Etiope and Ionescu, 2015). Ru is present in considerable abundance in chromitite bodies in ultramafic rock accumulations (Etiope et al., 2018). However, it has not been shown to catalyze CO_2 hydrogenation under aqueous conditions (Etiope and Ionescu, 2015). The relevance of this process, particularly to

aquifers whose fluid compositions appear to be dominantly influenced by water/harzburgite reactions, has been questioned (Etiope, 2017b; Miller et al., 2017a).

Low-temperature CH_4 production can also be mediated by microbes called "methanogens". It has been argued that serpentinizing settings contain only minor amounts of microbial CH_4 because CH_4 in serpentinizing settings is often more ^{13}C-enriched than CH_4 in sedimentary settings of microbial methanogenesis (Etiope, 2017b; Etiope and Whiticar, 2019). However, cultures of methanogens can produce CH_4 with minimal C isotope fractionation in H_2-rich, CO_2-poor fluids simulating serpentinizing systems (Miller et al., 2018). In these cultures, it has been inferred that the net C isotope effect of methanogenesis was attenuated due to microbial conversion of a large proportion of available CO_2 to CH_4 when CO_2 was the limiting substrate. Such results illustrate that ^{13}C-enriched CH_4 in natural serpentinizing settings does not necessarily derive from non-microbial sources. Still, the quantity and isotopic composition of microbial CH_4 in serpentinizing settings remains uncertain.

In this study, we assessed sources and sinks of CH_4 in the Samail Ophiolite of Oman, a site of active, low-temperature serpentinization and carbonation. For this purpose, isotopic compositions of CH_4 and co-occurring short-chain alkanes exsolved from pumped groundwaters were measured, including the multiply-substituted "clumped" isotopologues of CH_4, $^{13}CH_3D$ and $^{12}CH_2D_2$. To complement the isotopic data, 16S rRNA genes in biomass filter-concentrated from groundwaters were amplified and sequenced. We observed a wide range of C isotopic compositions of CH_4 and short-chain alkanes, intramolecular isotopologue disequilibrium in CH_4, and widespread occurrence of gene sequences affiliated with methanogens, which collectively indicate that substantial quantities of microbial CH_4 are produced and mix with abiotic CH_4 released from fluid inclusions in the Samail Ophiolite. Our finding that microbial methanogenesis proceeds even in hyperalkaline fluids lends insight into the functioning of microbial ecosystems that leverage reactions between water and ultramafic rocks to power metabolic processes on Earth and perhaps on other rocky bodies of the Solar System (Ménez, 2020; Glein and Zolotov, 2020).

2.2 Geologic Setting

The Samail Ophiolite (Figure 2.1) consists of pelagic sedimentary rocks (< 0.1 km), volcanic rocks (0.5 km to 2.0 km), sheeted dikes (1 km to 1.5 km), gabbro and igneous peridotite (0.5 km to 6.5 km), residual mantle peridotites, (8 km to 12 km), and a metamorphic sole of greenschist- to granulite-facies metamorphic rocks (< 0.5 km) (Glennie et al., 1973; Coleman and Hopson, 1981; Lippard et al., 1986; Nicolas, 1989; Nicolas et al., 2000). The ophiolite crust formed from 96.12 Ma to 95.50 Ma, and convergence began at about the same time (Rioux et al., 2016), or up to 10 My earlier (Guilmette et al., 2018; Soret et al., 2020). Ophiolite emplacement continued until 78 Ma to 71 Ma (Rabu et al., 1993). Part of the ophiolite was subaerially eroded in the Late Cretaceous, then became covered in parts by Maastrictian to Eocene limestones due to subsidence and transgression (Nolan et al., 1990; Skelton et al., 1990).

The mantle section of the ophiolite is mainly composed of highly depleted, residual mantle harzburgites, together with 5 % to 15 % dunite, which both contain a few percent chromian spinel (Godard et al., 2000; Hanghøj et al., 2010; Boudier and Coleman, 1981; Collier, 2012). The extent of serpentinization is typically 30 % to 60 %, reaching 100 % in some cases (Dewandel et al., 2003; Boudier et al., 2009; Miller et al., 2016; Kelemen et al., 2020a). Chromitites are most often found in association with dunites near the crust-mantle transition, possibly representing bases of cumulate piles, but are also found dispersed throughout the mantle section (Rollinson, 2005).

Geologic reservoirs of C underlying the ophiolite include Mid Permian to Late Cretaceous shallow marine carbonates, which host oil and gas fields in parts of northern Oman and the United Arab Emirates (Terken, 1999; Alsharhan, 1989; Etiope et al., 2015). Maastrictian to Eocene limestones that partially overly the ophiolite have been shown to transfer inorganic C to peridotites where they are in contact (de Obeso and Kelemen, 2018). C is also stored within the ophiolite, primarily in the form of carbonate minerals (Neal and Stanger, 1985; Kelemen and Matter, 2008; Kelemen et al., 2011; Noël et al., 2018). Hydration and

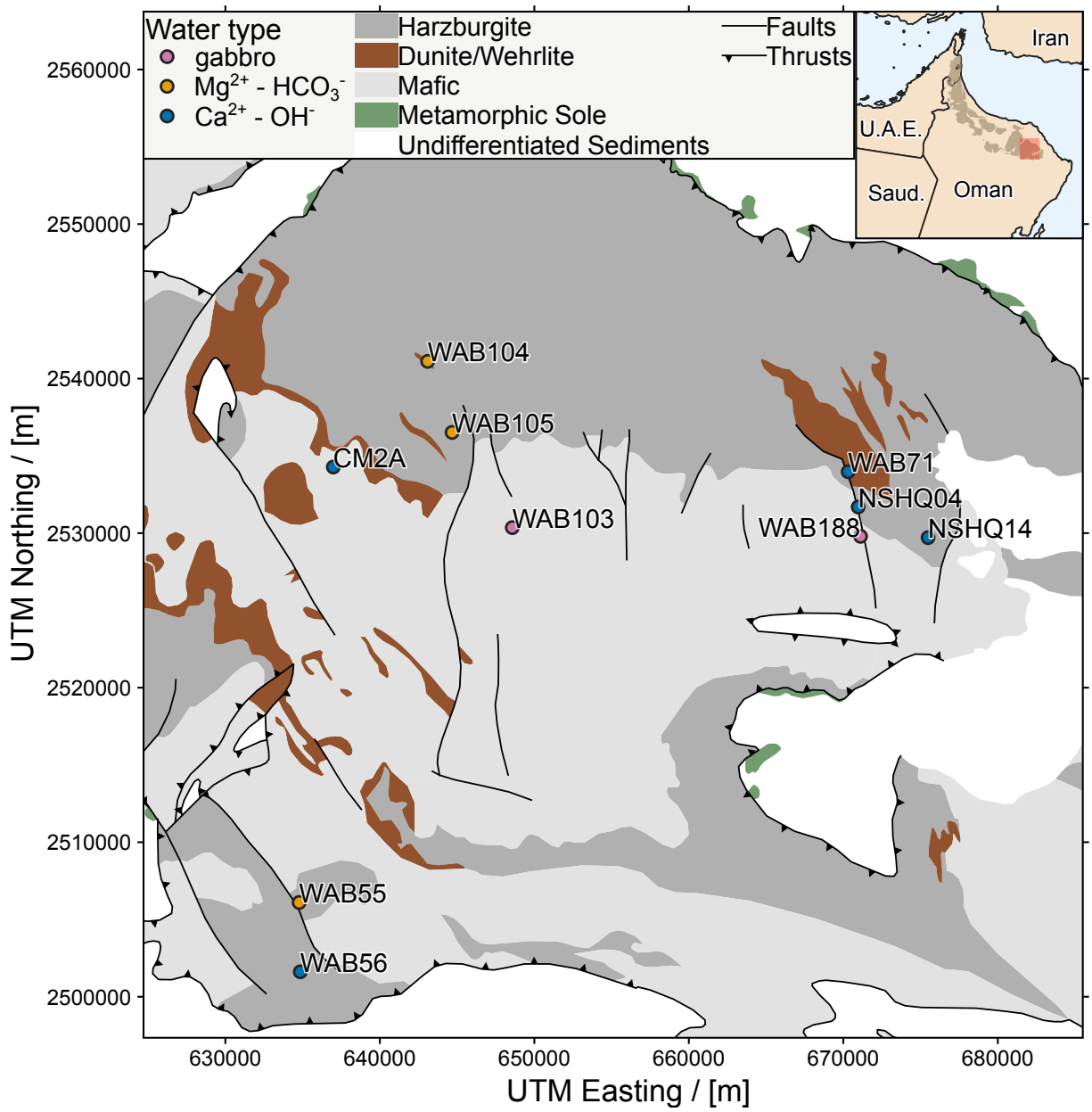

Figure 2.1: Study area in Samail Ophiolite, Sultanate of Oman. Geologic map data from Nicolas et al. (2000). Inset: overview of Samail Ophiolite (shaded in brown) with study area (larger map) indicated by the red shaded box. A topographic map of the study area is provided in Figure A.1.

carbonation of $> 20\,000\,\mathrm{km}^3$ of peridotite continue today in the Samail Ophiolite, largely at $< 60\,^{\circ}\mathrm{C}$ (Neal and Stanger, 1983, 1985; Kelemen and Matter, 2008; Kelemen et al., 2011; Streit et al., 2012; Paukert et al., 2012; Chavagnac et al., 2013a,b; Mervine et al., 2014; Falk et al., 2016; Miller et al., 2016; Vankeuren et al., 2019).

2.2.1 Fluid sampling and field measurements

Wells were drilled into the Samail Ophiolite by the Ministry of Regional Municipalities and Water Resources of the Sultanate of Oman prior to 2006 ("WAB" and "NSHQ" wells in this study) and by the Oman Drilling Project in 2016 through 2018 ("CM") (Parsons International & Co., 2005; Kelemen et al., 2013). Information on well location, construction, and water level are given in Table 4.4. In sampling campaigns in 2014 and 2015, a 12 V submersible Typhoon ® pump (Proactive Env. Products, Bradenton, FL, USA) with typical flow rates of $5\,\mathrm{L{\cdot}min^{-1}}$ was used. This pump was used in all years of sampling at well NSHQ04 due to partial obstruction of this well. In all other sampling from 2016 onwards, a larger submersible pump (Grundfos SQ 2-85) with typical flow rates of $20\,\mathrm{L{\cdot}min^{-1}}$ was used. The pumping depths are reported in Tables 4.4 and 3.4. For fluids sampled in 2018, temperature, conductivity, and pH were measured using a ColeParmer PC100 Meter, while *Eh* was measured using a Mettler Toledo SG2 SevenGo meter. The analytical uncertainties for temperature, conductivity, pH, and *Eh* are $0.5\,^{\circ}\mathrm{C}$, 1.0 % of measured value, 0.01, and 1 mV, respectively. Each well was pumped for $\geq 20\,\mathrm{min}$ prior to sampling. Sampling commenced once fluid pH and conductivity measurements stabilized.

2.2.2 Chemical and isotopic analyses of fluids

To analyze aqueous concentrations (c) of non-carbonaceous chemical species, samples were collected by passing groundwater through a $0.2\,\mu\mathrm{m}$ filter into polypropylene conical tubes. Aqueous concentrations of $\sum\mathrm{Na}$, $\sum\mathrm{Ca}$, $\sum\mathrm{Mg}$, $\sum\mathrm{Al}$, $\sum\mathrm{Fe}$, and $\sum\mathrm{Si}$ were measured by inductively coupled plasma (ICP) atomic emission spectroscopy on a PerkinElmer Optima

Table 2.1: Well data and field measurements.

Well	UTM coordinates (WGS-84)		Geologic description	Well depth / [mbgl]	Screen interval / [mbct]	Water level / [mbct]	Pump depth / [mbct]	Conductivity / $[\mu S \cdot cm^{-1}]$	Temperature / [°C]	pH	*Eh*/ [mV]	f_{O_2} / [bar][b]
	easting	northing										
WAB103	648 577	2 530 362	Gabbro	101	90 – 98	15	70.	1410	34.9	8.51	167[a]	$2.99 \cdot 10^{-36}$
WAB188	671 123	2 529 798	Gabbro, near contact with harzburgite	78	34.5 – 51	9.5	50.	1120	35.6	8.16	214[a]	$2.01 \cdot 10^{-34}$
WAB104	643 099	2 541 124	Harzburgite	120.4	100.8 – 104	40.	85	548	33.7	8.79	133	$1.23 \cdot 10^{-37}$
WAB105	644 678	2 536 524	Harzburgite	120.5	110 – 117	16.5	60.	498	33.7	8.66	162	$2.99 \cdot 10^{-36}$
WAB55	634 777	2 506 101	Harzburgite with abundant carbonate veins, near contact with gabbro	102	8 – 97	7.5[a]	50.[a]	1183[a]	36.2[a]	9.62[a]	269[a]	$7.17 \cdot 10^{-25}$
WAB56	634 851	2 501 617	Harzburgite	106	7 – 27	7.62[a]	30.[a]	930.[a]	35.6[a]	10.61[a]	20.2[a]	$2.81 \cdot 10^{-37}$
NSHQ04	670 971	2 531 699	Harzburgite, near fault with gabbro	304	open > 5.8	4.7	8	3350	33.4	10.51[a]	−174	$5.14 \cdot 10^{-51}$
WAB71	670 322	2 533 981	Dunite, near fault with harzburgite	136.5	128 – 131	8.3	70.	1970	34.9	11.22	−229	$2.52 \cdot 10^{-51}$
CM2A	636 988	2 534 284	Mostly dunite with occasional gabbro and harzburgite	400.	open > 23.7	13.4	75	2860	33.6	11.32	n.d.	n.d.
NSHQ14	675 495	2 529 716	Harzburgite	304	open > 5.8	9.2	85	2670	36.7	11.39	−253[a]	$1.19 \cdot 10^{-51}$

Measurements refer to sampling February-March, 2018, unless noted. Well elevations are given in Figure A.1. *Abbreviations:* n.d., not determined; mbgl, meters below ground level; mbct, meters below casing top. Casings extend ~ 1 m above ground level.

[a]Not determined during 2018 sampling, so most recent prior data is reported (2015 to 2017; Rempfert et al., 2017; Fones et al., 2019).

[b]Calculated from temperature, pH, and *Eh*. Where one or more of these parameters were obtained during different sampling years, f_{O_2} should be considered a representative estimate.

Table 2.2: Isotopic compositions of CH_4, C_2H_6, and C_3H_8.

Well	Sample year	Pump depth / [mbct]	laboratory	$\delta^{13}C_{CH_4}$	δD_{CH_4}	$\Delta^{13}CH_3D$	$\Delta^{12}CH_2D_2$	$\delta^{13}C_{C_2H_6}$	$\delta^{13}C_{C_3H_8}$
WAB188	2018	50.	CUB	−86.7	n.d.	n.d.	n.d.	n.d.	n.d.
	2017	78	CUB	−60.8	n.d.	n.d.	n.d.	n.d.	n.d.
	2015	20.	LBNL	−71.3	n.d.	n.d.	n.d.	n.d.	n.d.
WAB56	2015	12	LBNL	−83.2	n.d.	n.d.	n.d.	n.d.	n.d.
NSHQ04	2018	8	CUB	4.7	−229	n.d.	n.d.	n.d.	n.d.
			UCLA	4.177	−227.396	0.229 ± 0.288	-24.502 ± 0.944	n.d.	n.d.
	2017	5.8	CUB	6.8	−225	n.d.	n.d.	n.d.	n.d.
			MIT	3.59	−229.67	0.12 ± 0.17	n.d.	n.d.	n.d.
	2015	22	LBNL	0.8	−209	n.d.	n.d.	n.d.	n.d.
			MIT	1.60	−230.00	0.72 ± 0.29	n.d.	n.d.	n.d.
	2014	18	LBNL	2.4	−205	n.d.	n.d.	n.d.	n.d.
WAB71	2018	70.	CUB	3.6	−307	n.d.	n.d.	n.d.	n.d.
	2017	50.	CUB	3.9	−313	n.d.	n.d.	n.d.	n.d.
	2016	50.	LBNL	3.0	n.d.	n.d.	n.d.	n.d.	n.d.
	2015	18	LBNL	2.9	n.d.	n.d.	n.d.	n.d.	n.d.
CM2A	2018	75	CUB	−4.3	−206	n.d.	n.d.	n.d.	n.d.
			MIT	−3.83	−190.32	2.87 ± 0.57	n.d.	n.d.	n.d.
			UCLA	−4.710	−197.73	2.638 ± 0.284	-1.267 ± 0.886	n.d.	n.d.
NSHQ14	2018	85	CUB	−2.3	−314	n.d.	n.d.	n.d.	n.d.
			MIT	−5.02	−311.73	0.77 ± 0.44	n.d.	n.d.	n.d.
			UCLA	−3.352	−293.58	2.074 ± 0.298	-0.204 ± 1.358	n.d.	n.d.
	2017	85	CUB	0.2	−271	n.d.	n.d.	−6.0	+3.3
			MIT	−0.08	−268.82	0.69 ± 0.23	n.d.	n.d.	n.d.
	2016	70.	LBNL	1.8	−273	n.d.	n.d.	n.d.	n.d.
			MIT	−6.89	−308.52	0.69 ± 0.17	n.d.	n.d.	n.d.
	2015	20.	LBNL	3.7	n.d.	n.d.	n.d.	n.d.	n.d.
	2014	260.	LBNL	3.0	−232	n.d.	n.d.	n.d.	n.d.

All isotopic values reported in ‰ units. $\delta^{13}C$ and δD reported in the VPDB and VSMOW reference frames, respectively. Data from 2014 previously reported by Miller et al. (2016). *Abbreviations:* n.d., not determined; mbct, meters below casing top.

5300 (repeatability as median relative standard deviation of 3 %). Aqueous concentrations of Cl^-, Br^-, F^-, and SO_4^{2-} were measured on a Dionex IC25 ion chromatograph with an AS9-HC IonPac column, with the exception of NO_3^-, which was measured on a Dionex 4500I ion chromatograph with an IonPac AS14 column using EPA method 300.0 (analytical uncertainty of 2 %).

The concentration and $\delta^{13}C$ of dissolved inorganic C ($\sum CO_2$) were measured by acidification of water samples and transfer of resultant CO_2 (g) via a Thermo Fisher GasBench II to a Thermo Delta V Plus isotope ratio mass spectrometer. We optimized the methods of Assayag et al. (2006) for the wide range of $c_{\sum CO_2}$ observed in ophiolite groundwaters. Complete methodological details are available at `http://dx.doi.org/10.17504/protocols.io.zduf26w`. Conversion of sample $\delta^{13}C$ values to the VPDB reference frame using measured $\delta^{13}C$ values of international reference materials (Harding Iceland Spar and LSVEC) were performed using the statistical programming language, R (R Core Team, 2019) (Section A.1).

Water $\delta^{18}O$ and δD were measured on a Picarro L2120-i cavity ring down spectrometer. The instrument analyzed each sample six times, excluding the first three analyses to avoid memory effects. Reported precision is the standard deviation of the last three measurements. Reported accuracy is the mean difference between accepted values and measured values of standards. Mean precision in the run was 0.06 ‰ for $\delta^{18}O$ and 0.23 ‰ for δD; mean accuracy was 0.04 ‰ for $\delta^{18}O$ and 0.47 ‰ for δD.

Gases dissolved in pumped groundwaters were sampled by injecting water into N_2 purged vials for headspace gas analysis using methods described by Miller et al. (2016) in field campaigns occurring from 2014 to 2017. In addition, the bubble strip method (modified from Kampbell et al., 1998) was used from 2016 to 2018. Details on bubble strip gas sampling are available at `http://dx.doi.org/10.17504/protocols.io.2x5gfq6`. The gas concentrations reported in this study were determined from bubble strip samples. These concentrations were measured on an SRI 8610C gas chromatograph (GC) with N_2 as the carrier

gas. H_2, CO, CH_4, and CO_2 were separated with a 2 mm by 1 mm ID micropacked Shin-Carbon ST column, whereas alkanes of 2 to 6 C atoms ("$C_2 - C_6$ short-chain alkanes") were separated with a PORAPAK Q 6 ft by 0.085 in ID column. Peak intensities were measured concurrently using a thermal conductivity detector (TCD) and a flame ionization detector (FID) and calibrated with standard gas mixes (Supelco Analytical, Bellefonte, PA, USA; accuracy of ±2 % of reported concentration). Measurement repeatability expressed as relative standard deviation was 5 % over most of the calibrated range. The limit of quantitation was defined as the signal at which the relative standard deviation increased to 20 %. In 2018, H_2 and CO were analyzed on a Peak Performer 1 gas chromatograph equipped with a reducing compound photometer (RCP). Due to the high sensitivity of the RCP, the signal at limit of quantitation (S_{LQ}) for these analyses was defined as $S_{LQ} = S_b + 10 \cdot \sigma_b$, where S_{mb} is the mean signal of blanks prepared in field and σ_b is the population standard deviation of these blanks, in accordance with American Chemical Society guidelines (MacDougall et al., 1980). Gaseous concentrations were converted to aqueous concentrations using gas solubilities (Sander, 2015) and corrected for temperature and volume changes between sampling and analysis.

Prior to 2017, bulk stable isotope analyses of CH_4 were conducted at the Center for Isotope Geochemistry at the Lawrence Berkeley National Laboratory (LBNL) by gas chromatography/combustion/pyrolysis isotope-ratio mass spectrometry (GC/C/Pyr/IRMS) using methods described by Miller et al. (2016). The measurement repeatability expressed as 1 sample standard deviation (s) for these analyses is ±0.2 ‰ for $\delta^{13}C$ and ±5 ‰ for δD.

From 2017 onwards, bulk stable isotope analyses of CH_4 and co-occurring alkane gases were conducted at the University of Colorado - Boulder (CUB) by GC/C/Pyr/IRMS using a Trace 1310 GC equipped with an Agilent J & W GS-CarbonPLOT column (30 m length, 0.32 mm ID, 3.0 μm film) coupled to a Thermo Scientific MAT253 IRMS. CH_4 isotope standards purchased from Airgas (uncertainties of ±0.3 ‰ for $\delta^{13}C$ and ±5 ‰ for δD) were used for calibration. Over the range of peak amplitudes of analyses reported here, the repeata-

bility expressed as $1\,s$ on analyses of standards is $\pm 0.6\,‰$ for $\delta^{13}C$ and $\pm 7\,‰$ for δD. The analytical uncertainty (accuracy) expressed as 1 standard error on a 3-point calibration was $< 0.3\,‰$ for $\delta^{13}C$ and $< 9\,‰$ for δD (Section A.1).

The relative abundances of CH_4 isotopologues, including the doubly-substituted isotopologue, $^{13}CH_3D$, were measured at the Massachusetts Institute of Technology (MIT) by tunable infrared laser direct absorption spectroscopy following the methods described by Ono et al. (2014). Abundances of CH_4 isotopologues, including both $^{13}CH_3D$ and $^{12}CH_2D_2$, were measured at the University of California, Los Angeles (UCLA) by high-mass-resolution gas-source isotope ratio mass spectrometry following the procedure of Young et al. (2016). The abundance of $^{13}CH_3D$ relative to a random (stochastic) distribution of isotopes among the isotopologues in a CH_4 sample is described by its $\Delta^{13}CH_3D$ value, which is defined as: $\Delta^{13}CH_3D = \ln Q$, where Q is the reaction quotient of the isotope exchange reaction:

$$^{13}CH_4 + {}^{12}CH_3D \rightleftharpoons {}^{12}CH_4 + {}^{13}CH_3D. \tag{2.1}$$

Analogous expressions can be written for doubly-deuterated CH_4, $^{12}CH_2D_2$.

2.2.3 16S rRNA gene sequencing and analysis

Biomass for DNA extraction was concentrated by pumping 5 L to 20 L of groundwater through Millipore polycarbonate inline filters ($0.45\,\mu$m pore diameter, 47 mm filter diameter). At well NSHQ04, a $0.22\,\mu$m pore diameter polyethersulfone Millipore Sterivex filter was used instead due to the lower-flow pump used at this well (Section 3.5.1). Filters were placed in cryovials, transported frozen in liquid N_2, and stored in a $-70\,°C$ freezer until extraction. DNA was extracted from one quarter subsamples of each filter using a Qiagen PowerSoil DNA extraction kit. The V4 hypervariable region of the 16S rRNA gene was amplified by PCR in duplicate reactions using the 515 (Parada) - 806R (Apprill) primer pair modified to include Illumina adapters and the appropriate error-correcting barcodes. Each 25-μL reaction mixture included $12.5\,\mu$L of Promega HotStart Mastermix, $10.5\,\mu$L of PCR-grade water, $1\,\mu$L of PCR primers (combined at 10 M), and $1\,\mu$L of purified genomic

DNA. PCR consisted of an initial step at 94 °C for 3 min followed by 35 cycles of 94 °C for 45 s, 50 °C for 1 min, and 72 °C for 1.5 min. PCR concluded with a final elongation step at 72 °C for 10 min. No-template controls and DNA extraction controls were subjected to PCR to check for potential contamination in our PCR and DNA extraction reagents, respectively. Amplification was evaluated via electrophoresis in a 2 % agar gel. Amplicons from duplicate reactions were pooled, cleaned, and their concentrations normalized using a Thermo Fisher SequalPrep normalization plate kit. Amplicons were sequenced on an Illumina MiSeq at the CUB Next-Generation Sequencing Facility with 2-by-150 bp paired-end chemistry.

Sequences were demultiplexed with idemp (`https://github.com/yhwu/idemp`). The resultant fastq files were quality filtered using Figaro v1.1.1 (`https://github.com/Zymo-Research/figaro`) and the DADA2 v1.16 R package (Callahan et al., 2016). Amplicon sequence variants were assigned taxonomy to the genus level using the RDP classifier (Wang et al., 2007) trained on the Silva SSU 138 reference database (Quast et al., 2012) using the DADA2 assignTaxonomy function. Species level assignments were based on exact matching between amplicon sequence variants and sequenced reference strains using the DADA2 addSpecies function. Sequences assigned to mitochondria, chloroplast, and Eukaryota, or not assigned at the domain level (collectively < 1 % of sequences), were removed. In addition, 16S rRNA gene sequencing data from previous Oman sampling campaigns (2014 through 2017; Miller et al., 2016; Rempfert et al., 2017; Kraus et al., 2018) were reprocessed in accordance with the methods outlined here to facilitate comparisons across the data sets (`https://github.com/danote/Samail_16S_compilation`). For samples presented in this study, demultiplexed fastq files (without additional processing) are accessible on the NCBI Short Read Archive under accession PRJNA655565.

2.3 Results and discussion

2.3.1 Controls on groundwater chemistry

To assess the source and reaction histories of Samail Ophiolite groundwaters, we measured their stable isotopic compositions and solute concentrations. Groundwater δD and δ^{18}O plotted near local and global meteoric water lines (Weyhenmeyer et al., 2002; Terzer et al., 2013), indicating that the groundwaters derive from rain (Table 4.1; Figure A.2; Matter et al., 2006; Miller et al., 2016; Vankeuren et al., 2019). The sampled groundwaters included oxidized and moderately alkaline $Mg^{2+} - HCO_3^-$ waters, typical of reaction with peridotite in communication with the atmosphere, and reduced and hyperalkaline $Ca^{2+} - OH^-$ waters, typical of extensive hydration and oxidation of peridotite in closed-system conditions with respect to the atmosphere (Table 4.1; Barnes et al., 1967; Barnes and O'Neil, 1969; Neal and Stanger, 1985; Bruni et al., 2002; Cipolli et al., 2004; Kelemen et al., 2011; Paukert et al., 2012). $Ca^{2+} - OH^-$ waters had higher conductivities (930. $\mu S \cdot cm^{-1}$ to 3350 $\mu S \cdot cm^{-1}$) than $Mg^{2+} - HCO_3^-$ waters (498 $\mu S \cdot cm^{-1}$ to 1183 $\mu S \cdot cm^{-1}$) (Table 4.4). The increase in conductivity from $Mg^{2+} - HCO_3^-$ waters to $Ca^{2+} - OH^-$ waters is driven by enrichments in Ca^{2+} derived from dissolution of primary silicate minerals in addition to Na^+ and Cl^- derived from mineral dissolution, sea spray, and/or leaching of sea salts introduced during subseafloor alteration and/or ophiolite emplacement (Neal and Stanger, 1985; Stanger, 1986; Murad and Krishnamurthy, 2004; Paukert et al., 2012; Rempfert et al., 2017). The increase in pH from $Mg^{2+} - HCO_3^-$ waters (pH 8.66 to 9.62) to $Ca^{2+} - OH^-$ waters (10.51 to 11.39) was accompanied by a shift to lower f_{O_2} and Eh ($\sim 10^{-51}$ bar and -174 mV to -253 mV, respectively, in most $Ca^{2+} - OH^-$ waters) (Table 4.4), indicating reduced conditions in $Ca^{2+} - OH^-$ waters.

Concentrations of $\sum CO_2$ were relatively high in $Mg^{2+} - HCO_3^-$ waters and gabbro waters (up to 3490 $\mu mol \cdot L^{-1}$), but below the limit of quantitation ($< 12\,\mu mol \cdot L^{-1}$) in most $Ca^{2+} - OH^-$ waters (Table 4.1). This is consistent with water-harzburgite reaction path

Table 2.3: Chemical and isotopic composition of water samples.

Well	δD_{H_2O}	$\delta^{18}O_{H_2O}$	$\sum CO_2$	$\delta^{13}C_{\sum CO_2}$	$\sum Na$	$\sum Ca$	$\sum Mg$	$\sum Fe$	$\sum Si$	NO_3^-	SO_4^{2-}	Cl^-	Br^-
gabbro-hosted groundwaters													
WAB103	−0.5	+0.34	$2.67 \cdot 10^3$	−13.54	$1.18 \cdot 10^3$	$2.58 \cdot 10^2$	$1.87 \cdot 10^3$	7.35	$4.63 \cdot 10^2$	$4.72 \cdot 10^2$	$1.57 \cdot 10^3$	$6.25 \cdot 10^3$	$1.39 \cdot 10^2$
WAB188	−2.1	−0.71	$3.48 \cdot 10^3$	−13.52	$4.06 \cdot 10^3$	$1.41 \cdot 10^3$	$1.82 \cdot 10^3$	$2.90 \cdot 10^1$	$4.77 \cdot 10^2$	$3.21 \cdot 10^2$	$1.41 \cdot 10^3$	$4.22 \cdot 10^3$	$6.78 \cdot 10^1$
$Mg^{2+} - HCO_3^-$ *groundwaters*													
WAB104	−0.5	−0.53	$3.62 \cdot 10^3$	−13.88	$7.53 \cdot 10^2$	$1.96 \cdot 10^2$	$2.30 \cdot 10^3$	3.88	$4.15 \cdot 10^2$	$3.14 \cdot 10^2$	$3.80 \cdot 10^2$	$7.76 \cdot 10^2$	3.55
WAB105	+0.4	+0.50	$3.32 \cdot 10^3$	−10.88	$1.18 \cdot 10^3$	$2.58 \cdot 10^2$	$1.87 \cdot 10^3$	4.83	$2.83 \cdot 10^2$	$3.02 \cdot 10^2$	$2.92 \cdot 10^2$	$8.54 \cdot 10^2$	8.60
WAB55	+2.2	+0.26	$2.40 \cdot 10^3$	−12.63	$4.44 \cdot 10^3$	$5.06 \cdot 10^1$	$3.34 \cdot 10^3$	2.52	$3.58 \cdot 10^1$	$3.02 \cdot 10^2$	$8.03 \cdot 10^2$	$6.54 \cdot 10^3$	$1.12 \cdot 10^2$
$Ca^{2+} - OH^-$ *groundwaters*													
WAB56	n.d.	n.d.	$1.3 \cdot 10^{2a}$	n.d.	$3.56 \cdot 10^{3a}$	$5.43 \cdot 10^{2a}$	1.00^a	n.d.	$2.22 \cdot 10^2$	3.00^a	6.00^b	$1.33 \cdot 10^{1a}$	$1.79 \cdot 10^{-1a}$
NSHQ04	-15^a	-3.0^a	$1.8 \cdot 10^1$	−29.7	$1.04 \cdot 10^{4a}$	$7.79 \cdot 10^{3a}$	$1.80 \cdot 10^{1a}$	$8.20 \cdot 10^{-1a}$	$3.60 \cdot 10^{1a}$	3.00^a	$6.83 \cdot 10^{2a}$	$1.82 \cdot 10^{4a}$	1.25^a
WAB71	−3.0	−0.40	$< 1.2 \cdot 10^1$	n.d.	$6.25 \cdot 10^3$	$4.14 \cdot 10^3$	$< 2.06 \cdot 10^{-1}$	$8.48 \cdot 10^1$	$2.35 \cdot 10^1$	$1.84 \cdot 10^2$	$6.08 \cdot 10^1$	$1.17 \cdot 10^4$	$1.50 \cdot 10^2$
CM2A	+1.7	+0.67	$< 1.2 \cdot 10^1$	n.d.	$2.07 \cdot 10^4$	$1.75 \cdot 10^3$	9.49	$4.03 \cdot 10^1$	$2.81 \cdot 10^1$	$1.64 \cdot 10^2$	$5.56 \cdot 10^2$	$1.85 \cdot 10^4$	$2.48 \cdot 10^2$
NSHQ14	+0.2	+0.43	$< 1.2 \cdot 10^1$	n.d.	$1.03 \cdot 10^4$	$3.60 \cdot 10^3$	6.23	$8.48 \cdot 10^1$	$1.03 \cdot 10^1$	$3.60 \cdot 10^2$	$1.57 \cdot 10^2$	$1.36 \cdot 10^4$	$1.67 \cdot 10^2$

Concentrations reported in $\mu mol \cdot L^{-1}$. $\sum$ indicates the sum of all dissolved species of the element. All δ values reported in ‰ units. $\delta^{18}O$ and δD reported relative to VSMOW. $\delta^{13}C$ reported relative to VPDB. Samples obtained in February-March 2018, unless noted. *Abbreviations:* n.d., not determined.

[a]Not determined during 2018 sampling, so most recent prior data is reported (2015 to 2017; Rempfert et al., 2017; Fones et al., 2019).

modeling that terminates at chrysotile-brucite-diopside-calcite equilibrium, corresponding to a $c_{\sum CO_2}$ of $8\,\mu mol \cdot L^{-1}$ at 25 °C and 1 bar (Leong and Shock, 2020). Literature values for $c_{\sum CO_2}$ in ophiolitic $Ca^{2+} - OH^-$ waters are often higher than those predicted by reaction path modeling, but the lower range of reported values approaches $1\,\mu mol \cdot L^{-1}$ (Barnes et al., 1967; Barnes and O'Neil, 1969; Barnes et al., 1978; Neal and Stanger, 1985; Bruni et al., 2002; Cipolli et al., 2004; Paukert et al., 2012; Falk et al., 2016; Brazelton et al., 2017; Canovas III et al., 2017; Crespo-Medina et al., 2017; Rempfert et al., 2017; Fones et al., 2019; Vankeuren et al., 2019). This spread in the data could reflect groundwater mixing, atmospheric contamination during sampling, differences in reaction temperature and progress, and/or kinetic inhibitions to carbonate mineral precipitation. In $Mg^{2+} - HCO_3^-$ waters and waters from gabbroic aquifers, $\delta^{13}C_{\sum CO_2}$ ranged from −13.54 ‰ VPDB to −10.88 ‰ VPDB (Table 4.1), which is comparable to $\delta^{13}C_{\sum CO_2}$ of $Mg^{2+} - HCO_3^-$ waters elsewhere in the ophiolite (−15.56 ‰ VPDB to −13.60 ‰ VPDB; Matter et al., 2006).

Variable concentrations of H_2 and CH_4 across wells suggest spatial heterogeneities in sources and sinks of these gases in the ophiolite. In some $Ca^{2+} - OH^-$ waters, c_{H_2} was high (up to $253\,\mu mol \cdot L^{-1}$), but c_{H_2} was below limits of quantitation in other $Ca^{2+} - OH^-$ waters (Figure 2.2; Table 4.2). In $Mg^{2+} - HCO_3^-$ waters and waters from gabbroic aquifers, c_{H_2} was generally below limits of quantitation. However, up to $0.992\,\mu mol \cdot L^{-1}$ H_2 was measured in well WAB188, which is in gabbro near a faulted contact with peridotites that contain $Ca^{2+} - OH^-$ waters (Figure 2.1; Table 4.4). This suggests production of H_2 within the gabbro host rock or migration of H_2 from peridotites into gabbros surrounding WAB188. In most $Ca^{2+} - OH^-$ waters, c_{CH_4} was high (up to $483\,\mu mol \cdot L^{-1}$; Figure 2.2, Table 4.2). However, wells with high c_{CH_4} did not always have high c_{H_2} (Figure 2.2; Table 4.2). In $Mg^{2+} - HCO_3^-$ waters and gabbro waters, c_{CH_4} was typically lower ($\leq 0.1\,\mu mol \cdot L^{-1}$), although c_{CH_4} reached $1.83\,\mu mol \cdot L^{-1}$ in well WAB188, where c_{H_2} was also quantitatable.

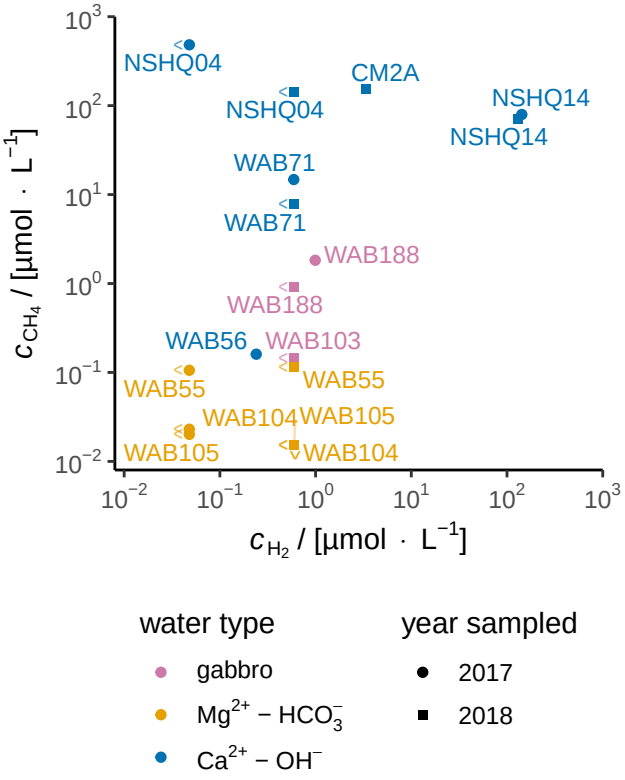

Figure 2.2: Aqueous concentrations of CH_4 and H_2 in Oman groundwater samples from 2017 and 2018. Left and down carrots denote "below limit of quantitation" for CH_4 and H_2, respectively, with the adjacent point plotted at the limit of quantitation for that gas and year of analysis.

Table 2.4: Aqueous gas concentrations, reported in $\mu\text{mol} \cdot \text{L}^{-1}$.

Well	Sample year	H_2	CO	CH_4	C_2H_6	C_3H_8	i-C_4H_{10}	n-C_4H_{10}	i-C_5H_{12}	n-C_5H_{12}	C_6H_{14}[a]
WAB103	2018	$< 5.98 \cdot 10^{-1}$	$< 1.32 \cdot 10^{-1}$	$1.45 \cdot 10^{-1}$	$< 9.88 \cdot 10^{-4}$	$< 7.60 \cdot 10^{-4}$	$< 4.61 \cdot 10^{-4}$	$6.05 \cdot 10^{-3}$	$< 3.43 \cdot 10^{-4}$	$8.73 \cdot 10^{-4}$	$< 2.81 \cdot 10^{-4}$
WAB188	2018	$< 5.98 \cdot 10^{-1}$	$< 1.32 \cdot 10^{-1}$	$9.17 \cdot 10^{-1}$	$< 9.88 \cdot 10^{-4}$	$< 7.60 \cdot 10^{-4}$	$< 4.61 \cdot 10^{-4}$	$< 5.78 \cdot 10^{-4}$	$< 3.43 \cdot 10^{-4}$	$< 3.81 \cdot 10^{-4}$	$< 2.81 \cdot 10^{-4}$
	2017	$9.92 \cdot 10^{-1}$	$< 2.79 \cdot 10^{-1}$	1.83	$< 1.01 \cdot 10^{-3}$	$< 7.79 \cdot 10^{-4}$	$< 4.72 \cdot 10^{-4}$	$< 6.01 \cdot 10^{-4}$	$< 3.50 \cdot 10^{-4}$	$< 3.91 \cdot 10^{-4}$	$< 2.88 \cdot 10^{-4}$
WAB104	2018	$< 5.98 \cdot 10^{-1}$	$< 1.32 \cdot 10^{-1}$	$< 1.53 \cdot 10^{-2}$	$< 9.88 \cdot 10^{-4}$	$< 7.60 \cdot 10^{-4}$	$4.82 \cdot 10^{-4}$	$< 5.78 \cdot 10^{-4}$	$7.56 \cdot 10^{-4}$	$< 3.81 \cdot 10^{-4}$	$< 2.81 \cdot 10^{-4}$
	2017	$< 4.80 \cdot 10^{-2}$	$< 2.79 \cdot 10^{-1}$	$2.30 \cdot 10^{-2}$	$< 1.01 \cdot 10^{-3}$	$< 7.79 \cdot 10^{-4}$	$< 4.72 \cdot 10^{-4}$	$< 6.01 \cdot 10^{-4}$	$< 3.50 \cdot 10^{-4}$	$< 3.91 \cdot 10^{-4}$	$< 2.88 \cdot 10^{-4}$
WAB105	2018	$< 5.98 \cdot 10^{-1}$	$< 1.32 \cdot 10^{-1}$	$< 1.53 \cdot 10^{-2}$	$< 9.88 \cdot 10^{-4}$	$< 7.60 \cdot 10^{-4}$	$3.70 \cdot 10^{-2}$	$< 5.78 \cdot 10^{-4}$	$< 3.43 \cdot 10^{-4}$	$< 3.81 \cdot 10^{-4}$	$< 2.81 \cdot 10^{-4}$
	2017	$< 4.80 \cdot 10^{-2}$	$< 2.79 \cdot 10^{-1}$	$2.01 \cdot 10^{-2}$	$< 1.01 \cdot 10^{-3}$	$< 7.79 \cdot 10^{-4}$	$< 4.72 \cdot 10^{-4}$	$< 6.01 \cdot 10^{-4}$	$< 3.50 \cdot 10^{-4}$	$< 3.91 \cdot 10^{-4}$	$< 2.88 \cdot 10^{-4}$
WAB55	2018	$< 5.98 \cdot 10^{-1}$	$< 1.32 \cdot 10^{-1}$	$1.15 \cdot 10^{-1}$	$1.55 \cdot 10^{-3}$	$< 7.60 \cdot 10^{-4}$	$2.25 \cdot 10^{-3}$	$7.91 \cdot 10^{-4}$	$1.60 \cdot 10^{-3}$	$< 3.81 \cdot 10^{-4}$	$5.52 \cdot 10^{-3}$
	2017	$< 4.80 \cdot 10^{-2}$	$< 2.79 \cdot 10^{-1}$	$1.06 \cdot 10^{-1}$	$< 1.01 \cdot 10^{-3}$	$< 7.79 \cdot 10^{-4}$	$< 4.72 \cdot 10^{-4}$	$< 6.01 \cdot 10^{-4}$	$< 3.50 \cdot 10^{-4}$	$< 3.91 \cdot 10^{-4}$	$< 2.88 \cdot 10^{-4}$
WAB56	2017	$2.40 \cdot 10^{-1}$	$< 2.79 \cdot 10^{-1}$	$1.60 \cdot 10^{-1}$	$< 1.01 \cdot 10^{-3}$	$< 7.79 \cdot 10^{-4}$	$< 4.72 \cdot 10^{-4}$	$< 6.01 \cdot 10^{-4}$	$< 3.50 \cdot 10^{-4}$	$< 3.91 \cdot 10^{-4}$	$< 2.88 \cdot 10^{-4}$
NSHQ04	2018	$< 5.98 \cdot 10^{-1}$	$< 1.32 \cdot 10^{-1}$	$1.44 \cdot 10^{2}$	$2.45 \cdot 10^{-2}$	$2.22 \cdot 10^{-3}$	$< 4.61 \cdot 10^{-4}$	$< 5.78 \cdot 10^{-4}$	$< 3.43 \cdot 10^{-4}$	$< 3.81 \cdot 10^{-4}$	$< 2.81 \cdot 10^{-4}$
	2017	$< 4.80 \cdot 10^{-2}$	$< 2.79 \cdot 10^{-1}$	$4.83 \cdot 10^{2}$	$< 1.01 \cdot 10^{-3}$ [b]	$1.03 \cdot 10^{-3}$	$< 4.72 \cdot 10^{-4}$	$< 6.01 \cdot 10^{-4}$	$< 3.50 \cdot 10^{-4}$	$< 3.91 \cdot 10^{-4}$	$< 2.88 \cdot 10^{-4}$
WAB71	2018	$< 5.98 \cdot 10^{-1}$	$< 1.32 \cdot 10^{-1}$	7.76	$1.00 \cdot 10^{-3}$	$< 7.60 \cdot 10^{-4}$	$< 4.61 \cdot 10^{-4}$	$< 5.78 \cdot 10^{-4}$	$< 3.43 \cdot 10^{-4}$	$< 3.81 \cdot 10^{-4}$	$< 2.81 \cdot 10^{-4}$
	2017	$5.92 \cdot 10^{-1}$	$< 2.79 \cdot 10^{-1}$	$1.48 \cdot 10^{1}$	$< 1.01 \cdot 10^{-3}$	$< 7.79 \cdot 10^{-4}$	$< 4.72 \cdot 10^{-4}$	$1.94 \cdot 10^{-2}$	$< 3.50 \cdot 10^{-4}$	$4.79 \cdot 10^{-4}$	$< 2.88 \cdot 10^{-4}$
CM2A	2018	3.38	$< 1.32 \cdot 10^{-1}$	$1.52 \cdot 10^{2}$	$4.11 \cdot 10^{-2}$	$1.75 \cdot 10^{-3}$	$< 4.61 \cdot 10^{-4}$	$6.48 \cdot 10^{-3}$	$< 3.43 \cdot 10^{-4}$	$< 3.81 \cdot 10^{-4}$	$< 2.81 \cdot 10^{-4}$
NSHQ14	2018	$1.31 \cdot 10^{2}$	$< 1.32 \cdot 10^{-1}$	$7.12 \cdot 10^{1}$	$7.32 \cdot 10^{-2}$	$7.64 \cdot 10^{-3}$	$2.26 \cdot 10^{-3}$	$2.88 \cdot 10^{-3}$	$1.27 \cdot 10^{-3}$	$2.23 \cdot 10^{-3}$	$1.12 \cdot 10^{-3}$
	2017	$2.53 \cdot 10^{2}$	$< 2.79 \cdot 10^{-1}$	$1.06 \cdot 10^{2}$	$7.98 \cdot 10^{-2}$	$9.00 \cdot 10^{-3}$	$1.53 \cdot 10^{-3}$	$4.77 \cdot 10^{-3}$	$< 3.50 \cdot 10^{-4}$	$< 3.91 \cdot 10^{-4}$	$9.70 \cdot 10^{-4}$

[a]Hexane isomers not chromatographically resolved.

[b]High $C_1/(C_2 + C_3)$ at NSHQ04 resulted in CH_4 tailing into and preventing quantitation of the C_2H_6 peak in 2017. Chromatographic improvements were made between analyses of 2017 and 2018 samples.

2.3.2 Origin of CH_4 and co-occurring short-chain alkanes in the Samail Ophiolite

In this study, we focus our discussion on fluid and particulate samples from a subset of wells (NSHQ14, NSHQ04, and WAB188) that yielded particularly rich datasets from which we infer key CH_4 cycle processes that likely occur widely in the Samail Ophiolite. We discuss three additional wells (WAB71, WAB56, and CM2A) in Section A.1, which illustrate that the processes outlined below are broadly applicable throughout the study area, although nuanced differences in CH_4 dynamics do occur depending on local hydrogeologic factors.

2.3.2.1 Abiotic, ^{13}C-enriched CH_4, C_2H_6, and C_3H_8 mixed with microbial CH_4 produced under C-limited conditions in the $Ca^{2+} - OH^-$ waters of well NSHQ14

Well NSHQ14 is situated in a catchment dominated by partially serpentinized harzburgite with meter-scale partially serpentinized dunite bands (Figure 2.1; Figure A.1; Table 4.4). The well is cased to 5.8 meters below ground level (mbgl) and drilled to 304 mbgl (Table 4.4). Geophysical logs of NSHQ14 (Paukert, 2014; Matter et al., 2018) indicate the presence of moderately fresh water ($1500\,\mu S \cdot cm^{-1}$) near the water table at 10 mbgl trending to more saline water ($3500\,\mu S \cdot cm^{-1}$) at 30 mbgl and more gradual, continued increase in conductivity towards the bottom of the well. The pH increases from 10.36 to 11.26, while f_{O_2} decreases from 10^{-30} bar to 10^{-74} bar and Eh decreases from 142 mV to -582 mV from 10 mbgl to 30 mbgl, and hyperalkaline and reduced conditions persist to the bottom of the well. These trends suggest that the upper 20 m of the water column contain a mixture of atmosphere-influenced water and deep water that has extensively reacted with peridotite in isolation from the atmosphere. The high extents of reaction experienced by deep fluids sampled from NSHQ14 are additionally reflected in their c_{H_2}, which was the highest among the studied wells ($253\,\mu mol \cdot L^{-1}$ and $131\,\mu mol \cdot L^{-1}$ in 2017 and 2018, respectively; Table 4.2; Figure 2.2). NSHQ14 waters also had high c_{CH_4} ($106\,\mu mol \cdot L^{-1}$ and $71.2\,\mu mol \cdot L^{-1}$ in 2017 and

2018, respectively).

CH_4 has ranged in $\delta^{13}C$ from $-6.89\,‰$ VPDB to $+3.7\,‰$ VPDB in fluid samples from NSHQ14, with a mean weighted by sample year of $-0.8\,‰$ VPDB (Figure 2.3a; Table 3.4). These $\delta^{13}C$ values are generally higher than those of CH_4 emanating from sediment-poor seafloor hydrothermal vents, where a dominantly abiotic origin has been proposed ((Welhan and Craig, 1983; Merlivat et al., 1987; Charlou et al., 1996, 2000, 2002; Proskurowski et al., 2008; Kumagai et al., 2008; McDermott et al., 2015; Wang et al., 2018); represented by Mid-Cayman Rise and Ashadze II in Figure 2.3a), higher than typical mantle values (Deines, 2002), and similar to marine carbonate (Schidlowski, 2001). CH_4 $\delta^{13}C$ at NSHQ14 is generally higher than $\delta^{13}C$ of carbonate veins in NSHQ14 ($-7.05\,‰$ VPDB to $-4.69\,‰$ VPDB; Miller et al., 2016), which is opposite to that which would be expected at equilibrium (Bottinga, 1969), indicating that CH_4 is not in isotopic equilibrium with co-existing carbonate minerals.

CH_4 is accompanied by $C_2 - C_6$ alkanes in fluids from NSHQ14 (Table 4.2). These alkanes had $C_1/(C_2 + C_3)$ ratios of 1240 in 2017 and 881 in 2018, which are similar to fluid samples and rock crushings from other ophiolites and sediment-poor seafloor hydrothermal vents (Abrajano et al., 1990; Charlou et al., 2010; McDermott et al., 2015; Grozeva et al., 2020), but 10^2 times higher than those of Kidd Creek mine, Canada, for which a low-temperature, abiotic origin of alkanes has been proposed (Sherwood Lollar et al., 2002, 2008; Young et al., 2017) (Figure 2.3c). Thus, $C_1/(C_2 + C_3)$ ratios could reflect differences in alkane formation mechanisms or extents of reaction in Precambrian shield sites like Kidd Creek versus ophiolites and sediment-poor seafloor hydrothermal vents.

C_2H_6 and C_3H_8 at NSHQ14 are strongly ^{13}C-enriched ($\delta^{13}C$ of $-6.0\,‰$ VPDB and $+3.3\,‰$ VPDB, respectively; Table 3.4; Figure 3.2). The observed $\delta^{13}C$ values are $\sim 15\,‰$ higher than those in the most mature (and therefore most ^{13}C-enriched) thermogenic C_2H_6 and C_3H_8 samples from confined systems (Milkov and Etiope, 2018; Fiebig et al., 2019). Increases in $\delta^{13}C_{C_3}$ of $\sim 15\,‰$ have been attributed to microbial oxidation of short-chain alka-

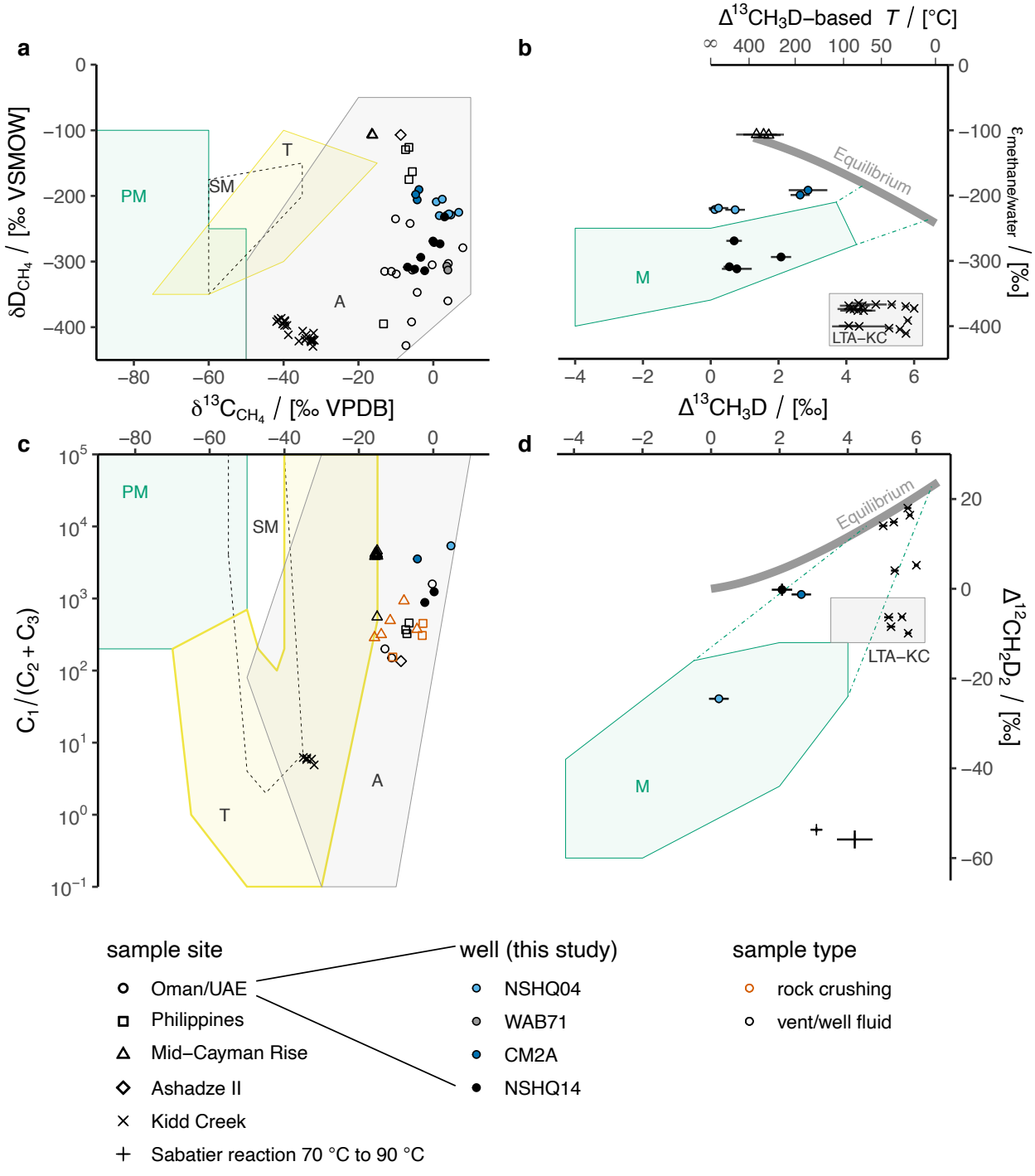
a
b
c
d
PM
SM
T
A
M
Equilibrium
LTA–KC
δD_CH4 / [‰ VSMOW]
δ13C_CH4 / [‰ VPDB]
Δ13CH3D–based T / [°C]
Δ13CH3D / [‰]
εmethane/water / [‰]
C1/(C2 + C3)
Δ12CH2D2 / [‰]
sample site
Oman/UAE
Philippines
Mid–Cayman Rise
Ashadze II
Kidd Creek
Sabatier reaction 70 °C to 90 °C
well (this study)
NSHQ04
WAB71
CM2A
NSHQ14
sample type
rock crushing
vent/well fluid

Figure 2.3: Molecular and isotopic compositions of natural gases. (a) Plot of δD_{CH_4} vs. $\delta^{13}C_{CH_4}$. Shaded fields of typical gas origin after Milkov and Etiope (2018). *Abbreviations:* PM, primary microbial; SM, secondary microbial; T, thermogenic; A, abiotic. (c) Plot of ratio of methane (C_1) to the sum of ethane (C_2) and propane (C_3) vs. $\delta^{13}C_{CH_4}$. Only analyses for which C_2 was above limit of quantitation are plotted. If C_3 was below limit of quantitation, its contribution to $C_1/(C_2 + C_3)$ was assumed to be negligible, and therefore C_1/C_2 is plotted. Fields and abbreviations same as in (a). In (a) and (c), uncertainties are smaller than plotted symbols. (b) Plot of $\varepsilon_{\text{methane/water}}$ vs. $\Delta^{13}CH_3D$. X and Y axes are swapped with respect to original publication of this type of plot (Wang et al., 2015) so that (b) is comparable against (d). The data from (b) are plotted in the Wang et al. (2015) orientation in Figure A.4. Equilibrium line from Horibe and Craig (1995) and Young et al. (2017). *Abbreviations:* LTA-KC, low-temperature abiotic (Kidd Creek-type); M, microbial. Green dot-dashed lines in (b) and (d) indicate a range of CH_4 isotopic compositions that have been attributed to either low cell-specific rates of methanogenesis or anaerobic oxidation of methane; that is, they start at isotopic compositions produced by methanogen cultures and end at isotopic equilibrium between 5 °C and 70 °C, which is the range of temperatures over which anaerobic oxidation of methane has been documented (Wang et al., 2015; Stolper et al., 2015; Young et al., 2017; Ash and Egger, 2019; Giunta et al., 2019). (d) Plot of $\Delta^{13}CH_3D$ vs. $\Delta^{12}CH_2D_2$, after Young et al. (2017). Fields, abbreviations, and temperature axis same as in (b). In (b) and (d), error bars represent 95 % confidence interval for analyses performed at MIT, and 1 standard error for analyses performed at UCLA. Contextual data from ophiolites: Oman/UAE (Fritz et al., 1992; Etiope et al., 2015; Boulart et al., 2013; Miller et al., 2016; Vacquand et al., 2018), the Philippines (Abrajano et al., 1990; Grozeva et al., 2020); sediment-poor seafloor hydrothermal vents: Mid-Cayman Rise (McDermott et al., 2015; Wang et al., 2018; Grozeva et al., 2020), Ashadze II (Charlou et al., 2010); Precambrian Shield: Kidd Creek, Canada (Sherwood Lollar et al., 2008; Young et al., 2017); and laboratory Sabatier reaction catalyzed by Ru (Young et al., 2017).

nes, which enriches the residual in ^{13}C (Martini et al., 2003). However, short-chain alkane oxidizing microbial species (Shennan, 2006; Singh et al., 2017; Laso-Pérez et al., 2019) were not detected in 16S rRNA gene sequences of DNA obtained from NSHQ14. Thus, there is not strong evidence to suggest that $\delta^{13}C_{C_2}$ and $\delta^{13}C_{C_3}$ at NSHQ14 result from post-genetic microbial alteration. Rather, $\delta^{13}C_{C_2}$ and $\delta^{13}C_{C_3}$ should reflect formation conditions and C source(s).

C_2H_6 and C_3H_8 at NSHQ14 are not likely to derive from nearby organic matter. Hydrocarbon-rich sedimentary formations in northern Oman not only lack a clear structural connection to the ophiolite aquifer, but also yield oils with $\delta^{13}C$ values (Terken, 1999) at least 20 ‰ lower than those of C_2H_6 and C_3H_8 at NSHQ14. Furthermore, total organic C in peridotites exposed to alteration at the seafloor, a proxy for organic C endogenous to the Samail Ophiolite, is also relatively ^{13}C-depleted (approximately -25 ± 5 ‰ VPDB; Alt et al., 2013, 2012a,b; Delacour et al., 2008). Closed-system thermal cracking of these organic matter sources is unlikely to have produced the comparatively ^{13}C-enriched C_2H_6 and C_3H_8 at NSHQ14 and previously reported elsewhere in the ophiolite (Figure 3.2; Fritz et al., 1992).

Thermal cracking of organic matter and open-system degassing can enrich late-produced short-chain alkanes in ^{13}C due to kinetic isotope effects associated with the cleavage of precursor sites in the parent organic matter and the resultant Rayleigh distillation of these sites (Fiebig et al., 2019). However, this process has only been shown to occur in hydrothermal settings where reservoir temperatures are 200 °C to 450 °C (Fiebig et al., 2019), which are higher than temperatures along groundwater flow paths intersecting the wells in this study. Measured groundwater temperatures in the study area are ~ 35 °C (Table 4.4), and $H_2 - H_2O$ isotope thermometry and $C - O$ clumped isotope thermometry on carbonate veins with significant ^{14}C contents in Samail Ophiolite peridotites both indicate equilibrium ≤ 60 °C (Kelemen and Matter, 2008; Kelemen et al., 2011; Mervine et al., 2014; Miller et al., 2016). At these low temperatures within the active alteration zone of the Samail Ophiolite, thermal cracking of organic matter is unlikely to proceed at sufficient rates to attain the high

extents of reaction progress necessary to explain the observed ^{13}C enrichments in short-chain alkanes at NSHQ14 over relevant timescales.

Alternatively, short-chain alkanes in NSHQ14 fluids may have an abiotic source. Several studies have demonstrated storage of large quantities of CH_4 and associated short-chain alkanes in fluid inclusions in ophiolites (Sachan et al., 2007; Klein et al., 2019; Grozeva et al., 2020). However, the findings of these studies disagree with those of Etiope et al. (2018), who measured relatively low concentrations of CH_4 stored in serpentinized peridotites from Greek ophiolites. Since the rocks analyzed by Etiope et al. (2018) were sampled from outcrops, it is possible that chemical or physical processes associated with surface exposure may have resulted in loss of CH_4 once stored in peridotite-hosted fluid inclusions prior to analysis. Although further study of the quantity and spatial distribution of CH_4 storage in ophiolitic rocks is warranted, the presence of $CH_4 + H_2$ inclusions in olivine and $CH_4 \pm$ graphite inclusions in orthopyroxene in Samail Ophiolite harzburgites (Miura et al., 2011) requires that fluid inclusions be considered as a potential source for abiotic CH_4 and associated short-chain alkanes at NSHQ14 and elsewhere in the ophiolite.

A fluid inclusion source of CH_4 and short-chain alkanes is compatible with C stable isotopic compositions of these compounds in groundwaters pumped from NSHQ14. CH_4, C_2H_6, and C_3H_8 $\delta^{13}C$ values at NSHQ14 (-6.89 ‰ VPDB to $+3.7$ ‰ VPDB; Table 3.4) overlap with CH_4 and C_2H_6 $\delta^{13}C$ values measured by Grozeva et al. (2020) in rock crushing experiments on CH_4-rich fluid inclusion-bearing peridotites and dunites sampled from the Zambales ophiolite in the Philippines (-12.4 ‰ VPDB to -0.9 ‰ VPDB; Figure 3.2), which, in turn, overlap with $\delta^{13}C$ values of CH_4 from nearby gas seeps at Los Fuegos Eternos and Nagsasa in the Philippines (-7.4 ‰ VPDB to -5.6 ‰ VPDB; Figure 2.3a; Abrajano et al., 1990; Vacquand et al., 2018). Grozeva et al. (2020) also crushed CH_4-rich fluid inclusion-bearing rocks from the Mid-Cayman Rise. Of the Mid-Cayman Rise samples that yielded sufficient CH_4 and C_2H_6 for precise C isotopic analysis, which were all mafic intrusive rocks, $\delta^{13}C$ values ranged from -14.0 ‰ VPDB to $+0.7$ ‰ VPDB. The lower end of Mid-Cayman

Rise rock crushing short-chain alkane $\delta^{13}C$ values are similar to those measured in Mid-Cayman Rise hydrothermal vent fluids (-15.8 ‰ VPDB to -9.7 ‰ VPDB; McDermott et al., 2015), whereas the higher end are similar to those of NSHQ14 (Figure 3.2). Furthermore, C_2H_6 and C_3H_8 $\delta^{13}C$ values of NSHQ14 fluids resemble those of fluids discharging from the sediment-poor hydrothermal vents at Ashadze II, Mid-Atlantic Ridge (Figure 3.2; Charlou et al. 2010). The similarities in short-chain alkane $\delta^{13}C$ values between circulating fluids and rock-hosted fluid inclusions in ophiolites and present-day oceanic lithospheric sites suggest that circulating fluids in both environments derive much of their CH_4 and short-chain alkanes from fluid inclusions.

Sources of CH_4 can also be assessed by measuring H isotopic compositions and clumped isotopologue relative abundances of CH_4 and comparing these isotopic compositions to temperature-dependent equilibria. $CH_4 - H_2O$ H isotopic equilibrium and intra-CH_4 isotopologue equilibrium are related because the dominant mechanism through which intra-CH_4 equilibrium is approached in nature is typically not direct reaction among CH_4 isotopologues (e.g. Equation 2.1), but rather isotopic exchange reactions involving co-existing compounds like H_2O and H_2 (Wang et al., 2018). These isotopic equilibria are represented by thick gray lines in Figure 2.3b and d. Intra-CH_4 equilibrium is governed by the increasing relative stability of bonds between two heavy isotopes (more "clumping") at lower temperatures, which is reflected in higher $\Delta^{13}CH_3D$ and $\Delta^{12}CH_2D_2$ values. However, isotopic equilibrium will only be expressed in a sample if kinetics allow it. This is not always the case because H isotope half-exchange timescales in the $CH_4 - H_2O$ system increase from 10 y at 300 °C to 10^6 y at 200 °C to 10^{12} y (extrapolated) at 100 °C (Koepp, 1978; Reeves et al., 2012). Furthermore, Wang et al. (2018) showed that CH_4- and H_2- rich gas samples from sediment-poor seafloor hydrothermal vents whose effluent fluid temperature ranged from 96 °C to 370 °C yielded apparent $CH_4 - H_2O$ H isotopic and $\Delta^{13}CH_3D$ equilibrium temperatures of 270 °C to 360 °C, suggesting a closure temperature of 270 °C for H isotope exchange in the $CH_4 - H_2O$ and $CH_4 - H_2$ systems in seafloor hydrothermal settings (e.g. Mid-Cayman Rise in Figure

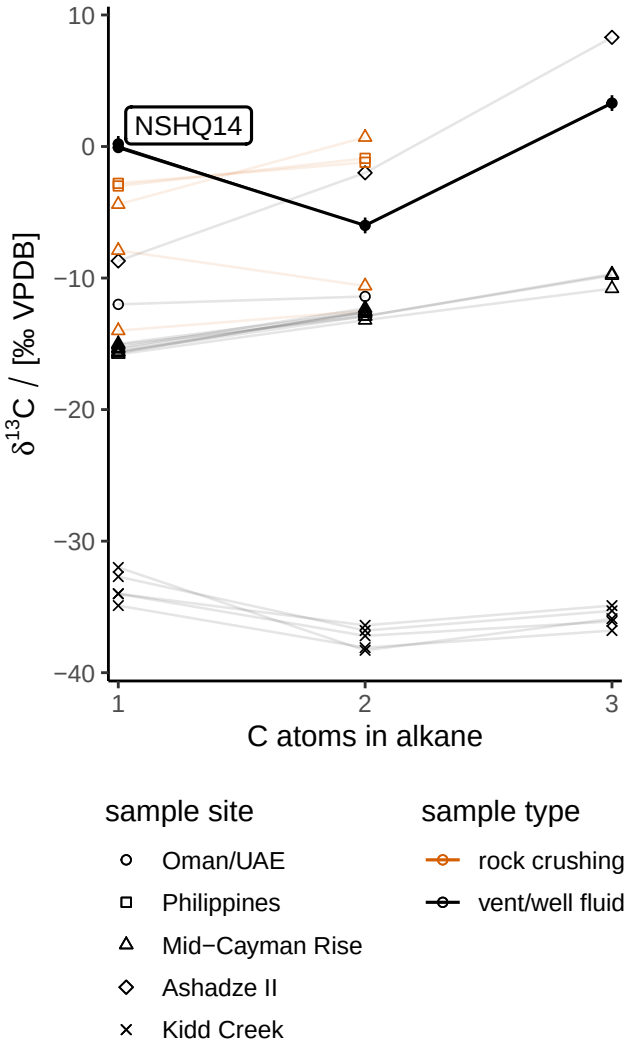

Figure 2.4: Plot of δ^{13}C of CH_4 and co-occurring n-alkanes vs. the number of C atoms per molecule. Error bars represent uncertainties on δ^{13}C analyses performed at CUB. Only samples for which $\delta^{13}C_{C_2}$ was determined are plotted. Contextual data from ophiolites: Oman/UAE (Fritz et al., 1992), the Philippines (Grozeva et al., 2020); sediment-poor seafloor hydrothermal vents: Mid-Cayman Rise (McDermott et al., 2015; Grozeva et al., 2020), Ashadze II (Charlou et al., 2010); and Precambrian Shield: Kidd Creek, Canada (Sherwood Lollar et al., 2008).

2.3b). Thus, if CH_4 at NSHQ14 were formed exclusively within fluid inclusions and was subsequently stored at relatively low temperatures ($< 200\,°C$) without subsequent alteration or mixing with CH_4 of other sources, then this CH_4 would be expected to exhibit H isotopic equilibrium with SMOW-like water and intra-CH_4 equilibrium reflecting temperatures above $200\,°C$.

Across five years of samples from NSHQ14, δD_{CH_4} has ranged from $-232\,‰$ VSMOW to $-311.73\,‰$ VSMOW, with a mean weighted by sample year of $-275\,‰$ VSMOW (Figure 2.3a; Table 3.4). This CH_4 is D-enriched with respect to coexisting H_2 ($\delta D_{H_2} = -685\,‰$ VSMOW; Miller et al., 2016) and D-depleted with respect to coexisting water ($\delta D_{H_2O} = +0.2\,‰$ VSMOW in 2018; Table 4.1). Although H_2 and water reflect H isotopic equilibrium at $\sim 50\,°C$ (Miller et al., 2016), both H_2 and water are in H isotopic disequilibrium with CH_4 (Figure 2.3b). Moreover, NSHQ14 fluids exhibit intra-CH_4 disequilibrium, as indicated by $\Delta^{13}CH_3D$ and $\Delta^{12}CH_2D_2$ values (Table 3.4) plotting below the equilibrium line in Figure 2.3d. These non-equilibrium isotopic compositions indicate that post-genetic alteration of CH_4 must have occurred or that fluid inclusions are not the only source of CH_4 at NSHQ14.

One such post-genetic alteration mechanism is diffusion. However, CH_4 at NSHQ14 cannot be the diffusion residual of CH_4 that was originally at intramolecular equilibrium, as that would have increased $\Delta^{13}CH_3D$ and $\Delta^{12}CH_2D_2$ of the residual (Young et al., 2017), pushing those values above the equilibrium line in Figure 2.3d. Another potential alteration mechanism is microbial CH_4 oxidation. Two types of microbial CH_4 oxidation have been studied for their effects on CH_4 clumped isotopologue relative abundances: anaerobic methane oxidation of the ANME type and aerobic CH_4 oxidation. ANME-type anaerobic methane oxidation is suggested to be a highly reversible metabolic pathway (Knittel and Boetius, 2009; Timmers et al., 2017). This reversibility has been proposed to bring $\Delta^{13}CH_3D$ towards equilibrium at low temperatures ($70\,°C$ to $30\,°C$) through continuous breaking and reforming of bonds in the CH_4 molecule (Young et al., 2017; Ash and Egger, 2019; Giunta et al., 2019). Thus, the

comparatively low $\Delta^{13}CH_3D$ values observed in samples from NSHQ14 and other wells in this study (Figure 2.3b and d) do not support a major role for anaerobic methane oxidation in the CH_4 cycle within the study area. Aerobic CH_4 oxidation is less reversible than ANME-type anaerobic methane oxidation due to differences in the enzymes and electron acceptors used for those respective processes. For this reason, aerobic CH_4 oxidation does not bring CH_4 into isotopic equilibrium, but rather imparts a normal, classical kinetic isotope effect during CH_4 consumption. In a study of the effect of aerobic CH_4 oxidation on $\Delta^{13}CH_3D$, Wang et al. (2016) found that the fractionation factor for $^{13}CH_3D$ was closely approximated by the product of the fractionation factors for $^{13}CH_4$ and $^{12}CH_3D$. Although it has not yet been demonstrated experimentally, it is hypothesized that the fractionation factor for $^{12}CH_2D_2$ during aerobic CH_4 oxidation is likewise equivalent to the square of the fractionation factor for $^{12}CH_3D$ (Young, 2020). This "product rule" for isotopic fractionation during aerobic CH_4 oxidation results in decreases in $\Delta^{13}CH_3D$ and $\Delta^{12}CH_2D_2$ with concomitant increases in $\delta^{13}C$ and δD in residual CH_4 (Wang et al., 2016; Young, 2020). Thus, aerobic CH_4 oxidation could in principle draw $\Delta^{13}CH_3D$ and $\Delta^{12}CH_2D_2$ values originally reflecting 200 °C to 360 °C equilibrium down below the equilibrium line in Figure 2.3d. However, if CH_4 samples from NSHQ14 were originally at 200 °C to 360 °C equilibrium with water of SMOW-like isotopic composition, aerobic methane oxidation would push the residual CH_4 towards higher δD (and $\varepsilon_{\text{methane/water}}$) values (above the equilibrium line in Figure 2.3b), which is inconsistent with the comparatively low δD_{CH_4} observed at NSHQ14.

For the reasons outlined above, post-genetic alteration of CH_4 in $CH_4 - H_2O$ and intramolecular isotopic equilibrium at 200 °C to 360 °C does not explain the observed isotopic compositions of CH_4 sampled from NSHQ14. Therefore, the release of CH_4 stored in fluid inclusions cannot account for all the CH_4 at NSHQ14. Alternative processes that do produce CH_4 with $\Delta^{13}CH_3D$ and $\Delta^{12}CH_2D_2$ values lower than equilibrium include microbial methanogenesis (green shaded area in Figure 2.3b and d; Wang et al., 2015; Stolper et al., 2015; Young et al., 2017; Gruen et al., 2018; Young, 2020) and low-temperature ($\leq$ 90 °C)

abiotic reduction of CO_2 or CO through Sabatier or Fischer-Tropsch-type reactions (represented in Figure 2.3 d by samples from Kidd Creek (gray shaded area) (Young et al., 2017; Sherwood Lollar et al., 2002, 2008) and Ru-catalyzed Sabatier reaction experiments (Young et al., 2017; Etiope and Ionescu, 2015)).

To independently assess the potential influences of microbial processes on CH_4 concentration and isotopic composition, DNA was extracted from biomass in pumped groundwaters and subjected to amplification and sequencing of 16S rRNA genes. 16S rRNA gene sequences of biomass collected in 2018 were searched for matches to known CH_4-cycling taxa, as compiled previously by Crespo-Medina et al. (2017). Sequences closely affiliated with both methanogenic and methanotrophic taxa were found to be widespread in the aquifer (Figure 2.5). Based on phylogenetic inference, the dominant methanogenic taxon was related to the genus *Methanobacterium*, whose members can produce CH_4 from H_2 and CO_2, CO, or formate (Balch et al., 1979). *Methanobacterium* comprised a high proportion (24 %) of 16S rRNA gene sequences at NSHQ14 in 2018. Relative abundances of *Methanobacterium* 16S rRNA gene reads were similarly high in 2017 (12 %) and 2016 (28 %), but lower (< 1 %) in 2015 and 2014 (Miller et al., 2016; Rempfert et al., 2017; Kraus et al., 2018). The increase in the relative abundance of 16S rRNA genes affiliated with *Methanobacterium* in samples collected in 2016 and onwards versus those collected in 2014 and 2015 coincided with our transition from a smaller, lower-flow pump (maximum depth 20 m) to larger, higher-flow pumps (maximum depth 90 m). The obligate anaerobic nature of this methanogen genus (Boone, 2015) is consistent with its higher relative gene abundances in fluids sampled from greater depths, which presumably receive less input of atmospheric O_2 than do shallower fluids.

Consortia capable of anaerobic oxidation of CH_4 coupled to SO_4^{2-} reduction, including ANME, were not detected by 16S rRNA gene sequencing of samples obtained from NSHQ14 in 2018 (Figure 2.5), 2016, or 2014 (Miller et al., 2016; Rempfert et al., 2017), although sequences affiliated with order ANME-1b were detected in low abundance (< 1 % of reads) in

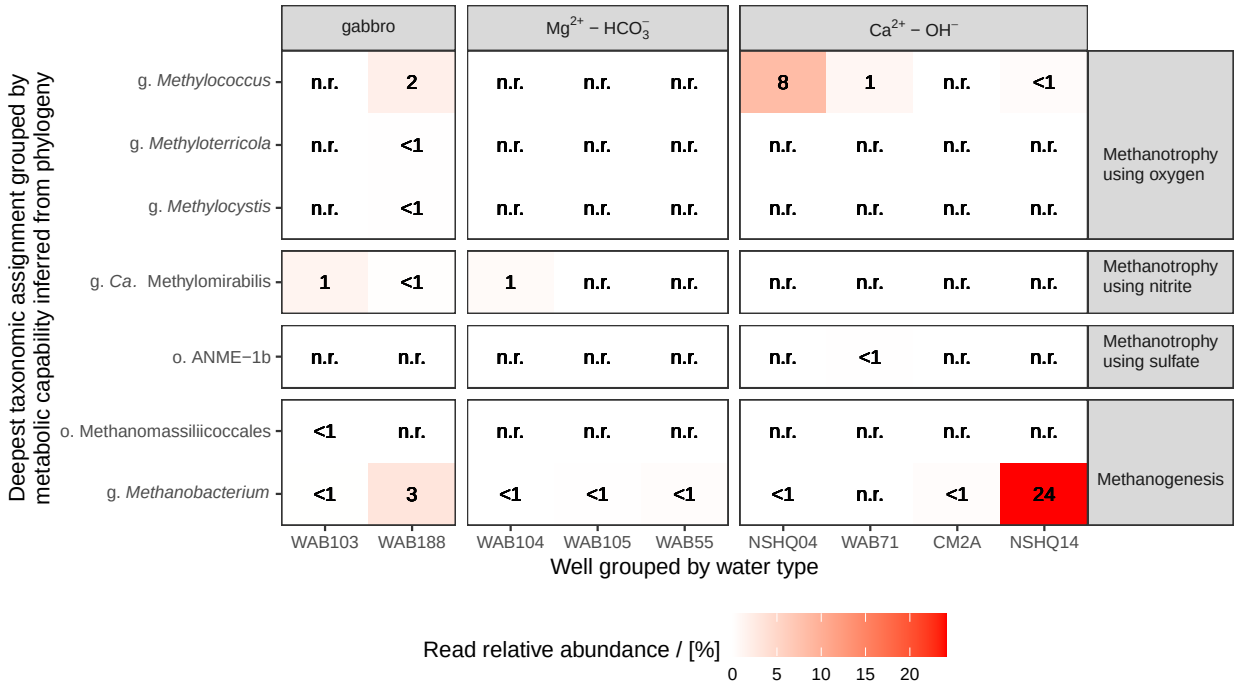

Figure 2.5: 16S rRNA gene read relative abundances of DNA extracted from Samail Ophiolite groundwaters sampled in 2018 affiliated with CH_4-cycling taxa. Read relative abundances are reported as percentages rounded to the ones place. Cases when a taxon was detected in a sample and was $< 1\,\%$ read relative abundance after rounding are labeled "< 1". Cases when no reads of a taxon were detected in a sample are labeled "n.r."

samples obtained from NSHQ14 in 2017 and 2015 (Rempfert et al., 2017; Kraus et al., 2018). This scarcity of ANME may result from metabolic inhibition by high c_{H_2} in groundwaters at NSHQ14 and elsewhere in the Samail Ophiolite. It has been proposed that the thermodynamics of "reverse methanogenesis" require low c_{H_2} (0.1 nM to 1 nM at Hydrate Ridge, a marine cold seep environment (Boetius et al., 2000), where CH_4 and SO_4^{2-} concentrations can be a factor of 10 or more higher than those typically measured in ophiolitic groundwaters such as in Oman). Indeed, the bioenergetics of SO_4^{2-}-driven oxidation of CH_4 are less favorable than SO_4^{2-}-driven oxidation of H_2 or non-CH_4 organics, or other metabolisms such as methanogenesis or acetogenesis in the Samail Ophiolite (Canovas III et al., 2017), as in deep continental settings where radiolytic H_2 accumulates (Kieft et al., 2005; Moser et al., 2005; Kieft, 2016).

While 16S rRNA gene sequences affiliated with anaerobic CH_4 oxidizing microbes have only occasionally been detected at NSHQ14, 16S rRNA gene sequences affiliated with the genus *Methylococcus*, which contains aerobic methanotrophs (Hanson and Hanson, 1996), have been detected in all samples from NSHQ14, ranging from 1 % to $<$ 1 % of reads in samples obtained from 2014 to 2018 (Figure 2.5; Miller et al., 2016; Rempfert et al., 2017; Kraus et al., 2018). Since the aerobic lifestyle of *Methylococcus* is at odds with that of the obligate anaerobe, *Methanobacterium*, it seems most likely that these two taxa are spatially separated in the aquifer, and that waters containing each of them were mixed during open borehole pumping. Still, the $>$ 10 times higher abundances of *Methanobacterium*-related 16S rRNA genes relative to those of *Methylococcus* at NSHQ14 in samples from 2016 to 2018 suggest that the microbial CH_4 cycle at this well is dominated by CH_4 production, rather than consumption.

16S rRNA gene sequencing of subsurface biomass from NSHQ14 is complemented by other observations that suggest that methanogens are not only prevalent, but active. The functional potential to perform hydrogenotrophic and acetoclastic methanogenesis at NSHQ14 has been demonstrated through metagenomic sequencing (Fones et al., 2019), and genes

involved in methanogenesis are actively transcribed (Kraus et al., 2018). Transformation of ^{14}C-labeled HCO_3^- to CH_4 has been shown to occur in water samples from NSHQ14 at significantly higher rates than in killed controls (Fones et al., 2019), indicating that methanogenesis occurs *in situ*. Taken together with a cell abundance of $1.15 \cdot 10^5$ cells $\cdot$ mL^{-1} in groundwater at NSHQ14 (Fones et al., 2019), these data suggest that some depths of the aquifer accessed by NSHQ14 host abundant active methanogenic cells (thousands per mL, assuming $\sim 24\,\%$ of cells are methanogens based on 16S rRNA gene data). These active cells could influence CH_4 concentration and isotopic composition.

Methanogens could produce CH_4 through direct uptake of $\sum CO_2$ in H_2-rich $Ca^{2+} - OH^-$ water, where kinetic inhibitions to abiotic $\sum CO_2$ reduction to CH_4 allow for a modest energy yield for hydrogenotrophic methanogens (Leong and Shock, 2020). Methanogens using $\sum CO_2$ could benefit from greater chemical disequilibrium if they inhabit zones where deeply-sourced, H_2-rich $Ca^{2+} - OH^-$ water mixes with shallow, $Mg^{2+} - HCO_3^-$ water (Zwicker et al., 2018; Leong and Shock, 2020). This niche could be supported by rapid microbial O_2 consumption by aerobes, such as those that may belong to the genera *Meiothermus* and *Hydrogenophaga*, whose 16S rRNA gene sequences have been detected in multiple years of sampling at NSHQ14 (Figure A.3; Miller et al., 2016; Rempfert et al., 2017; Kraus et al., 2018; Fones et al., 2019), and kinetic limitations on carbonate precipitation (Kelemen et al., 2011; Gadikota et al., 2014; National Academies, 2019; Gadikota et al., 2020; Kelemen et al., 2020b). In addition to direct uptake of $\sum CO_2$, carbonate minerals may serve as a C source for methanogenesis in carbonated peridotites (Miller et al., 2018). Other potential C sources include formate ($HCOO^-$) and carbon monoxide (CO). Formate and CO are related to $\sum CO_2$ through reversible reactions involving H_2 and H_2O, which are known to occur during serpentinization (McCollom and Seewald, 2003; McDermott et al., 2015). CO has always been below limits of quantitation in Oman wells ($< 132\,\mathrm{nmol} \cdot \mathrm{L}^{-1}$ in 2018; Table 4.2), and formate concentrations are $1\,\mu\mathrm{mol} \cdot \mathrm{L}^{-1}$ to $2\,\mu\mathrm{mol} \cdot \mathrm{L}^{-1}$ in the studied wells (Rempfert et al., 2017). The relatively low concentrations of these single-C compounds suggest that they could

be limiting substrates for methanogenesis, similarly to $\sum CO_2$. Further physiological studies are needed to determine which C compounds *Methanobacterium* most actively metabolizes in $Ca^{2+} - OH^-$ waters and how substrate selection/limitation under these conditions affects isotopic compositions of produced CH_4.

The microbiological data from NSHQ14 fluids are compatible with δD_{CH_4}, $\Delta^{13}CH_3D$, and $\Delta^{12}CH_2D_2$ values that collectively indicate a substantial addition of microbial CH_4 to an otherwise abiotic pool of CH_4. Although the data presented here do not enable us to precisely determine the mole fractions and isotopic compositions of the microbial and abiotic components of CH_4 at NSHQ14, the high $\delta^{13}C$ of this CH_4 suggests that the microbial component is more ^{13}C-enriched than microbial CH_4 formed in sedimentary environments. The small apparent C isotope fractionation imparted by microbial methanogenesis at NSHQ14 is perhaps less than that observed by Miller et al. (2018) in growth of *Methanobacterium* on $CaCO_3\,(s)$ at pH $\sim$ 9 ($\alpha_{CO_2/CH_4} = 1.028$). This could be a result of the higher pH in natural $Ca^{2+} - OH^-$ fluids (up to pH $\sim$ 12) compared to the maximum experimental pH of 9.66 at which sufficient CH_4 was produced for isotopic analysis by Miller et al. (2018) and the potential for increased pH to further limit CO_2 availability. In natural settings, the suppression of C isotope fractionation during methanogenesis under severe C limitation is supported by observations of high $\delta^{13}C$ values (up to $+14\,‰$ VPDB) of lipid biomarkers thought to be produced by methanogens at serpentinite-hosted seeps at Chimaera, Turkey (Zwicker et al., 2018) and at the Lost City Hydrothermal Vent Field, Mid-Atlantic Ridge (Bradley et al., 2009). Evaluation of these hypotheses will require further research on the isotope effects of methanogenesis at hyperalkaline conditions using various C sources.

While our data support substantial microbial CH_4 and abiotic, fluid inclusion-derived CH_4 in NSHQ14 fluids, we find less evidence for abiotic CH_4 production at low temperatures ($< 200\,°C$). At low temperatures, access of gas-phase H_2 and CO_2 or CO to catalytic metals such as Ru is required for CH_4 to form at appreciable rates (Etiope and Ionescu, 2015; McCollom, 2016). It has been proposed that the spatial concentration of potentially-catalytic

Ru-rich chromites in chromitites is important for catalysis of low-temperature CO_2 reduction to CH_4 in ophiolites (Etiope and Ionescu, 2015; Etiope et al., 2018). While peridotites in Oman ubiquitously contain a few percent distributed chromite (Hanghøj et al., 2010), massive chromitites were not reported in lithologic descriptions of cores or drill cuttings from NSHQ14 or any of the six additional wells ranging from 300 m to 400 m depth that have been drilled in the same catchment by the Oman Drilling Project (Kelemen et al., 2020a). Nor are chromitites notably abundant in outcrop within this catchment. Furthermore, although some flow paths of meteoric water through the ophiolite may result in saturation in H_2 and separation of a free gas phase (Canovas III et al., 2017), the depth to water is < 20 m in all wells in the catchment of NSHQ14, suggesting water-saturated conditions in the subsurface. Moreover, if free H_2 (g) were generated at high extents of reaction progress, co-existing $CO_2\,(g)$ would be extremely scarce due to precipitation of carbonate minerals and high pH (Etiope and Ionescu, 2015; Leong and Shock, 2020). It has been proposed that CH_4 in ophiolites can form through reduction of $CO_2\,(g)$ from non-atmospheric sources such as magma, the mantle, or sedimentary carbonate formations (Etiope and Ionescu, 2015). A magmatic/mantle CO_2 source is not supported at NSHQ14 because excess He above air saturation in groundwaters from this well has a dominantly radiogenic isotopic composition that is distinct from mantle-derived He (Vankeuren et al., 2019). Further, although sedimentary carbonates are present in the vicinity of NSHQ14 and elsewhere in the ophiolite (Boudier and Coleman, 1981; de Obeso and Kelemen, 2018), there is no clear mechanism to liberate $CO_2\,(g)$ from mineral carbonates and transfer that $CO_2\,(g)$ to catalytic sites of reaction on chromites where $H_2\,(g)$ is also present. Thus, the apparent lack of massive chromites and free gaseous potential reactants suggest that the subsurface surrounding NSHQ14 is not conducive to low-temperature abiotic CH_4 production.

While low-temperature CH_4 production in the catchment of NSHQ14 seems unlikely, NSHQ14 groundwaters could be mere carriers of CH_4 that was produced elsewhere in the ophiolite under gaseous conditions and that has subsequently migrated into the aquifer.

Some studies of CH_4 origin in other peridotite bodies have favored such a hypothesis (Etiope et al., 2016; Marques et al., 2018). However, it is not clear how this hypothesis could be tested in the case of the NSHQ14, nor how it addresses the issue of CO_2 source.

In summary, isotopic and microbiological data lead us to conclude that the high concentrations of CH_4 ($10^2\,\mu mol{\cdot}L^{-1}$) in groundwaters accessed by NSHQ14 primarily result from microbial methanogenesis and the release of abiotic CH_4 from fluid inclusions. A portion of this CH_4 may be oxidized by aerobic methanotrophs.

2.3.2.2 Abundant microbial CH_4 produced under C-limited conditions and substantial microbial CH_4 oxidation in the $Ca^{2+} - OH^-$ waters of well NSHQ04

NSHQ04 is situated in partially serpentinized harzburgite 10 m away from a faulted contact with crustal gabbros (Figure 2.1; Figure A.1). Surface rock exposures surrounding NSHQ04 are dominated by serpentinized harzburgites, with lesser dunites, gabbro lenses, and pyroxenite dikes. NSHQ04 is cased to 5.8 mbgl and drilled to 304 m depth (Table 4.4). As of 2017, the well is obstructed at 8 m below the casing top, precluding deeper sampling (Section 3.5.1; Table 4.4).

Primary differences in fluid composition between NSHQ04 and NSHQ14 include lower pH by ~ 1 and higher $c_{\sum Ca}$ and $c_{\sum Si}$ at NSHQ04 (Tables 4.4 and 4.1; Miller et al., 2016; Rempfert et al., 2017; Vankeuren et al., 2019; Fones et al., 2019). These differences could be related to the scarcity of fresh, near-surface olivine at NSHQ04, which may result in a greater influence of pyroxene serpentinization at NSHQ04 (Miller et al., 2016). Low-temperature pyroxene serpentinization generally continues after olivine is exhausted, and leads to higher $c_{\sum Si}$ and, depending on pyroxene chemical composition, can also lead to higher $c_{\sum Ca}$ and lower pH (Bach et al., 2006; Leong and Shock, 2020). The relatively low pH and high $c_{\sum Si}$ could also stem from mixing of $Ca^{2+} - OH^-$ waters with gabbro- or atmosphere-influenced fluids.

Compared to NSHQ14, NSHQ04 has generally had lower c_{H_2} (detected in 2014, but not in 2018, 2017, 2015, or 2012; Table 4.2; Figure 2.2; Miller et al., 2016; Rempfert et al., 2017; Vankeuren et al., 2019). The relatively low c_{H_2} measured in waters pumped from NSHQ04 is probably due at least in part to microbial H_2 oxidation. Although there are multiple enzymes with which which a diversity of microbes oxidize H_2 (Peters et al., 2015), aerobic H_2 oxidation by bacteria of the genus *Hydrogenophaga* has been identified as a particularly prevalent process in serpentinizing settings, including the Samail Ophiolite (Suzuki et al., 2014; Rempfert et al., 2017; Marques et al., 2018). Sequences affiliated with *Hydrogenophaga* accounted for 20 % of 16S rRNA gene reads in DNA extracted from biomass in waters pumped from NSHQ04 in 2018, which is similar to previous years of sampling at NSHQ04 (6 % to 18 % in 2014, 2015, and 2017; inter-annual mean of 12 %) and higher than all other studied wells (Figure A.3; Rempfert et al., 2017; Miller et al., 2016; Kraus et al., 2018).

While H_2 has only been transiently detected at NSHQ04, c_{CH_4} at this well has consistently been the highest among our sample sites ($144\,\mu\text{mol}\cdot\text{L}^{-1}$ in 2018 and $483\,\mu\text{mol}\cdot\text{L}^{-1}$ in 2017. In comparison to NSHQ14, CH_4 at NSHQ04 is more ^{13}C- and D-enriched (mean weighted by sample year $\delta^{13}\text{C} = +3.3\,‰\,\text{VPDB}$, $s = 1.8\,‰$; $\delta\text{D} = -220\,‰\,\text{VSMOW}$, $s = 11\,‰$; $n = 4$; Table 3.4; Figure 2.3a). Fluids sampled from NSHQ04 are in $CH_4 - H_2O$ H isotopic disequilibrium and intra-CH_4 disequilibrium (Figure 2.3b and d), which is also true of fluids from NSHQ14. However, CH_4 sampled from NSHQ04 has distinctly negative $\Delta^{12}CH_2D_2$ ($-24.502\,‰$) and low $\Delta^{13}CH_3D$ (mean weighted by sample year of $0.36\,‰$, $s = 0.32\,‰$, $n = 3$; Table 3.4). As such, CH_4 from NSHQ04 plots squarely among methanogen culture samples in $\Delta^{13}CH_3D/\Delta^{12}CH_2D_2$ space (Figure 2.3d), suggesting that CH_4 is dominantly microbial at NSHQ04. Moreover, alkane gases dissolved in waters pumped from NSHQ04 exhibited a $C_1/(C_2 + C_3)$ ratio of $5.4 \cdot 10^3$ in 2018, which is higher than other wells in this study (Table 4.2; Figure 2.3c), further supporting a major component of microbial CH_4 at NSHQ04.

Microbial CH_4 production at NSHQ04 is also indicated by microbiological data. 16S

rRNA gene sequences affiliated with *Methanobacterium* have been detected in DNA extracted from biomass filtered from waters pumped from NSHQ04, albeit in low relative abundance ($< 1\,\%$ of reads in 2018; Figure 2.5; also detected in $< 1\,\%$ of reads in 2014, but not detected in 2015 and 2017; Rempfert et al., 2017; Miller et al., 2016; Kraus et al., 2018). The apparent low relative abundance of *Methanobacterium* at NSHQ04 could have resulted from the relatively shallow depth from which samples were collected at NSHQ04 due to well obstruction and the consequential sampling of groundwaters that may have experienced atmospheric O_2 infiltration. High relative read abundances of sequences affiliated with aerobes and transient H_2 across years of sampling NSHQ04 suggest that zones of the aquifer that are not always anoxic were accessed. These conditions may restrict methanogen abundance to greater depths than were sampled, but not constrain the upward diffusion of the product of their metabolism, CH_4. Nevertheless, fluids obtained from NSHQ04 have yielded robust cultures of *Methanobacterium*. These cultures have been shown to produce CH_4 with suppressed C isotope fractionation when provided H_2 and $CaCO_3$ (s) at alkaline conditions (Miller et al., 2018). Carbonate minerals could therefore be an important C source for methanogens in subsurface fluids near NSHQ04. Miller et al. (2016) analyzed the isotopic composition of one carbonate mineral sample from NSHQ04 drill cuttings, which yielded a $\delta^{13}C$ value of $-1.48\,‰$ VPDB. This places an upper estimate on the $\delta^{13}C$ of CH_4 that could be produced from carbonate mineral substrates in the subsurface near NSHQ04. Since this is lower than the measured $\delta^{13}C$ of CH_4 at NSHQ04 (Table 3.4), a secondary mechanism, such as methanotrophy, could have further enriched this CH_4 in ^{13}C. High relative abundances of 16S rRNA gene reads of DNA extracted from biomass in waters sampled from NSHQ04 were related to an aerobic methanotroph of the genus *Methylococcus* ($8\,\%$ of reads in 2018; inter-annual mean of $11\,\%$; Figure 2.5; Miller et al., 2016; Rempfert et al., 2017; Kraus et al., 2018). Greater aerobic methanotrophy at NSHQ04 relative to NSHQ14 may have contributed in part to the lower $\Delta^{13}CH_3D$ and $\Delta^{12}CH_2D_2$ and higher $\delta^{13}C$ and δD of CH_4 sampled from NSHQ04.

Methanotrophic activity at NSHQ04 is consistent with the observed ^{13}C-depletion in $\sum CO_2$ at NSHQ04 (-29.7 ‰ VPDB δ^{13}C; Table 3.4) relative to the other studied wells because environments of active methanotrophy often have ^{13}C-depleted $\sum CO_2$ (Barker and Fritz, 1981; Michaelis et al., 2002). Indeed, $\delta^{13}C_{\sum CO_2}$ at NSHQ04 is compatible with aerobic oxidation of CH_4 of ~ 0 ‰ VPDB δ^{13}C (Barker and Fritz, 1981; Feisthauer et al., 2011). Alternatively, ^{13}C-depletion in $\sum CO_2$ could be explained by kinetic isotope fractionation during hydroxylation of atmospheric CO_2 upon contact with $Ca^{2+} - OH^-$ water, which has been interpreted as the cause of δ^{13}C as low as -27.21 ‰ VPDB in Ca-rich carbonates from hyperalkaline seeps in the Samail Ophiolite (Clark et al., 1992; Kelemen et al., 2011; Falk et al., 2016). The similarity in δ^{13}C of travertines from Samail Ophiolite hyperalkaline seeps and $\sum CO_2$ in waters pumped from NSHQ04 could reflect a shared mechanism of CO_2 uptake. Considering the relatively shallow sampling depth at NSHQ04 in 2018 (Table 4.4), it is plausible that the sampled groundwaters continuously interact with atmospheric CO_2. Although the relative influences of methanotrophy and atmospheric CO_2 hydroxylation cannot be determined based on the available data, both processes could affect $\delta^{13}C_{\sum CO_2}$ at NSHQ04.

In summary, low $\Delta^{13}CH_3D$ and $\Delta^{12}CH_2D_2$, high $C_1/(C_2 + C_3)$, the presence of *Methanobacterium* that were readily cultured, and high 16S rRNA gene relative abundances of *Methylococcus* lead us to conclude that microbial production and consumption of CH_4 are the dominant factors controlling CH_4 concentration and isotopic composition at NSHQ04.

2.3.2.3 H_2-limited microbial methanogenesis with classic C isotope effect expressed at well WAB188

WAB188 is situated 2 km down-gradient from NSHQ04 and is set in gabbro on the opposite side of a fault from NSHQ04 (Figure 2.1; Figure A.1; Table 4.4). Fluids pumped from WAB188 have had variable pH (8.72 to 5.75) and oxidation-reduction potential (f_{O_2} of 10^{-61} bar to 10^{-34} bar and Eh of -220 mV to $+214$ mV) across four years of sampling (Table

4.4; Rempfert et al., 2017; Fones et al., 2019). WAB188 has consistently had major ion composition similar to the gabbro-hosted well WAB103, except that WAB188 has had higher $c_{\sum \mathrm{Ca}}$ (Table 4.1; Rempfert et al., 2017; Fones et al., 2019). H_2 has occasionally been detected in fluids pumped from WAB188 ($c_{H_2} = 0.992\,\mu\mathrm{mol} \cdot \mathrm{L}^{-1}$ in 2017), and CH_4 has consistently been detected at moderate concentrations ($c_{CH_4} = 1.83\,\mu\mathrm{mol}{\cdot}\mathrm{L}^{-1}$ in 2017 and $0.917\,\mu\mathrm{mol}{\cdot}\mathrm{L}^{-1}$ in 2018) (Table 4.2; Rempfert et al., 2017; Fones et al., 2019). The high $c_{\sum \mathrm{Ca}}$ and moderate but variable pH, *Eh*, and c_{H_2} in fluids sampled from WAB188 suggest that fluid chemical composition at WAB188 is dominantly controlled by water-rock reaction with gabbro, but may also be affected by inputs of fresh rainwater and/or H_2-bearing $Ca^{2+} - OH^-$ water flowing from the peridotite aquifer into the gabbro aquifer across a fault at depth. Flows of water from higher-head, lower-permeability peridotite aquifers into gabbro aquifers in the Samail Ophiolite has been proposed on the basis of physical hydrologic data (Dewandel et al., 2005). Instead or in addition, serpentinization of olivine and pyroxene entirely within gabbro might have produced some of the H_2 observed in water samples from WAB188.

Microbial methanogenesis at WAB188 is indicated by high relative abundances of 16S rRNA gene reads affiliated with methanogens in pumped groundwaters. Sequences affiliated with *Methanobacterium* accounted for 3 % of 16S rRNA gene reads of DNA extracted from subsurface fluids sampled from WAB188 in 2018, which was second only to NSHQ14 among our sampling sites, and consistent with prior years of sampling at WAB188 (mean 2015 to 2018 of 4 %; Figure 2.5; Rempfert et al., 2017; Kraus et al., 2018). Further, 2 % of 16S rRNA gene reads from WAB188 were affiliated with *Methylococcus* in 2018, which was second only to NSHQ04 among our sampling sites, and consistent with prior years of sampling (Figure 2.5; Rempfert et al., 2017; Kraus et al., 2018). In addition, 16S rRNA gene sequences affiliated with genus *Candidatus* Methylomirabilis, which includes species that mediate anaerobic methane oxidation coupled to nitrite reduction (Ettwig et al., 2010; Luesken et al., 2012; Welte et al., 2016), were detected in samples from WAB188 in 2018 albeit at low relative gene abundance ($< 1\,\%$). As a whole, the 16S rRNA gene sequencing data from WAB188

fluids are consistent with microbial production of CH_4 and, secondarily, methanotrophy using O_2 and/or NO_2^- .

While subsurface fluids sampled at WAB188, NSHQ14, and NSHQ04 all bear microbiological and isotopic evidence of methanogenic activity, the conditions under which methanogenesis proceeds at WAB188 are fundamentally distinct. In contrast to the $Ca^{2+}-OH^-$ fluids from NSHQ14 and NSHQ04, the circumneutral fluids from WAB188 have $\sim 10^2$ to $\sim 10^3$ times higher $c_{\sum CO_2}$ (inter-annual mean of 2910 μmol $\cdot$ L^{-1}, $s = 620\,\mu$mol $\cdot$ L^{-1}, $n = 3$; Table 4.1) and ~ 75 ‰ lower $\delta^{13}C_{CH_4}$ (inter-annual mean $\delta^{13}C = -73$ ‰ VPDB, $s = 13$ ‰, $n = 3$; Table 3.4). Since WAB188 fluids contain relatively ^{13}C-depleted CH_4 that is not associated with substantial concentrations of $C_2 - C_6$ alkanes (Table 4.2), a standard interpretation (Bernard et al., 1977; Milkov and Etiope, 2018) would be that the source of CH_4 at WAB188 is dominantly microbial. Such an interpretation is largely predicated on data from sedimentary settings, where H_2 is typically more scarce than CO_2. H_2 may be the limiting substrate for methanogenesis at WAB188, as indicated by transient H_2 at moderate concentrations co-occurring with abundant $\sum CO_2$. These conditions contrast starkly with those that prevail in $Ca^{2+} - OH^-$ fluids, where C substrates for methanogenesis are more scarce than H_2. Indeed, the apparent α_{CO_2/CH_4} at WAB188 (based on measured $\delta^{13}C_{\sum CO_2}$ of -13.52 ‰ VPDB; Table 4.1) is compatible with that of CH_4 produced by *Methanobacterium* cultures provided limiting H_2 and excess HCO_3^- (aq), which was greater than the α_{CO_2/CH_4} observed for parallel cultures under CO_2-poor conditions (Miller et al., 2018). Therefore, the inverse relationship between $c_{\sum CO_2}$ and $\delta^{13}C_{CH_4}$ across fluids from wells WAB188, NSHQ14, and NSHQ04 is consistent with an effect of CO_2 availability on α_{CO_2/CH_4} of microbial methanogenesis.

2.4 Conclusions

Through integration of isotopic, microbiological, and hydrogeochemical data, we conclude that substantial microbial CH_4 is produced under varying degrees of C or H_2 limitation in

subsurface waters of the Samail Ophiolite and mixes with abiotic CH_4 released from fluid inclusions. Across subsurface fluids ranging in pH from circumneutral to 11.39, microbial CH_4 production is evidenced by 16S rRNA gene sequencing and other microbiological data indicating that methanogens are widespread and active in groundwaters in the ophiolite. We propose that CH_4 produced by these microbes constitutes a substantial portion of the total CH_4 pool, which is consistent with our finding of $^{13}CH_3D$ and $^{12}CH_2D_2$ relative abundances significantly less than equilibrium. An abiotic, fluid inclusion-derived source of CH_4, C_2H_6, and C_3H_8 is inferred from the widespread occurrence of CH_4 in fluid inclusions in peridotites, including those in Oman, and is supported by the relatively ^{13}C-enriched C_2H_6 and C_3H_8 measured in gases exsolved from peridotite-hosted groundwaters in this study. In contrast, abiotic, low-temperature reduction of CO_2 to CH_4 is less likely to contribute substantially to the CH_4 pool in the study area due to an apparent scarcity of conditions favorable to catalysis: access of gas-phase H_2 and CO_2/CO to Ru-bearing chromites. The 16S rRNA gene sequencing data also indicate the presence of microbes capable of CH_4 oxidation, particularly using O_2 as an oxidant, but this oxidation is apparently not extensive enough to obscure the underlying CH_4 sources. In addition, we note an inverse relationship between $c_{\sum CO_2}$ and $\delta^{13}C_{CH_4}$ across groundwaters bearing microbiological evidence of methanogenic activity. This finding supports the hypothesis that C isotope fractionation between the C substrate used by methanogens and the CH_4 they produce is suppressed when the C substrate is limiting. Thus, our finding that $\delta^{13}C_{CH_4}$ varies by 90 ‰ in the Samail Ophiolite suggests that, in some settings, $\delta^{13}C_{CH_4}$ may be a powerful indicator of transitions from H_2-limited to C-limited conditions for microbial methanogenesis, rather than a discriminant between microbial versus abiotic CH_4.

This study supports the premise that H_2 produced from water/rock reaction can fuel microbial life, even under challenging conditions of high pH and low oxidant availability. By identifying where and how microbial methanogenesis can reasonably be expected to occur in H_2-rich, subsurface environments, this work complements theoretical models in guiding

the search for rock-hosted life, including extraterrestrial life. For example, our findings substantiate predictions that microbial methanogenesis could occur in the reduced, alkaline ocean of Saturn's moon, Enceladus (McKay et al., 2008; Glein et al., 2015; Waite et al., 2017), and that methanogens may use H_2 and carbonate minerals in the Martian subsurface (Kral et al., 2014).

2.5 Acknowledgements

This research was directly supported by the Rock-Powered Life NASA Astrobiology Institute (NNA15BB02A). This research also used samples and/or data provided by the Oman Drilling Project. The Oman Drilling Project (OmanDP) has been possible through co-mingled funds from the International Continental Scientific Drilling Project (ICDP), the Sloan Foundation – Deep Carbon Observatory (Grant 2014-3-01, Kelemen PI), the National Science Foundation (NSF-EAR-1516300, Kelemen PI), the NASA Astrobiology Institute (NNA15BB02A), the German Research Foundation (DFG), the Japanese Society for the Promotion of Science (JSPS), the European Research Council, the Swiss National Science Foundation, JAMSTEC, the TAMU-JR Science operator, and contributions from the Sultanate of Oman Ministry of Regional Municipalities and Water Resources, the Oman Public Authority of Mining, Sultan Qaboos University, CRNS-Univ. Montpellier II, Columbia University, and the University of Southampton. Work at LBNL was supported by the U.S. Department of Energy, Office of Science, Office of Basic Energy Sciences, Chemical Sciences, Geosciences, and Biosciences Division, under Award Number DE-AC02-05CH11231.

We thank the Ministry of Regional Municipalities and Water Resources in the Sultanate of Oman (particularly Said Al Habsi, Rashid Al Abri, Salim Al Khanbashi, and Haider Ahmed Mohammed Alajmi) for allowing access to wells and logistical support, Zaher Al Sulaimani and Mazin Al Sulaimani from the Oman Water Centre and AZD Engineering for their technical and logistical support, Jude Coggon for coordinating Oman Drilling Project

activities, Benoît Ildefonse for sharing geologic map data, Eric Ellison and Kaitlin Rempfert for their assistance in the field and laboratory, Elizabeth Fones for sharing biomass samples, Emily Kraus for critical discussion of Oman CH_4 cycle processes, and Noah Fierer, Jen Reeves, Corinne Walsh, Matthew Gebert, and Angela Oliverio for assisting with DNA sequencing and interpretation.

Data (in Excel format) and source code (in R Markdown format) used to produce the figures, data tables and analyses for this paper (as well as additional data on analytical uncertainties and trace element concentrations) are available online at `https://github.com/danote/Oman_CH4_stable_isotopes`. Additional DNA sequence data processing codes are available at `https://github.com/danote/Samail_16S_compilation`. The sequences are accessible on the NCBI Short Read Archive under accession PRJNA655565.

Chapter 3

Active conversion of atmospheric CO_2 to CH_4 in serpentinites of the Samail ophiolite, Oman

Daniel B. Nothaft, Alexis S. Templeton, Peter Kelemen, Eric S. Boyd, Juerg M. Matter, and The Oman Drilling Project Science Team

Abstract

Methane (CH_4) is often the most abundant form of C in high pH fluids that are generated during the hydration of ultramafic rocks, a process known as "serpentinization". Although it is often assumed that this methane is produced from the reduction of CO_2, the processes and timescales required for CH_4 formation are uncertain within serpentinite aquifers at near-surface temperatures. By accessing subsurface fluids in the Samail Ophiolite in Oman, we show that some CH_4 had ^{14}C contents up to 0.304 fraction modern. This is the first definitive indication of active (within the last 10 kyr) conversion of atmospheric CO_2 to CH_4 in a serpentinizing setting. Detailed investigation of the fluid geochemistry, hydrocarbon gases, microbiology and the ^{14}C content of carbonate minerals present in the serpentinites demonstrate that atmospheric CO_2 infiltrates into the subsurface, and methanogens inhabiting zones where H_2-rich fluids mix with fluids bearing C recently derived from air produce the ^{14}C-rich CH_4. This "young" microbial CH_4 is added to the pre-existing pool of isotopically-heavy hydrocarbon gases that are probably abiotic in origin. These results demonstrate the activity of H_2-based subsurface ecosystems, even at pH $>$ 11 and advances understanding of how subaerial peridotite exposures exchange greenhouse gases such as CO_2 and CH_4 with the atmosphere.

3.1 Introduction

At temperatures and pressures near the Earth's surface ($< 400\,^{\circ}C$, < 100 MPa), ultramafic rocks such as peridotite in contact with water are thermodynamically driven to hydrate and oxidize, forming variable amounts of serpentine, magnetite, brucite, hydrogen (H_2), and other phases (Evans, 1977; Frost, 1985; McCollom and Bach, 2009; Klein and Bach, 2009; Klein et al., 2009, 2019). This process, often called "serpentinization", can produce H_2 at temperatures at least as low as $55\,^{\circ}C$ (Miller et al., 2017b). The resultant H_2 can be thermodynamically favored to reduce carbon dioxide (CO_2) to methane (CH_4) (Shock, 1992).

In continental settings undergoing serpentinization, where fluid-rock reactions typically occur at low temperatures ($< 150\,^{\circ}C$), there is disagreement regarding the origin of CH_4. Three key potential CH_4 sources have been identified in these environments. One potential source is the abiotic reduction of CO_2 to CH_4 at warmer-than-present temperatures in fluid inclusions within crystals that can store CH_4 and subsequently release it (Kelley, 1996; Kelley and Früh-Green, 1999; McDermott et al., 2015; Wang et al., 2018). Another potential source is the abiotic, mineral-catalyzed reduction of CO_2 to CH_4 at the low temperatures that prevail in the present-day weathering environment (Etiope and Ionescu, 2015; Etiope et al., 2018). A third potential source is microbial methanogenesis (Wang et al., 2015; Miller et al., 2016, 2018; Fones et al., 2019; Zwicker et al., 2018).

An important characteristic of CH_4 in serpentinizing settings is its lack of ^{14}C activity significantly above analytical blanks (i.e. it is "radiocarbon-dead"). This has been documented in 5 total analyses from ophiolites in Spain, Turkey, Italy, and the Philippines (Abrajano et al., 1990; Etiope and Schoell, 2014; Etiope et al., 2016; Etiope and Whiticar, 2019) and in 6 analyses from the Lost City Hydrothermal Vent Field at the Mid-Atlantic Ridge (Proskurowski et al., 2008). This has contributed in part to the hypothesis that CH_4 in ophiolites forms from CO_2 sources that are "fossil" (not derived from the atmosphere within the last 50 kyr) such as mantle-derived CO_2 or limestones in contact with ophiolites (Etiope and Ionescu, 2015; Etiope and Whiticar, 2019).

In the Samail Ophiolite of Oman, a site of active, low-temperature serpentinization and carbonation, microbiological evidence points to active microbial methanogenesis (Miller et al., 2016; Rempfert et al., 2017; Nothaft et al., 2020; Kraus et al., in press; Fones et al., in press). In this study, we sought to answer whether the microbial contribution is rapid and quantitively important. Further, we asked whether the C source of CH_4 was fossil, or present-day atmospheric CO_2. If this site of abiotic H_2 production shows vigorous microbial transformation of CO_2, it would have far-reaching implications for subsurface habitability in the Solar System. The Samail Ophiolite is also notable for its well-documented rapid con-

version of atmospheric CO_2 to carbonate minerals, which has been particularly motivated by the the prospect of *in situ* mineral carbonation as a climate change mitigation technique (Clark and Fontes, 1990; Kelemen and Matter, 2008; Kelemen et al., 2011; Mervine et al., 2014). What may be the implications for this promising technology if CH_4, a potent greenhouse, is actively produced from atmospheric CO_2 in the subsurface and is then emitted to the atmosphere?

3.2 Results

3.2.1 ^{14}C content of CH_4

To assess timescales of CH_4 formation in the Samail Ophiolite, we analyzed the ^{14}C contents of CH_4 exsolved from groundwater samples pumped from wells previously drilled into the ophiolite. Our $^{14}CH_4$ data set (Table 3.1) consists of nine analyses including samples from four wells collected over the course of three sampling campaigns: February 2017, February 2018, and January 2019. Two wells had ^{14}C content in CH_4 that was significantly above analytical blanks. The CH_4 extracted from groundwaters sampled at well NSHQ14 had 0.192 fraction modern ($F^{14}C$) in a sample obtained in 2017, 0.304 $F^{14}C$ in a sample obtained in 2018, and 0.06 ± 0.01 ($1\,s$) $F^{14}C$ in three field replicate samples obtained in 2019. The CH_4 extracted from groundwaters sampled at well NSHQ04 had $F^{14}C$ of 0.007. Two other wells, CM2A and WAB71, yielded CH_4 samples with ^{14}C contents that were indistinguishable from analytical blanks, indicating that the CH_4 sampled from these sites was produced from one or more radiocarbon-dead C source(s), was produced > 50 ka, or both. Our measurement of radiocarbon-dead samples in the same analytical sessions in which we measured the radiocarbon-live samples is also important in that it demonstrates that there was not systematic ^{14}C contamination introduced by our sample preparation methods.

Table 3.1: Radiocarbon measurements.

Well	Year sampled	Depth sampled / [m]	Sample type	Accession #[a]	δ^{13}C / [‰ VPDB][b]	Fraction modern ($F^{14}C$)[c]	Conventional ^{14}C age / [yr BP][c]
NSHQ14	2019	84	CH_4	OS-152137	n.d.	$0.0614 \pm 0.001\,40$	$22\,400 \pm 180$
NSHQ14	2019	84	CH_4	CURL-26148	0.5	0.0566 ± 0.0006	$23\,070 \pm 90$
NSHQ14[d]	2019	84	CH_4	CURL-26147	2.5	0.0497 ± 0.0006	$24\,110 \pm 100$
NSHQ14	2018	84	CH_4	CURL-24538	−3.2	0.3038 ± 0.0015	9570 ± 45
NSHQ14	2017	84	CH_4	CURL-24539	1.1	0.1918 ± 0.0010	$13\,265 \pm 45$
WAB71	2019	79	CH_4	CURL-26149	3.2	-0.0001 ± 0.005	$> 42\,600$
WAB71	2018	69	CH_4	CURL-24537	3.0	-0.002 ± 0.0000	$> 42\,200$
NSHQ04	2018	7	CH_4	CURL-24535	−0.7	0.0069 ± 0.0010	$39\,950 \pm 1210$
CM2A	2018	74	CH_4	CURL-24536	−7.0	0.0002 ± 0.0011	$> 48\,100$
BA3A	2018	4.4	dolomite/calcite	OS-146309	−8.6	$0.078\,20 \pm 0.001\,00$	$20\,500 \pm 100$
BA3A	2018	5.2	dolomite	OS-146310	−7.7	$0.056\,80 \pm 0.001\,00$	$23\,000 \pm 140$
BA3A	2018	7.4	calcite	OS-146311	−15.0	$0.011\,00 \pm 0.001\,00$	$36\,200 \pm 740$
BA3A	2018	5.7	calcite	OS-147575	−9.7	$0.041\,40 \pm 0.001\,00$	$25\,600 \pm 190$
BA3A	2018	5.7	calcite	OS-147525	−9.6	$0.015\,70 \pm 0.000\,90$	$33\,400 \pm 470$
BA3A	2018	8.2	dolomite	OS-147526	−12.9	$0.003\,70 \pm 0.000\,90$	$45\,000 \pm 1900$

n.d. = not determined.
Depths referenced to ground level.
[a]"CURL" samples analyzed at UCI. "OS" samples analyzed at NOSAMS.
[b]For CH_4 samples, the reported δ^{13}C value is the AMS measurement, which can be fractionated from the original sample material (often by 1 ‰ to 3 ‰) due to the graphitization process. For carbonate mineral samples, the reported δ^{13}C value was measured by GC-IRMS of a CO_2 split, and has an uncertainty of 0.1 ‰.
[c]Following refs. Stuiver and Polach, 1977 and Reimer et al., 2004.
[d]Well not purged (NP) prior to sampling.

As detailed in Materials and Methods, two laboratories independently prepared hydrocarbon gas samples and sent them for analysis at two different AMS laboratories for replicate samples from NSQH14 obtained and analyzed in 2019. The general agreement between these replicates ($0.0614 \pm 0.001\,40$ and 0.0566 ± 0.0006 $F^{14}C$; Table 3.1) validates our analytical methods and highlights their reproducibility.

The geochemical and microbiological context of hyperalkaline well NSHQ14 is of great interest since it hosts CH_4 with the highest $F^{14}C$ of the studied wells. Some discussion of well WAB71 is also provided for comparison because the fluids sampled from WAB71 are also hyperalkaline, but have CH_4 that is radiocarbon-dead. Although our sample set spans three years, we focus our presentation of supporting geochemical and geomicrobiological data here on samples obtained in 2019 because the supporting data for samples obtained

in 2017 and 2018 have been presented elsewhere (Fones et al., 2019; Nothaft et al., 2020) and are generally consistent with our observations from samples obtained in 2019. Aqueous geochemical data for all years of Samail Ophiolite well sampling performed by the authors and collaborators is accessible at `https://github.com/danote/Oman-14CH4`.

3.2.2 Chemical composition of subsurface fluids

Groundwaters sampled from the wells had δD and δ^{18}O values that were within 4 ‰ and 1 ‰ of VSMOW, respectively, and plotted near local and global meteoric water lines (Weyhenmeyer et al., 2002; Terzer et al., 2013), which is consistent with a rainwater source and their low-latitude (23 °N), low-elevation (600 m), and coastal (within 45 km of coast) location (Section B.1; Matter et al., 2006; Miller et al., 2016; Vankeuren et al., 2019; Nothaft et al., 2020). Groundwater temperatures were 34.5 °C to 37.1 °C (Table 3.2), which is within 10 °C of the mean annual air temperature of $\sim$ 28 °C in the region (Dewandel et al., 2005), suggesting that the groundwaters flow through the local weathering horizon, and are not related to any potential distant hydrothermal sources.

Table 3.2: Chemical compositions of water samples. Concentrations reported in $\mu\text{mol} \cdot \text{L}^{-1}$.

Well	Depth to water / [m]	Pump depth / [m]	Conductivity / [$\text{mS} \cdot \text{cm}^{-1}$]	Temperature / [°C]	pH	Eh / [mV]	$\sum$Na	$\sum$Ca	SO_4^{2-}	Cl^-
NSHQ14	8.36	84	2.43	37.1	11.07	-290.3	$8.92 \cdot 10^3$	$4.02 \cdot 10^3$	$4.73 \cdot 10^1$	$1.45 \cdot 10^4$
NSHQ14[a]	8.39	84	2.84	36.7	11.20	-479.7	$1.08 \cdot 10^4$	$4.09 \cdot 10^3$	5.09	$1.62 \cdot 10^4$
WAB71	7.30	79	2.08	34.5	11.09	-339.4	$5.61 \cdot 10^3$	$3.82 \cdot 10^3$	$5.10 \cdot 10^1$	$1.26 \cdot 10^4$

Depths referenced to ground level.
[a]Well not purged (NP) prior to sampling.

Groundwaters were reduced (Eh of -290.3 mV to -339.4 mV) and hyperalkaline (pH 11.07 to 11.20) $Ca^{2+} - OH^-$ waters (Table 3.2), typical of extensive hydration and oxidation of peridotite in closed-system conditions with respect to the atmosphere (Barnes et al., 1967; Barnes and O'Neil, 1969; Neal and Stanger, 1985; Bruni et al., 2002; Cipolli et al., 2004; Kelemen et al., 2011; Paukert et al., 2012). Conductivities ranged from 2.08 $\text{mS} \cdot \text{cm}^{-1}$

to $2.84\,\mathrm{mS \cdot cm^{-1}}$, which are higher than other groundwaters of lower pH and shorter residence times in the ophiolite (Rempfert et al., 2017; Nothaft et al., 2020; Vankeuren et al., 2019). The increase in conductivity is driven by enrichments in Ca^{2+} derived from dissolution of primary silicate minerals in addition to Na^{+} and Cl^{-} derived from mineral dissolution, sea spray, and/or leaching of sea salts introduced during subseafloor alteration and/or ophiolite emplacement (Neal and Stanger, 1985; Stanger, 1986; Murad and Krishnamurthy, 2004; Paukert et al., 2012; Rempfert et al., 2017). Concentrations (c) of SO_4^{2-} ranged from $5.09\,\mu\mathrm{mol \cdot L^{-1}}$ to $51.0\,\mu\mathrm{mol \cdot L^{-1}}$ (Table 3.2), which is lower than groundwaters in more oxidized sections of the aquifer, which generally range from $300\,\mu\mathrm{mol \cdot L^{-1}}$ to $1000\,\mu\mathrm{mol \cdot L^{-1}}$ (Rempfert et al., 2017; Nothaft et al., 2020), suggesting that microbial SO_4^{2-} reduction may occur or may have occurred in groundwaters sampled at NSHQ14 and WAB71.

Concentrations of dissolved inorganic C ($\sum CO_2$) in groundwaters sampled at NSHQ14 and WAB71 were below the limit of quantitation in 2019 ($< 282\,\mu\mathrm{mol \cdot L^{-1}}$) and also below the lower limit of quantitation of $12\,\mu\mathrm{mol \cdot L^{-1}}$ in measurements performed in 2018 with slightly different sample preparation methods (Nothaft et al., 2020). These data are consistent with water-harzburgite reaction path modeling that terminates at chrysotile-brucite-diopside-calcite equilibrium, corresponding to a $c_{\sum CO_2}$ of $8\,\mu\mathrm{mol \cdot L^{-1}}$ at $25\,^{\circ}\mathrm{C}$ and 1 bar (Leong and Shock, 2020). These data highlight the extremely low $c_{\sum CO_2}$ in $Ca^{2+} - OH^{-}$ waters, which could result in autotrophic metabolisms such as hydrogenotrophic methanogenesis being limited by C availability in these waters.

Two different pumping methods were used to sample fluids from NSHQ14 in order to test the effect of pumping methods on fluid chemistry. As detailed in Materials and Methods, we first purged the well through extensive pumping and then sampled, as is our normal practice; 8 days later, we returned to the well and sampled it immediately upon turning on the pump. Compared to the purged sample of NSHQ14, the subsequent, non-purged sample of NSHQ14 was more alkaline by 0.13 pH units, had marginally higher concentrations of major ions, and had lower Eh by 189.4 mV (Table 3.2). These data suggest that the non-purged sample of

NSHQ14 may have have been more similar to a classic $Ca^{2+} - OH^-$ endmember fluid than the purged sample.

This hypothesis is further supported by the non-purged sample of NSHQ14 having higher concentrations of H_2, CH_4, and alkanes of 2 to 6 C atoms ("$C_2 - C_6$ alkanes") than the purged sample by a factor of ~ 2 (Table 3.3). Nonetheless, both samples of NSHQ14 had high concentrations of these gases ($245\,\mu mol \cdot L^{-1}$ to $467\,\mu mol \cdot L^{-1}$ H_2, $73.1\,\mu mol \cdot L^{-1}$ to $128\,\mu mol \cdot L^{-1}$ CH_4, and from below limits of quantitation to $0.291\,\mu mol \cdot L^{-1}$ $C_2 - C_6$ alkanes) and similar relative concentrations of these gases. This suggests that, although these gases may have been diluted in the purged sample relative to the non-purged sample, the underlying source of the gas is the same between samples. In addition, the gas compositions of both samples of NSHQ14 were markedly different than those of WAB71, for which H_2 was below the limit of quantitation ($< 3.29\,\mu mol \cdot L^{-1}$), most $C_2 - C_6$ alkanes were below limits of quantitation, and CH_4 (at $25.4\,\mu mol \cdot L^{-1}$) was ~ 4 times lower than samples from NSHQ14 (Table 3.3). CO was below the limit of quantitation ($< 2.05 \cdot 10^{-2}\,\mu mol \cdot L^{-1}$) in all sampled groundwaters, indicating that CO is not produced in high abundance, or that it is readily consumed by biotic or abiotic processes.

Table 3.3: Aqueous gas concentrations, reported in $\mu mol \cdot L^{-1}$.

Well	H_2	CH_4	C_2H_6	C_3H_8	i-C_4H_{10}	n-C_4H_{10}	i-C_5H_{12}	n-C_5H_{12}	C_6H_{14}
NSHQ14	$2.45 \cdot 10^2$	$7.31 \cdot 10^1$	$1.08 \cdot 10^{-1}$	$1.27 \cdot 10^{-2}$	$< 4.13 \cdot 10^{-3}$	$< 5.45 \cdot 10^{-3}$	$< 3.27 \cdot 10^{-3}$	$4.04 \cdot 10^{-3}$	$7.17 \cdot 10^{-3}$
NSHQ14[a]	$4.67 \cdot 10^2$	$1.28 \cdot 10^2$	$2.91 \cdot 10^{-1}$	$3.11 \cdot 10^{-2}$	$< 4.13 \cdot 10^{-3}$	$< 5.45 \cdot 10^{-3}$	$< 3.27 \cdot 10^{-3}$	$< 3.63 \cdot 10^{-3}$	$8.34 \cdot 10^{-3}$
WAB71	< 3.29	$2.54 \cdot 10^1$	$< 8.63 \cdot 10^{-3}$	$< 6.81 \cdot 10^{-3}$	$< 4.13 \cdot 10^{-3}$	$< 5.45 \cdot 10^{-3}$	$< 3.27 \cdot 10^{-3}$	$< 3.63 \cdot 10^{-3}$	$7.13 \cdot 10^{-3}$

[a]Well not purged (NP) prior to sampling.

In addition to chemical analyses of subsurface fluids sampled by pumping, chemical properties were logged *in situ* along depth profiles in wells NSHQ14 and BA3A (Matter et al., 2018). Well BA3A is located 10 m from NSHQ14 (Figure B.1). NSHQ14 was drilled in 2004 to 2005 (Parsons International & Co., 2005), then BA3A was drilled in January 2018 (Kelemen et al., 2020a). The geochemical profiles shown in Figure 4.3 were logged in March 2018. In the well temperature profiles (Figure 4.3A), regressing temperature (T) upon depth (d) over

the depth range of 100 m to 300 m yielded a line of the equation $T/[°C] = 34\,°C - 0.25d/[m]$ ($R^2 = 1.00$, $p < 0.001$). This represents a geothermal gradient of $25\,°C\,km^{-1}$, which is typical of near-surface, continental settings (Lowell et al., 2014), again indicating that these waters derive from groundwater circulation through the local weathering horizon as opposed to a water source exogenous to the ophiolite or contact with an anomalous heat source. At depths less than 100 m, temperatures deviated slightly (within 2 °C) from this linear trend towards warmer values, which may reflect seasonal or diurnal surface temperature variations. From 10 m to 30 m depth in NSHQ14, pH increased from 10.36 to 11.26, while Eh decreased from 142 mV to −582 mV, and conductivity increased from $1.59\,mS{\cdot}cm^{-1}$ to $3.52\,mS{\cdot}cm^{-1}$ (Figure 4.3B-D). These trends suggest that, within the upper 20 m of the water column, shallowly-sourced, relatively dilute, atmosphere-influenced fluids of presumably shorter residence time mix with deeply-sourced, hyperalkaline and reduced fluids with higher ionic strength that have extensively reacted with peridotite in isolation from the atmosphere. The aqueous geochemical trends found in NSHQ14 were generally similar in BA3A, although BA3A waters were 0.43 pH units less alkaline and $2.12\,mS \cdot cm^{-1}$ less conductive (Figure 4.3A-D). This suggests that the general conditions of high pH and low Eh are laterally extensive in the aquifer surrounding NSHQ14, although there are some spatial heterogeneities in lithology and/or extents of water-rock reaction that affect groundwater chemical composition. While hyperalkaline, reduced, and high-conductivity conditions persisted from 30 m to the bottom of both wells, these parameters varied somewhat with depth. For instance, conductivity, which was nearly constant from 30 m to 170 m depth, increased by $\sim 1\,mS \cdot cm^{-1}$ at 175 m depth in NSHQ14 and 200 m depth in BA3A (Figure 4.3D). The interval with increased conductivity also had decreased Eh in NSHQ14, and to a greater extent, in BA3A (Figure 4.3D; Figure B.2). Within this interval, the stability limit of water with respect to H_2 was closely approached in NSHQ14, and even more closely, in BA3A (Figure B.2). This suggests an influx at depth of highly reacted and extremely reduced fluids, where water may coexist with a separate H_2 (g) phase.

Comparing the geochemical profile of NSHQ14 to the pumped samples of subsurface fluids, the conductivity is $\sim 1\,\mathrm{mS \cdot cm^{-1}}$ higher and the Eh is $\sim 250\,\mathrm{mV}$ lower in the profile at a depth equivalent to the pump intake depth (Table 3.2; Figure 4.3C-D). The conductivity measurements on pumped fluids from the same depth of NSHQ14 were similar between 2019 and 2018 (when conductivity was $2665\,\mathrm{mS \cdot cm^{-1}}$) (Nothaft et al., 2020), bracketing the time when the geochemical profile was logged. These observations are consistent with the hypothesis that, during open well pumping, deeply-sourced, reduced, and high-conductivity fluids mix with more shallowly-sourced fluids that are more oxidized and lower-conductivity. This may also explain the trends previously discussed for the purged versus non-purged samples of NSHQ14, whereby purging larger volumes of water prior to sampling may result in sampling greater proportions of fluids that derive from a shallower section of the aquifer, where higher-transmissivity fractures may be more prevalent (Dewandel et al., 2005; Lods et al., 2020).

3.2.3 Stable isotope composition of CH_4, C_2H_6, and C_3H_8

The $\delta^{13}C$ of CH_4 from the purged sample of well NSHQ14 agreed within analytical uncertainty between GC-C-IRMS measurements performed at University of Colorado - Boulder (7.2 ‰ VPDB) and at Isotech (6.5 ‰ VPDB) (Table 3.4). CH_4 from the non-purged sample of NSHQ14 had somewhat lower $\delta^{13}C$ (4.5 ‰ VPDB). These $\delta^{13}C$ values are 30 ‰ to 100 ‰ higher than those of biogenic CH_4 found in sedimentary settings and 15 ‰ to 20 ‰ higher than is typical of CH_4 emanating from sediment-poor seafloor hydrothermal vents, where a dominantly abiotic origin has been proposed (Welhan and Craig, 1983; Merlivat et al., 1987; Charlou et al., 1996, 2000, 2002; Proskurowski et al., 2008; Kumagai et al., 2008; McDermott et al., 2015; Wang et al., 2018). CH_4 in continental sites of serpentinization generally has high but variable $\delta^{13}C$ values (Etiope and Whiticar, 2019), and the $\delta^{13}C$ of CH_4 at NSHQ14 is on the high end of values reported for similar settings, although even higher $\delta^{13}C_{CH_4}$ values (up to 7.9 ‰ VPDB) have previously been reported from the Samail Ophiolite (Vacquand

et al., 2018). The δD of CH_4 from NSHQ14 was -263 ‰ VSMOW for the purged sample and -251 ‰ VSMOW for the non-purged sample (Table 3.4). The δD of CH_4 from NSHQ14 is lower than that which would be expected if H isotopic equilibrium between CH_4 and water (Horibe and Craig, 1995) were attained at the measured groundwater temperatures.

Table 3.4: Isotopic compositions of CH_4, C_2H_6, and C_3H_8.

Well	$\delta^{13}C_{CH_4}$	δD_{CH_4}	$\delta^{13}C_{C_2H_6}$	$\delta^{13}C_{C_3H_8}$
NSHQ14	6.5[a], 7.2	-263	-5.5	4.9
NSHQ14[b]	4.5	-251	n.d.	n.d.
WAB71	7.0	-304	n.d.	n.d.

All isotopic values reported in ‰ units. δ^{13}C and δD reported in the VPDB and VSMOW reference frames, respectively. *Abbreviations:* n.d., not determined,
[a]Measured by Isotech.
[b]Well not purged (NP) prior to sampling.

For samples from NSHQ14, regressing $\delta^{13}C_{CH_4}$ upon $F^{14}C_{CH_4}$ yielded a line of the equation $\delta^{13}C_{CH_4}/[‰\,\text{VPDB}] = 7.9\,‰\,\text{VPDB} - 34.9F^{14}C_{CH_4}$ ($R^2 = 0.91$, $p = 0.01$), suggesting a strong, negative linear relationship between $\delta^{13}C_{CH_4}$ and $F^{14}C_{CH_4}$ (Figure 3.1). Regressing δD_{CH_4} upon $F^{14}C_{CH_4}$ yielded a line of the equation $\delta D_{CH_4}/[‰\,\text{VSMOW}] = -243\,‰\,\text{VSMOW} - 212F^{14}C_{CH_4}$ ($R^2 = 0.88$, $p = 0.06$), suggesting a potentially strong, negative linear relationship between δD_{CH_4} and $F^{14}C_{CH_4}$ (Figure 3.1), although the p-value indicates that the null hypothesis that δD_{CH_4} and $F^{14}C_{CH_4}$ are not correlated is not rejected at the traditional 5 % probability threshold. We note that one CH_4 sample for which $F^{14}C$ was measured had a δ^{13}C measurement but not a δD measurement, which resulted in the $\delta^{13}C_{CH_4}$ vs. $F^{14}C_{CH_4}$ regression having a sample size 5, while the δD_{CH_4} vs. $F^{14}C_{CH_4}$ regression had a sample size of only 4. This difference in sample size may have more to do with the differences in p-values between these two regressions than real differences in the strengths of correlations between $\delta^{13}C_{CH_4}$ vs. $F^{14}C_{CH_4}$ and δD_{CH_4} vs. $F^{14}C_{CH_4}$. Further insight into the relationship between $\delta^{13}C_{CH_4}$ and δD_{CH_4} can been gleaned from analysis of the larger data set of all samples of CH_4 from NSHQ14 taken from 2014 through 2019 for which both δ^{13}C and δD were measured ($n = 10$). In this data set, regressing δD_{CH_4} upon $\delta^{13}C_{CH_4}$ yields

a line of the equation $\delta D_{CH_4}/[‰\,\text{VSMOW}] = -278\,‰\,\text{VSMOW} - 5.14\delta^{13}C_{CH_4}/[‰\,\text{VPDB}]$ ($R^2 = 0.67$, $p = 0.004$) (Section 3.5.1, Figure B.3; Nothaft et al., 2020), suggesting a moderately strong, positive linear relationship between δD_{CH_4} and $\delta^{13}C_{CH_4}$. Thus, if $\delta^{13}C_{CH_4}$ has a negative, linear correlation with $F^{14}C_{CH_4}$, as the data indicate, the same is probably true for δD_{CH_4} and $F^{14}C_{CH_4}$ also. These correlations are compatible with mixing of a CH_4 source that is relatively ^{13}C- and D-depleted and ^{14}C-rich (relatively modern) with another source that is relatively ^{13}C- and D-enriched and that contains little to no ^{14}C.

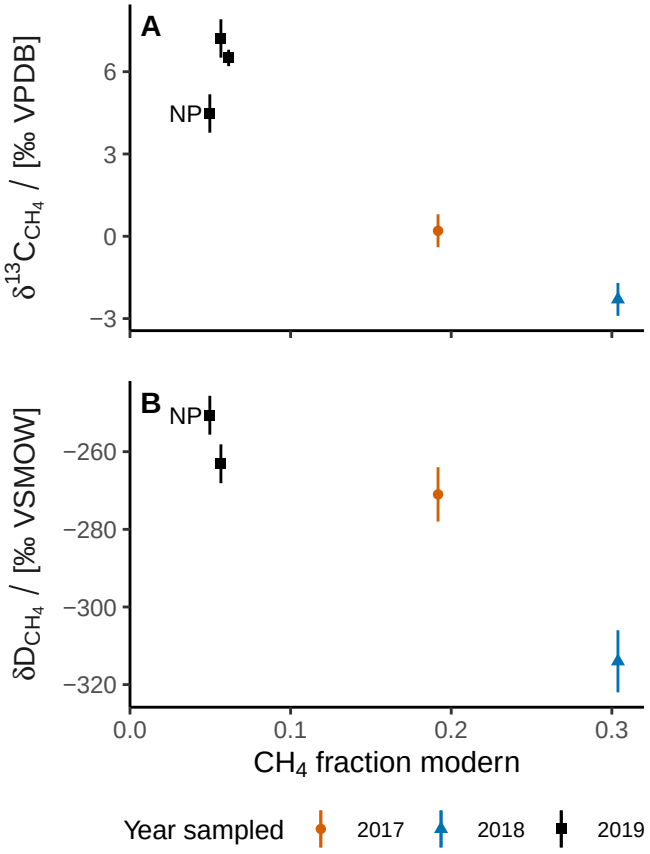

Figure 3.1: Radiocarbon and stable isotopic composition of CH_4 at NSHQ14. The "NP" label indicates that the well was not purged prior to sampling.

The $\delta^{13}C$ of ethane (C_2H_6) and propane (C_3H_8) from NSHQ14 were $-5.5\,‰$ VPDB and $4.9\,‰$ VPDB, respectively (Table 3.4; Figure 3.2). These values are $\sim 15\,‰$ higher than those in the most mature (and therefore most ^{13}C-enriched) thermogenic C_2H_6 and C_3H_8 samples from confined systems (Milkov and Etiope, 2018; Fiebig et al., 2019). Rather, the $\delta^{13}C_{C_2H_6}$

and $\delta^{13}C_{C_3H_8}$ values are similar to those reported in studies of CH_4-rich inclusions in rocks from oceanic lithosphere, including rocks from the Mid-Cayman Rise and the Zambales Ophiolite, Philippines (Grozeva et al., 2020; Figure 3.2). While $\delta^{13}C_{CH_4}$ in samples from NSHQ14 has varied between sampling years, $\delta^{13}C_{C_2H_6}$ and $\delta^{13}C_{C_3H_8}$ have been practically invariant (Figure 3.2; Nothaft et al., 2020), suggesting that the dynamics of CH_4 may be decoupled to some degree from those of $C_2 - C_6$ alkanes.

The $\delta^{13}C$ of CH_4 sampled from WAB71 in 2019 was 7.0 ‰ VPDB, which is similar to that of CH_4 sampled from NSHQ14 in 2019 (Table 3.4). The $\delta^{13}C$ of CH_4 sampled from WAB71 in 2019 was somewhat higher than in previous sampling of this well (range of 2.9 ‰ VPDB to 2.9 ‰ VPDB from 2015 to 2018; Nothaft et al., 2020). The δD of CH_4 sampled from WAB71 in 2019 was −304 ‰ VSMOW, which is 40 ‰ lower than that of CH_4 sampled from NSHQ14 in 2019 (Table 3.4). The δD of CH_4 sampled from WAB71 in 2019 was generally consistent with previous sampling of this well (−307 ‰ VSMOW in 2018 and −313 ‰ VSMOW in 2017, the only prior years when δD_{CH_4} was measured for samples from WAB71; Nothaft et al., 2020).

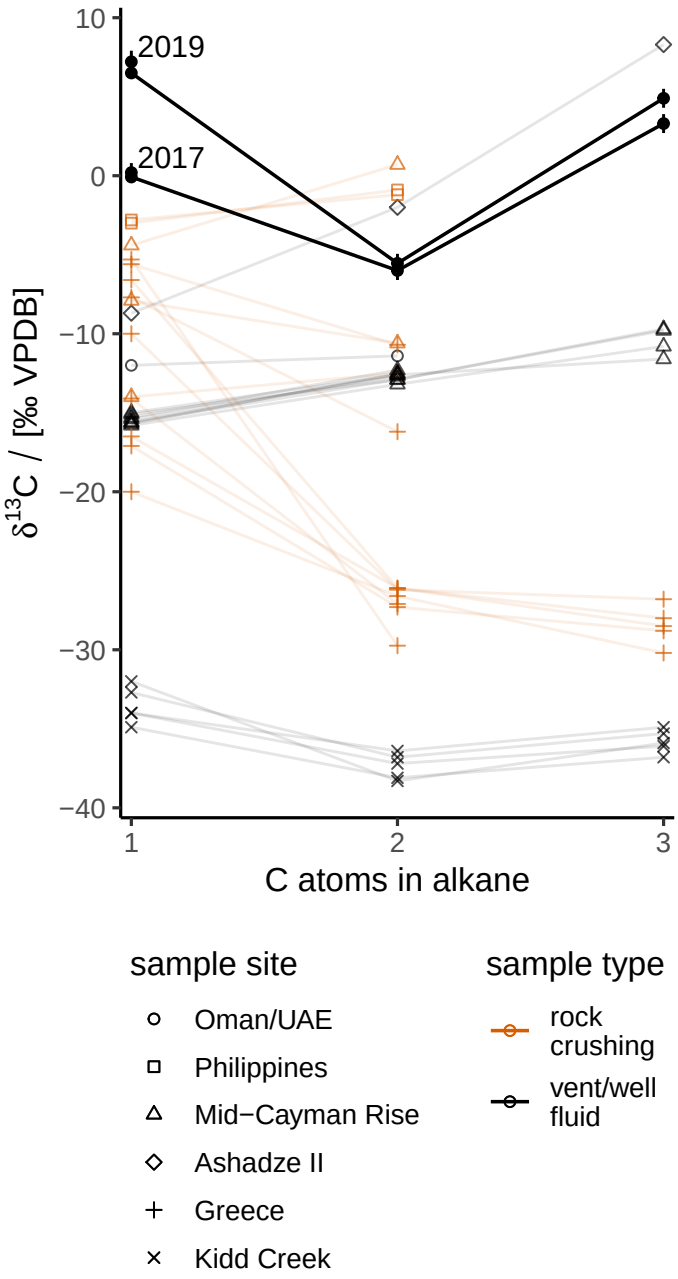

Figure 3.2: Plot of δ^{13}C of CH_4 and co-occurring n-alkanes vs. the number of C atoms per molecule for samples from NSHQ14 and the literature. NSHQ14 samples are labeled by the year in which they were sampled. Analyses from the same samples are connected by lines. Error bars represent uncertainties on δ^{13}C analyses of NSHQ14 samples. Only samples for which $\delta^{13}C_{C_2}$ was determined are plotted. Contextual data from ophiolites: Oman/UAE (Fritz et al., 1992; Nothaft et al., 2020), the Philippines (Grozeva et al., 2020), Greece (Etiope et al., 2018); sediment-poor seafloor hydrothermal vents: Mid-Cayman Rise (McDermott et al., 2015; Grozeva et al., 2020), Ashadze II (Charlou et al., 2010); and Precambrian Shield: Kidd Creek, Canada (Sherwood Lollar et al., 2008).

3.2.4 Subsurface carbonate mineralogy and ^{14}C content

The ^{14}C contents of subsurface carbonate minerals from well BA3A are reported in (Table 3.1). Whereas the other wells in this study were drilled by rotary drilling, well BA3A was drilled by diamond wireline drilling. As such, rock core samples are available for BA3A, enabling sampling of in-place carbonate minerals, while only rock chips from approximate depths are available for the rotary-drilled wells. However, due to the smaller diameter of the diamond-wireline-drilled wells relative to the rotary-drilled wells in our study area, we were concerned about the risk of our pump getting stuck in diamond wireline-drilled wells, and thus we only pumped fluids from the rotary-drilled wells.

The primary rock type of BA3A and NSHQ14 is partially-serpentinized harzburgite throughout the entire drilled depth (300 m for BA3A, 304 m for NSHQ14) (Kelemen et al., 2020a; Paukert, 2014; Miller et al., 2016). Veins bearing carbonate minerals were most abundant in the top 10 m of BA3A cores (where 19 carbonate-bearing veins were identified) and were scarce below $\sim$ 100 m (Figure 4.3E). This is generally consistent with the distribution of white chips that effervesce upon acidification (presumably Ca-rich carbonates) in rock chips from NSHQ14 (Paukert, 2014). At the time of writing, 6 carbonate veins from the upper 10 m of BA3A have been analyzed for C stable and radio- isotopic composition and mineralogy (Table 3.1). All of these samples had ^{14}C contents significantly above analytical blanks, with $F^{14}C$ ranging from 0.0037 to 0.078 (Table 3.1; Figure 4.3G), indicating that these carbonates were formed at least in part from atmospheric CO_2 in geologically recent times (< 50 ka). The $\delta^{13}C$ of carbonates from BA3A ranged from -15.0 ‰ VPDB to -7.7 ‰ VPDB. These $\delta^{13}C$ values are within a similar range as those of $\sum CO_2$ in $Mg^{2+} - HCO_3^-$ waters in the ophiolite (-15.56 ‰ VPDB to -10.88 ‰ VPDB; (Matter et al., 2006; Nothaft et al., 2020)), which is less than that which would be expected based on equilibrium with atmospheric CO_2 (Zeebe and Wolf-Gladrow, 2001). This could be a result of kinetic isotope effects associated with CO_2 hydroxylation as these groundwaters uptake CO_2 from air (Clark and Fontes, 1990; Clark et al., 1992). The BA3A carbonates were Ca-bearing (calcite and dolomite; Table 3.1),

which is consistent with their possible precipitation upon mixing of $Ca^{2+} - OH^-$ fluid with air or a $Mg^{2+} - OH^-$ fluid.

3.2.5 16S rRNA gene sequencing

To investigate potential relationships between CH_4 cycle processes and subsurface microbial communities, biomass was filter-concentrated from groundwaters pumped in 2019; DNA was extracted from this biomass, and 16S rRNA genes of this DNA were amplified and sequenced. For well NSHQ14, only DNA from the sample acquired without pre-purging the well (Materials and Methods—Pumping and in-field measurements) was sequenced. In this sample, the most abundant taxonomic affiliation inferred from 16S rRNA gene phylogeny was genus *Methanobacterium* (24 % of reads; Table 2.5), whose members are obligately anaerobic and can produce CH_4 from H_2 and CO_2, CO, or formate (Balch et al., 1979). Other taxa presumed capable of anaerobic, hydrogenotrophic, and autotrophic metabolisms on the basis of phylogenetic inference were detected at NSHQ14, including members of candidate phylum Acetothermia (former OP1) (23 % of reads; Figure 2.5), for which an autotrophic acetogenic metabolism using the Wood-Ljungdahl (acetyl-CoA) pathway has been inferred from metagenome-assembled genomes obtained from microbial mat samples in an oligotrophic, reduced, hydrothermal stream environment (Takami et al., 2012). In addition, 16S rRNA gene sequences affiliated with taxa whose cultured reference strains are capable of obligately or facultatively aerobic lifestyles were found in subsurface DNA from NSHQ14, including members of the genera *Silanimonas* (Lee et al., 2005) (21 % of reads), *Meiothermus* (Raposo et al., 2019) (15 % of reads), *Hydrogenophaga* (Suzuki et al., 2014) (7 % of reads), and *Brachymonas* (Halpern et al., 2009) (6 % of reads). In contrast to the microbial community composition of NSHQ14 inferred from 16S rRNA gene phylogeny, that of WAB71 was dominated by class Thermodesulfovibrionia (93 % of reads) in samples from 2019. Cultured representatives of Thermodesulfovibrionia are capable of SO_4^{2-} reduction coupled to H_2 oxidation and may additionally/alternatively oxidize C_1-C_3 acids and use thiosulfate, sulfite,

Fe^{3+} or NO_3^- as terminal electron acceptors for anaerobic respiration (Henry et al., 1994; Sekiguchi et al., 2008). 16S rRNA gene sequences affiliated with *Methanobacterium* were not detected in samples from WAB71. 16S rRNA gene sequences of biomass were searched for matches to known CH_4-cycling taxa, as compiled previously (Crespo-Medina et al., 2017). Apart from *Methanobacterium,* the only other known CH_4-cycling taxon in this data set was affiliated with the genus *Methylococcus* ($< 1\,\%$ of reads in both NSHQ14 and WAB71; Section B.1), which contains aerobic methanotrophs (Hanson and Hanson, 1996).

3.3 Discussion

CH_4 samples from two out of the four studied wells had ^{14}C contents significantly above analytical blanks (Table 3.1). $F^{14}C$ of up to 0.304 was measured in CH_4 sampled from well NSHQ14, indicating conversion of substantial quantities of atmospheric CO_2 to CH_4 actively (within the last 10 kyr) under some conditions within the Samail Ophiolite. The sample with 0.304 $F^{14}C$ at NSHQ14 must have consisted of $\sim 30\,\%$ CH_4 that was currently (within the last $\sim$ 100 years) being produced from atmospheric CO_2 and $70\,\%$ CH_4 produced > 50 ka and/or produced from one or more radiocarbon-dead C source(s), or it consisted wholly of CH_4 produced from atmospheric $CO_2 \sim 10$ ka (Table 3.1) on average, or it consisted of CH_4 derived from a combination of processes like these.

Not only is the finding of substantial ^{14}C content in CH_4 at NSHQ14 reproducible across two laboratories and three years of sample acquisition (Results—^{14}C content of CH_4), it is also unlikely to derive from potential drilling contamination. Twelve years had passed between the drilling of NSHQ14 by Omani authorities and our first sampling of CH_4 from this well for ^{14}C analysis in 2017. The intervening period should have allowed time for the aquifer surrounding NSHQ14 to recover to its natural state. Further, NSHQ14 had been previously pumped for sampling in 2014, 2015, and 2016 (Miller et al., 2016; Rempfert et al., 2017; Nothaft et al., 2020), helping to clear the well of potentially stagnant fluids prior to

sampling in 2017. In 2018, drilling of well BA3A (10 m from NSHQ14; Figure B.1) occurred two months prior to pump sampling of NSHQ14. This drilling activity had the potential to introduce modern C into the aquifer surrounding NSHQ14 in 2018. However, the broad consistency in ^{14}C content of CH_4 sampled in 2017 ($F^{14}C = 0.192$) and 2018 ($F^{14}C = 0.304$) and the subsequent decrease in ^{14}C content of CH_4 sampled in 2019 ($F^{14}C = 0.06 \pm 0.01$, $1s$, $n = 3$) (Table 3.1) indicate that drilling fluids are not the primary source of modern C in the sampled CH_4. Moreover, even if drilling did introduce modern C into the aquifer that was converted to CH_4 on months to years timescales, that would in itself be remarkable, as it would point to a system poised for rapid turnover of C (presumably in the form of aqueous $\sum CO_2$) to CH_4. That said, we maintain that modern C that may have been present in drilling fluids was probably not a major contributor to the ^{14}C content of sampled CH_4; rather, our observations predominantly reflect processes that occur in the aquifer in the absence of human influence.

They key question is what processes underpin the formation of CH_4 with a measurable ^{14}C content at NSHQ14 and its variation between sampling events The negative and linear correlations we observe between $F^{14}C_{CH_4}$ and both $\delta^{13}C_{CH_4}$ and δD_{CH_4} (Figure 3.1; Results—Stable isotope composition of CH_4, C_2H_6, and C_3H_8), and what these correlations indicate about the relative importance of production versus consumption of CH_4 at NSHQ14. It has been proposed that positive, linear correlations between $\delta^{13}C_{CH_4}$ and δD_{CH_4} in the Samail Ophiolite (e.g. Section B.1, Figure B.3) arise from microbial oxidation of CH_4, which could result in residual CH_4 having the isotopic composition observed at NSHQ14 starting from an initial isotopic composition of approximately -30 ‰ VPDB to -10 ‰ VPDB $\delta^{13}C$ and -300 ‰ VSMOW to -350 ‰ VSMOW δD (Etiope, 2017b; Miller et al., 2018). The added dimension provided by our $F^{14}C$ data leads to a different interpretation. In the case of aerobic CH_4 oxidation, which is characterized by a minor (not detectable) degree of reversibility (Wang et al., 2016), oxidation would not be expected to affect the $F^{14}C$ of CH_4 ($F^{14}C$ is, by definition, corrected for mass-dependent fractionation (Reimer et al., 2004)). In the

case of anaerobic methane oxidation (of the SO_4^{2-}-driven, ANME-type; the isotope effects of other types have not been thoroughly investigated), which is suggested to be a highly reversible metabolic pathway (Knittel and Boetius, 2009; Timmers et al., 2017), C stable isotopic equilibration between CO_2 and CH_4 has been proposed to occur due to partial back-reaction of CO_2 to CH_4 (Yoshinaga et al., 2014). In this way, microbially-mediated isotopic exchange between CO_2 and CH_4 could theoretically introduce ^{14}C into CH_4, even if net CH_4 production were negative. If this were occurring, equilibration of H isotopes between CH_4 and water, and isotopic bond order equilibration ("clumped" CH_4 isotopes, $^{13}CH_3D$ and $^{12}CH_2D_2$) might also be expected to approach equilibrium (Ash and Egger, 2019; Young et al., 2017). However, none of the metrics of C or H bulk or clumped isotopic composition of CH_4 indicate an approach towards isotopic equilibrium at NSHQ14 (Nothaft et al., 2020), suggesting that back-reaction of $^{14}CO_2$ to $^{14}CH_4$ through anaerobic CH_4 oxidation is not a major process at NSHQ14. Moreover, 16S rRNA gene sequences related to ANME were not detected in 2019, and have always accounted for $< 1\,\%$ of reads in samples of NSHQ14 groundwaters from 2014 through 2018, suggesting that ANME do not comprise a major portion of the microbial community at NSHQ14 (Section B.1; Nothaft et al., 2020; Kraus et al., 2018; Rempfert et al., 2017; Miller et al., 2016). Thus, the isotopic correlations of CH_4 sampled from NSHQ14 are unlikely to result primarily from CH_4 oxidation. Rather, these correlations are better explained by mixing of at least two sources of CH_4: e.g. one that is relatively ^{13}C- and D-depleted and ^{14}C-rich (relatively modern) and another that is relatively ^{13}C- and D-enriched and that contains little to no ^{14}C. These two sources may derive from different regions of the subsurface. In each sampling event, we may have accessed different regions of the aquifer, resulting in the sampling of CH_4 originating from these two sources in varying proportions.

The hypothesis that we accessed different regions of the subsurface at NSHQ14 across sampling events is consistent with our findings of aqueous geochemical variation across samples obtained through different pre-purging techniques in 2019 and our findings from the

down-hole geochemical profiles that chemical compositions of subsurface fluids at NSHQ14 vary with depth and differ between the down-hole geochemical profiles and the pumped fluid sample at equivalent depths of measurement/sampling (Results—Chemical composition of subsurface fluids; Figure 4.3B-D, Table 3.2; Table 3.3). These findings suggest that the pump draws fluids from parts of the aquifer that do not exactly correspond to the depth of the pump intake and that the source of fluids sampled during pumping may vary depending on how the well was purged prior to sampling. This is to be expected of open well pumping in heterogeneous fractured-rock aquifers, of which the Samail Ophiolite is a prime example (Dewandel et al., 2005; Lods et al., 2020). Indeed, our methods of purging NSHQ14 prior to sampling have differed between sampling events. For example, in 2019, NSHQ14 was purged for 233 minutes prior to sampling, whereas, in 2018, it was purged for 45 minutes. Another factor that could have resulted in our sampling of different regions of the subsurface across years of sampling is the potential that the drilling of BA3A opened or clogged fractures in the subsurface surrounding NSHQ14. If such changes to the hydrologic properties of the aquifer occurred, they could have changed the source of our fluid samples, even if the pumping methods were exactly the same. Some evidence for this is that the conductivity increase from 160 m to 180 m depth in the NSHQ14 down-hole geochemical profile logged in 2018 (Figure 4.3D) was not present in an earlier (circa 2005) down-hole geophysical log of NSHQ14 (Paukert, 2014), suggesting that the conductivity increase may have been induced by the activation of a fracture. Collectively, these observations are consistent with the hypothesis that variation in the purging of NSHQ14 prior to sampling and/or variations in subsurface hydrologic properties potentially resulting from the drilling of BA3A could have led to our samples containing varying proportions of fluids from different regions of the aquifer, where CH_4 production from modern C sources was active to greater or lesser extents.

The mechanism(s) of CH_4 production from modern C could in principle be abiotic or biotic. If abiotic, at the low temperatures ($\approx 40\,^{\circ}C$) that prevail in the subsurface near NSHQ14, laboratory experiments indicate that gas-phase reaction of H_2 and CO_2 on a Ru

catalyst is required to yield CH_4 at appreciable rates (Etiope and Ionescu, 2015; McCollom, 2016). In ophiolites, the highest concentrations of ruthenium (Ru) are found in chromites, which can be concentrated in chromitites (Etiope and Ionescu, 2015; Etiope et al., 2018). Chromitites were not found in cores or drill chips of any of the seven wells in the catchment of NSHQ14 (Kelemen et al., 2020a; Miller et al., 2016; Paukert, 2014). Nonetheless, peridotites in Oman ubiquitously contain a few percent distributed chromite (Hanghøj et al., 2010) that could host lesser amounts of catalytic Ru. In the case of NSHQ14, though, a greater obstacle to low-temperature CH_4 production than the presence of Ru may be the access of gaseous H_2 and CO_2 to Ru. The depth to water of $\sim 8\,\mathrm{m}$ (Table 3.2) at NSHQ14 indicates predominantly water-saturated conditions in the subsurface near NSHQ14. However, in some regions of the subsurface, exceedingly reduced conditions could result in separation of a H_2-rich gas phase (Figure 4.3C, Figure B.2, Results—Chemical composition of subsurface fluids; (Leong and Shock, 2020)). Although such a gas phase could theoretically allow for methanation catalysis, it would be surrounded by highly alkaline (pH > 10.5; Figure 4.3B) and $\sum CO_2$-poor ($< 12\,\mu\mathrm{mol} \cdot \mathrm{L}^{-1}$ (Nothaft et al., 2020)) water, making CO_2 (g) extremely scarce. Under these conditions, the opportunities for Ru, H_2 (g), and CO_2 (g) recently derived from air to come into contact seem limited, perhaps too limited to account for the tens of $\mu\mathrm{mol} \cdot \mathrm{L}^{-1}$ of ^{14}C-modern CH_4 in our samples.

Alternatively, the production of CH_4 from modern C sources could be mediated by microbes. Sequences affiliated with *Methanobacterium* accounted for 24 % of 16S rRNA gene reads in biomass filter-concentrated from groundwaters pumped at NSHQ14 in 2019 (Figure 2.5). 16S rRNA gene reads affiliated with *Methanobacterium* were in similarly high relative abundance in previous years of sampling NSHQ14 (e.g. 24 % in 2018 (Nothaft et al., 2020) and 12 % in 2017 (Kraus et al., 2018)). The sustained high relative abundance of *Methanobacterium* 16S rRNA gene reads in NSHQ14 fluids indicates that methanogenic microbes comprise a major portion of the subsurface microbial community at NSHQ14. 16S rRNA gene sequencing of subsurface biomass from NSHQ14 is complemented by other ob-

servations that suggest that methanogens are not only prevalent, but active. The functional potential to perform hydrogenotrophic and acetoclastic methanogenesis at NSHQ14 has been demonstrated through metagenomic sequencing (Fones et al., 2019), and genes involved in methanogenesis are actively transcribed (Kraus et al., 2018). Transformation of ^{14}C-labeled HCO_3^- to CH_4 has been shown to occur in water samples from NSHQ14 at significantly higher rates than in killed controls (Fones et al., 2019), indicating active microbial methanogenesis in the sampled groundwater. Taken together with a cell abundance of $1.15 \cdot 10^5\,\text{cells} \cdot \text{mL}^{-1}$ in groundwater at NSHQ14 (Fones et al., 2019), these data suggest that some depths of the aquifer accessed by NSHQ14 host abundant active methanogenic cells (thousands per mL, assuming $\sim 24\,\%$ of cells are methanogens based on 16S rRNA gene data). Thus, there is little doubt that microbes are capable of active, subsurface CH_4 production at NSHQ14. The question then becomes: *how* might methanogens access this modern C?

To address this, the spatial extent of modern C in the subsurface must first be assessed. Since concentrations of $\sum CO_2$ in $Ca^{2+} - OH^-$ groundwaters within ophiolites are generally too low to yield reliable ^{14}C measurements (Vankeuren et al., 2019), we can instead look to the ^{14}C contents of subsurface carbonate minerals and other geochemical parameters as recorders of recent groundwater-air interaction. The presence of ^{14}C-live carbonates in rock cores from BA3A (Table 3.1; Figure 4.3E-G) demonstrates that at least the upper $\sim 10\,\text{m}$ of the subsurface near BA3A and NSHQ14 actively uptakes atmospheric CO_2. Sharp decreases in pH and increases in Eh towards the surface at $\sim 30\,\text{m}$ depth in BA3A and NSHQ14 down-hole geochemical profiles (Figure 4.3B-C) suggest that the influence of air on subsurface geochemical conditions extends to at least 30 m below ground level. These findings, taken together with our measurement of $245\,\mu\text{mol} \cdot \text{L}^{-1}$ to $467\,\mu\text{mol} \cdot \text{L}^{-1}$ H_2 (aq) in NSHQ14 groundwaters 2019 (Table 3.3) and measurements dating back to 2014 indicating that hundreds of $\mu\text{mol} \cdot \text{L}^{-1}$ concentrations of H_2 (aq) persist to depths at least as shallow as 17 m below ground level at NSHQ14 (Miller et al., 2016), imply that high concentrations of H_2 and low but (bio)geochemically impactful concentrations of modern $\sum CO_2$ coexist

in groundwaters at some depths of the subsurface near NSHQ14. Collectively, these data are compatible with a scenario in which deeply-sourced H_2-rich $Ca^{2+} - OH^-$ fluids mix with downward-infiltrating fluids bearing $\sum CO_2$ recently derived from air, creating a niche well-suited to microbial methanogenesis.

Such a niche has been predicted through thermodynamic modeling. Using reaction path and bioenergetic modeling, Leong and Shock (Leong and Shock, 2020) predicted that hydrogenotrophic methanogenesis is energetically favorable in end-member $Ca^{2+} - OH^-$ fluids out of contact with the atmosphere at 1 bar and 25 °C (if abiotic CH_4 production is suppressed due to kinetic limitations). In addition, they found that when $Ca^{2+} - OH^-$ fluids equilibrated with 1 bar of H_2 mix with relatively small proportions ($\sim 10\,\%$) of $Mg^{2+} - HCO_3^-$ fluids equilibrated with air, the energetic yield of methanogenesis per unit of fluid mass increases by a factor of $\sim$ 10 to $\sim$ 15 due to increased $\sum CO_2$ availability. Similar mixing and thermodynamic models were employed by Zwicker et al. (Zwicker et al., 2018) to explain their findings of hydromagnesite bearing the ^{13}C-depleted signature of atmospheric CO_2 hydroxylation co-located with lipid biomarkers affiliated with methanogens (but not methanotrophs), from which they concluded that deeply-sourced fluids produced through serpentinization mixed with fluids containing $\sum CO_2$ derived from air, thereby facilitating hydrogenotrophic methanogenesis within the terrestrial weathering environment. Thus, prior work has anticipated active microbial methanogenesis in terrestrial serpentinizing settings where H_2-rich fluids come into contact with C derived from atmospheric CO_2, and this study now demonstrates this process in action.

Ideally, our $F^{14}C_{CH_4}$ could yield information of about the stable isotopic compositions of end member CH_4 sources, which could be used to infer their CH_4 production mechanisms. Unfortunately, there are too many unconstrained variables to precisely estimate the isotopic composition of microbial CH_4 produced at NSHQ14, but the range of potential compositions predicted by extrapolating correlations between $F^{14}C_{CH_4}$, $\delta^{13}C_{CH_4}$, and δD_{CH_4} does intersect with plausible compositions based on comparison to culturing studies. Multiple factors make

estimating the isotopic composition of microbial CH_4 difficult. First, there may be more than one mode of microbial methanogenesis. For instance, methanogenesis in deep-seated fluids out of touch with the atmosphere would be expected to have lower ^{14}C content and proceed at slower rates than CH_4 produced at mixing zones where C is more available, and thus may also have a different stable isotopic composition. Second, an abiotic contribution of the ^{14}C-bearing CH_4 cannot be ruled out. Third, even it were assumed that there is one mode of microbial methanogenesis and that it is the only source of ^{14}C-bearing CH_4, the $F^{14}C$ of microbial CH_4 would remain unknown. In this scenario, the microbial CH_4 could have been produced thousands of years ago and account for the majority of the total CH_4 pool. On the opposite extreme, the microbial CH_4 could have been produced in the latter half of the 20^{th} century, when the ^{14}C content of atmospheric CO_2 increased due to nuclear bomb testing, in which case the fraction of microbial CH_4 relative to the total CH_4 pool may be as little as half that of the measured $F^{14}C$. Lastly, the confidence intervals on our regressions of $F^{14}C_{CH_4}$ upon $\delta^{13}C_{CH_4}$ and δD_{CH_4} encompass a wide range of values, which may be due in part to our relatively small sample size. Still, we can calculate a potential isotopic composition of microbial CH_4 under the same assumptions described above by taking our regressions at face value and plugging in the simple, albeit arbitrary, condition of $F^{14}C = 1.00$ for the hypothesized microbial end member, which would correspond to production in 1950 or approximately contemporaneously with the start of our $^{14}CH_4$ sampling in 2017 (Hammer and Levin, 2017). Doing so yields a predicted isotopic composition of the microbial end member of $\delta^{13}C_{CH_4} = -27.1\,‰\,\text{VPDB}$ and $\delta D_{CH_4} = -455\,‰\,\text{VSMOW}$ *(*Section B.1). These values are similar to those produced by *Methanobacterium* cultured at pH 9.66 to 9.23 provided $CaCO_3$ as the C source in experiments simulating methanogenesis under alkaline, C-limited conditions during serpentinization ($\delta^{13}C_{CH_4} = -28.0\,‰\,\text{VPDB}$ and $\delta D_{CH_4} = -431\,‰\,\text{VSMOW}$ from $\delta^{13}C_{CaCO_3} = -0.1\,‰\,\text{VPDB}$ and $\delta D_{H_2O} = -108\,‰\,\text{VSMOW}$; (Miller et al., 2018)). While this similarity may be coincidental, it does demonstrate that the hypothesized ^{14}C-rich microbial end member is plausible from a stable isotopic perspective. We note that high $\delta^{13}C$

values (up to +14 ‰ VPDB) of lipid biomarkers thought to be produced by methanogens at serpentinite-hosted seeps at Chimaera, Turkey (Zwicker et al., 2018) and at the Lost City Hydrothermal Vent Field, Mid-Atlantic Ridge (Bradley et al., 2009) indicate that C limitation in serpentinizing settings results in ^{13}C enrichments in methanogen biomass, and further suggests the possibility of production of microbial CH_4 in these settings that is more ^{13}C-enriched than microbial CH_4 produced in sedimentary environments, which is generally ≤ -50 ‰ VPDB (Milkov and Etiope, 2018).

Having discussed the evidence for mixing of two more sources of CH_4 with different ^{14}C contents and the hypothesis that a ^{14}C-rich component is microbial, we now turn our attention to sources of CH_4 having little to no ^{14}C. The presence of $C_2 - C_6$ alkanes in samples from NSHQ14 (Table 3.3; (Nothaft et al., 2020)) indicates a component of non-microbial CH_4 because, of the $C_2 - C_6$ alkanes, microbes are only known to produce C_2H_6 and C_3H_8, and then, only under specific conditions in seafloor sediments and at much lower quantities than CH_4 (Formolo, 2010). The high $\delta^{13}C$ values of C_2H_6 (-5.5 ‰ VPDB) and C_3H_8 (4.9 ‰ VPDB) (Table 3.4; Figure 3.2) are also indicative of their source. These values are ~ 15 ‰ higher than those in the most mature (and therefore most ^{13}C-enriched) thermogenic C_2H_6 and C_3H_8 samples from confined systems (Milkov and Etiope, 2018; Fiebig et al., 2019), indicating an abiotic source (Nothaft et al., 2020). The observed values are similar to those of C_2H_6 released during crushing of peridotites and other oceanic lithospheric rocks demonstrated through Raman spectroscopy to host CH_4-rich fluid inclusions (Grozeva et al., 2020) and are also similar to C_2H_6 and C_3H_8 from sediment-poor seafloor hydrothermal vents (Charlou et al., 2010; McDermott et al., 2015) (Figure 3.2), where a large body of evidence indicates that CH_4 is released from fluid inclusions rather than being produced from seawater $\sum CO_2$ reduction during hydrothermal circulation (Kelley and Früh-Green, 1999; McDermott et al., 2015; Wang et al., 2018; Klein et al., 2019). CH_4-rich fluid inclusions have been documented in olivine and orthopyroxene within harzburgite from the Samail Ophiolite (Miura et al., 2011), supporting the possibility of a fluid inclusion source of CH_4 and $C_2 - C_6$

alkanes. Low-temperature ($< 150\,^{\circ}C$) CH_4 generation can also produce $C_2 - C_6$ alkanes through Fischer-Tropsch Type reactions (Etiope and Ionescu, 2015), but less is known about the isotopic composition of alkanes produced via this mechanism in natural settings. The best-documented case is that of Kidd Creek, Canadian Shield (Sherwood Lollar et al., 2008), where $\delta^{13}C$ values are $\sim 20\,‰$ lower than sites where $C_2 - C_6$ alkane production is proposed to occur at higher temperatures within fluid inclusions (Figure 3.2). Crushings of Ru-rich chromitites from Greek ophiolites where low-temperature abiotic CH_4 production has been proposed to occur (Etiope et al., 2018) have $\delta^{13}C_{C_2H_6}$ values that are mostly $\sim 20\,‰$ lower than those measured in samples from NSHQ14, but some Greek chromitite $\delta^{13}C_{C_2H_6}$ values are similar to $\delta^{13}C_{C_2H_6}$ values reported elsewhere in the Samail Ophiolite ($\sim -10\,‰$ VPDB) (Fritz et al., 1992) (Figure 3.2). In sum, although $\delta^{13}C_{C_2H_6}$ and $\delta^{13}C_{C_3H_8}$ are not conclusive signatures of production mechanism, they do favor a predominant fluid inclusion source at NSHQ14.

Regarding the $\delta^{13}C$ of the the the low-to-no-^{14}C CH_4 end member, our finding of CH_4 with $\delta^{13}C$ as high as $7.2\,‰$ VPDB that also had $F^{14}C = 0.057$ and the negative correlation between $F^{14}C_{CH_4}$ and $\delta^{13}C_{CH_4}$ (Tables 3.1 and 3.4; Figure 3.1A) suggests that the $\delta^{13}C$ of the low-to-no-^{14}C end member is $> 7.2\,‰$ VPDB. The C precursor to CH_4 formed in fluid inclusions would be expected to be mantle CO_2 at $\sim -5\,‰$ VPDB (Deines, 2002), and the C isotope fractionation of CH_4 formation may be minimal due to the high temperatures of reaction and complete consumption of reactant CO_2 (Bottinga, 1969; Kelley and Früh-Green, 1999; Klein et al., 2019; Grozeva et al., 2020). Reaction of CO_2 to ^{13}C-depleted graphite is known to enrich residual CO_2 in ^{13}C in fluid inclusions (Luque et al., 2012; Satish-Kumar, 2005), which could also enrich CH_4 to $\delta^{13}C$ values above that of mantle CO_2 if CH_4 is subsequently produced from the residual CO_2. This is plausible in the Samail Ophiolite because CH_4 and graphite have been found to coexist in orthopyroxene-hosted fluid inclusions in Samail Ophiolite peridotite (Miura et al., 2011). CH_4 produced at low temperatures in the present-day weathering environment could form from a C source that

is more ^{13}C-enriched than mantle CO_2 (i.e. marine carbonates up to 4 ‰ VPDB; (Richoz et al., 2010; Etiope, 2017b)), but there are no documented mechanisms to enrich CH_4 in ^{13}C above its C precursor because the reaction would proceed at lower temperatures, which could inhibit graphite formation, and not in a strictly closed system, in contrast to the fluid inclusion case. However, it is possible that our CH_4 samples have undergone partial microbial oxidation, which could have enriched residual CH_4 in ^{13}C and D. This is consistent with our detection of 16S rRNA gene sequences related to aerobic methanotrophs of the genus *Methylococcus* in samples from NSHQ14 groundwaters in low but consistent relative abundance (< 1 ‰ of reads in all samples, 2019 through 2014; Section B.1; (Miller et al., 2016; Rempfert et al., 2017; Kraus et al., 2018; Nothaft et al., 2020)). We reiterate that our F^{14}C data indicate that mixing of CH_4 sources with different ^{14}C contents accounts for most of variation observed in the C and D stable isotopic compositions of CH_4 at NSHQ14, but even a minor overprint of microbial CH_4 oxidation could reasonably enrich CH_4 (Miller et al., 2018) from a marine carbonate δ^{13}C value to something close to the extrapolated δ^{13}C of the low-to-no-^{14}C CH_4 end member. Thus, $\delta^{13}C_{CH_4}$ at NSHQ14 does not distinguish between abiotic reaction mechanisms given the available data.

While $\delta^{13}C_{CH_4}$ provides information primarily on C source, δD_{CH_4} carries more information about formation conditions, particularly temperature. This is because H isotope equilibrium between CH_4, H_2, and water, as well as intra-CH_4 "clumped isotopologue" equilibrium, are typically attained during relatively high-temperature formation of CH_4. For instance, in a study of four sediment-poor seafloor hydrothermal vent settings, Wang et al. (Wang et al., 2018) determined that CH_4 in vent effluent exhibited H isotope and clumped isotopologue ($^{13}CH_3D$) equilibrium at temperatures of 270 °C to 360 °C and showed no apparent relation to the wide range of effluent temperatures (96 °C to 370 °C), suggesting that this CH_4 formed in fluid inclusions rather than during ongoing hydrothermal fluid circulation, and that the closure temperature for H isotope exchange in the $CH_4 - H_2 - H_2O$ system is $\sim$ 270 °C in seafloor hydrothermal settings. Formation of CH_4 at lower temperatures through either

abiotic or microbial mechanisms typically results in greater D depletion in CH_4 relative to the dominant reservoir of H (generally water), reflecting lower-temperature equilibrium or kinetic isotope effects. Assuming $\delta D_{H_2O} = 0$ ‰ VSMOW (valid for ocean water or NSHQ14 groundwater; Section B.1), calculated equilibrium δD_{CH_4} values using fractionation factors from ref. Horibe and Craig, 1995 are −122 ‰ VSMOW at 270 °C (a plausible temperature for CH_4 formed in fluid inclusions (Wang et al., 2018)) and −208 ‰ VSMOW at 35 °C (approximate NSHQ14 groundwater temperature; Table 3.2; Figure 4.3A). The δD_{CH_4} predicted at $F^{14}C_{CH_4} = 0$ based on our regression of NSHQ14 samples (Results—Stable isotope composition of CH_4, C_2H_6, and C_3H_8; Section B.1, Figure 3.1B) is −242 ‰ VSMOW (95 % confidence interval of −287 ‰ VSMOW to −198 ‰ VSMOW). Thus, the δD predicted for the low-to-no-^{14}C CH_4 end member at NSHQ14 is below that which would be expected from formation within fluid inclusions. It is compatible with H isotopic equilibrium at present groundwater temperatures within uncertainty, although it may also be below this, suggesting potential CH_4 production through mechanisms that express kinetic isotope effects. These calculations suggest that ^{14}C-poor CH_4 at NSHQ14 is not entirely sourced from fluid inclusions. However, fluid inclusions could still comprise a substantial proportion of the low-to-no-^{14}C CH_4 end member if there is another, low-temperature source of ^{14}C-poor CH_4, which could be abiotic or microbial.

A prediction based on our hypothesis that NSHQ14 CH_4 is a mixture of ^{14}C-rich CH_4 that is dominantly microbial and ^{14}C-poor CH_4, of which a substantial portion is abiotic, is that $F^{14}C_{CH_4}$ should exhibit a positive correlation with $C_1/(C_2 + C_3)$ at NSHQ14. In fact, $F^{14}C_{CH_4}$ increased from 0.192 to 0.304 in samples taken at NSHQ14 from 2017 to 2018 (Table 3.1), while $C_1/(C_2 + C_3)$ decreased from 1190 to 881, which is contrary to what would be predicted from our hypothesis (Figure B.4). However, samples of NSHQ14 taken in 2019, which had starkly lower $F^{14}C_{CH_4}$ (0.06 ± 0.01, $1s$, $n = 3$; Table 3.1), had lower $C_1/(C_2 + C_3)$ (397 to 605) than samples from 2017 and 2018 (Figure B.4), which is consistent with our hypothesis. Gas sampling and quantitation methods differed across sampling years in our

data set (Nothaft et al., 2020), so measurement artifacts could account for some of the observed inter-annual variability in $C_1/(C_2 + C_3)$. Additionally, or alternatively, we may have tapped into reservoirs of abiotic $C_1 - C_6$ alkanes with truly distinct $C_1/(C_2 + C_3)$, which is compatible with our hypothesis that variations in our pumping methods across sampling events resulted in our accessing of different regions of the aquifer at NSHQ14. Additional sampling and measurement of $C_1 - C_6$ alkanes at NSHQ14, controlled for methodological differences, will be necessary in order to assess whether $C_1/(C_2 + C_3)$ supports or contradicts our hypothesis of a ^{14}C-rich, microbial component of CH_4 at NSHQ14.

If microbes convert atmospheric CO_2 to CH_4 on timescales of thousands of years or less in ophiolite aquifers, they likely also convert atmospheric CO_2 to intermediate redox state carbonaceous compounds on similar timescales. One such compound is acetate (CH_3COO^-), which could be produced from H_2 and CO_2 by members of candidate phylum Acetothermia (former OP1) (Takami et al., 2012), which were notably abundant in NSHQ14 16S rRNA gene sequences in 2019 (23 % of reads; Figure 2.5) and in previous years sampling this well and others in the ophiolite (Miller et al., 2016; Rempfert et al., 2017; Kraus et al., 2018; Nothaft et al., 2020). Methanogens, acetogens, and other microbes may also assimilate C recently derived from atmospheric CO_2 into biomass in the ophiolite. While research on CO_2 reactivity in peridotites has largely focused on carbonation reactions (Bruni et al., 2002; Cipolli et al., 2004; Kelemen and Matter, 2008; Kelemen et al., 2011; Paukert et al., 2012), our findings suggest that microbial production of carbonaceous compounds of varied redox states is an additional sink of atmospheric CO_2 in the ophiolite aquifer. Determining the turnover rates and eventual fates of these organic compounds is an increasingly important area of C cycle research in serpentinizing environments.

This task will be challenging because the turnover rates and eventual fates of C-containing compounds in serpentinizing settings may be spatially variable, as illustrated by the contrasts between well NSHQ14, where CH_4 had up to 0.304 $F^{14}C$ and well WAB71, where CH_4 did not have ^{14}C content significantly above analytical blanks in samples from both 2018 and 2019

(Table 3.1). In DNA extracted from pumped groundwater samples of WAB71, 16S rRNA gene sequences of methanogens were not detected in 2018 (Nothaft et al., 2020) or 2019, but bacteria related to class Thermodesulfovibrionia, which are thought to be capable of sulfate reduction (Henry et al., 1994; Sekiguchi et al., 2008), comprised a large proportion of 16S rRNA reads in 2019 (93 %; Figure 2.5) and in 2018 (20 %; (Nothaft et al., 2020)). WAB71 also contrasts with NSHQ14 in that groundwaters at WAB71 had below quantitatable concentrations of H_2 in 2019 ($< 3.29\,\mu\text{mol} \cdot \text{L}^{-1}$; Table 3.3) and in 2018 ($< 0.598\,\mu\text{mol} \cdot \text{L}^{-1}$; (Nothaft et al., 2020)).. That said, the origin of CH_4 at WAB71 cannot be determined from the available data. All that can be said with certainty is that CH_4 at WAB71 was not produced from atmospheric CO_2 within the last 50 kyr, indicating heterogeneous timescales and/or mechanisms of CH_4 production in the ophiolite.

On the topic of heterogeneity, we consider whether the ^{14}C content of CH_4 in the Samail Ophiolite is representative of low-temperature serpentinizing settings or if it is an anomaly. On this subject, we must first note that the number of $^{14}CH_4$ analyses in ophiolites was more than doubled by this study. More analyses would serve to better assess what is the rule and what is the exception. We do note in particular that the well with the highest $F^{14}C$ of CH_4 also had particularly high c_{H_2} (hundreds to thousands of $\mu\text{mol}\,\text{L}^{-1}$). This may suggest that systems must be poised at very reduced conditions for microbial methanogenesis to be strongly active. Additionally, NSHQ14 stands out in that a lineage of *Methanobacterium* has been identified in this well that is apparently incapable of producing CH_4 from CO_2, but can do so using formate ($HCOO^-$), which has been proposed to be an adaptation to hyperalkaline, CO_2-poor conditions (Fones et al., in press). It is plausible that this *Methanobacterium* widely dispersed in other serpentinizing settings in which ^{14}C activity in CH_4 was non-detectable. Atmospheric CO_2 may be rapidly converted to formate under the highly reduced conditions of NSHQ14, which is then converted to CH_4 by *Methanobacterium*. Further metagenomic and culturing studies will be necessary to assess the global distribution and functioning of this lineage of *Methanobacterium*.

3.4 Conclusions and Implications

In this study, we report the first measurement of ^{14}C content significantly above analytical blanks in CH_4 from a serpentinizing setting. Our finding of $F^{14}C_{CH_4}$ up to 0.304 indicates conversion of atmospheric CO_2 to CH_4 within the last 10 kyr in parts of the ophiolite. CH_4 samples from two out of the four studied wells were radiocarbon-dead, indicating that, elsewhere in the ophiolite, CH_4 was produced before $\sim$ 50 ka and/or from non-atmospheric C sources. Integrating microbiological and geochemical data, we infer that the recent conversion of atmospheric CO_2 to CH_4 was predominantly mediated by microbes. This implies that in some samples, microbial CH_4 may account for $\sim$ 30 % or more of the total CH_4 pool, which contrasts with existing paradigms that would interpret this CH_4 as wholly abiotic due to its high $\delta^{13}C$ (-3 ‰ VPDB for the samples with $F^{14}C_{CH_4} = 0.304$). Multiple isotopic measurements, including of C_2H_6 and C_3H_8, reveal that ^{14}C-poor abiotic CH_4 mixes with the ^{14}C-rich microbial CH_4. There may be an additional ^{14}C-poor component of microbial CH_4.

We recommend more widespread measurement of $^{14}CH_4$ in ophiolites not only because of its utility as a tracer of the C source for CH_4 production, but also because of its potential as an indicator of groundwater age or mixing, particularly in hyperalkaline waters in which low $\sum CO_2$ concentrations often preclude accurate ^{14}C dating of $\sum CO_2$. In addition, this study supports the premise that H_2 produced from water/rock reaction can fuel microbial life, even under challenging conditions of high pH and low oxidant availability, when C is available. By identifying where and how microbial methanogenesis can reasonably be expected to occur in H_2-rich, subsurface environments, this work complements theoretical models in guiding the search for rock-hosted life, including extraterrestrial life. For example, our findings substantiate predictions that microbial methanogenesis could occur in the reduced, alkaline ocean of Saturn's moon, Enceladus (McKay et al., 2008; Glein et al., 2015; Waite et al., 2017), and that methanogens may use H_2 and carbonate minerals in the Martian subsurface (Kral et al., 2014).

These implications of this study for greenhouse gas management via *in situ* mineral carbonation of peridotite (Kelemen and Matter, 2008; National Academies, 2019) should also be carefully considered. Our findings suggest that CO_2 injected into peridotites could be partially converted to CH_4 by methanogens that normally subsist in conditions of extreme C limitation. In addition, drilling and fracturing of peridotite could unintentionally release CH_4 stored in fluid inclusions. Due to differences in infrared absorbance band saturations of CH_4 and CO_2 (Archer, 2011; Myhre et al., 2013), if 1 unit mass of CH_4 were released to the atmosphere for every 30 unit mass of CO_2 injected and stored as subsurface carbonate minerals, the decrease in global warming potential resulting from mineral carbonation would be negated. Thus, our findings imply that the responses of CH_4 flux and microbial activity to engineered CO_2 injection into peridotite should be monitored.

3.5 Materials and Methods

3.5.1 Pumping and in-field measurements

Information on well location and construction are given in ref. Nothaft et al., 2020. Fluids were sampled with a submersible pump (Grundfos SQ 2-85). The pumping depths are reported in Table 3.2 and Table 3.1. Each well was pumped for ≥ 20 min prior to sampling. Sampling commenced once fluid pH and conductivity measurements stabilized. The only exception to this was a replicate from NSHQ14 that was not purged prior to sampling, which is labeled as "NP", or indicated in table footnotes, where applicable. This was done as a test of the effect of purging methods on water chemical composition. The NP sampling was conducted 8 days after a normal sampling of NSHQ14, when the well was pumped for 233 minutes at a rate of $20\,\mathrm{L}\cdot\mathrm{min}^{-1}$ prior to sample acquisition.

3.5.2 ^{14}C analysis of CH_4

CH_4 was prepared for ^{14}C analysis at the Institute for Alpine and Arctic Research (INSTAAR) Laboratory for AMS Radiocarbon Preparation and Research at CU-Boulder. The INSTAAR CH_4 preparation line is based on the designs of refs. Lowe et al., 1991 and Petrenko et al., 2008. Gas was extracted from 37 mL blue butyl-stoppered serum vials by flowing C-free air at $100\,mL \cdot min^{-1}$ through the vial and onto the main preparation line for 15 min, using BD PrecisionGlide needles (0.124 cm outer diameter, 3.8 cm length) to puncture the stopper. Extracted gas flowed across a series of cryogenic traps to remove water and CO_2. CO was quantitatively oxidized over Sofnacat, and the resultant CO_2 was removed by additional cryogenic trapping. Residual sample was then combusted over platinized glass wool to yield CO_2 from (primarily) CH_4. The yield was quantified and the process CO_2 transferred to flame-sealed tubes for eventual graphitization and measurement by accelerator mass spectrometry at the University of California - Irvine using the procedures of ref. Turnbull et al., 2007.

"CH_4" prepared for ^{14}C analysis at INSTAAR technically reflects all combustible gases after removal of CO and CO_2, which includes $C_2 - C_6$ alkanes. Isolation of CH_4 through gas chromatography (GC) is not employed on the CH_4 radiocarbon prep line at INSTAAR because it was designed for atmospheric samples in which CH_4 is the dominant hydrocarbon. Similarly, we calculated that the potential uncertainty in $^{14}C/^{12}C$ introduced by non-methane hydrocarbons is negligible in our samples due to their high C_1/C_{2+} ratios calculated from hydrocarbon gas quantitation via gas chromatography - flame ionization detection.

To independently verify our methodology and calculations, a replicate sample of CH_4 from one of the studied wells (NSHQ14) was sent to Isotech laboratories, where CH_4 was quantitatively separated from the other components by gas chromatography and then converted to CO_2, which was purified and captured in a Pyrex tube. This captured CO_2 was sent to National Ocean Sciences Accelerator Mass Spectrometry (NOSAMS), where it was converted to graphite, which was then analyzed for its $^{14}C/^{12}C$ ratio.

3.5.3 Identification and ^{14}C analysis of carbonate minerals

Vein types in cores from well BA3A were classified on the basis of macroscopic observation and, for a subset of samples, on thin section optical petrography and X-ray diffraction (XRD), as detailed in ref. Kelemen et al., 2020a. A subset of veins bearing carbonate minerals were subsampled for ^{14}C analysis. The mineralogy of these subsamples was confirmed by XRD. For XRD, carbonate samples were powdered and sieved to 100 mesh ($< 150\,\mu$mol) and analyzed on an Olympus BTX-II XRD Analyzer. Diffractograms were analyzed using Match! software to identify main minerals. Carbonate mineral samples were sent to NOSAMS where they were leached for 1 minute in a 10 % HCl solution to remove potential surface contamination, washed with Milli-Q, dried, and then converted to CO_2 via hydrolysis. The resultant CO_2 was converted to graphite, which was then analyzed for its $^{14}C/^{12}C$ ratio.

3.5.4 Chemical and stable isotopic analyses of fluids

To analyze aqueous concentrations (c) of non-carbonaceous chemical species, samples were collected by passing groundwater through a $0.2\,\mu$m filter into polypropylene conical tubes. Aqueous concentrations were measured by inductively coupled plasma atomic emission spectroscopy (repeatability as median relative standard deviation of 3 % for most ions). Aqueous concentrations of F^- Cl^-, SO_4^{2-}, Br^-, and NO_3^- were measured on by ion chromatography (analytical uncertainty of 5 %). The concentration and $\delta^{13}C$ of dissolved inorganic C ($\sum CO_2$) were measured by acidification of water samples and transfer of resultant CO_2 (g) via a Thermo Fisher GasBench II to a Thermo Delta V Plus isotope ratio mass spectrometer. Complete methodological details are available at `http://dx.doi.org/10.17504/protocols.io.zduf26w`.

Groundwaters and gases dissolved therein were sampled via syringe from a luer-lok port on the pump manifold. 60. mL of this water was then passed through a $0.2\,\mu$m filter and needle into an evacuated 117 mL glass vial capped with a blue chlorobutyl rubber stopper and Al crimp top. These are referred to as "headspace" samples. In addition, gases were

sampled with the "bubble" strip method modified from ref. Kampbell et al., 1998. Details on bubble strip gas sampling are available at `http://dx.doi.org/10.17504/protocols.io.bkb9ksr6`. H_2, CH_4, and CO concentrations in this study are reported from headspace samples due to the better accuracy of this method versus the bubble strip method, as determined in comparisons by the authors. Ethane through hexane concentrations were determined from the bubble strip samples because of the lower detection limit offered by bubble strip samples, and were normalized to the headspace gas samples through the CH_4 concentration and assumption of constant C_1/C_n ratio of both sample types, where C_n is an alkane of n C atoms. Gas concentrations were determined according to the methods of ref. Nothaft et al., 2020.

Bulk stable isotope analyses of CH_4 and co-occurring alkane gases were conducted at the University of Colorado - Boulder by GC/C/Pyr/IRMS using a Trace 1310 GC equipped with an Agilent J & W GS-CarbonPLOT column (30 m length, 0.32 mm ID, 3.0 μm film) coupled to a Thermo Scientific MAT253 IRMS. Three CH_4 isotope standards purchased from Airgas (uncertainties of ± 0.3 ‰ for δ^{13}C and ± 5 ‰ for δD) and three additional standards obtained from the U.S. Geological Survey (uncertainties of ± 0.2 ‰ for δ^{13}C and ± 3 ‰ for δD) were used for calibration. Over the range of peak amplitudes of analyses reported here, the repeatability expressed as 1 s on analyses of standards is ± 0.2 ‰ for δ^{13}C and ± 3 ‰ for δD. The analytical uncertainty (accuracy) expressed as 1 standard error on a 3-point calibration was 0.4 ‰ to 0.7 ‰ for δ^{13}C and 4 ‰ to 5 ‰ for δD (Section B.1). As a consistency check, an additional analysis of $\delta^{13}C_{CH_4}$ of one sample was performed by GC/C/IRMS by Isotech laboratories with a precision of 0.3 ‰ (1 σ).

3.5.5 16S rRNA gene sequencing and analysis

Biomass for DNA extraction was concentrated by pumping 5 L to 20 L of groundwater through Millipore polycarbonate inline filters (0.22 μm pore diameter, 47 mm filter diameter). Filters were placed in cryovials, transported frozen in liquid N_2, and stored in a

−70 °C freezer until extraction. DNA was extracted from one quarter subsamples of each filter using a Qiagen PowerSoil DNA extraction kit. The V4 hypervariable region of the 16S SSU rRNA gene was amplified from purified DNA by PCR. PCR was performed in triplicate reactions using the 515F/806R primer pair at an annealing temperature of 50°C, as described previously (Hamilton et al., 2013). Amplicons from triplicate reactions were pooled, and adapters were added in triplicate reactions via five cycles of nested PCR (following the same conditions as above) with 515F/816R primers modified to include Illumina adapters. Amplicons from triplicate reactions were pooled and purified using the Wizard® PCR Preps DNA Purification System (Promega Corp.). Sequencing on the 2x150 Illumina Miseq platform was performed at the UW-Madison Biotechnology Center DNA Sequencing Facility.

Demultiplexed fastq files were quality filtered using Figaro v1.1.1 (`https://github.com/Zymo-Research/figaro`) and the DADA2 v1.16 R package (Callahan et al., 2016). Amplicon sequence variants were assigned taxonomy to the genus level using the RDP classifier (Wang et al., 2007) trained on the Silva SSU 138 reference database (Quast et al., 2012) using the DADA2 assignTaxonomy function. Sequences assigned to mitochondria, chloroplast, and Eukaryota, or not assigned at the domain level (collectively $< 1\,\%$ of sequences), were removed.

3.6 Acknowledgements

This research was directly supported by the Rock-Powered Life NASA Astrobiology Institute (NNA15BB02A). This research also used samples and/or data provided by the Oman Drilling Project. The Oman Drilling Project (OmanDP) has been possible through co-mingled funds from the International Continental Scientific Drilling Project (ICDP), the Sloan Foundation – Deep Carbon Observatory (Grant 2014-3-01, Kelemen PI), the National Science Foundation (NSF-EAR-1516300, Kelemen PI), the NASA Astrobiology Institute (NNA15BB02A), the

German Research Foundation (DFG), the Japanese Society for the Promotion of Science (JSPS), the European Research Council, the Swiss National Science Foundation, JAMSTEC, the TAMU-JR Science operator, and contributions from the Sultanate of Oman Ministry of Regional Municipalities and Water Resources, the Oman Public Authority of Mining, Sultan Qaboos University, CRNS-Univ. Montpellier II, Columbia University, and the University of Southampton.

We thank the Ministry of Regional Municipalities and Water Resources in the Sultanate of Oman (particularly Said Al Habsi, Rashid Al Abri, Salim Al Khanbashi, and Haider Ahmed Mohammed Alajmi) for allowing access to wells and logistical support, Zaher Al Sulaimani and Mazin Al Sulaimani from the Oman Water Centre and AZD Engineering for their technical and logistical support, Jude Coggon for coordinating Oman Drilling Project activities, Scott Lehman, Steve Morgan, and Chad Wolak of the INSTAAR Laboratory for AMS Radiocarbon Preparation and Research (NSRL) as well as Isotech laboratories for help with preparing CH_4 for ^{14}C analyses, Elizabeth Fones for assistance DNA sequencing, Mark Dreier for supplying CH_4 stable isotope standards, and Juan Carlos de Obeso for preparing carbonate mineral samples for mineralogical and ^{14}C analyses.

Chapter 4

Aqueous geochemical and microbial variation across discrete depth intervals in a peridotite aquifer assessed using a packer system in the Samail Ophiolite, Oman

Daniel B. Nothaft, Alexis S. Templeton, Eric S. Boyd, Juerg M. Matter, Martin Stute, Amelia N. Paukert Vankeuren, and The Oman Drilling Project Science Team

Abstract

The potential for H_2 generated via serpentinization to fuel subsurface microbial ecosystems independent from photosynthesis has prompted biogeochemical investigations of serpentinization-influenced fluids. However, samples are typically obtained from surface seeps or through open-borehole pumping. These depth-indiscriminate sampling methods have hindered the assessment of groundwater reaction histories and mixing extents, thereby obscuring the real energy availability and discrete biomes present at depth. In order to resolve distinct groundwater masses and their resident microbial communities in a low-temperature serpentinizing environment, we deployed a packer system in two 400 m-deep, peridotite-hosted wells in the Samail Ophiolite, Oman. Through isolation and pumping of discrete intervals as deep as 108 m to 132 m below ground level, multiple aquifers ranging in pH from 8 to 11 were accessed. Aqueous chemical analyses and 16S rRNA gene sequencing of deep, highly-reacted $Ca^{2+} - OH^-$ groundwaters bearing up to 4.05 μmol $\cdot$ L^{-1} H_2, 3.81 μmol $\cdot$ L^{-1} CH_4 and 946 μmol $\cdot$ L^{-1} SO_4^{2-} revealed the presence of an ecosystem dominated by bacteria related affiliated with class Thermodesulfovibrionia that likely reduce SO_4^{2-} coupled to the oxidation of H_2 and/or small organic acids generated through serpentinization. In shallower, oxidized $Mg^{2+} - HCO_3^-$ groundwaters, heterotrophic aerobes and denitrifiers were relatively more abundant. CH_4 had high $\delta^{13}C$ and δD (up to 23.9 ‰ VPDB and 45 ‰ VSMOW, respectively), indicating microbial CH_4 oxidation, particularly in $Ca^{2+} - OH^-$ that showed evidence of mixing with $Mg^{2+} - HCO_3^-$ waters. This study demonstrates how to spatially resolve subsurface energy availability and microbial community structure, which is critical for predicting the microbial activity in fractured rock ecosystems and for detecting life beyond Earth..

4.1 Introduction

Serpentinization reactions between peridotite and water can generate molecular hydrogen (H_2) (Neal and Stanger, 1983; McCollom and Bach, 2009; Miller et al., 2017b), a powerful and labile electron donor that may fuel microbial communities whose nutrient and energy cycles are independent from photosynthesis (Nealson et al., 2005). The potential relevance of such ecosystems to subsurface life on the modern and early Earth, as well as life beyond Earth, has led to numerous biogeochemical investigations of groundwaters from peridotite aquifers accessed at surface seeps or through open well pumping in ophiolites, which are continental exposures of mantle-derived rocks, including peridotites (Brazelton et al., 2012; Suzuki et al., 2014; Crespo-Medina et al., 2014; Meyer-Dombard et al., 2015; Woycheese et al., 2015; Postec et al., 2015; Rempfert et al., 2017; Canovas III et al., 2017; Brazelton et al., 2017; Crespo-Medina et al., 2017; Marques et al., 2018). These studies have produced important information about the chemistry and biology of peridotite-hosted ecosystems, but collection of surface waters, or subsurface waters sampled using depth-indiscriminate methods, tend to include significant mixing of waters with the O_2 and CO_2-bearing atmosphere, or mixing of shallow and deep fluids that are hydrologically segregated. Thus sampling methods have often hindered assessment of groundwater source regions, reaction histories, subsurface fluid mixing extents, and associated differences in microbial community structure.

The inability to differentiate the sources, residence times, and geochemical states of discrete fluids is problematic because it obscures the real energy availability and distinct biomes present. Mixing of groundwaters with disparate concentrations of dissolved inorganic carbon ($\sum CO_2$) and other redox-sensitive chemical species such as H_2, CH_4, nitrate (NO_3^-), and sulfate (SO_4^{2-}) may be widespread and underestimated in samples from seeps and open boreholes in ophiolites. Such mixing may distort understanding of the deep, peridotite-hosted biosphere by enriching samples in microbes that opportunistically consume oxidants recently derived from the atmosphere, which is a lifestyle that is incompatible with the more reduced, subsurface ecosystems that many studies seek to probe. Although there

have been few hydrologic studies of ophiolite aquifers, it is known that groundwater flow in these systems is fracture-dominated, and that these fractures occur on multiple spatial scales and are heterogeneously distributed, although generally more abundant within $\sim$ 50 m to $\sim$ 100 m of the surface (Dewandel et al., 2005; Lods et al., 2020). Variations in transmissivity and fracture spacing in ophiolite aquifers make it difficult to predict subsurface hydrologic properties at any given location, but it does suggest that when deep, long-residence time groundwaters approach the surface, they have the potential to mix with lower-residence time groundwaters hosted in shallow, relatively high-transmissivity fracture networks. This mixing may often escape notice because groundwater pH is commonly used as an indicator of the extent of reaction of the water with peridotite out of contact with the atmosphere (with highly reacted waters being hyperalkaline, often defined as pH $>$ 11), but pH is weakly sensitive to mixing of hyperalkaline groundwaters with circumneutral to moderately alkaline (pH 7 to 9) groundwaters derived from water-rock reaction in contact with the atmosphere (Leong et al., 2020).

In this study, we directly assessed the relationship between spatially heterogeneous hydrogeochemical parameters and subsurface microbial community compositions in ophiolite aquifers through the use of packers to sample groundwaters from discrete, isolated depth intervals within two 400 m-deep wells in the Samail Ophiolite, Oman. Our samples were obtained concurrently with hydrologic pumping tests (Lods et al., 2020), enabling direct comparisons of our biogeochemical data against previously and independently reported physical hydrologic interpretations. We obtained depth-resolved aqueous geochemical data from both downhole wireline logging and measurements of solute concentrations in groundwater samples pumped from defined packer intervals. Gases dissolved in the pumped groundwaters were analyzed for their aqueous concentrations and the stable isotopic compositions of CH_4 and C_2H_6. Microbial community compositions of biomass filter-concentrated from pumped groundwaters was assessed through 16S rRNA gene sequencing of DNA. We accessed discrete aquifers at multiple depths, which ranged in pH from 8 to 11 and hosted distinct microbial

communities. Hyperalkaline and reduced waters were dominated by bacteria related to class Thermodesulfovibrionia, of which cultured representatives are capable of SO_4^{2-} reduction coupled to oxidation of H_2 and/or small organic acids (Henry et al., 1994; Sekiguchi et al., 2008), while moderately alkaline waters also contained Thermodesulfovibrionia, but in comparable relative gene abundances to relatives of heterotrophic bacteria capable of respiration using O_2 and/or NO_3^-. The deployment of packers to probe the biogeochemistry of subsurface, peridotite-hosted aquifers in this study marks a considerable advance in the ability to sample deep, serpentinization-influenced fluids isolated from surficial fluids and assess the effect of mixing these fluids on microbial processes. In doing so, this study furthers understanding of where and how serpentinization-influenced ecosystems may inhabit the subsurface of Earth and celestial rocky bodies.

4.2 Site and methods

4.2.1 Site description and drilling

The Oman Drilling Project (Kelemen et al., 2013, 2020a) established a multi-borehole observatory in Wadi Lawayni in the Wadi Tayin massif of the Samail Ophiolite, which has been previously described in detail (Lods et al., 2020). Here, we focus on two 400 m deep, 6-inch diameter, rotary-drilled wells, BA1A and BA1D (Figure C.1). Well BA1A was drilled in 2017, from February 20$^{\text{th}}$ to March 2$^{\text{nd}}$, and BA1D was drilled in 2018, from February 24$^{\text{th}}$ to March 15$^{\text{th}}$. These wells are situated in the mantle section of the ophiolite, 3 km north of the crust-mantle transition zone of the ophiolite, and are spaced 15 m apart from one another. Shallow alluvium was isolated from the boreholes by installing casing during drilling, which extends to 22 m below ground level in BA1A and 26 m below ground level in BA1D. Below the surficial alluvium, drill cuttings from these wells were predominantly fully serpentinized dunite in the upper 150 m to 250 m and partially serpentinized harzburgite at greater depths (Kelemen et al., 2020a; Lods et al., 2020). The drilling fluid was a mixture of

1 volume percent "DrillFoam," a biodegradable sodium alcohol ethoxyl sulfate with chelating agents, and 99 volume percent fresh water sourced from wells elsewhere in the region. BA1A and BA1D were air lift tested immediately after well completion for well development. The air lift tests involved pumping a mixture of water and air into the well at different depths and monitoring the air-lifted discharge.

4.2.2 Fluid sampling and field measurements

Downhole wireline logs (Matter et al., 2018) were obtained using an ALT QL40 OCEAN multi parameter probe, from which temperature, electrical conductivity, pH, and oxidation-reduction potential are reported with accuracy/precision of 0.005/0.001 °C, 5/0.1 μS $\cdot$ cm^{-1}, 0.01/0.001, and 1/0.1 mV, respectively. BA1A was logged on April 22$^{\text{nd}}$, 2017 and March 16$^{\text{th}}$, 2018. BA1D was logged on March 19$^{\text{th}}$, 2018 and February 13$^{\text{th}}$, 2019.

The packer system (SolExperts) includes two inflatable rubber bladders ("packers") and a submersible pump (Grundfos SQE 1–140) (Lods et al., 2020). Inflating one or both of the packers at depth in a well enables the isolation of discrete subsurface intervals for targeted pumping. The depth intervals from which samples were collected in this study are reported in Table 4.4. The sampling setup is pictured in Figures C.2. At least a pipe string's volume of water was pumped and discarded prior to taking biogeochemical samples of groundwaters. Temperature, pH, electrical conductivity, and oxidation-reduction potential (Eh), were monitored with probes at the pump outflow before and during sampling. The values of these parameters reported in Table 4.4 reflect the time point nearest to the start of biogeochemical sampling. Shorthand sample identifiers used throughout this manuscript consist of a well name, sampling year, and sampling interval, all concatenated (see Tables 4.4 and 4.1).

4.2.3 Chemical and stable isotopic analyses of fluids

Chemical and stable isotopic analyses of fluids sampled in 2018 were conducted according to the methods reported by Nothaft et al. (2020). Analytical methods for fluids sampled

in 2019 were similar and are reported below. To analyze aqueous concentrations (c) of non-carbonaceous chemical species, samples were collected by passing groundwater through a 0.2 μm filter into polypropylene conical tubes. Solute concentrations were measured by inductively coupled plasma atomic emission spectroscopy (repeatability as median relative standard deviation of 3 % for most elements). Aqueous concentrations of F^- Cl^-, SO_4^{2-}, Br^-, and NO_3^- were measured by ion chromatography (analytical uncertainty of 5 %). Molybdate-reactive SiO_2 (reported here as $\sum$Si) was quantitated using a spectrophotometric method (ASTM, 2016). The concentration and $\delta^{13}C$ of dissolved inorganic C ($\sum CO_2$) were measured by acidification of water samples and transfer of resultant CO_2 (g) via a Thermo Fisher GasBench II to a Thermo Delta V Plus isotope ratio mass spectrometer. Details of $\sum CO_2$ analyses are available at `http://dx.doi.org/10.17504/protocols.io.zduf26w`.

Groundwaters and gases dissolved therein were sampled via syringe from a luer-lok port on the pump manifold. 60. mL of this water was then passed through a 0.2 μm filter and needle into an evacuated 117 mL glass vial capped with a blue chlorobutyl rubber stopper and Al crimp top. These are referred to as "headspace" samples. In addition, gases were sampled with the "bubble strip" method modified from Kampbell et al. (1998). Details on bubble strip gas sampling are available at `http://dx.doi.org/10.17504/protocols.io.bkb9ksr6`. H_2, CH_4, and CO concentrations in this study are reported from headspace samples due to the better accuracy of this method versus the bubble strip method, as determined in comparisons by the authors. Ethane through hexane concentrations were determined from the bubble strip samples because of the lower detection limit offered by bubble strip samples, and were normalized to the headspace gas samples through the CH_4 concentration and assumption of constant C_1/C_n ratio of both sample types, where C_n is an alkane of n C atoms. Gas concentrations were determined according to the methods of Nothaft et al. (2020).

Bulk stable isotope analyses of CH_4 and co-occurring alkane gases were conducted at the University of Colorado - Boulder (CUB) by GC/C/Pyr/IRMS using a Trace 1310 GC equipped with an Agilent J & W GS-CarbonPLOT column (30 m length, 0.32 mm ID, 3.0 μm

film) coupled to a Thermo Scientific MAT253 IRMS. Three CH_4 isotope standards purchased from Airgas (uncertainties of ±0.3 ‰ for $\delta^{13}C$ and ±5 ‰ for δD) and three additional standards obtained from the U.S. Geological Survey (uncertainties of ±0.2 ‰ for $\delta^{13}C$ and ±3 ‰ for δD) were used for calibration. Over the range of peak amplitudes of analyses reported here, the repeatability expressed as 1 s on analyses of standards is ±0.2 ‰ for $\delta^{13}C$ and ±3 ‰ for δD. The analytical uncertainty (accuracy) expressed as 1 standard error on a 3-point calibration was 0.4 ‰ to 0.7 ‰ for $\delta^{13}C$ and 4 ‰ to 5 ‰ for δD.

4.2.4 16S rRNA gene sequencing and analysis

Biomass for DNA extraction was concentrated by pumping 5 L to 20 L of groundwater through Millipore polycarbonate inline filters. In 2018, groundwaters were passed sequentially through filters with pore diameters of 0.45 μm, 0.22 μm, then 0.10 μm to test whether cell size and microbial community composition were correlated. In 2019, only 0.22 μm pore diameter filters were used. The diameter of filters was 47 mm in both years. Filters were placed in cryovials and stored for transport in liquid N_2 dewars immediately following biomass collection. Upon their arrival at CUB, filters were stored in a −70 °C freezer until extraction.

For samples collected in 2018, DNA was extracted from one quarter subsamples of each filter using a Qiagen PowerSoil DNA extraction kit. The V4 hypervariable region of the 16S rRNA gene was amplified by PCR in duplicate reactions using the 515 (Parada) - 806R (Apprill) primer pair modified to include Illumina adapters and the appropriate error-correcting barcodes, as described previously (Nothaft et al., 2020). Amplicons from duplicate reactions were pooled, cleaned, and their concentrations normalized using a Thermo Fisher SequalPrep normalization plate kit. Amplicons were sequenced on an Illumina MiSeq at the CUB Next-Generation Sequencing Facility using 2-by-150 bp paired-end chemistry.

For samples collected in 2019, DNA was extracted from one quarter subsamples of each filter using a Qiagen PowerSoil DNA extraction kit. The V4 hypervariable region of the 16S

SSU rRNA gene was amplified from purified DNA by PCR. PCR was performed in triplicate reactions using the 515 (Parada) - 806R (Apprill) primer pair at an annealing temperature of 50°C, as described previously (Hamilton et al., 2013). Amplicons from triplicate reactions were pooled, and adapters were added in triplicate reactions via five cycles of nested PCR (following the same conditions as above) with 515 (Parada) - 806R (Apprill) primers modified to include Illumina adapters. Amplicons from triplicate reactions were pooled and purified using the Wizard® PCR Preps DNA Purification System (Promega Corp.). Amplicons were sequenced on an Illumina Miseq at the UW-Madison Biotechnology Center DNA Sequencing Facility using 2-by-150 bp paired-end chemistry.

Demultiplexed fastq files were quality filtered using Figaro v1.1.1 (`https://github.com/Zymo-Research/figaro`) and the DADA2 v1.16 R package (Callahan et al., 2016). Amplicon sequence variants were assigned taxonomy to the genus level using the RDP classifier (Wang et al., 2007) trained on the Silva SSU 138 reference database (Quast et al., 2012) using the DADA2 assignTaxonomy function. Sequences assigned to mitochondria, chloroplast, and Eukaryota, or not assigned at the domain level (collectively $< 1\,\%$ of sequences), were removed.

4.3 Prior study of site hydrology

To provide context for the geochemical results that will follow, we summarize here the findings of Lods et al. (2020), who analyzed flowmeter and pumping tests at boreholes BA1A and BA1D to arrive at an integrated interpretation of the physical hydrology of BA1A and BA1D. Our samples from 2019 (Table 4.4) were collected simultaneously with, or immediately following, the pumping tests of Lods et al. (2020), facilitating comparison of our results to theirs. The depth intervals pumped by these studies were chosen to target hydraulically conductive zones in the subsurface, which were identified through the analysis of temperature profiles and flowmeter data (Lods et al., 2020). All hydraulically conductive

regions were above the transition from dunite to harzburgite in these wells, which occurs at depths of 150 m to 250 m. Interpretations of open-borehole pumping tests by Lods et al. (2020) revealed transmissivity of BA1D one order of magnitude lower than that of BA1A, with BA1D having an important leakage, which means a component of vertical flow within the formation. Pumping tests of packed intervals determined hydrologic properties with depth resolution. There were four main hydraulically productive depth regions in BA1A and BA1D: a surficial alluvial aquifer (< 22 m in BA1A, < 26 m in BA1D), an upper dunite aquifer (41 m to 75 m), an intermediate dunite aquifer (102 m to 132 m), and a lower dunite aquifer (> 133 m, only pumpable in BA1D). The interpretations of each of these intervals are paraphrased from Lods et al. (2020) below.

Flowmeter tests under ambient and forced hydraulic conditions indicated that there was an aquifer in the alluvium above the casings and that both wells were connected to it via horizontal and vertical fracture networks surrounding the wells. The transmissivity in the shallow regions of BA1A was higher than in BA1D due to BA1A's stronger connection to the surficial aquifer. An ambient downflow of $1\,\mathrm{L}\cdot\mathrm{min}^{-1}$ measured in BA1A from 22 m to 59 m indicated the displacement of substantial volumes of water from the surficial aquifer to the upper dunite aquifer at BA1A. Lesser flow may extend to the intermediate dunite aquifer at BA1A at rates below the detection limit of the flowmeter used in the experiments of Lods et al. (2020) ($< 0.1\,\mathrm{L}\cdot\mathrm{min}^{-1}$). Ambient flow was not below detectable levels at BA1D, suggesting minimal flow of surficial aquifer waters to deeper aquifers at BA1D.

The upper dunite aquifer hosted highly conductive fractures between 41 m and 75 m depth. Tests of pumping in BA1A indicated channelized, 1-dimensional flow between BA1A and BA1D in this interval. This channelized structure was interpreted as an open or partially mineralized fracture connected to the boreholes directly or through a conduit. All the pumped flow from BA1A in that interval could be accommodated through this channel. However, during pumping of BA1D in that interval, additional vertical flow from the formation near BA1D above and below the pumped interval was required to accommodate the

pumped flow.

In contrast to the upper dunite aquifer, the intermediate dunite aquifer located between 102 m and 132 m displayed no evidence of conductive structures with channelized flow. Rather, heterogeneities in the directions of flow contributing to the pumping tests were inferred. Specifically, the pumping in BA1A was supplied by both horizontal and vertical flows that were located near and far from the pumped borehole. Pumping in BA1D was also supplied by horizontal and vertical flows near the pumped borehole, but only horizontal flows further away, in the vicinity BA1A. The authors speculated that a component the water pumped during the BA1D test could have derived from the highly conductive fractures in the shallower regions near BA1A, with this water flowing downward through the BA1A borehole and then horizontally to BA1D via fractures in the intermediate dunite aquifer region.

A lower dunite aquifer (> 133 m) was found to be pumpable only in BA1D. Vertical connections around BA1D link this lower part of the system to the intermediate part of BA1D (and then to BA1A via horizontal connections). Heterogeneities in vertical connections between BA1A and BA1D (i.e. less vertical connection in BA1A) resulted in this deep interval being pumpable in BA1D, but not BA1A. No samples of the lower dunite aquifer were obtained for the present study due to low sustainable flow rates in this interval ($0.5\,\mathrm{L\cdot min^{-1}}$).

4.4 Results

4.4.1 Aquifer geochemistry: drilling, mixing, and recovery

During drilling, a strong smell of sulfide was evident within tens of meters of BA1A, suggesting sulfidic conditions in the subsurface at the time of drilling. In well logs acquired shortly after drilling of BA1A in 2017 and BA1D in 2018, Eh values were 100 mV to 200 mV throughout most of the depth profile (Figure 4.1), indicating the presence of oxidized fluids that were likely introduced at depth through drilling. In well logs obtained at BA1A in

2018, a year after the drilling of that well, the chemical state of the upper 200 m of the depth profile was essentially unchanged since 2017, but the lower 200 m of the depth profile showed a relative increase in pH of 0.4, a stark decrease in *Eh* of 800 mV, and an increase in conductivity of up to 0.3 $mS \cdot cm^{-1}$. These data indicate at least partial recovery towards reduced, hyperalkaline conditions at depths > 200 m at BA1A from 2017 to 2018. Similarly, in BA1D well logs obtained in 2019, a year after the drilling of that well, an increase in pH of 0.5, a stark decrease in *Eh* of up to 700 mV, and an increase in conductivity of up to 0.8 $mS \cdot cm^{-1}$ relative to the 2018 log were observed throughout most of the depth profile. A notable difference between BA1A and BA1D well logs recorded a year after drilling is that the conditions in BA1A transition from moderately alkaline and oxidized to hyperalkaline and reduced at $\sim$ 150 m depth, while in BA1D, hyperalkaline and reduced conditions are reached at relatively shallow depths (40 m) and maintained to the bottom of the well (Figure 4.1).

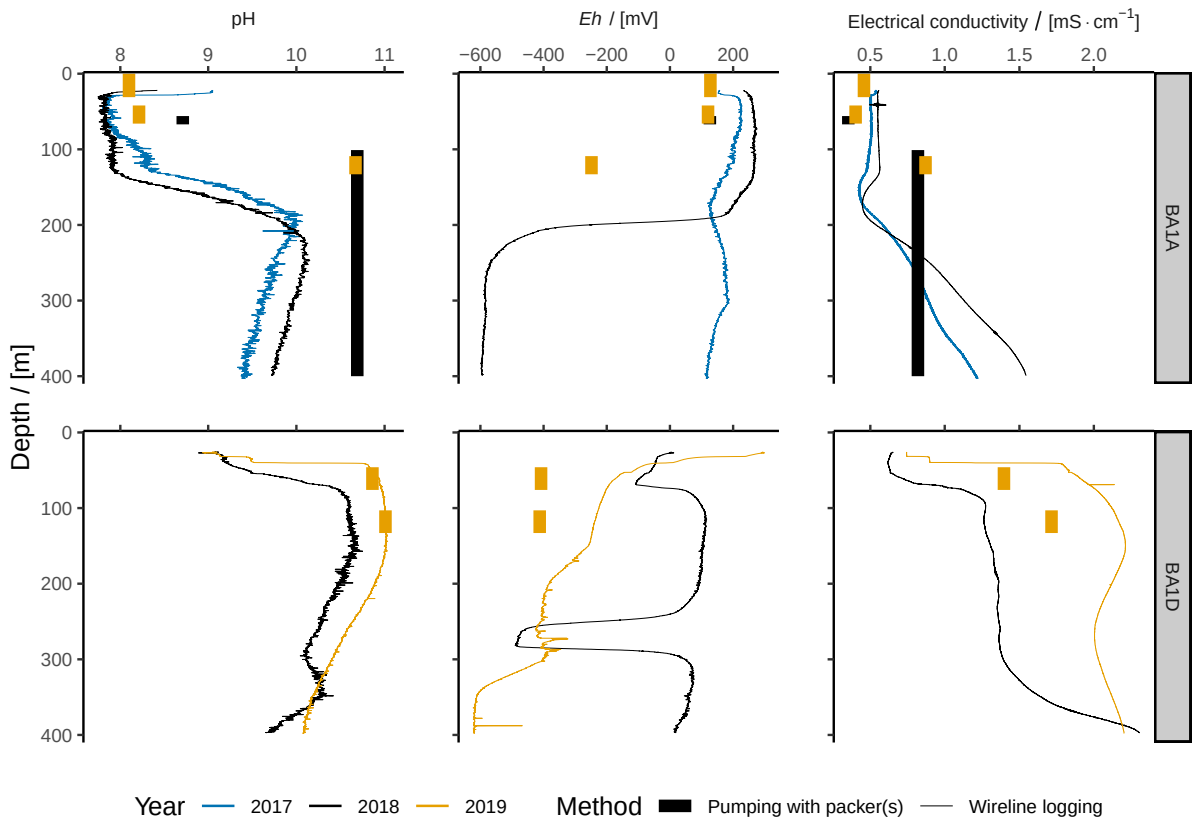

Figure 4.1: *Eh*, pH, and conductivity from well logs and pumped samples from BA1A and BA1D. All depths referenced to ground level. Well log data within the cased intervals (above 22 m for BA1A and 26 m for BA1D) are not shown to better highlight trends in the sections of the wells that direct communicate with surrounding formation fluids.

The *Eh*, pH, and electrical conductivity values of samples pumped from discrete intervals using packers generally exhibit similar trends with depth to those of the well logs obtained a year after drilling, but there are some discrepancies between the logs and pumped samples (Figure 4.1; Table 4.4). For instance, the transition from moderately alkaline, oxidized, low-electrical conductivity fluids to hyperalkaline, reduced, high-electrical conductivity conditions in BA1A occurs $\sim$ 50 m deeper in the well logs relative to the pumped samples. In addition, the pumped samples of BA1A reach a maximum pH that is 0.5 higher than that recorded in its well logs. At BA1D, pH values of pumped samples from 2019 overlap with those of well logs measured in the same year and at equivalent intervals, but the pumped samples had *Eh* values 200 mV lower and electrical conductivity values 0.5 mS $\cdot$ cm^{-1} lower

than the well logs.

As expected based on pH, Eh, and electrical conductivity (Figure 4.1, Table 4.4), the pH 8.1 to 8.7 waters in the upper 70 m of BA1A are $Mg^{2+}-HCO_3^-$ waters, and the pH 10.6 to 11.0 waters at both sampled depths in BA1D and in the ≥ 100 m-depth samples from BA1A are $Ca^{2+}-OH^-$ waters (Table 4.1). These are the two commonly observed water compositions in ophiolite aquifers, where $Mg^{2+}-HCO_3^-$ waters are considered to communicate openly with the atmosphere and have shorter residence times, while $Ca^{2+}-OH^-$ waters have extensively reacted with peridotite in regions of the subsurface closed to atmospheric inputs (Barnes et al., 1967; Barnes and O'Neil, 1969; Neal and Stanger, 1985; Bruni et al., 2002; Cipolli et al., 2004; Kelemen et al., 2011; Paukert et al., 2012; Leong and Shock, 2020). These water types are known to vary widely in $\sum$Si concentrations, as mineral dissolution in waters open to the atmosphere increases $c_{\sum \mathrm{Si}}$ in $Mg^{2+}-HCO_3^-$ waters, while continued reaction under closed system, lower water/rock conditions leads towards chrysotile-brucite-calcite-diopside equilibrium in $Ca^{2+}-OH^-$ waters and draws $\sum$Si to $\mu\mathrm{mol}\cdot\mathrm{L}^{-1}$ to $10^2\,\mathrm{nmol}\cdot\mathrm{L}^{-1}$ levels (Leong et al., 2020). Leong et al. (2020) proposed the use of $\sum$Si as a tracer of mixing in ophiolitic groundwaters, noting its relatively conservative behavior in these systems and its stronger sensitivity to mixing than pH. Adopting the Leong et al. (2020) framework, we have plotted the $c_{\sum \mathrm{Si}}$ and pH of our samples in Figure 4.2. The shallowest sample in this study, BA1A_2019_0–30, had the highest $c_{\sum \mathrm{Si}}$ of the data set ($333\,\mu\mathrm{mol}\cdot\mathrm{L}^{-1}$), which is typical of $Mg^{2+}-HCO_3^-$ waters. Other samples fall below this, but do not quite reach the low levels representative of chrysotile-brucite-calcite±diopside equilibrium as in end member $Ca^{2+}-OH^-$ waters, suggesting that they represent mixtures of varying proportions of $Mg^{2+}-HCO_3^-$ and $Ca^{2+}-OH^-$ end-member waters.

Table 4.1: Chemical composition of water samples.

Sample ID	$\sum CO_2$	$\sum Na$	$\sum Ca$	$\sum Mg$	$\sum Si$	NO_3^-	SO_4^{2-}	Cl^-
BA1A_2018_55-66	1.32×10^3	8.36×10^2	3.91×10^2	7.06×10^2	1.97×10^2	2.40×10^2	2.70×10^2	1.27×10^3
BA1A_2018_100-400	3.74×10^1	2.81×10^3	1.57×10^3	5.00×10^1	4.49×10^1	1.85×10^2	5.18×10^2	4.65×10^3
BA1A_2019_0-30	3.18×10^3	5.13×10^2	5.89×10^2	1.38×10^3	3.33×10^2	1.21×10^2	3.21×10^2	9.34×10^2
BA1A_2019_41-65	1.42×10^3	6.83×10^2	3.64×10^2	1.05×10^3	1.56×10^2	9.03×10^1	3.36×10^2	1.27×10^3
BA1A_2019_108-132	$< 2.82 \times 10^2$	3.36×10^3	1.69×10^3	1.02×10^1	2.13×10^1	$< 8.06 \times 10^{-1}$	4.67×10^2	5.96×10^3
BA1D_2019_45-75	n.d.	4.03×10^3	2.55×10^3	2.20×10^1	8.51	$< 8.06 \times 10^{-1}$	9.46×10^2	8.51×10^3
BA1D_2019_102-132	n.d.	5.18×10^3	2.92×10^3	1.56	5.88	$< 8.06 \times 10^{-1}$	5.91×10^2	6.87×10^3

Concentrations reported in μmol $\cdot$ L^{-1}. $\sum$ indicates the sum of all dissolved species of the element. "n.d." = "not determined."

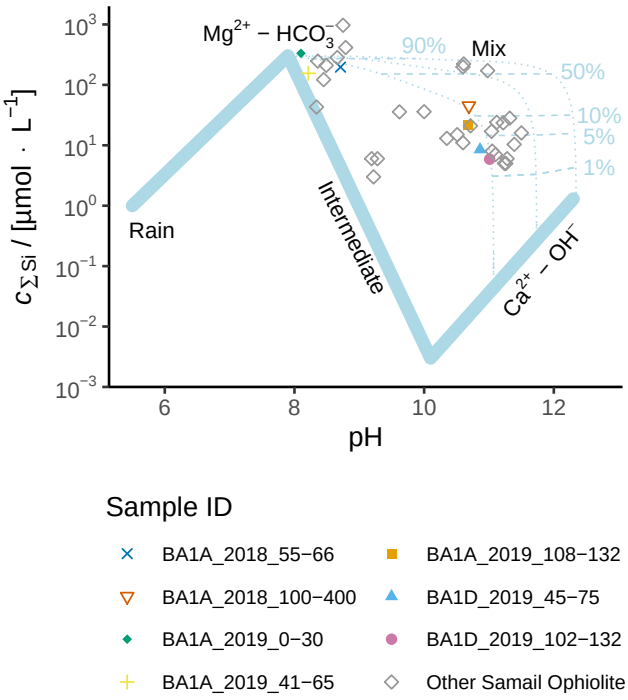

Figure 4.2: $\sum$Si vs. pH plot, after Leong et al. (2020). The thick blue line corresponds to reaction path modeling starting from rain, progressing to moderately alkaline $Mg^{2+} - HCO_3$ waters as a response to mineral dissolution open to the atmosphere, then intermediate waters in early stages of serpentinization closed to the atmosphere, which later become hyperalkaline $Ca^{2+} - OH^-$ waters as they approach chrysotile-brucite-calcite±diopside equilibrium. Three potential end member $Ca^{2+} - OH^-$ water compositions (differing in their $c_{\sum CO_2}$ from 8 μmol $\cdot$ kg^{-1} to 20 μmol $\cdot$ kg^{-1}) form one side of a mixing trend to a typical $Mg^{2+} - HCO_3$ water composition. Si, which is the most conservative tracer of mixing available in ophiolites, is used to distinguish extents of mixing between $Ca^{2+} - OH^-$ and $Mg^{2+} - HCO_3$ waters (shown in plot as percentages next to mixing tie-lines). Mixing extents calculated for our samples are tabulated in Table C.1. Other Samail Ophiolite data from Miller et al., 2016; Rempfert et al., 2017; Kraus et al., 2018; Nothaft et al., 2020

In the $Mg^{2+} - HCO_3^-$ waters in the upper 70 m of BA1A, the dissolved inorganic carbon ($\sum CO_2$) ranged in concentration (c) from 1320 μmol·L^{-1} to 3180 μmol·L^{-1}, which is similar to $c_{\sum CO_2}$ in other $Mg^{2+} - HCO_3^-$ waters in the ophiolite (Neal and Stanger, 1985; Rempfert et al., 2017; Vankeuren et al., 2019; Nothaft et al., 2020), and consistent with uptake of atmospheric CO_2 into these moderately alkaline waters (Bruni et al., 2002; Cipolli et al., 2004; Paukert et al., 2012; Leong and Shock, 2020). In the $Ca^{2+} - OH^-$ waters sampled at $\geq$ 100 m depths at BA1A, $c_{\sum CO_2}$ was 37.4 $\mu mol \cdot L^{-1}$ in 2018 and below the limit of quantitation in 2019 ($< 282\,\mu mol \cdot L^{-1}$; Table 4.1). Hyperalkaline groundwaters sampled from certain other wells in 2018, including the nearby (within 2 km), pH $\sim$ 11.4 well, NSHQ14, for which $c_{\sum CO_2}$ was measured in the same analytical session as BA1A_2018_100-400, had $c_{\sum CO_2}$ below the limit of quantitation in 2018 ($< 12\,\mu mol \cdot L^{-1}$; Nothaft et al., 2020). These lower values are consistent with water-harzburgite reaction path modeling that terminates at chrysotile-brucite-diopside-calcite equilibrium, corresponding to a $c_{\sum CO_2}$ of 8 $\mu mol \cdot L^{-1}$ at 25 °C and 1 bar (Leong and Shock, 2020). Thus, the relatively higher $c_{\sum CO_2}$ in BA1A_2018_100-400 suggests that that sample does not represent true $Ca^{2+} - OH^-$ end-member water, but rather is the product of groundwater mixing or moderate extents of water-rock reaction. Though not necessarily on the compositional extremes of peridotite-hosted groundwaters, $\sum CO_2$ concentrations in the tens of $\mu mol \cdot L^{-1}$ or less in the $Ca^{2+} - OH^-$ waters of BA1A and BA1D are still quite low in a general sense (e.g. compared to seawater at 2.1 mmol $\cdot$ L^{-1} or river water at 50 $\mu mol \cdot L^{-1}$ to 500 $\mu mol \cdot L^{-1}$; Zeebe and Wolf-Gladrow, 2001; Waldron et al., 2007). Thus, inorganic C limitation may affect microbial metabolic processes in the $Ca^{2+} - OH^-$ waters within BA1A and BA1D aquifers, particularly considering that inorganic C would be speciated primarily as the relatively bio-unavailable forms, CO_3^{2-} and $CaCO_3$ (aq), at these conditions.

Concentrations of the reduced gases H_2 and CH_4 ranged up to 4.05 $\mu mol \cdot L^{-1}$ and 3.81 $\mu mol \cdot L^{-1}$, respectively, in $Ca^{2+} - OH^-$ waters of BA1A and BA1D, but H_2 and CH_4 were below limits of quantitation in the $Mg^{2+} - HCO_3^-$ waters of the upper 70 m of BA1A

(Table 4.2), consistent with the differing Eh of these waters (Table 4.4). The concentrations of H_2 and CH_4 in the $Ca^{2+} - OH^-$ waters are high in comparison to near-surface aquifers in sedimentary settings, where H_2 concentrations rarely exceed $10\,\mathrm{nmol \cdot L^{-1}}$, even under the most reduced conditions (Lovley et al., 1994; Kampbell et al., 1998), but they are moderate in the context of peridotite aquifers, as in the Samail Ophiolite, where groundwaters accessed at wells can have H_2 and CH_4 concentrations in the hundreds to thousands of $\mu\mathrm{mol \cdot L^{-1}}$ (Paukert, 2014; Nothaft et al., 2020). In addition, $C_2 - C_6$ alkane gases were detected in some samples (Table 4.2). In samples with quantitatable C_2H_6, CH_4/C_2H_6 ratios ranged from 14.6 to 106, which is lower than $CH_4/(C_2H_6 \pm C_3H_8)$ ratios previously reported in samples from the Samail Ophiolite, which have ranged from 10^2 to 10^4 (Figure C.3; Etiope et al., 2015; Vacquand et al., 2018; Nothaft et al., 2020).

In order to assess the availability of oxyanions as terminal electron acceptors for microbial metabolism, NO_3^- and SO_4^{2-} concentrations were measured (Table 4.1). In samples of BA1A taken in 2018, NO_3^- concentrations were higher in samples from depths of 55 m to 66 m ($240.\,\mu\mathrm{mol \cdot L^{-1}}$) than in samples from depths of 100 m to 400 m ($185\,\mu\mathrm{mol \cdot L^{-1}}$). In samples of BA1A taken in 2019, a trend of decreasing $c_{NO_3^-}$ with increasing depth was also observed, with samples from depths of 0 m to 30 m, 41 m to 65 m, and 108 m to 132 m having NO_3^- concentrations of $132\,\mu\mathrm{mol \cdot L^{-1}}$, $90.3\,\mu\mathrm{mol \cdot L^{-1}}$, and below the limit of quantitation ($< 0.806\,\mu\mathrm{mol \cdot L^{-1}}$), respectively. The higher end of these NO_3^- concentrations are within the range previously reported for $Mg^{2+} - HCO_3^-$ waters sampled from wells in the ophiolite (Rempfert et al., 2017; Nothaft et al., 2020). NO_3^- was below the limit of quantitation in samples from BA1D. Thus, concentrations of NO_3^- were higher in more oxidized aquifers at BA1A and BA1D (Table 4.4; Figure 4.1).

In contrast, SO_4^{2-} concentrations were generally higher in more reduced water samples (Table 4.1; Figure C.5). SO_4^{2-} was present at notably high concentrations for $Ca^{2+} - OH^-$ waters in a freshwater serpentinizing setting (cf. Sabuda et al., 2020), with $c_{SO_4^{2-}}$ reaching $946\,\mu\mathrm{mol \cdot L^{-1}}$ in BA1D_2019_45-75. To compare these values with other groundwaters

Table 4.2: Aqueous gas concentrations, reported in $\mu\text{mol} \cdot \text{L}^{-1}$.

Sample ID	H_2	CO	CH_4	C_2H_6	C_3H_8	i-C_4H_{10}	n-C_4H_{10}	i-C_5H_{12}	n-C_5H_{12}	C_6H_{14}[a]
BA1A_2018_55-66	$< 5.98 \times 10^{-1}$	$< 1.32 \times 10^{-1}$	$< 1.18 \times 10^{-1}$	$< 9.88 \times 10^{-4}$	$< 7.60 \times 10^{-4}$	$< 4.61 \times 10^{-4}$	$< 5.78 \times 10^{-4}$	$< 3.43 \times 10^{-4}$	$< 3.81 \times 10^{-4}$	$< 2.81 \times 10^{-4}$
BA1A_2018_100-400	4.05	$< 1.32 \times 10^{-1}$	2.42×10^{-1}	$< 9.88 \times 10^{-4}$	$< 7.60 \times 10^{-4}$	$< 4.61 \times 10^{-4}$	3.89×10^{-2}	$< 3.43 \times 10^{-4}$	$< 3.81 \times 10^{-4}$	8.80×10^{-4}
BA1A_2019_0-30	< 3.29	$< 2.04 \times 10^{-2}$	$< 6.70 \times 10^{-1}$	$< 8.63 \times 10^{-3}$	$< 6.81 \times 10^{-3}$	$< 4.13 \times 10^{-3}$	$< 5.45 \times 10^{-3}$	$< 3.27 \times 10^{-3}$	$< 3.63 \times 10^{-3}$	$< 2.77 \times 10^{-3}$
BA1A_2019_41-65	< 3.29	$< 2.04 \times 10^{-2}$	$< 6.70 \times 10^{-1}$	$< 8.63 \times 10^{-3}$	$< 6.81 \times 10^{-3}$	$< 4.13 \times 10^{-3}$	$< 5.45 \times 10^{-3}$	$< 3.27 \times 10^{-3}$	$< 3.63 \times 10^{-3}$	$< 2.77 \times 10^{-3}$
BA1A_2019_108-132	< 3.29	$< 2.04 \times 10^{-2}$	1.05	7.16×10^{-2}	$< 6.81 \times 10^{-3}$	$< 4.13 \times 10^{-3}$	$< 5.45 \times 10^{-3}$	$< 3.27 \times 10^{-3}$	$< 3.63 \times 10^{-3}$	$< 2.77 \times 10^{-3}$
BA1D_2019_45-75	< 3.29	$< 2.04 \times 10^{-2}$	2.30	2.16×10^{-2}	$< 6.81 \times 10^{-3}$	$< 4.13 \times 10^{-3}$	$< 5.45 \times 10^{-3}$	$< 3.27 \times 10^{-3}$	$< 3.63 \times 10^{-3}$	$< 2.77 \times 10^{-3}$
BA1D_2019_102-132	3.55	$< 2.04 \times 10^{-2}$	3.81	1.27×10^{-1}	$< 6.81 \times 10^{-3}$	$< 4.13 \times 10^{-3}$	$< 5.45 \times 10^{-3}$	$< 3.27 \times 10^{-3}$	$< 3.63 \times 10^{-3}$	$< 2.77 \times 10^{-3}$

[a]Hexane isomers not chromatographically resolved.

sampled from wells in Oman (Figure C.5), most $Ca^{2+}-OH^-$ waters have SO_4^{2-} concentrations in the tens of $\mu mol \cdot L^{-1}$ and rarely exceed $500\,\mu mol \cdot L^{-1}$, while $Mg^{2+}-HCO_3^-$ waters typically range from $100\,\mu mol \cdot L^{-1}$ to $1000\,\mu mol \cdot L^{-1}$, and gabbro waters range from $500\,\mu mol \cdot L^{-1}$ to $4000\,\mu mol \cdot L^{-1}$. The co-existence of SO_4^{2-} approaching $mmol \cdot L^{-1}$ levels and H_2 at $\mu mol \cdot L^{-1}$ levels in some $Ca^{2+} - OH^-$ waters at BA1A and BA1D could make microbial SO_4^{2-} reduction coupled to H_2 oxidation a viable metabolism in those waters.

4.4.2 Stable isotopic compositions of water, $\sum CO_2$, CH_4 and C_2H_6

To trace H and C through the BA1 system, the stable isotopic compositions of water, $\sum CO_2$, CH_4 and C_2H_6 were measured. Groundwater δD and $\delta^{18}O$ plotted near local and global meteoric water lines (Weyhenmeyer et al., 2002; Terzer et al., 2013), indicating that the groundwaters derive from rain (Table 3.4; Figure C.4; Matter et al., 2006; Miller et al., 2016; Vankeuren et al., 2019; Nothaft et al., 2020). The $\delta^{13}C_{\sum CO_2}$ of $Mg^{2+} - HCO_3^-$ waters in the upper 70 m of BA1A ranged from $-14.64\,‰$ VPDB to $-14.15\,‰$ VPDB (Table 4.1), which is within the range of $\delta^{13}C_{\sum CO_2}$ of $Mg^{2+} - HCO_3^-$ waters elsewhere in the ophiolite ($-15.56\,‰$ VPDB to $-10.88\,‰$ VPDB; Matter et al., 2006; Nothaft et al., 2020). These values are considerably lower than seawater $\delta^{13}C_{\sum CO_2}$, which ranges from $0\,‰$ VPDB to $2\,‰$ VPDB (Zeebe and Wolf-Gladrow, 2001). This difference is peculiar because, like seawater, $Mg^{2+} - HCO_3^-$ waters in ophiolites have HCO_3^- as the dominant $\sum CO_2$ species and are widely thought to be in equilibrium with atmospheric CO_2 (Neal and Stanger, 1985; Bruni et al., 2002; Cipolli et al., 2004; Paukert et al., 2012; Leong and Shock, 2020). In comparison to the $Mg^{2+} - HCO_3^-$ water at BA1A, a deeper sample (BA1A_2018_100-400) bearing $Ca^{2+} - OH^-$ water had notably lower $\delta^{13}C_{\sum CO_2}$ ($-18.0\,‰$ VPDB; Table 4.3). The dynamics of $\delta^{13}C_{\sum CO_2}$ in this system will be discussed further in Section 4.5.4.

Three samples had sufficient CH_4 for accurate isotopic analysis through our methods (Table 4.3). BA1D_2019_102-132 had a $\delta^{13}C_{CH_4}$ of $3.8\,‰$ VPDB, which is high compared to CH_4 typically found in sedimentary settings, but within the range of CH_4 in serpen-

Table 4.3: Stable isotopic compositions of water, $\sum CO_2$, CH_4 and C_2H_6.

Sample ID	δD_{H_2O}	$\delta^{18}O_{H_2O}$	$\delta^{13}C_{\sum CO_2}$	$\delta^{13}C_{CH_4}$	δD_{CH_4}	$\delta^{13}C_{C_2H_6}$
BA1A_2018_55-66	−10.9	−2.55	−14.64	n.d.	n.d.	n.d.
BA1A_2018_100-400	−9.4	−2.17	−18.0	n.d.	n.d.	n.d.
BA1A_2019_0-30	−10.8	−2.44	−14.15	n.d.	n.d.	n.d.
BA1A_2019_41-65	−9.77	−2.27	−14.32	n.d.	n.d.	n.d.
BA1A_2019_108-132	−3.92	−0.91	n.d.	23.9	45	n.d.
BA1D_2019_45-75	−4.52	−1.04	n.d.	12.8	−111	n.d.
BA1D_2019_102-132	−6.9	−1.59	n.d.	3.8	−112	−2.5

All δ values reported in ‰ units. $\delta^{18}O$ and δD reported relative to VSMOW. $\delta^{13}C$ reported relative to VPDB. "n.d." = "not determined."

tinizing settings, including the Samail Ophiolite (Figure 4.3; Milkov and Etiope, 2018). BA1D_2019_45-75 had a $\delta^{13}C_{CH_4}$ of 12.8 ‰ VPDB, which is higher than previously reported for CH_4 in Samail Ophiolite, and BA1A_2019_108-132 had even higher $\delta^{13}C_{CH_4}$ (23.9 ‰ VPDB).

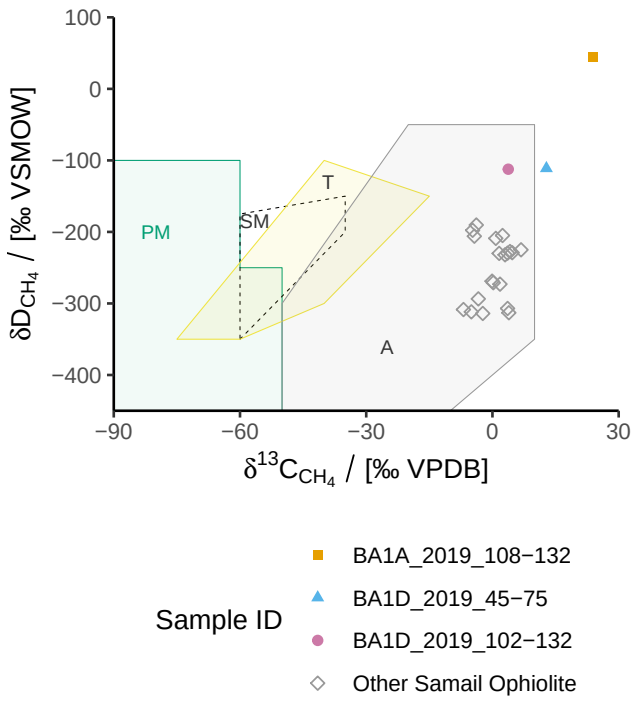

Figure 4.3: Plot of δD_{CH_4} vs. $\delta^{13}C_{CH_4}$ of samples from BA1A and BA1D with previously published Samail Ophiolite samples (Etiope et al., 2015; Vacquand et al., 2018; Nothaft et al., 2020) shown in black for context. Shaded fields of typical gas origin after Milkov and Etiope (2018). *Abbreviations:* PM, primary microbial; SM, secondary microbial; T, thermogenic; A, abiotic.

In addition to CH_4, there was sufficient C_2H_6 for isotopic analysis in sample BA1D_2019_102-132, and this C_2H_6 was also ^{13}C-enriched (−2.5 ‰ VPDB; Table 4.3) compared to C_2H_6 typically found in sedimentary settings (Prinzhofer and Huc, 1995), but this $\delta^{13}C_{C_2H_6}$ value is generally similar to that previously reported for C_2H_6 in the Samail Ophiolite (Figure 4.4; Fritz et al., 1992; Nothaft et al., 2020), suggesting an abiotic source of C_2H_6 at BA1D. The $\delta^{13}C_{C_2H_6}$ of BA1D_2019_102-132 is notably similar (within 3.5 ‰) to that of well NSHQ14 (Nothaft et al., 2020), which is only 2 km down-gradient within the same catchment, potentially suggesting a similar source of C_2H_6 in these wells.

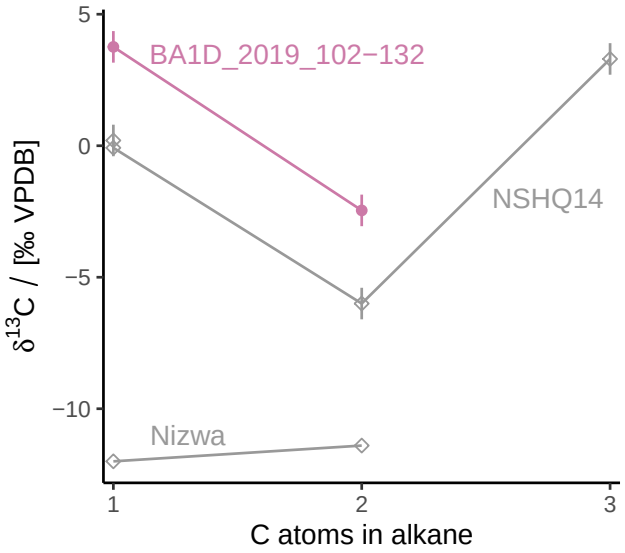

Figure 4.4: Plot of $\delta^{13}C$ of CH_4 and co-occurring n-alkanes vs. the number of C atoms per molecule. Error bars represent uncertainties on $\delta^{13}C$ analyses performed at CUB. Only samples for which $\delta^{13}C_{C_2}$ was determined are plotted. Contextual data from the Samail Ophiolite at Nizwa (Fritz et al., 1992) and well NSHQ14 (Nothaft et al., 2020).

The δD_{CH_4} at BA1D (−111 ‰ VSMOW to −112 ‰ VSMOW; Table 4.3) is higher than that of samples previously reported from the Samail Ophiolite (Figure 4.3), but is similar to that of samples from sediment-poor seafloor hydrothermal vents that are near isotopic equilibrium with ocean water at 270 °C to 360 °C (Wang et al., 2018) and is similar to some samples from ophiolites, including those in the Philippines (Abrajano et al., 1990) and Turkey (Young et al., 2017), where dominantly abiotic sources of CH_4 have been proposed. Thus, it is plausible, from the perspective of δD_{CH_4}, that BA1D CH_4 formed abiotically and equilibrated, potentially at 270 °C to 360 °C, with water with δD similar to that of seawater. The δD_{CH_4} of BA1A_2019_108-132, however, is extraordinarily high (45 ‰ VSMOW). Noting that the δD of water at BA1A, BA1D, and other wells in the Samail Ophiolite is within 15 ‰ of VSMOW (Table 4.1; Miller et al., 2016; Vankeuren et al., 2019; Nothaft et al., 2020), such high δD of CH_4 from BA1A_2019_108-132 cannot plausibly be explained by CH_4 having equilibrated with water (Horibe and Craig, 1995), and it is unlikely to have been produced through kinetic processes, in which CH_4 would be expected to be D-depleted with respect to the H of its precursor. Thus, the δD_{CH_4} of BA1A_2019_108-132 likely indi-

cates post-genetic fractionating processes, such as microbial CH_4 oxidation. CH_4 oxidation is also compatible with the low $CH_4/(C_2H_6 + C_3H_8)$ in BA1A and BA1D samples, particularly BA1A_2019_108-132 ($CH_4/C_2H_6 = 14.6$), relative to other samples from the Samail Ophiolite (Figure C.3).

4.4.3 16S rRNA gene sequencing

To assess microbial community composition, 16S rRNA genes of DNA extracted from biomass filter-concentrated from groundwaters pumped from wells were amplified and sequenced. 16S rRNA gene reads affiliated with class Thermodesulfovibrionia were dominant in the BA1A and BA1D data set, accounting for upwards of 90 % of reads in some samples (Figure 4.5), particularly those with low *Eh* (Table 4.4). Cultured representatives of Thermodesulfovibrionia are capable of SO_4^{2-} reduction coupled to H_2 oxidation and may additionally/alternatively oxidize C_1-C_3 acids and use thiosulfate, sulfite, Fe^{3+} or NO_3^- as terminal electron acceptors for anaerobic respiration (Henry et al., 1994; Sekiguchi et al., 2008). The high relative abundance of Thermodesulfovibrionia, especially in samples that are reduced, contain up to $\mu mol \cdot L^{-1}$ levels of H_2, approach $mmol \cdot L^{-1}$ levels of SO_4^{2-}, and have below quantitatable (sub-$\mu mol \cdot L^{-1}$) levels of NO_3^-, suggests that microbial sulfate reduction may be an important process in the subsurface at BA1A and BA1D.

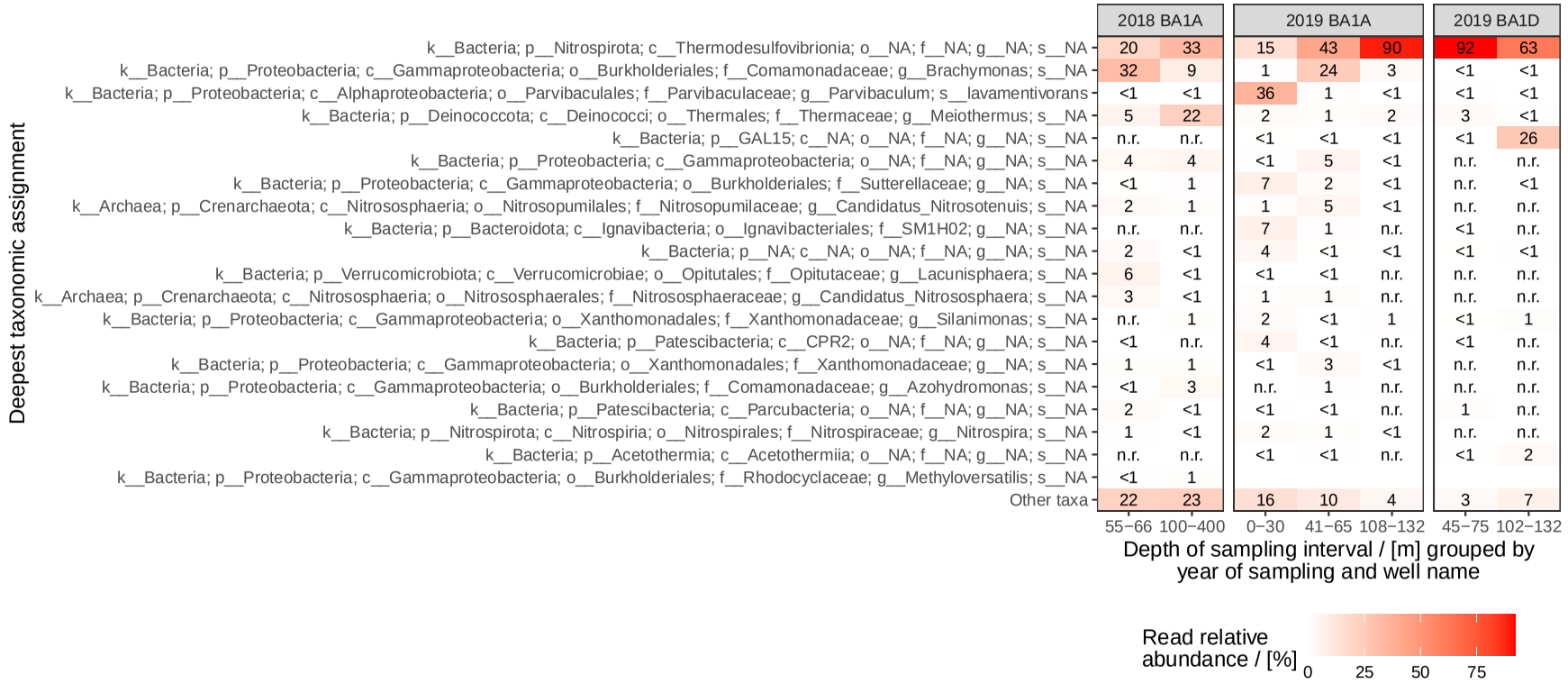

Figure 4.5: 16S rRNA gene read relative abundances of 20 most abundant taxonomic assignments in DNA extracted from 0.22 μm-filter-concentrated groundwaters from BA1A and BA1D . Read relative abundances are reported as percentages rounded to the ones place. Cases when a taxon was detected in a sample and was $< 1\,\%$ read relative abundance after rounding are labeled "< 1". Cases when no reads of a taxon were detected in a sample, but when that taxon was detected in 16S gene reads of other Oman samples obtained during the same sampling year, are labeled "n.r." Cases when no reads were detected in any Oman sample within the data set of a given year are blank.

Taxa that had markedly higher relative abundances of 16S rRNA genes in the more oxidized waters sampled from the upper 70 m of BA1A include relatives of the genus *Brachymonas* and the species *Parvibaculum lavamentivorans* (Figure 4.5). Cultured representatives of *Brachymonas* are heterotrophic and respire using molecular oxygen, and in some cases nitrate, as terminal electron acceptors (Hiraishi et al., 1995; Halpern et al., 2009). A close relative of *Brachymonas denitrificans* was enriched for in a microcosm given a H_2 headspace and amended with formate innoculated with groundwater sampled from wells in the Coast Range Ophiolite, USA (Crespo-Medina et al., 2014), indicating that *Brachymonas* relatives can thrive in anaerobic conditions in serpentinization-derived fluids. *Parvibaculum lavamentivorans* isolates are aerobic heterotrophs (Schleheck et al., 2011), but *Parvibaculum* species have also been detected through culture-independent methods in enrichment cultures under anaerobic, denitrifying conditions (Blöthe and Roden, 2009; De Weert et al., 2011). The high relative abundances of *Brachymonas*- and *Parvibaculum lavamentivorans*-affiliated 16S rRNA gene reads in the more oxidized parts of BA1A, taken together with the trends of decreasing $c_{NO_3^-}$ with increasing depth at BA1A (Section 4.4.1), suggest that heterotrophic, aerobic and/or denitrifying microbial metabolisms may be active in those regions of the subsurface.

Taxa that also had high 16S rRNA gene relative abundances in some samples, but whose metabolic functions are more enigmatic, include relatives of the genus *Meiothermus*. 16S rRNA gene reads affiliated with *Meiothermus* were detected in all BA1A and BA1D samples, but had the highest relative abundance (22 % of reads) in the sample BA1A_2018_100-400 (Figure 4.5). Although *Eh* was not directly measured for BA1A_2018_100-400, this sample had $4.05\,\mu\text{mol} \cdot \text{L}^{-1}$ H_2 (Table 4.2) and a pH of 10.69 (Table 4.1), indicating that it was reduced, which would be consistent with a sample from a similar depth interval taken the following year (BA1A_2019_108-132), which had an *Eh* of $-249\,\text{mV}$ (Table 4.4). *Meiothermus* has been a confounding taxon in 16S rRNA gene surveys of the Samail Ophiolite subsurface because *Meiothermus* isolates from the literature are obligately aerobic (although

some can reduce NO_3^- to NO_2^-; Habib et al., 2017; Raposo et al., 2019), yet *Meiothermus*-affiliated 16S rRNA gene sequences have consistently accounted for high percentages of reads from the most reduced (lowest f_{O_2}) groundwater samples from wells in the Samail Ophiolite, where they apparently cohabitate with obligate anaerobes (Miller et al., 2016; Rempfert et al., 2017; Kraus et al., 2018; Nothaft et al., 2020). Previous studies of the ophiolite have suggested that *Meiothermus* could have been respiring anaerobically, or could have been inhabiting shallow, oxic waters that were mixed in with deeper, anoxic waters during open-borehole pumping (Miller et al., 2016; Rempfert et al., 2017). The present study's finding of high relative abundances of *Meiothermus* 16S rRNA gene reads in a sample obtained through pumping of a > 100 m depth interval isolated using packers favors the interpetation that *Meiothermus* are indeed capable of functioning anaerobically in the subsurface, rather than being strictly aerobic, shallow-residing microbes entrained into samples through depth-indiscriminate pumping methods.

Another enigmatic taxon is candidate phylum GAL15, which comprised 26 % of 16S rRNA gene reads in the sample BA1D_2019_102-132 (Figure 4.5). No genomes or cultured isolates from this taxon have been published, so its traits can only be inferred indirectly. The relative abundance of GAL15 in 16S rRNA gene amplicon sequences and shotgun metagenomic sequences was found to positively correlate with increasing soil depth in a study of 20 soil profiles in diverse ecological settings throughout the United States, suggesting that members of GAL15 are well-suited to the oligotrophic conditions of relatively deep (1 m) soil horizons (Brewer et al., 2019). Members of GAL15 have also been detected in sediments at radionuclide-contaminated sites (Lin et al., 2012) and in high-altitude, cold fumarolic environments (Costello et al., 2009), suggesting that members of GAL15 have outstanding stress tolerance. Members of GAL15 were found to be more abundant in oxic than anoxic zones of a profile of sediment cores (Lin et al., 2012), suggesting that some members of GAL15 are capable of aerobic respiration. However, our finding of a high relative abundance of GAL15-affiliated 16S rRNA gene reads in a sample of strongly reduced waters (-412 mV

Eh and 3.55 μmol $\cdot$ L^{-1} H_2; Tables 4.4 and 4.2) pumped from an isolated depth interval of 102 m to 132 m in a peridotite aquifer suggests that some members of GAL15 can function anaerobically.

16S rRNA gene sequences were searched for matches to known CH_4-cycling taxa, as compiled previously (Crespo-Medina et al., 2017; Nothaft et al., 2020). Sequences closely affiliated with both methanogenic and aerobic methanotrophic taxa were found in multiple samples, but always in low relative abundance (< 1 % of reads; Figure C.6). These included sequences related to the genus *Methanobacterium*, whose members can produce CH_4 from H_2 and CO_2, CO, or formate (Balch et al., 1979) and are widespread in Samail Ophiolite groundwaters (Nothaft et al., 2020). In addition, relatives aerobic methanotrophs of the genus *Methylocaldum* (Hanson and Hanson, 1996) and the family Methylacidiphilaceae (Op den Camp et al., 2009) were detected.

In order to explore how microbial community composition relates to cell size, biomass was collected onto filters with pore diameters of 0.45 μm, 0.22 μm, and 0.10 μm by connecting three inline filter housings in series when sampling BA1A in 2018 (Figure C.7, Text C.1, Figure C.7). The microbial community composition was overall similar across filters of different pore diameters (Figure C.7), with the exception of relatives of the genus *Brachymonas*, which had highest relative abundance in the 0.10 μm pore-diameter filter in the sample from > 100 m depth (80 % of reads, compared to 9 % to 10 % in filters of other pore diameters), but showed decreased relative read abundance with decreasing pore size in samples of the 55 m to 66 m depth interval (44 %, 32 %, and 26 % in the 0.45 μm, 0.22 μm, and 0.10 μm pore-diameter filters, respectively). Although a greater sample size would be required to robustly interpret trends of microbial community composition as a function of cell size in this environment, our ability to extract and sequence DNA from cells between 0.22 μm and 0.10 μm in diameter is in itself notable because streamlining (shrinking) of cell and/or genome sizes has been proposed as an adaptive strategy to reduce the energetic costs of replication under conditions of environmental stress (Giovannoni et al., 2014), including the challenging con-

ditions of high pH and low electron acceptor and inorganic C availability found in parts of the Samail Ophiolite (Fones et al., 2019).

In addition to biomass samples obtained during pumping, a sample of drill foam/fluid was taken as it emerged from BA1A during drilling in order to evaluate potential contamination of the subsurface with exogenous microbes. The most abundant 16S rRNA gene sequences in the drill foam/fluid sample were distinct from those of samples obtained during subsequent groundwater pumping (Figure C.8, Text C.1). This suggests that the taxa identified in samples subsequently obtained from pumping groundwaters from the subsurface were for the most part not derived from drill fluids.

4.5 Discussion

4.5.1 Sources and mixing of groundwaters

To derive an integrated hydrologic and geochemical conceptual model of the BA1A/BA1D system, we revisit the trends in the wireline logs and pumped samples in light of the physical hydrological conclusions of Lods et al. (2020) (Section 4.3). We then compare these physical hydrological conclusions with groundwater mixing calculations based on pH and $c_{\sum \mathrm{Si}}$.

In the case of BA1A, where downward flow within the borehole under ambient conditions has been recorded (Section 4.3), it appears that the wireline log pH, Eh, and electrical conductivity trends (Figure 4.1; Section 4.4.1) reflect displacement of moderately alkaline water from the surficial alluvium aquifer down to depths approaching 200 m, where it mixes in the borehole with hyperalkaline $Ca^{2+} - OH^{-}$ waters from deeper aquifers. In contrast, pumped samples of packed intervals at depths $\geq$ 100 m in BA1A drew water from the surrounding rock formations that was more hyperalkaline and reduced (Table 4.4) than resting borehole water. In BA1D, where no ambient flow within the borehole was recorded (Section 4.3), the well logs and pumped samples show closer agreement. Thus, differences in logs and pumped sample chemical compositions in BA1A and BA1D may result from

variable within-borehole flow regimes. We speculate that, prior to drilling, the upper dunite aquifer (41 m to 75 m) near BA1A may have been reduced and hyperalkaline, as BA1D was in that depth interval during sampling in 2019, and that the drilling-induced strong connection of the surficial alluvium aquifer to the upper dunite aquifer through the borehole at BA1A resulted in the oxidized and moderately alkaline conditions recorded in our samples of BA1A at depths < 70 m (Table 4.4).

The downward ambient flow in BA1A implies that the surficial alluvium aquifer had a higher hydraulic head than the upper dunite aquifer at the time of drilling. When a higher-elevation aquifer is at a higher hydraulic head than a lower-elevation aquifer, and the two are hydraulically separated by a low-permeability layer, the upper aquifer is said to be "perched". Thus, the surficial alluvium aquifer at BA1A can be described as a perched aquifer. A perched near-surface (above $\sim$ 10 m depth) aquifer has also been inferred in serpentinites of the Coast Range Ophiolite, USA through electrical resistivity tomography surveys (Ortiz et al., 2018). It is interesting to consider why the surficial alluvium aquifer at BA1A had higher hydraulic head than the the upper dunite aquifer at BA1A at the time of drilling. If the recharge elevation of both aquifers were the same, their hydraulic heads should also be the same, all else being equal. However, all else is not equal because the high pH of the upper dunite aquifer at BA1D (and, presumably also at BA1A prior to drilling) indicates that these fluids experienced high extents of rock/water reaction. At rock/water ratio of 1 (i.e. 1 kg of peridotitite reacted with 1 kg of water), reaction path modelling by Leong et al. (2020) calculated a water loss due to hydration of 15 %. If the volumetric decrease in water is greater than that of the volume increase in hydrated minerals and potential H_2 production, then rock/water reaction could in principle lower the hydraulic head of a reacted water mass in a confined peridotite aquifer. This is one possible explanation for the head differential between the surficial alluvium aquifer and the upper dunite aquifer at BA1A. It is relevant here to note an apparent trend of higher $\delta^{18}O$ and δD of water with increasing pH among BA1A and BA1D samples (Tables 4.4 and 4.3; Figure C.4), although it is unclear if this is

Table 4.4: Pumping data and field measurements.

Well	Sampling date			Sampling interval / [m]		Initial depth to water / [m]	Conductivity / [mS · cm^{-1}]	Temperature / [°C]	pH	*Eh*/ [mV]
	Year	Month	Day	Top	Bottom					
BA1A	2018	2	2	55	66	13.47	0.353	35.7	8.71	126
			8	100	400 (open)		0.820	37.5	10.69	n.d.
	2019	1	14	0 (open)	30	17.25	0.458	34.9	8.10	128
			16	41	65		0.402	35.0	8.21	120.
			16	108	132		0.871	36.5	10.67	−249
BA1D	2019	1	11	45	75	17.03	1.40	34.6	10.86	−408
			13	102	132		1.72	35.2	11.01	−412

Depths referenced to casing top. "n.d." = "not determined."

related to differences of water source or extents of rock/water reaction.

The Si and pH data provide further insights into aquifer dynamics. Although the aquifers are nominally in dunite, the pH of $Ca^{2+} - OH^-$ waters (≥ 10.67; Table 4.4) indicates that they must have been contacted diopside within their flow paths. Reaction of water with solely forsterite will attain chrysotile-brucite equilibrium at pH ~ 10 (Leong and Shock, 2020). The addition of enstatite is also insufficient to increas pH past 11. This can be accomplished only when diopside is present, as it reacts with brucite to form chrysotile, releasing Ca^{2+} into the aqueous phase and consuming protons (Leong and Shock, 2020). Thus, there may be some small amount of diopside within the dunites, or the waters may have sourced from outside of the immediate, dunitic surroundings of the boreholes, and perhaps from further afield harzburgitic terrains. This is unsurprising because harzburgites are present throughout the catchment where BA1A and BA1D are situated, and the lenses of dunite are more rare. The shallower parts (above $\approx 200\,\mathrm{m}$) of BA1A and BA1D just happen to intersect dunites.

The indication that these waters have reacted with harzburgites validates the use of the Leong et al. (2020) Si mixing model. Our samples plot close to the mixing line associated with the $20\,\mu\mathrm{mol} \cdot \mathrm{kg}^{-1}$ $c_{\sum \mathrm{CO_2}}$ chrysotile-brucite-calcite end member of Leong et al. (2020) (leftmost dotted mixing line in Figure 4.2). Assuming this as a compositional end-member, the extent of mixing with a $Mg^{2+} - HCO_3^-$ water endmember is tabulated in Table C.1. These calculations reveal a trend of decreasing contribution of $Mg^{2+} - HCO_3^-$ water to the total water mass with increasing depth in BA1A. This is consistent with the hydrologic flowmeter

tests that showed strong downflow in the upper 60 m at BA1. The downflow tapers off below this, but remains influential to depths approaching 200 m, as evidenced by the wireline logs (Figure 4.1). Compared to BA1A, BA1D has lower calculated proportions of $Mg^{2+} - HCO_3^-$ water (only 2.8 % $Mg^{2+} - HCO_3^-$ at in the 45 m to 75 m interval and 1.9 % $Mg^{2+} - HCO_3^-$ in the 102 m to 132 m interval; Table C.1; Figure 4.2). This is consistent with the lack of evidence of downflow within BA1D. The collection of nearly end-member $Ca^{2+} - OH^-$ fluids from these deeper intervals in BA1D indicates that the packer system is a promising tool for retrieving relatively pure $Ca^{2+} - OH^-$ waters from depth in ophiolite aquifers.

4.5.2 Dissolved gas dynamics

Before interpreting our gas chemistry results, the possibility of degassing during sampling must be addressed. Bubbles were observed in the pumped outflow when pumping the hyperalkaline intervals. In addition, interferences with in-line flow meter (Figure C.2) readings were observed during pumping of BA1D in 2019, which were rectified by tilting the flow meter at an incline, suggesting that bubbles in the flow meter were causing the unstable readings. These observations suggest that partial gas exsolution may have occured upstream of the flow-splitting manifold (Figure C.2) used for collecting our samples for H_2, CO, CH_4, and other short-chain alkanes reported in Table 4.2. The deepest of our samples were pumped from $\sim$ 100 m below ground level, where hydrostatic pressure is $\sim$ 10 bar, and the thick-walled black tubing (Figure C.2) connecting the pump outflow to the flow meter is rated for pressures of up to 30 bar, indicating that this tubing should have been able to maintain pressure on the pumped water, thereby preventing gas exsolution. A more likely cause of degassing is cavitation associated with the fittings or measurement mechanisms of the flow meter. That said, some simple calculations of tubing diameters and flow rates suggest that degassing probably had a minor effect on our data. The black tubing connecting from the pipe string outlet to the flow meter, and then downstream towards the flow-splitting manifold (Figure C.2), had a diameter of $\sim$ 1 inch and a length of $\sim$ 10 m. Given our typical

flow rates of $20\,\mathrm{L}\cdot\mathrm{min}^{-1}$, the residence time of water in this tubing was 15 s, suggesting that kinetics of exsolution would have limited degassing over the short time period between fluids exiting the pipe string and arriving at the gas sampling apparatus. Further, noting that packed intervals were generally pumped on for an hour or more prior to geochemical sampling, upwards of 200 tubing-volumes of water were pumped through the black tubing prior to sampling (assuming flow of $20\,\mathrm{L}\cdot\mathrm{min}^{-1}$ for 60 min). This suggests that, if gas bubbles were present at some locations within the sampling tubing or flow meter, they would have had time to approach equilibrium with gases in the pumped waters, resulting in gas partial pressures in the sampled fluids approaching those of the fluids in the pumped interval. Thus, while we cannot strictly rule out that degassing affected our measured gas concentrations and isotopic compositions, these simple calculations suggest that our data are likely representative and informative. Still, the gas concentrations reported here should be considered minimum values until future work in which gas samples are taken closer to the pipe string outlet at BA1A and BA1D corroborates our results.

The concentration of H_2 at BA1A and BA1D, which ranged up to $4\,\mu\mathrm{mol}\cdot\mathrm{L}^{-1}$ (Table 4.2), is modest in comparison to other hyperalkaline waters in the ophiolite. Well NSHQ14, which is located 2 km down-gradient within the same catchment as BA1A and BA1D, hosts waters of pH $\sim$ 11.4 with two orders of magnitude higher c_{H_2} (Nothaft et al., 2020) than the maximum c_{H_2} observed at BA1A and BA1D. These differences could stem from variations in reaction extent and/or lithology between the two wells. In addition, microbial H_2 consumption, notably coupled to SO_4^{2-} reduction (Section 4.4.3), could exert a control on c_{H_2} at BA1A and BA1D.

Regarding hydrocarbon gases, the high $\delta^{13}C$ value of C_2H_6 (-2.5 ‰ VPDB; Table 4.3; Figure 4.4) in sample BA1D_2019_102-132 indicates an abiotic source of C_2H_6, which has also been proposed for C_2H_6 elsewhere in the ophiolite (Fritz et al., 1992; Nothaft et al., 2020). If C_2H_6 is indeed abiotic at BA1D, then at least some of the CH_4 at BA1A and BA1D is likely also abiotic. The detection of 16S rRNA gene sequences affiliated with methanogens

of the genus *Methanobacterium* at BA1A and BA1D, albeit in low abundances ($< 1\,\%$ of reads; Section 4.4.3; Figure C.6), suggests a potential additional contribution of microbial CH_4.

Perhaps the most remarkable aspect of our gas data is the ^{13}C and D enrichment of CH_4, particularly in sample BA1A_2019_108-132 (23.9 ‰ VPDB and 45 ‰ VSMOW; Table 4.3). This isotopic composition on its own, and especially in relation to the relatively less ^{13}C- and D-enriched (but still quite enriched) samples from BA1D (Figure 4.3), is hard to explain without invoking microbial CH_4 oxidation (Section 4.4.2). This inference is further supported by the lower c_{CH_4} and C_1/C_2 ratio of BA1A_2019_108-132 relative to the BA1D samples (Table 4.2; Figure C.3). This is not to say that the CH_4 samples from BA1D haven't also undergone microbial oxidation; the samples may have experienced variable extents of oxidation.

4.5.3 Microbial ecology

As proposed in Section 4.5.1, hydrologic and geochemical data indicate that the upper dunite aquifer (41 m to 75 m) may have been hyperalkaline and reduced at BA1A prior to drilling, similar to the geochemical state of BA1D in 2019 at equivalent depths. If this is so, we infer that, prior to drilling, BA1A and BA1D below ~ 40 m hosted a microbial ecosystem dominated by sulfate reduction coupled to H_2 oxidation. This is indicated by the high relative 16S rRNA gene abundance (up to 92 % of reads) of sequences related to Thermodesulfovibriona, particularly in BA1D and in OM19_BA1A_108_132. It is also consistent with the sulfidic smell observed during drilling of BA1A. In addition, there was notable blackening and sulfurization of the drill chips recovered during BA1A drilling and analyzed by optical and Raman spectroscopy (Ellison and Templeton, unpublished data). Further, it is in agreement with the potentially energy-yielding reactions in this system, as Further, it is in agreement with the potentially energy-yielding reactions in this system, as reflected in the co-existence of SO_4^{2-} approaching $\text{mmol} \cdot \text{L}^{-1}$ levels and H_2 at $\mu\text{mol} \cdot \text{L}^{-1}$ levels in some $Ca^{2+} - OH^-$

waters at BA1A and BA1D (Tables 4.1 and 4.2; Section 4.4.1). Bioenergetic, metagenomic, and metatranscriptomic evidence of bacterial SO_4^{2-} reduction has been found at other sites of serpentinization such as the Coast Range Ophiolite (Sabuda et al., 2020) and the Lost City Hydrothermal Vent Field, Mid-Atlantic ridge (Lang et al., 2018). Moreover, low but detectable rates of microbial SO_4^{2-} reduction have been measured in groundwaters sampled from wells in the Samail Ophiolite and the Coast Range Ophiolite (Glombitza et al., 2019).

The source of the nearly mmol $\cdot$ L^{-1} levels SO_4^{2-} at BA1D is unclear. One explanation is leaching of SO_4^{2-} salts previously loaded into these rocks during partial serpentinization during seafloor alteration and obduction. Another is the oxidation of reduced S in the rocks, which can occur either abiotically or biotically at the low temperatures observed *in situ* and in the presence of O_2 or NO_3^- (Luther et al., 2011). The reduced sulfur may source from more S-rich gabbros, which are present in intrusive veins at the BA1 wells, or from sulfide minerals, which are pervasive in partially altered peridotites in the BA1 wells (Lods et al., 2020; Kelemen et al., 2020a). Fluids carrying O_2 or NO_3^- may have come into contact with these subsurface, rock-hosted, reduced S reservoirs through natural groundwater circulation and mixing prior to drilling and/or through an influx of oxidized water resulting from drilling (Sections 4.2.1 and 4.4.1).

S-oxidizing bacteria including relatives of the genera *Sulfuritalea* and *Cupriavidus*, as well as the family Rhodocyclaceae, have accounted for particularly high relative abundances of 16S rRNA gene reads in groundwaters sampled from wells in the Samail Ophiolite that show evidence of mixing of reduced, hyperalkaline waters with more oxidized $Mg^{2+} - HCO_3^-$ waters and/or gabbro-reacted waters, suggesting that microbial S oxidation occurs at redox interfaces and mixing zones in the ophiolite (Rempfert et al., 2017). In searching the BA1A and BA1D 16S rRNA gene sequences for the S-oxidizing bacteria noted by Rempfert et al. (2017), sequences related to Rhodocyclaceae and *Cupriavidus* were found at up to 2 % of reads at BA1A, indicating that similar microbial S-oxidizing processes to those described by Rempfert et al. (2017) may occur at BA1A, although the extent of these processes may be

minor compared to other microbial processes, such as microbial SO_4^{2-} reduction. We also note that the DrillFoam used in drilling (Section 4.2.1) is a biodegradable, sulfate-containing compound, so this may have been an additional source of SO_4^{2-} to the system, although it is not necessary to invoke this biodegradation process as the source of SO_4^{2-}, given the presence of the natural S reservoirs discussed above.

In addition to SO_4^{2-} reduction coupled to H_2 oxidation, secondary anaerobic, autotrophic processes at BA1A and BA1D may include hydrogenotrophic methanogenesis, evidenced by the presence of 16S rRNA genes affiliated with genus *Methanobacterium* in $< 1\,\%$ of reads (Figure C.6; Section 4.4.3), and homoacetogenesis, evidenced by the presence of 16S rRNA genes affiliated with putative acetogens of the class *Acetothermiia* (Takami et al. 2012) in up to $2\,\%$ of reads (Figure 2.5). The apparent dominance of SO_4^{2-} reduction over methanogenesis at BA1A and BA1D presents an interesting contrast to the relative influences of these processes at the nearby (within 2 km) and more H_2-rich ($10^2\,\mu mol{\cdot}L^{-1}$ to $10^3\,\mu mol{\cdot}L^{-1}$; Paukert, 2014; Nothaft et al., 2020) well NSHQ14, where the abundance and activity of methanogens is comparable to, if not substantially greater than, that of SO_4^{2-} reducers (Miller et al., 2016; Rempfert et al., 2017; Kraus et al., 2018; Fones et al., 2019; Nothaft et al., 2020). This implies the potential existence of a threshold level of production of reduced compounds, such as H_2 or formate ($HCOO^-$), in continental, low-temperature serpentinizing settings, at which methanogenesis becomes energetically competitive with SO_4^{2-} reduction. The juxtaposition of the BA1 wells vs. NSHQ14 suggests that this transition may occur at H_2 concentrations in the range of $10\,\mu mol \cdot L^{-1}$ to $10^2\,\mu mol \cdot L^{-1}$ in the Samail Ophiolite. Such a transition has been described in sedimentary settings, but at orders of magnitude lower c_{H_2} ($\sim 5\,nmol{\cdot}L^{-1}$; Lovley et al., 1994; Kampbell et al., 1998). The higher apparent c_{H_2} threshold in serpentinizing settings such as the Samail Ophiolite may be a consequence of the stressors of high pH and low CO_2 availability unique to serpentinizing settings. At hyperalkaline conditions, microbes must expend additional energy to regulate cytoplasmic pH and to maintain a proton motive force across the cell membrane to generate ATP (Mitchell, 2011; Mulkidjanian et al.,

2008). High pH has been shown to be more important than substrate availability in limiting microbial SO_4^{2-} reduction rates in serpentinization-influenced waters from the Samail Ophiolite and the Coast Range Ophiolite (Glombitza et al., 2019). One might expect high pH to be an even greater burden for hydrogenotrophic methanogens due to their reliance on CO_2 for both C fixation and energy metabolism. Thus, a higher c_{H_2} threshold for competition between SO_4^{2-} reducers and methanogens in serpentinizing settings relative to sedimentary settings may result from the high pH and related geochemical challenges associated with H_2-rich waters influenced by serpentinization.

Our detection of high relative abundances of genes related to heterotrophic bacteria capable of respiration using O_2 or potentially NO_3^- such as *Brachymonas* and *Parvibaculum lavamentivorans* in samples of BA1A taken from < 70 m depth (Figure 4.5; Section 4.4.3), taken together with the trends of decreasing $c_{NO_3^-}$ with increasing depth at BA1A (Section 4.4.1), suggest that heterotrophic, aerobic and/or denitrifying microbial metabolisms may be active in those regions of the subsurface. *Brachymonas* and *Parvibaculum lavamentivorans* have been detected in 16S rRNA gene surveys of the Samail Ophiolite prior to Oman Drilling Project activities in low relative abundance (typically < 1 % of reads and not exceeding 6 %; Miller et al., 2016; Rempfert et al., 2017; Kraus et al., 2018; Nothaft et al., 2020), but these taxa were not detected in samples of the drilling fluids used at BA1A (Sections 4.4.3 and C.1; Figure C.8). This suggests that these taxa are Samail Ophiolite natives rather than foreign drilling contaminants. Natural *Brachymonas* and *Parvibaculum* populations may have bloomed in response to an influx of oxidized water at depth when the previously separated surficial alluvium aquifer and upper dunite aquifer were connected by drilling at BA1A (Section 4.3). Interestingly, *Parvibaculum lavamentivorans* has been noted for its ability to degrade synthetic laundry surfactants (Schleheck et al., 2011), suggesting that it could have participated in the biodegradation of DrillFoam (Section 4.2.1) introduced into the aquifer during drilling.

As discussed in Sections 4.4.2 and 4.5.2, there is strong isotopic evidence of microbial

CH_4 oxidation in fluids accessed by both wells, and especially at BA1A (Figure 4.3). A search of 16S rRNA gene sequences related to cultured CH_4 oxidizers yielded few matches at BA1A ($< 1\,\%$ of reads) and none at BA1D, and all of the potential CH_4 oxidizers we found are thought to use exclusively O_2 to oxidize CH_4 (Figure S6; Section 4.4.3). It is possible that microbial CH_4 oxidizers are truly rare at BA1A and BA1D and that their numbers are scant in comparison to dominant taxa such as Thermodesulfovibrionia. CH_4 oxidation may just be a minor process that could have been briefly stimulated by O_2 influx during drilling. Alternatively, there may be organisms at BA1A and BA1D whose capacity to oxidize CH_4 under anaerobic conditions has not yet been documented. Future work could employ shotgun metagenomic sequencing to search for genes related to CH_4 oxidation or amend enrichment cultures from BA1A and BA1D with CH_4 to identify microbes whose abilities to oxidize CH_4 are currently unknown.

On the topic of future experimental directions, we wish to express to the broader scientific community that a microbial "observatory" now exists in the BA borehole array, where it is possible to do both intra-hole and cross-hole experimentation. Such observatories have been established to a limited extent in the ocean crust (e.g. North Pond; Wheat et al., 2020) and in ophiolites (e.g. CROMO; Cardace et al., 2013). North Pond is situated in oceanic crustal rocks. CROMO is situated in ultramafic rocks, but the groundwaters there are considerably impacted by nearby non-ultramafic lithologies, and boreholes extend to a maximum of 76 m. In contrast the BA site represents a truly peridotite-buffered, fractured rock system that can be investigated via deep (400 m) boreholes.

4.5.4 Isotopic composition of $\sum CO_2$

It is commonly stated in the literature that ophiolitic $Mg^{2+} - HCO_3^-$ waters are in open-system communication with the atmosphere (Neal and Stanger, 1985; Bruni et al., 2002; Cipolli et al., 2004; Paukert et al., 2012; Leong and Shock, 2020). It is widely known that this is also true of seawater, which sets the $\delta^{13}C$ of seawater $\sum CO_2$ at $0\,‰$ VPDB to

2 ‰ VPDB, reflecting a series of isotopic equilibria connecting seawater HCO_3^-, the dominant $\sum CO_2$ species in seawater, to the isotopic composition of atmospheric CO_2 (Zeebe and Wolf-Gladrow, 2001). Yet, the $\delta^{13}C$ values of $\sum CO_2$ in the $Mg^{2+} - HCO_3^-$ waters in the upper 70 m of BA1A (Table 4.3; Section 4.4.2) and in other $Mg^{2+} - HCO_3^-$ waters pumped from wells in the ophiolite (Matter et al., 2006; Nothaft et al., 2020) are $\sim$ 15 ‰ lower than that of marine $\sum CO_2$. This discrepancy raises the question of whether equilibrium with atmospheric CO_2 is the only factor affecting $\sum CO_2$ in ophiolitic $Mg^{2+} - HCO_3^-$ waters.

Studies of the $\delta^{13}C$ of $\sum CO_2$ in rivers have found that coupled changes in pH and carbonate speciation, and their resultant equilibrium isotopic effects, can only partially account for variations in riverine $\delta^{13}C_{\sum CO_2}$, which is also affected by microbial respiration and changes in C sources to the rivers (Waldron et al., 2007). In the Samail Ophiolite, particularly at the BA site, vegetation and soil cover is sparse and the catchment is lithologically homogeneous (See Figure C.1), so soil respiration and changes in C sources seem to be of questionable relevance. However, an additional organic C reservoir may be present within the crystalline bedrock. Total organic C in peridotites exposed to alteration at the seafloor, a proxy for organic C endogenous to the Samail Ophiolite, is relatively ^{13}C-depleted (approximately -25 ± 5 ‰ VPDB; Alt et al., 2013, 2012a,b; Delacour et al., 2008). Microbial oxidation of CH_4, potentially sourced from fluid inclusions could be another source of ^{13}C depleted $\sum CO_2$ in ophiolite groundwaters. Microbial respiration of these rock-hosted reduced C sources could deplete $\delta^{13}C_{\sum CO_2}$ below atmospheric equilibrium if this respiration occurs at rates comparable to or faster than air-water CO_2 exchange.

This hypothesis should be testable by measuring the ^{14}C content of $\sum CO_2$ in $Mg^{2+} - HCO_3^-$ waters waters. To our knowledge, there is one such analysis in the literature on the Samail Ophiolite. This is from well WDA17 that is situated in peridodite, has a groundwater pH of 9.10, $c_{\sum CO_2}$ of 2.481 mmol $\cdot$ kg^{-1}, $\delta^{13}C_{\sum CO_2}$ of -12.3 ‰ VPDB, $F^{14}C_{\sum CO_2}$ of 0.205 (corresponding to a ^{14}C age of 12 700 years B.P.), and a $^3H/^3He$ recharge age of 21.5 years (Vankeuren et al., 2019). It is interesting that the ^{14}C age of the $\sum CO_2$ in this sample is

considerably older than its $^{3}H/^{3}He$-derived recharge age and that its $\delta^{13}C_{\sum CO_2}$ is well below that which would be expected based on carbonate equilibrium with atmospheric CO_2. These characteristics are compatible with the hypothesis of recent microbial oxidation of ancient organic matter stored in the partially-serpentinized peridotites.

An alternative explanation would be that the ^{14}C-free C derives from dissolution/reprecipitation of carbonate veins that are ^{14}C-free. Such veins could have inherited C from marine organic C through thermochemical sulfate reduction (Goldstein and Aizenshtat, 1994), which can produce relatively ^{13}C-depleted inorganic C. However, this suggestion is complicated by the fact that calcite, dolomite, and magnesite are typically at or above saturation in $Mg^{2+} - HCO_3^-$ waters in the Samail Ophiolite (Neal and Stanger, 1985; Matter et al., 2006), and magnesite should precipitate (rather than dissolve) from these waters upon moderate degrees of reaction progress (Bruni et al., 2002).

The ^{13}C depletion of $\sum CO_2$ below equilibrium with atmospheric CO_2 in $Mg^{2+} - HCO_3^-$ waters could alternatively be explained by these waters expressing a muted signal of the kinetic isotope effects associated with hydroxylation of aqueous CO_2, which have been invoked to explain the stark ^{13}C depletion in Ca-rich carbonate travertine deposits found at hyperalkaline springs in ophiolites (Clark and Fontes, 1990; Kelemen et al., 2011). However, this seems unlikely because a rapid CO_2 uptake process would be necessary to achieve these kinetic isotopic effects. Further, in contrast to the travertine deposits, there is no clear mechanism to preserve such a signature in a $Mg^{2+} - HCO_3^-$ water (as in a precipitation process), so CO_2 (aq) and HCO_3^- would be expected to quickly re-equilibrate.

Although we cannot resolve the compositional and isotopic dynamics of inorganic C in $Mg^{2+} - HCO_3^-$ waters given the available data, this discussion has highlighted that there are important aspects of the C cycle of low-temperature serpentinizing systems that remain unanswered. Further analyses of the stable and radio isotopic compositions of inorganic C in ophiolitic $Mg^{2+} - HCO_3^-$ waters, especially if coupled to $^{3}H/^{3}He$-derived recharge ages, could advance understanding of the timescales and sources of CO_2 uptake in near-surface

serpentinizing aquifers.

4.6 Conclusions

In this study, vertically- and horizontally-resolved sample acquistion via the deployment of a packer system in two 400 m-deep wells enabled a holistic geochemical, hydrologic, and biological investigation into an aquifer experiencing ongoing low-temperature serpentinization. In addition, a temporal component was assessed through monitoring of variations in subsurface biogeochemical states from the time of well completion to three years afterwards. The isolation and pumping of discrete intervals as deep as 108 m to 132 m below ground level enabled us to interrogate how microbial ecological dynamics of minimally-disturbed, hyperalkaline, and reduced groundwaters differed from those of pervasively mixed and oxidized groundwaters. Aqueous chemical analyses and 16S rRNA gene sequencing of deep, $Ca^{2+} - OH^{-}$ groundwaters revealed the presence of an ecosystem dominated by microbial SO_4^{2-} reduction coupled to the oxidation of H_2 and/or small organic acids generated through serpentinization. Based on these findings, we propose that future investigations of the borehole lithology seek evidence for late stage sulfurization induced by microbial activity. In oxidized $Mg^{2+} - HCO_3^{-}$ groundwaters, the dominance of SO_4^{2-}-reducing bacteria was challenged by heterotrophic aerobes or denitrifiers that may have been stimulated by drilling-induced groundwater mixing. Isotopic data point to intriguing future avenues of C cycle investigations in this system. Stark ^{13}C and D enrichments in CH_4 and ^{13}C depletions in $\sum CO_2$ of $Mg^{2+} - HCO_3^{-}$ groundwaters below the expectation of equilibrium with atmospheric CO_2 suggest the importance of cryptic microbial oxidation of stored CH_4 and potentially other forms of reduced C. Overall, the results of this study, and moreover its methods, mark an important step towards an integrated hydrologic and biogeochemical understanding of the deep biosphere, particularly in low-temperature serpentinizing settings. This study presents a framework for exploring where subsurface energy availability is greatest and how that

maps onto microbial abundance and activity, which is needed for improving strategies for life detection beyond Earth.

4.7 Acknowledgements

This research was directly supported by the Rock-Powered Life NASA Astrobiology Institute (NNA15BB02A). This research also used samples and/or data provided by the Oman Drilling Project. The Oman Drilling Project (OmanDP) has been possible through co-mingled funds from the International Continental Scientific Drilling Project (ICDP), the Sloan Foundation – Deep Carbon Observatory (Grant 2014-3-01, Kelemen PI), the National Science Foundation (NSF-EAR-1516300, Kelemen PI), the NASA Astrobiology Institute (NNA15BB02A), the German Research Foundation (DFG), the Japanese Society for the Promotion of Science (JSPS), the European Research Council, the Swiss National Science Foundation, JAMSTEC, the TAMU-JR Science operator, and contributions from the Sultanate of Oman Ministry of Regional Municipalities and Water Resources, the Oman Public Authority of Mining, Sultan Qaboos University, CRNS-Univ. Montpellier II, Columbia University, and the University of Southampton. Work at LBNL was supported by the U.S. Department of Energy, Office of Science, Office of Basic Energy Sciences, Chemical Sciences, Geosciences, and Biosciences Division, under Award Number DE-AC02-05CH11231.

We thank the Ministry of Regional Municipalities and Water Resources in the Sultanate of Oman (particularly Said Al Habsi, Rashid Al Abri, Salim Al Khanbashi, and Haider Ahmed Mohammed Alajmi) for allowing access to wells and logistical support, Zaher Al Sulaimani and Mazin Al Sulaimani from the Oman Water Centre and AZD Engineering for their technical and logistical support, Jude Coggon for coordinating Oman Drilling Project activities, Benoît Ildefonse for sharing geologic map data, Eric Ellison, Elizabeth Fones, and Emily Kraus for assistance in the field and laboratory, and Noah Fierer, Jen Reeves, Corinne Walsh, Matthew Gebert, and Angela Oliverio for assisting with DNA sequencing

and interpretation.

Data (in Excel format) and source code (in R Markdown format) used to produce the figures, data tables and analyses for this paper (as well as additional data on analytical uncertainties and trace element concentrations) are available online at `https://github.com/danote/Oman-packers-2018-2019`. Additional DNA sequence data processing codes are available at `https://github.com/danote/Samail_16S_compilation`.

Chapter 5

Conclusions and future directions

5.1 Contributions of this dissertation

This dissertation set out to address the following overarching research questions as they relate to low-temperature serpentinizing settings, as exemplified by the Samail Ophiolite:

1. What are the source(s) of CH_4 in highly reacted fluids, and in what ways can the contributions of microbial CH_4 production be recognized?

2. How can subsurface hydrologic and biogeochemical data sets be obtained and integrated to arrive at a more holistic model of microbial ecology and predicted metabolic activity?

To contextualize the contributions of this dissertation to these objectives, I will revisit the state of research concerning these topics when my dissertation began. At that time, the viewpoint that ^{13}C-enriched CH_4 in ophiolites was practically all abiotic was vocally advocated (Etiope, 2017a), and the hypothesis that microbial CH_4 production could proceed with suppressed C isotope fractionation due to C-limited conditions resulting from serpentinization could only be inferred indirectly through 16S rRNA gene sequencing of DNA (Brazelton et al., 2006; Blank et al., 2009; Suzuki et al., 2013; Miller et al., 2016) and compound-specific isotopic analyses of lipid biomarkers (Bradley et al., 2009).

In this dissertation, I have presented the first direct evidence that microbial methanogenesis is a quantitatively important process contributing to ^{13}C-enriched CH_4 in low-temperature serpentinizing settings. In Chapter 2, in analyzing dissolved gases from hyperalkaline fluids sampled at well NSHQ04, where $\delta^{13}C_{CH_4}$ was 4 ‰ VPDB, I observed deficits in the clumped isotopologues, $^{13}CH_3D$ and $^{12}CH_2D_2$, relative to equilibrium, which were similar to those of CH_4 generated by methanogenic cultures and distinct from those of CH_4 produced in abiotic experiments. Well NSHQ04 also had notably high $C_1/(C_2 + C_3)$ relative to other samples from the ophiolite, suggesting addition of CH_4 to a background source. Further, fluids pumped from the well NSQH04 have yielded vibrant enrichment cultures of methanogens affiliated with genus *Methanobacterium* (Miller et al., 2018). Thus, clumped isotopologue data, from which source effects are normalized out (Young, 2020), and other data support a substantial, potentially dominant, microbial contribution to this strongly ^{13}C-enriched CH_4. Then in Chapter 3, I found that hyperalkaline groundwaters pumped from another well, NSHQ14, contained CH_4 with $F^{14}C$ of 0.304 and $\delta^{13}C$ of -3 ‰ VPDB in addition to DNA for which 12 % of 16S rRNA gene reads were affiliated with *Methanobacterium*. This suggests active microbial production of considerable (30 % or more) of the total pool of CH_4, which was also remarkably ^{13}C-enriched. These data are complimented by a wide range of geochemical, theoretical, and microbiological evidence pointing to methanogenic activity in mixing zones of H_2-rich and CO_2-rich fluids in the aquifers surrounding these wells (Fones et al., 2019; Leong and Shock, 2020; Kraus et al., in press). In light of these data, the viewpoint that the microbial contribution to ^{13}C-enriched CH_4 in low-temperature serpentinizing settings is negligible is no longer tenable.

Beyond the fundamental finding that microbial methanogenesis can contribute substantially to the pool of ^{13}C-enriched CH_4 in low-temperature serpentinizing environments, this dissertation has identified key systematics of microbial CH_4 production. First, the comparison of wells WAB188 and NSHQ04 in Chapter 2, which are situated only 2 km apart and both harbor active *Methanobacterium* populations (Miller et al., 2016, 2018; Rempfert et al.,

2017; Kraus et al., 2018; Fones et al., in press), but host CH_4 that differs in $\delta^{13}C$ by 80 ‰, with the more ^{13}C-depleted CH_4 in well WAB188, which had higher $c_{\sum CO_2}$ than NSHQ04 by a factor of 100, supports the hypothesis that C availability modulates the expression of C isotope fractionation of microbial methanogenesis. Second, the finding of significant ^{14}C content in CH_4 suggests that methanogens and potentially other microbes can rapidly metabolize C sourced recently from atmospheric CO_2, either directly, or via simple organic C compounds that may rapidly form from $\sum CO_2$, such as formate (McCollom and Seewald, 2003; McDermott et al., 2015; Miller et al., 2017b; Lang et al., 2018). Third, while Chapter 2 emphasized the influence of C availability on methanogenesis, Chapters 3 and 4 drew contrasts between the high-H_2 ($10^2\,\mu mol\,L^{-1}$ to $10^3\,\mu mol\,L^{-1}$) well, NSHQ14, where methanogens are abundant and active at comparable or greater extents than sulfate reducers or acetogens (Rempfert et al., 2017; Kraus et al., in press; Fones et al., 2019, in press), vs. the wells WAB71, BA1A, and BA1D, where H_2 and CH_4 were present at lower concentrations (typically $< 10\,\mu mol\,L^{-1}$), and sulfate reducing bacteria dominate the microbial community. These contrasts in H_2 and the relative abundances/activities of methanogens vs. sulfate reducers suggest that reduced compounds such as H_2 or formate produced through serpentinization may, in addition to CO_2, be critical determinants of where microbial CH_4 production may be most prevalent.

The second objective of this dissertation (unifying hydrogeology and biogeochemistry) was framed in Chapter 1 within the context of abiotic CH_4 synthesis. Specifically, the prevalence of colocation of $H_2\,(g)$, $CO_2\,(g)$, and Ru in water-unsaturated conditions was queried. In Chapter 3, wireline log Eh profiles suggested the potential for a H_2-rich vapor phase to coexist with water at depths below ≈ 170 m in wells BA3A and NSHQ14. However, it was also noted in Chapter 3 that conditions where a H_2-rich vapor phase may exist coincided with pH > 10.5 and $c_{\sum CO_2} < 12\,\mu mol\,L^{-1}$, implying that the p_{CO_2} would be negligible in these locations. Further, we have seen evidence for active CH_4 production in settings without evidence for proximity to chromitites, which are the most Ru-rich rocks in

ophiolites. Thus, we do not find evidence that the reaction of H_2 (g) and CO_2 (g) on Ru in water-unsaturated conditions is required for CH_4 to be abundant or actively produced in the Samail Ophiolite.

My investigations into coupled hydrogeologic and biogeochemical dynamics took me far beyond C cycling. In Chapter 4, I reported the first sampling of peridotite-hosted aquifers at discrete depth intervals using a packer system and calculated mixing extents of $Mg^{2+} - HCO_3^-$ and $Ca^{2+} - OH^-$ waters using $\sum$Si and pH, which were interpreted alongside the concentrations of $\sum CO_2$, NO_3^-, SO_4^-, H_2, and CH_4 to contribute to a detailed hydrogeochemical conceptual model of the system. This framework enabled me to explain the presence of distinct microbial communities dominated by sulfate reducers vs. aerobes and denitrifiers in discrete loci within dimensions of depth, lateral distance, and time.

5.2 Potential avenues of future research

The findings of this dissertation lead to new interesting questions, and some of the tools that we have begun to employ will be integral to further investigation of the biogeochemistry of low-temperature serpentinizing environments. Among these tools, the packer system in particular opens many new doors. The ability to target discrete depth intervals is critical to understanding the true energy availabilities and distinct biomes present at different locations in the subsurface. Further, the capacity to limit mixing of water masses during pumping enables the application of advanced groundwater age tracers such as ^{39}Ar and ^{81}Kr (Ritterbusch et al., 2014; Vankeuren et al., 2019). Evaluating fluid residence times and coupling this information to geochemical analyses and microbial rate assays would help calculate nutrient and energy fluxes (power) through time, which is critical to assessing the habitability of serpentinizing systems.

The $\delta^{13}C$ measured for C_2H_6 and C_3H_8 in Chapters 2, 3, and 4 of this dissertation were strikingly similar to C_2H_6 and C_3H_8 found in some sediment-poor seafloor hydrothermal vent

settings, and in rock crushing experiments performed on mafic and ultramafic rocks known to contain CH_4-rich fluid inclusions (Charlou et al., 2010; Grozeva et al., 2020). CH_4-bearing fluid inclusions have been previously documented in Samail Ophiolite harzburgites (Miura et al., 2011), but the quantity of CH_4 present per unit mass of rock and the isotopic composition of this CH_4 are unknown. These data would be immensely valuable for interpreting the source of abiotic CH_4 in the ophiolite. If a reasonable end-member isotopic composition of this CH_4 could be determined, then mixing proportions or isotopic compositions of commingled microbial CH_4 may in turn be evaluated. Thus, there is ample justification for a fluid inclusion rock-crushing study on Samail Ophiolite rocks. The rock material is already available from Oman Drilling Project cores, and the analytical techniques are established (Etiope et al., 2018; Grozeva et al., 2020). However, only $\delta^{13}C$ has been measured in CH_4 and C_2H_6 liberated from from rock crushings. This is no small feat, but if δD_{CH_4} could additionally be accurately measured, it could offer new insights into the isotopic composition of abiotic CH_4 in low-temperature serpentinizing settings and the rates of H isotopic exchange between water, H_2, and CH_4 over long (tens to hundreds of Myr) time scales. The rate of isotopic exchange in CH_4 is an area of active debate, as illustrated by recent CH_4 clumped isotopologue studies suggesting that isotopic exchange in CH_4, possibly involving interactions with water, may occur at appreciable rates at lower temperatures than was previously thought (Young et al., 2017; Labidi et al., 2020). Further, acquiring more data on the concentrations of CH_4 present in continental peridotites such as the Samail Ophiolite could inform strategies of CO_2 injection into these rocks for the purpose of climate change mitigation via *in situ* mineral carbonation (Kelemen and Matter, 2008; Kelemen et al., 2011; National Academies, 2019).

In addition to refining constraints on abiotic CH_4 isotopic compositions in the ophiolite, further cultivation of methanogens supplied with varying substrates under C limitation is an essential step towards understanding the controls on microbial CH_4 production in low-temperature serpentinizing environments. Miller et al. (2018) demonstrated that

Methanobacterium sp. prevalent in the Samail Ophiolite can utilize carbonate minerals as a C source for CH_4 production at high pH, resulting in unusually ^{13}C-enriched microbial CH_4. However, Fones et al. (in press) recently demonstrated that two lineages within the genus *Methanobacterium* exist in the Samail Ophiolite, and a different lineage than that cultured by Miller et al. (2018) is more prevalent in the most hyperalkaline waters and is capable of CH_4 production using formate, but not CO_2. The bulk stable isotopic composition of CH_4 produced by this novel *Methanobacterium* lineage, let alone its clumped isotopologue composition, are complete unknowns. In 2018, I attended the São Paolo School of Advanced Methane Science, at which Prof. Brendan Bohannan, who researches Microbial Biodiversity at the University of Oregon told me, "I you can't grow it, you don't know it." This sage wisdom ought to be heeded by all environmental microbiologists, and those working on serpentinizing settings are no exception.

The use of ^{14}C as a tracer of C source and reaction rates should be expanded in ophiolites including the Samail Ophiolite. Carbonate mineral ^{14}C has been widely deployed in the Samail Ophiolite to track carbonation rates (Clark and Fontes, 1990; Kelemen and Matter, 2008; Mervine et al., 2014; Kelemen et al., 2011). The utility of $^{14}CH_4$ in assessing C turnover processes and rates in the Samail Ophiolite has begun to be explored in this dissertation, but $^{14}CH_4$ analysis should become a routine measurement in CH_4-rich samples in this ophiolite and others. Additional ^{14}C analyses of $\sum CO_2$ in $Mg^{2+} - HCO_3^-$ waters in ophiolites could shed light the timescales and sources of CO_2 uptake in near-surface serpentinizing aquifers, as discussed in Chapter 4. These analyses would be particularly useful if coupled to $^3H/^3He$-derived recharge ages. Concentrations and stable C isotopic compositions of organic matter in the rocks as a function of depth and in relation to downhole geochemical profiles could also be powerful, alongside ^{14}C analyses of $\sum CO_2$, to assess whether microbial respiration of ancient C may contribute to the $\sum CO_2$ pool.

To expand understanding of how CH_4 fits into the broader C cycle of serpentinizing settings, additional CH_4 flux measurements are needed. I believe that portable flux meter

measurements are already underway in the Samail Ophiolite. This is a great and much-needed start. However, dual frequency comb spectrometer methods could offer additional insights. This technique is essentially a laser that can scan over an entire field site and remotely detect small concentrations of CH_4 (i.e. a $1.6\,\mathrm{g\,min^{-1}}$ emission from a distance of 1 km) (Coburn et al., 2018). It has been deployed to monitor leaks in commercial oil and gas operations, but the full scope of its natural environmental applications are yet to be realized.

Bibliography

Abrajano, T., Sturchio, N., Kennedy, B., Lyon, G., Muehlenbachs, K., and Bohlke, J. (1990). Geochemistry of reduced gas related to serpentinization of the Zambales ophiolite, Philippines. *Appl. Geochem.* 5, 625 – 630. doi:10.1016/0883-2927(90)90060-I. Water-Rock Interactions Special Memorial Issue Ivan Barnes (1931–1989)

Alsharhan, A. S. (1989). PETROLEUM GEOLOGY OF THE UNITED ARAB EMIRATES. *J. Pet. Geol.* 12, 253–288. doi:10.1111/j.1747-5457.1989.tb00197.x

Alt, J. C., Garrido, C. J., Shanks, W., Turchyn, A., Padrón-Navarta, J. A., Sánchez-Vizcaíno, V. L., et al. (2012a). Recycling of water, carbon, and sulfur during subduction of serpentinites: A stable isotope study of Cerro del Almirez, Spain. *Earth Planet. Sci. Lett.* 327-328, 50 – 60. doi:10.1016/j.epsl.2012.01.029

Alt, J. C., Schwarzenbach, E. M., Früh-Green, G. L., Shanks, W. C., Bernasconi, S. M., Garrido, C. J., et al. (2013). The role of serpentinites in cycling of carbon and sulfur: Seafloor serpentinization and subduction metamorphism. *Lithos* 178, 40 – 54. doi:10.1016/j.lithos.2012.12.006. Serpentinites from mid-oceanic ridges to subduction

Alt, J. C., Shanks, W., Crispini, L., Gaggero, L., Schwarzenbach, E. M., Früh-Green, G. L., et al. (2012b). Uptake of carbon and sulfur during seafloor serpentinization and the effects of subduction metamorphism in Ligurian peridotites. *Chem. Geol.* 322-323, 268 – 277. doi:10.1016/j.chemgeo.2012.07.009

Archer, D. (2011). *Global warming: understanding the forecast* (John Wiley & Sons), chap. Greenhouse Gases. 4

Ash, J. L. and Egger, M. (2019). Exchange catalysis during anaerobic methanotrophy revealed by $^{12}CH_2D_2$ and $^{13}CH_3D$ in methane. *Geochem. Perspect. Lett.* 10, 26–30. doi: 10.7185/geochemlet.1910

Assayag, N., Rivé, K., Ader, M., Jézéquel, D., and Agrinier, P. (2006). Improved method for isotopic and quantitative analysis of dissolved inorganic carbon in natural water samples. *Rapid Commun. Mass Spectrom.* 20, 2243–2251. doi:10.1002/rcm.2585

ASTM (2016). *ASTM D859-16, Standard Test Method for Silica in Water*. Tech. rep., ASTM International. doi:10.1520/D0859-16

Bach, W., Paulick, H., Garrido, C. J., Ildefonse, B., Meurer, W. P., and Humphris, S. E. (2006). Unraveling the sequence of serpentinization reactions: petrography, mineral chemistry, and petrophysics of serpentinites from MAR 15 °N (ODP Leg 209, Site 1274). *Geophys. Res. Lett.* 33. doi:10.1029/2006GL025681

Balch, W. E., Fox, G. E., Magrum, L. J., Woese, C. R., and Wolfe, R. S. (1979). Methanogens: reevaluation of a unique biological group. *Microbiol. Rev.* 43, 260

Barker, J. F. and Fritz, P. (1981). Carbon isotope fractionation during microbial methane oxidation. *Nature* 293, 289–291. doi:10.1038/293289a0

Barnes, I., LaMarche, j. V., and Himmelberg, G. (1967). Geochemical evidence of present-day serpentinization. *Science* 156, 830–832. doi:10.1126/science.156.3776.830

Barnes, I., O'Neil, J., and Trescases, J. (1978). Present day serpentinization in New Caledonia, Oman and Yugoslavia. *Geochim. Cosmochim. Acta* 42, 144 – 145. doi: 10.1016/0016-7037(78)90225-9

Barnes, I. and O'Neil, J. R. (1969). The relationship between fluids in some fresh alpine-type ultramafics and possible modern serpentinization, western United States. *Geol. Soc. Am. Bull.* 80, 1947–1960. doi:10.1130/0016-7606(1969)80[1947:TRBFIS]2.0.CO;2

Bernard, B., Brooks, J. M., Sackett, W. M., et al. (1977). A geochemical model for characterization of hydrocarbon gas sources in marine sediments. In *Offshore Technology Conference* (Offshore Technology Conference), 435–438. doi:10.4043/2934-MS

Blank, J., Green, S., Blake, D., Valley, J., Kita, N., Treiman, A., et al. (2009). An alkaline spring system within the Del Puerto Ophiolite (California, USA): a Mars analog site. *Planet. Space Sci.* 57, 533–540. doi:10.1016/j.pss.2008.11.018

Blöthe, M. and Roden, E. E. (2009). Composition and Activity of an Autotrophic Fe(II)-Oxidizing, Nitrate-Reducing Enrichment Culture. *Appl. Environ. Microbiol.* 75, 6937–6940. doi:10.1128/AEM.01742-09

Boetius, A., Ravenschlag, K., Schubert, C. J., Rickert, D., Widdel, F., Gieseke, A., et al. (2000). A marine microbial consortium apparently mediating anaerobic oxidation of methane. *Nature* 407, 623–626. doi:10.1038/35036572

Boone, D. R. (2015). *Methanobacterium* (American Cancer Society). 1–8. doi:10.1002/9781118960608.gbm00495

Bottinga, Y. (1969). Calculated fractionation factors for carbon and hydrogen isotope exchange in the system calcite-carbon dioxide-graphite-methane-hydrogen-water vapor. *Geochim. Cosmochim. Acta* 33, 49 – 64. doi:10.1016/0016-7037(69)90092-1

Boudier, F., Baronnet, A., and Mainprice, D. (2009). Serpentine Mineral Replacements of Natural Olivine and their Seismic Implications: Oceanic Lizardite versus Subduction-Related Antigorite. *J. Petrol.* 51, 495–512. doi:10.1093/petrology/egp049

Boudier, F. and Coleman, R. G. (1981). Cross section through the peridotite in the Samail Ophiolite, southeastern Oman Mountains. *J. Geophys. Res.: Solid Earth* 86, 2573–2592. doi:10.1029/JB086iB04p02573

Boulart, C., Chavagnac, V., Monnin, C., Delacour, A., Ceuleneer, G., and Hoareau, G. (2013). Differences in gas venting from ultramafic-hosted warm springs: the example of Oman and Voltri ophiolites. *Ofioliti* 38, 142–156. doi:10.4454/ofioliti.v38i2.423

Bradley, A. S. (2016). The sluggish speed of making abiotic methane. *Proc. Natl. Acad. Sci. U. S. A.* 113, 13944–13946. doi:10.1073/pnas.1617103113

Bradley, A. S., Hayes, J. M., and Summons, R. E. (2009). Extraordinary ^{13}C enrichment of diether lipids at the Lost City Hydrothermal Field indicates a carbon-limited ecosystem. *Geochim. Cosmochim. Acta* 73, 102–118. doi:10.1016/j.gca.2008.10.005

Brazelton, W., Nelson, B., and Schrenk, M. (2012). Metagenomic Evidence for H_2 Oxidation and H_2 Production by Serpentinite-Hosted Subsurface Microbial Communities. *Front. Microb.* 2, 268. doi:10.3389/fmicb.2011.00268

Brazelton, W. J., Schrenk, M. O., Kelley, D. S., and Baross, J. A. (2006). Methane- and Sulfur-Metabolizing Microbial Communities Dominate the Lost City Hydrothermal Field Ecosystem. *Appl. Environ. Microbiol.* 72, 6257–6270. doi:10.1128/AEM.00574-06

Brazelton, W. J., Thornton, C. N., Hyer, A., Twing, K. I., Longino, A. A., Lang, S. Q., et al. (2017). Metagenomic identification of active methanogens and methanotrophs in serpentinite springs of the Voltri Massif, Italy. *PeerJ* 5, e2945. doi:10.7717/peerj.2945

Brewer, T. E., Aronson, E. L., Arogyaswamy, K., Billings, S. A., Botthoff, J. K., Campbell, A. N., et al. (2019). Ecological and Genomic Attributes of Novel Bacterial Taxa That Thrive in Subsurface Soil Horizons. *mBio* 10. doi:10.1128/mBio.01318-19

Bruni, J., Canepa, M., Chiodini, G., Cioni, R., Cipolli, F., Longinelli, A., et al. (2002). Irreversible water–rock mass transfer accompanying the generation of the neutral, Mg–HCO3 and high-pH, Ca–OH spring waters of the Genova province, Italy. *Appl. Geochem.* 17, 455–474. doi:10.1016/S0883-2927(01)00113-5

Callahan, B. J., McMurdie, P. J., Rosen, M. J., Han, A. W., Johnson, A. J. A., and Holmes, S. P. (2016). DADA2: High-resolution sample inference from Illumina amplicon data. *Nat. Methods* 13, 581. doi:10.1038/nmeth.3869

Canovas III, P. A., Hoehler, T., and Shock, E. L. (2017). Geochemical bioenergetics during low-temperature serpentinization: An example from the Samail ophiolite, Sultanate of Oman. *J. Geophys. Res.: Biogeosci.* 122, 1821–1847. doi:10.1002/2017JG003825

Cardace, D., Hoehler, T., McCollom, T., Schrenk, M., Carnevale, D., Kubo, M., et al. (2013). Establishment of the Coast Range ophiolite microbial observatory (CROMO): drilling objectives and preliminary outcomes. *Sci. Drilling* 16, 45–55. doi:10.5194/sd-16-45-2013

Charlou, J., Donval, J., Douville, E., Jean-Baptiste, P., Radford-Knoery, J., Fouquet, Y., et al. (2000). Compared geochemical signatures and the evolution of Menez Gwen (37°50′N) and Lucky Strike (37°17′N) hydrothermal fluids, south of the Azores Triple Junction on the Mid-Atlantic Ridge. *Chem. Geol.* 171, 49 – 75. doi:10.1016/S0009-2541(00)00244-8

Charlou, J., Donval, J., Fouquet, Y., Jean-Baptiste, P., and Holm, N. (2002). Geochemistry of high H_2 and CH_4 vent fluids issuing from ultramafic rocks at the Rainbow hydrothermal field (36° 14′ N, MAR). *Chem. Geol.* 191, 345–359. doi:10.1016/S0009-2541(02)00134-1

Charlou, J. L., Donval, J. P., Konn, C., Ondréas, H., Fouquet, Y., Jean-Baptiste, P., et al. (2010). *High production and fluxes of H_2 and CH_4 and evidence of abiotic hydrocarbon synthesis by serpentinization in ultramafic-hosted hydrothermal systems on the Mid-Atlantic Ridge* (American Geophysical Union (AGU)). 265–296. doi:10.1029/2008GM000752

Charlou, J. L., Fouquet, Y., Donval, J. P., Auzende, J. M., Jean-Baptiste, P., Stievenard, M., et al. (1996). Mineral and gas chemistry of hydrothermal fluids on an ultrafast spreading ridge: East Pacific Rise, 17 ° to 19 °S (Naudur cruise, 1993) phase separation processes controlled by volcanic and tectonic activity. *J. Geophys. Res.: Solid Earth* 101, 15899–15919. doi:10.1029/96JB00880

Chavagnac, V., Ceuleneer, G., Monnin, C., Lansac, B., Hoareau, G., and Boulart, C. (2013a). Mineralogical assemblages forming at hyperalkaline warm springs hosted on ultramafic rocks: A case study of Oman and Ligurian ophiolites. *Geochem., Geophys., Geosyst.* 14, 2474–2495. doi:10.1002/ggge.20146

Chavagnac, V., Monnin, C., Ceuleneer, G., Boulart, C., and Hoareau, G. (2013b). Characterization of hyperalkaline fluids produced by low-temperature serpentinization of mantle peridotites in the Oman and Ligurian ophiolites. *Geochem., Geophys., Geosyst.* 14, 2496–2522. doi:10.1002/ggge.20147

Cheng, L., Normandeau, C., Bowden, R., Doucett, R., Gallagher, B., Gillikin, D. P., et al. (2019). An international intercomparison of stable carbon isotope composition measurements of dissolved inorganic carbon in seawater. *Limnology and Oceanography: Methods* 17, 200–209. doi:10.1002/lom3.10300

Cipolli, F., Gambardella, B., Marini, L., Ottonello, G., and Zuccolini, M. V. (2004). Geochemistry of high-pH waters from serpentinites of the Gruppo di Voltri (Genova, Italy) and reaction path modeling of CO_2 sequestration in serpentinite aquifers. *Appl. Geochem.* 19, 787 – 802. doi:10.1016/j.apgeochem.2003.10.007

Clark, I. D. and Fontes, J.-C. (1990). Paleoclimatic Reconstruction in Northern Oman Based on Carbonates from Hyperalkaline Groundwaters. *Quat. Res.* 33, 320–336. doi:10.1016/0033-5894(90)90059-T

Clark, I. D., Fontes, J.-C., and Fritz, P. (1992). Stable isotope disequilibria in travertine from

high pH waters: Laboratory investigations and field observations from Oman. *Geochim. Cosmochim. Acta* 56, 2041 – 2050. doi:10.1016/0016-7037(92)90328-G

Coburn, S., Alden, C. B., Wright, R., Cossel, K., Baumann, E., Truong, G.-W., et al. (2018). Regional trace-gas source attribution using a field-deployed dual frequency comb spectrometer. *Optica* 5, 320–327. doi:10.1364/OPTICA.5.000320

Coleman, R. G. and Hopson, C. A. (1981). Introduction to the Oman Ophiolite Special Issue. *J. Geophys. Res.: Solid Earth* 86, 2495–2496. doi:10.1029/JB086iB04p02495

Collier, M. L. (2012). *Spatial-Statistical Properties of Geochemical Variability as Constraints on Magma Transport and Evolution Processes at Ocean Ridges.* Ph.D. thesis, Columbia University. doi:10.7916/D82V2P43

Costello, E. K., Halloy, S. R. P., Reed, S. C., Sowell, P., and Schmidt, S. K. (2009). Fumarole-Supported Islands of Biodiversity within a Hyperarid, High-Elevation Landscape on Socompa Volcano, Puna de Atacama, Andes. *Appl. Environ. Microbiol.* 75, 735–747. doi: 10.1128/AEM.01469-08

Crespo-Medina, M., Twing, K. I., Kubo, M. D. Y., Hoehler, T. M., Cardace, D., McCollom, T., et al. (2014). Insights into environmental controls on microbial communities in a continental serpentinite aquifer using a microcosm-based approach. *Front. Microb.* 5, 604. doi:10.3389/fmicb.2014.00604

Crespo-Medina, M., Twing, K. I., Sánchez-Murillo, R., Brazelton, W. J., McCollom, T. M., and Schrenk, M. O. (2017). Methane Dynamics in a Tropical Serpentinizing Environment: The Santa Elena Ophiolite, Costa Rica. *Front. Microb.* 8. doi:10.3389/fmicb.2017.00916

de Obeso, J. C. and Kelemen, P. B. (2018). Fluid rock interactions on residual mantle peridotites overlain by shallow oceanic limestones: Insights from Wadi Fins, Sultanate of Oman. *Chem. Geol.* 498, 139 – 149. doi:10.1016/j.chemgeo.2018.09.022

De Weert, J. P. A., Viñas, M., Grotenhuis, T., Rijnaarts, H. H. M., and Langenhoff, A. A. M. (2011). Degradation of 4-n-nonylphenol under nitrate reducing conditions. *Biodegradation* 22, 175–187. doi:10.1007/s10532-010-9386-4

Deines, P. (2002). The carbon isotope geochemistry of mantle xenoliths. *Earth-Sci. Rev.* 58, 247 – 278. doi:10.1016/S0012-8252(02)00064-8

Delacour, A., Früh-Green, G. L., Bernasconi, S. M., Schaeffer, P., and Kelley, D. S. (2008). Carbon geochemistry of serpentinites in the Lost City Hydrothermal System (30 °N, MAR). *Geochim. Cosmochim. Acta* 72, 3681 – 3702. doi:10.1016/j.gca.2008.04.039

Dewandel, B., Boudier, F., Kern, H., Warsi, W., and Mainprice, D. (2003). Seismic wave velocity and anisotropy of serpentinized peridotite in the Oman ophiolite. *Tectonophysics* 370, 77 – 94. doi:10.1016/S0040-1951(03)00178-1. Physical Properties of Rocks and other Geomaterials, a Special Volume to honour Professor H. Kern

Dewandel, B., Lachassagne, P., Boudier, F., Al-Hattali, S., Ladouche, B., Pinault, J.-L., et al. (2005). A conceptual hydrogeological model of ophiolite hard-rock aquifers in Oman based on a multiscale and a multidisciplinary approach. *Hydrogeol. J.* 13, 708–726. doi: 10.1007/s10040-005-0449-2

Economou-Eliopoulos, M. (1996). Platinum-group element distribution in chromite ores from ophiolite complexes: implications for their exploration. *Ore Geol. Rev.* 11, 363–381. doi:10.1016/S0169-1368(96)00008-X

Etiope, G. (2017a). Abiotic methane in continental serpentinization sites: an overview. *Procedia Earth Planet. Sci.* 17, 9–12. doi:10.1016/j.proeps.2016.12.006

Etiope, G. (2017b). Methane origin in the Samail ophiolite: Comment on "Modern water/rock reactions in Oman hyperalkaline peridotite aquifers and implications for microbial habitability" [Geochim. Cosmochim. Acta 179 (2016) 217–241]. *Geochim. Cosmochim. Acta* 197, 467 – 470. doi:10.1016/j.gca.2016.08.001

Etiope, G., Ifandi, E., Nazzari, M., Procesi, M., Tsikouras, B., Ventura, G., et al. (2018). Widespread abiotic methane in chromitites. *Sci. Rep.* 8. doi:10.1038/s41598-018-27082-0

Etiope, G. and Ionescu, A. (2015). Low-temperature catalytic CO_2 hydrogenation with geological quantities of ruthenium: a possible abiotic CH_4 source in chromitite-rich serpentinized rocks. *Geofluids* 15, 438–452. doi:10.1111/gfl.12106

Etiope, G., Judas, J., and Whiticar, M. (2015). Occurrence of abiotic methane in the eastern United Arab Emirates ophiolite aquifer. *Arabian J. Geosci.* 8, 11345–11348. doi:10.1007/s12517-015-1975-4

Etiope, G. and Schoell, M. (2014). Abiotic Gas: Atypical, But Not Rare. *Elements* 10, 291–296. doi:10.2113/gselements.10.4.291

Etiope, G., Schoell, M., and Hosgörmez, H. (2011). Abiotic methane flux from the Chimaera seep and Tekirova ophiolites (Turkey): understanding gas exhalation from low temperature serpentinization and implications for Mars. *Earth Planet. Sci. Lett.* 310, 96–104. doi:10.1016/j.epsl.2011.08.001

Etiope, G., Vadillo, I., Whiticar, M., Marques, J., Carreira, P., Tiago, I., et al. (2016). Abiotic methane seepage in the Ronda peridotite massif, southern Spain. *Appl. Geochem.* 66, 101–113. doi:doi.org/10.1016/j.apgeochem.2015.12.001

Etiope, G. and Whiticar, M. (2019). Abiotic methane in continental ultramafic rock systems: Towards a genetic model. *Appl. Geochem.* 102, 139 – 152. doi:10.1016/j.apgeochem.2019.01.012

Ettwig, K. F., Butler, M. K., Le Paslier, D., Pelletier, E., Mangenot, S., Kuypers, M. M. M., et al. (2010). Nitrite-driven anaerobic methane oxidation by oxygenic bacteria. *Nature* 464, 543. doi:10.1038/nature08883

Evans, B. W. (1977). Metamorphism of alpine peridotite and serpentinite. *Annu. Rev. Earth Planet. Sci.* 5, 397–447. doi:10.1146/annurev.ea.05.050177.002145

Falk, E., Guo, W., Paukert, A., Matter, J., Mervine, E., and Kelemen, P. (2016). Controls on the stable isotope compositions of travertine from hyperalkaline springs in Oman: Insights from clumped isotope measurements. *Geochim. Cosmochim. Acta* 192, 1 – 28. doi:10.1016/j.gca.2016.06.026

Feisthauer, S., Vogt, C., Modrzynski, J., Szlenkier, M., Krüger, M., Siegert, M., et al. (2011). Different types of methane monooxygenases produce similar carbon and hydrogen isotope fractionation patterns during methane oxidation. *Geochim. Cosmochim. Acta* 75, 1173 – 1184. doi:10.1016/j.gca.2010.12.006

Fiebig, J., Stefánsson, A., Ricci, A., Tassi, F., Viveiros, F., Silva, C., et al. (2019). Abiogenesis not required to explain the origin of volcanic-hydrothermal hydrocarbons. *Geochem. Perspect. Lett.* 11, 23–27. doi:10.7185/geochemlet.1920

Fones, E. M., Colman, D. R., Kraus, E. A., Nothaft, D. B., Poudel, S., Rempfert, K. R., et al. (2019). Physiological adaptations to serpentinization in the Samail Ophiolite, Oman. *ISME J.* , 1doi:10.1038/s41396-019-0391-2

Fones, E. M., Colman, D. R., Kraus, E. A., Stepanauskas, R., Templeton, A. S., Spear, J. R., et al. (in press). Diversification of methanogens into hyperalkaline serpentinizing environments through adaptations to minimize oxidant limitation. *ISME J.*

Formolo, M. (2010). *Handbook ofHydrocarbon and Lipid Microbiology* (Springer-Verlag Berlin Heidelberg), chap. The Microbial Production of Methane and Other Volatile Hydrocarbons. 6. doi:10.1007/978-3-540-77587-4_6

Friedlingstein, P., Jones, M. W., O'Sullivan, M., Andrew, R. M., Hauck, J., Peters, G. P., et al. (2019). Global Carbon Budget 2019. *Earth Syst. Sci. Data* 11, 1783–1838. doi:10.5194/essd-11-1783-2019

Fritz, P., Clark, I., Fontes, J.-C., Whiticar, M., and Faber, E. (1992). Deuterium and ^{13}C evidence for low temperature production of hydrogen and methane in a highly alkaline groundwater environment in Oman. In *International symposium on water-rock interaction* (AA Balkema Rotterdam), vol. 1, 793–796

Frost, B. R. (1985). On the Stability of Sulfides, Oxides, and Native Metals in Serpentinite. *J. Petrol.* 26, 31–63. doi:10.1093/petrology/26.1.31

Gadikota, G., Matter, J., Kelemen, P., Brady, P. V., and Park, A.-H. A. (2020). Elucidating the differences in the carbon mineralization behaviors of calcium and magnesium bearing alumino-silicates and magnesium silicates for CO_2 storage. *Fuel* 277, 117900. doi:10.1016/j.fuel.2020.117900

Gadikota, G., Matter, J., Kelemen, P., and Park, A.-h. A. (2014). Chemical and morphological changes during olivine carbonation for CO_2 storage in the presence of NaCl and $NaHCO_3$. *Phys. Chem. Chem. Phys.* 16, 4679–4693. doi:10.1039/C3CP54903H

Garuti, G. and Zaccarini, F. (1997). In situ alteration of platinum-group minerals at low temperature; evidence from serpentinized and weathered chromitite of the Vourinos Complex, Greece. *Canad. Mineral.* 35, 611–626

Giovannoni, S. J., Cameron Thrash, J., and Temperton, B. (2014). Implications of streamlining theory for microbial ecology. *ISME J.* 8, 1553–1565. doi:10.1038/ismej.2014.60

Giunta, T., Young, E. D., Warr, O., Kohl, I., Ash, J. L., Martini, A., et al. (2019). Methane sources and sinks in continental sedimentary systems: New insights from paired clumped isotopologues $^{1}3CH_3D$ and $^{1}2CH_2D^{2}$. *Geochim. Cosmochim. Acta* 245, 327 – 351. doi:10.1016/j.gca.2018.10.030

Glein, C. R., Baross, J. A., and Waite Jr, J. H. (2015). The pH of Enceladus' ocean. *Geochim. Cosmochim. Acta* 162, 202–219. doi:10.1016/j.gca.2015.04.017

Glein, C. R. and Zolotov, M. Y. (2020). Hydrogen, Hydrocarbons, and Habitability Across the Solar System. *Elements* 16, 47–52. doi:10.2138/gselements.16.1.47

Glennie, K., Boeuf, M., Clarke, M. H., Moody-Stuart, M., Pilaar, W., and Reinhardt, B. (1973). Late Cretaceous nappes in Oman Mountains and their geologic evolution. *AAPG Bull.* 57, 5–27. doi:10.1306/819A4240-16C5-11D7-8645000102C1865D

Glombitza, C., Kubo, M. D., Ellison, E. T., Rempfert, K. R., Matter, J. M., Templeton, A. S., et al. (2019). Microbial sulfate reduction rates in low temperature serpentinizing mantle rocks. In *AGU Fall Meeting Abstracts*. vol. 2019, B44C–06

Godard, M., Jousselin, D., and Bodinier, J.-L. (2000). Relationships between geochemistry and structure beneath a palaeo-spreading centre: a study of the mantle section in the Oman ophiolite. *Earth Planet. Sci. Lett.* 180, 133 – 148. doi:10.1016/S0012-821X(00)00149-7

Goldstein, T. P. and Aizenshtat, Z. (1994). Thermochemical sulfate reduction a review. *J. Therm. Anal.* 42, 241–290. doi:10.1007/BF02547004

Grozeva, N. G., Klein, F., Seewald, J. S., and Sylva, S. P. (2020). Chemical and isotopic analyses of hydrocarbon-bearing fluid inclusions in olivine-rich rocks. *Philos. Trans. R. Soc., A* 378. doi:10.1098/rsta.2018.0431

Gruen, D. S., Wang, D. T., Könneke, M., Topçuoğlu, B. D., Stewart, L. C., Goldhammer, T., et al. (2018). Experimental investigation on the controls of clumped isotopologue and hydrogen isotope ratios in microbial methane. *Geochim. Cosmochim. Acta* 237, 339 – 356. doi:10.1016/j.gca.2018.06.029

Guillot, S. and Hattori, K. (2013). Serpentinites: Essential Roles in Geodynamics, Arc Volcanism, Sustainable Development, and the Origin of Life. *Elements* 9, 95–98. doi:10.2113/gselements.9.2.95

Guilmette, C., Smit, M. A., van Hinsbergen, D. J. J., Gürer, D., Corfu, F., Charette, B., et al. (2018). Forced subduction initiation recorded in the sole and crust of the Semail Ophiolite of Oman. *Nat. Geosci.* 11, 688–695. doi:10.1038/s41561-018-0209-2

Habib, N., Khan, I. U., Hussain, F., Zhou, E.-M., Xiao, M., Dong, L., et al. (2017). Meiothermus luteus sp. nov., a slightly thermophilic bacterium isolated from a hot spring. *Int. J. Syst. Evol. Microbiol.* 67, 2910–2914. doi:10.1099/ijsem.0.002040

Halpern, M., Shakèd, T., and Schumann, P. (2009). Brachymonas chironomi sp. nov., isolated from a chironomid egg mass, and emended description of the genus Brachymonas. *International Journal of Systematic and Evolutionary Microbiology* 59, 3025–3029. doi: https://doi.org/10.1099/ijs.0.007211-0

Hamilton, T. L., Peters, J. W., Skidmore, M. L., and Boyd, E. S. (2013). Molecular evidence for an active endogenous microbiome beneath glacial ice. *ISME J.* 7, 1402–1412. doi: 10.1038/ismej.2013.31

Hammer, S. and Levin, I. (2017). Monthly mean atmospheric D14CO2 at Jungfraujoch and Schauinsland from 1986 to 2016. doi:10.11588/data/10100

Hand, K. P., Carlson, R. W., and Chyba, C. F. (2007). Energy, chemical disequilibrium, and geological constraints on Europa. *Astrobiology* 7, 1006–1022. doi:10.1089/ast.2007.0156

Hanghøj, K., Kelemen, P. B., Hassler, D., and Godard, M. (2010). Composition and Genesis of Depleted Mantle Peridotites from the Wadi Tayin Massif, Oman Ophiolite; Major and Trace Element Geochemistry, and Os Isotope and PGE Systematics. *J. Petrol.* 51, 201–227. doi:10.1093/petrology/egp077

Hanson, R. S. and Hanson, T. E. (1996). Methanotrophic bacteria. *Microbiol. Mol. Biol. Rev.* 60, 439–471

Henry, E. A., Devereux, R., Maki, J. S., Gilmour, C. C., Woese, C. R., Mandelco, L., et al. (1994). Characterization of a new thermophilic sulfate-reducing bacterium. *Arch. Microbiol.* 161, 62–69. doi:10.1007/BF00248894

Hiraishi, A., Sugiyama, J., and Shin, Y. K. (1995). BRACHYMONAS DENITRIFICANS GEN. NOV., SP. NOV., AN AEROBIC CHEMOORGANOTROPHIC BACTERIUM WHICH CONTAINS RHODOQUINONES, AND EVOLUTIONARY RELATIONSHIPS OF RHODOQUINONE PRODUCERS TO BACTERIAL SPECIES WITH VARIOUS QUINONE CLASSES. *J. Gen. Appl. Microbiol.* 41, 99–117. doi:10.2323/jgam.41.99

Hirschmann, M. M. (2018). Comparative deep Earth volatile cycles: The case for C recycling from exosphere/mantle fractionation of major (H_2O, C, N) volatiles and from H_2O/Ce, CO_2/Ba, and CO_2/Nb exosphere ratios. *Earth Planet. Sci. Lett.* 502, 262 – 273. doi:10.1016/j.epsl.2018.08.023

Horibe, Y. and Craig, H. (1995). DH fractionation in the system methane-hydrogen-water. *Geochim. Cosmochim. Acta* 59, 5209–5217. doi:10.1016/0016-7037(95)00391-6

Jacquemin, M., Beuls, A., and Ruiz, P. (2010). Catalytic production of methane from CO_2 and H_2 at low temperature: Insight on the reaction mechanism. *Catal. Today* 157, 462–466. doi:10.1016/j.cattod.2010.06.016

Jones, L. C., Rosenbauer, R., Goldsmith, J. I., and Oze, C. (2010). Carbonate control of H_2 and CH_4 production in serpentinization systems at elevated P-Ts. *Geophys. Res. Lett.* 37. doi:10.1029/2010GL043769

Kampbell, D., Wilson, J., and McInnes, D. (1998). Determining dissolved hydrogen, methane, and vinyl chloride concentrations in aqueous solution on a nanomolar scale with the bubble strip method. In *Proceedings of the 1998 Conference on Hazardous Waste Research*. 176–190

Kelemen, P., Al Rajhi, A., Godard, M., Ildefonse, B., Köpke, J., MacLeod, C., et al. (2013). Scientific drilling and related research in the samail ophiolite, sultanate of Oman. *Scientific Drilling 2013 (2013), Nr. 15* 2013, 64–71

Kelemen, P., Matter, J., Teagle, D., Coggon, J., and the Oman Drilling Project Science Team (2020a). Proceedings of the oman drilling project. In *Proceedings of the Oman Drilling Project* (College Station, TX: International Ocean Discovery Program), All pages. doi: 10.14379/OmanDP.proc.2020

Kelemen, P. B. and Manning, C. E. (2015). Reevaluating carbon fluxes in subduction zones, what goes down, mostly comes up. *Proc. Natl. Acad. Sci. U. S. A.* 112, E3997–E4006. doi:10.1073/pnas.1507889112

Kelemen, P. B. and Matter, J. (2008). In situ carbonation of peridotite for CO_2 storage. *Proc. Natl. Acad. Sci. U. S. A.* 105, 17295–17300. doi:10.1073/pnas.0805794105

Kelemen, P. B., Matter, J., Streit, E. E., Rudge, J. F., Curry, W. B., and Blusztajn, J. (2011). Rates and mechanisms of mineral carbonation in peridotite: natural processes and recipes for enhanced, in situ CO_2 capture and storage. *Annu. Rev. Earth Planet. Sci.* 39, 545–576. doi:10.1146/annurev-earth-092010-152509

Kelemen, P. B., McQueen, N., Wilcox, J., Renforth, P., Dipple, G., and Vankeuren, A. P. (2020b). Engineered carbon mineralization in ultramafic rocks for CO_2 removal from air: Review and new insights. *Chem. Geol.* 550, 119628. doi:10.1016/j.chemgeo.2020.119628

Kelley, D. S. (1996). Methane-rich fluids in the oceanic crust. *J. Geophys. Res.: Solid Earth* 101, 2943–2962. doi:10.1029/95JB02252

Kelley, D. S. and Früh-Green, G. L. (1999). Abiogenic methane in deep-seated mid-ocean ridge environments: Insights from stable isotope analyses. *J. Geophys. Res.: Solid Earth* 104, 10439–10460. doi:10.1029/1999JB900058

Kieft, T. L. (2016). *Microbiology of the Deep Continental Biosphere* (Cham: Springer International Publishing). 225–249. doi:10.1007/978-3-319-28071-4_6

Kieft, T. L., McCuddy, S. M., Onstott, T. C., Davidson, M., Lin, L.-H., Mislowack, B., et al. (2005). Geochemically Generated, Energy-Rich Substrates and Indigenous Microorganisms in Deep, Ancient Groundwater. *Geomicrobiol. J.* 22, 325–335. doi: 10.1080/01490450500184876

Klein, F. and Bach, W. (2009). Fe–Ni–Co–O–S Phase Relations in Peridotite–Seawater Interactions. *J. Petrol.* 50, 37–59. doi:10.1093/petrology/egn071

Klein, F., Bach, W., Jöns, N., McCollom, T., Moskowitz, B., and Berquó, T. (2009). Iron partitioning and hydrogen generation during serpentinization of abyssal peridotites from 15 °N on the Mid-Atlantic Ridge. *Geochim. Cosmochim. Acta* 73, 6868 – 6893. doi: 10.1016/j.gca.2009.08.021

Klein, F., Grozeva, N. G., and Seewald, J. S. (2019). Abiotic methane synthesis and serpentinization in olivine-hosted fluid inclusions. *Proc. Natl. Acad. Sci. U. S. A.* 116, 17666–17672. doi:10.1073/pnas.1907871116

Knittel, K. and Boetius, A. (2009). Anaerobic Oxidation of Methane: Progress with an Unknown Process. *Annu. Rev. Microbiol.* 63, 311–334. doi:10.1146/annurev.micro.61.080706.093130. PMID: 19575572

Koepp, M. (1978). D/H isotope exchange reaction between petroleum and water: a contributory determinant for D/H- isotope ratios in crude oils. In *Short papers of the Fourth International Conference, Geochronology, Cosmochronology, Isotope Geology, 1978*, ed. R. E. Zartman. 221–222. doi:10.3133/ofr78701

Kral, T. A., Birch, W., Lavender, L. E., and Virden, B. T. (2014). Potential use of highly insoluble carbonates as carbon sources by methanogens in the subsurface of Mars. *Planet. Space Sci.* 101, 181 – 185. doi:10.1016/j.pss.2014.07.008

Kraus, E. A., Stamps, B. W., Rempfert, K. R., Nothaft, D. B., Boyd, E. S., Matter, J. M., et al. (2018). Biological methane cycling in serpentinization-impacted fluids of the Samail ophiolite of Oman. *AGU Fall Meeting Abstracts*

Kraus, E. A., Stamps, B. W., Rempfert, K. R., Nothaft, D. B., Boyd, E. S., Matter, J. M., et al. (in press). Active biological methane cycling in serpentinization-impacted fluids of the samail ophiolite of oman and implications for methane isotopic biosignatures. *Appl. Environ. Microbiol.*

Kumagai, H., Nakamura, K., Toki, T., Morishita, T., Okino, K., Ishibashi, J.-i., et al. (2008). Geological background of the Kairei and Edmond hydrothermal fields along the Central Indian Ridge : Implications for the distinct chemistry between their vent fluids. *Geofluids* 8, 239–251. doi:10.1111/j.1468-8123.2008.00223.x

Labidi, J., Young, E., Giunta, T., Kohl, I., Seewald, J., Tang, H., et al. (2020). Methane thermometry in deep-sea hydrothermal systems: Evidence for re-ordering of doubly-substituted isotopologues during fluid cooling. *Geochim. Cosmochim. Acta* 288, 248 – 261. doi:10.1016/j.gca.2020.08.013

Lang, S. Q., Früh-Green, G. L., Bernasconi, S. M., Brazelton, W. J., Schrenk, M. O., and McGonigle, J. M. (2018). Deeply-sourced formate fuels sulfate reducers but not methanogens at Lost City hydrothermal field. *Sci. Rep.* 8, 755. doi:10.1038/s41598-017-19002-5

Laso-Pérez, R., Hahn, C., van Vliet, D. M., Tegetmeyer, H. E., Schubotz, F., Smit, N. T., et al. (2019). Anaerobic Degradation of Non-Methane Alkanes by "Candidatus Methanoliparia" in Hydrocarbon Seeps of the Gulf of Mexico. *mBio* 10. doi:10.1128/mBio.01814-19

Lee, E. M., Jeon, C. O., Choi, I., Chang, K.-S., and Kim, C.-J. (2005). Silanimonas lenta gen. nov., sp. nov., a slightly thermophilic and alkaliphilic gammaproteobacterium isolated from a hot spring. *Int. J. Syst. Evol. Microbiol.* 55, 385–389. doi:10.1099/ijs.0.63328-0

Leong, J., Howells, A., Robinson, K., and Shock, E. (2020). Diversity in the compositions of fluids hosted in continental serpentinizing systems. In *International Conference on Ophiolites and the Oceanic Lithosphere: Proceeding and Abstract Book*. 130–131

Leong, J. A. M. and Shock, E. L. (2020). Thermodynamic constraints on the geochemistry of low-temperature, continental, serpentinization-generated fluids. *Am. J. Sci.* 320, 185–235. doi:10.2475/03.2020.01

Lin, X., Kennedy, D., Fredrickson, J., Bjornstad, B., and Konopka, A. (2012). Vertical stratification of subsurface microbial community composition across geological formations at the Hanford Site. *Environ. Microbiol.* 14, 414–425. doi:10.1111/j.1462-2920.2011.02659.x

Lippard, S., Shelton, A., and Gass, I. (1986). *The Ophiolite of Northern Oman*, vol. 11 (Geological Society of London). doi:10.1144/GSL.MEM.1986.011.01.03

Lods, G., Roubinet, D., Matter, J. M., Leprovost, R., and Gouze, P. (2020). Groundwater flow characterization of an ophiolitic hard-rock aquifer from cross-borehole multi-level hydraulic experiments. *Journal of Hydrology* 589, 125152. doi:https://doi.org/10.1016/j.jhydrol.2020.125152

Lovley, D. R., Chapelle, F. H., and Woodward, J. C. (1994). Use of Dissolved H_2 Concentrations To Determine Distribution of Microbially Catalyzed Redox Reactions in Anoxic Groundwater. *Environ. Sci. Technol.* 28, 1205–1210. doi:10.1021/es00056a005

Lowe, D. C., Brenninkmeijer, C. A., Tyler, S. C., and Dlugkencky, E. J. (1991). Determination of the isotopic composition of atmospheric methane and its application in the Antarctic. *J. Geophys. Res.: Atmos.* 96, 15455–15467. doi:10.1029/91JD01119

Lowell, R., Kolandaivelu, K., and Rona, P. (2014). Hydrothermal Activity. In *Reference Module in Earth Systems and Environmental Sciences* (Elsevier). doi:10.1016/B978-0-12-409548-9.09132-6

Luesken, F. A., Wu, M. L., Op den Camp, H. J. M., Keltjens, J. T., Stunnenberg, H., Francoijs, K.-J., et al. (2012). Effect of oxygen on the anaerobic methanotroph 'Candidatus Methylomirabilis oxyfera': kinetic and transcriptional analysis. *Environ. Microbiol.* 14, 1024–1034. doi:10.1111/j.1462-2920.2011.02682.x

Luque, F., Crespo-Feo, E., Barrenechea, J., and Ortega, L. (2012). Carbon isotopes of graphite: Implications on fluid history. *Geosci. Front.* 3, 197 – 207. doi:10.1016/j.gsf.2011.11.006

Luther, G. W., Findlay, A., MacDonald, D., Owings, S., Hanson, T., Beinart, R., et al. (2011). Thermodynamics and Kinetics of Sulfide Oxidation by Oxygen: A Look at Inorganically Controlled Reactions and Biologically Mediated Processes in the Environment. *Front. Microb.* 2, 62. doi:10.3389/fmicb.2011.00062

MacDougall, D., Crummett, W. B., et al. (1980). Guidelines for data acquisition and data quality evaluation in environmental chemistry. *Anal. Chem.* 52, 2242–2249

Marques, J., Etiope, G., Neves, M., Carreira, P., Rocha, C., Vance, S., et al. (2018). Linking serpentinization, hyperalkaline mineral waters and abiotic methane production in continental peridotites: an integrated hydrogeological-bio-geochemical model from the Cabeço de Vide CH_4-rich aquifer (Portugal). *Appl. Geochem.* 96, 287 – 301. doi:10.1016/j.apgeochem.2018.07.011

Martini, A. M., Walter, L. M., Ku, T. C. W., Budai, J. M., McIntosh, J. C., and Schoell, M. (2003). Microbial production and modification of gases in sedimentary basins: A geochemical case study from a Devonian shale gas play, Michigan basin. *AAPG Bull.* 87, 1355–1375. doi:10.1306/031903200184

Matter, J. M., Pezard, P. A., Moe, K., Henry, G., Paris, J., Brun, L., et al. (2018). Advanced downhole hydrogeophysical logging during Oman Drilling Project Phase 2 - Correlation of hydraulic and fluid properties. *AGU Fall Meeting Abstracts*

Matter, J. M., Waber, H., Loew, S., and Matter, A. (2006). Recharge areas and geochemical evolution of groundwater in an alluvial aquifer system in the Sultanate of Oman. *Hydrogeol. J.* 14, 203–224. doi:10.1007/s10040-004-0425-2

Mayhew, L. E., Ellison, E., McCollom, T., Trainor, T., and Templeton, A. (2013). Hydrogen generation from low-temperature water–rock reactions. *Nat. Geosci.* 6, 478. doi:10.1038/ngeo1825

McCollom, T. M. (1999). Methanogenesis as a potential source of chemical energy for primary biomass production by autotrophic organisms in hydrothermal systems on Europa. *Journal of Geophysical Research: Planets* 104, 30729–30742. doi:10.1029/1999JE001126

McCollom, T. M. (2016). Abiotic methane formation during experimental serpentinization of olivine. *Proc. Natl. Acad. Sci. U. S. A.* 113, 13965–13970. doi:10.1073/pnas.1611843113

McCollom, T. M. and Bach, W. (2009). Thermodynamic constraints on hydrogen generation during serpentinization of ultramafic rocks. *Geochim. Cosmochim. Acta* 73, 856–875. doi:10.1016/j.gca.2008.10.032

McCollom, T. M. and Seewald, J. S. (2003). Experimental constraints on the hydrothermal reactivity of organic acids and acid anions: I. Formic acid and formate. *Geochim. Cosmochim. Acta* 67, 3625 – 3644. doi:10.1016/S0016-7037(03)00136-4

McDermott, J. M., Seewald, J. S., German, C. R., and Sylva, S. P. (2015). Pathways for abiotic organic synthesis at submarine hydrothermal fields. *Proc. Natl. Acad. Sci. U. S. A.* 112, 7668–7672. doi:10.1073/pnas.1506295112

McKay, C. P., Porco, C. C., Altheide, T., Davis, W. L., and Kral, T. A. (2008). The Possible Origin and Persistence of Life on Enceladus and Detection of Biomarkers in the Plume. *Astrobiology* 8, 909–919. doi:10.1089/ast.2008.0265. PMID: 18950287

Ménez, B. (2020). Abiotic Hydrogen and Methane: Fuels for Life. *Elements* 16, 39–46. doi:10.2138/gselements.16.1.39

Merlivat, L., Pineau, F., and Javoy, M. (1987). Hydrothermal vent waters at 13 °N on the East Pacific Rise: isotopic composition and gas concentration. *Earth Planet. Sci. Lett.* 84, 100 – 108. doi:10.1016/0012-821X(87)90180-4

Mervine, E. M., Humphris, S. E., Sims, K. W., Kelemen, P. B., and Jenkins, W. J. (2014). Carbonation rates of peridotite in the Samail Ophiolite, Sultanate of Oman, constrained through ^{14}C dating and stable isotopes. *Geochim. Cosmochim. Acta* 126, 371 – 397. doi: 10.1016/j.gca.2013.11.007

Meyer-Dombard, D. R., Woycheese, K. M., YargÄ±*olu*, *E. N.*, *Cardace*, *D.*, *Shock*, *E. L.*, *Gleal*−
Pektas, *Y.*, *et al.*(2015). *HighpHmicrobialecosystemsinanewlydiscovered*, *ephemeral*, *serpentinizingfluic*
Meyer-Dombard_ea_2015_Turkey

Michaelis, W., Seifert, R., Nauhaus, K., Treude, T., Thiel, V., Blumenberg, M., et al. (2002). Microbial Reefs in the Black Sea Fueled by Anaerobic Oxidation of Methane. *Science* 297, 1013–1015. 10.1126/science.1072502 Michaelis_ea_2002_black_sea_AOM_carb

Milkov, A. V. and Etiope, G. (2018). Revised genetic diagrams for natural gases based on a global dataset of >20,000 samples. *Org. Geochem.* 125, 109–120. 10.1016/j.orggeochem.2018.09.002 Milkov_Etiope_2018_CH4_origin_diagrams

Miller, H. M., Chaudhry, N., Conrad, M. E., Bill, M., Kopf, S. H., and Templeton, A. S. (2018). Large carbon isotope variability during methanogenesis under alkaline conditions. *Geochim. Cosmochim. Acta* 237, 18 – 31. 10.1016/j.gca.2018.06.007 Miller_ea_2018_pH_methanogens

Miller, H. M., Matter, J. M., Kelemen, P., Ellison, E. T., Conrad, M., Fierer, N., et al. (2017a). Reply to "Methane origin in the Samail ophiolite: Comment on 'Modern water/rock reactions in Oman hyperalkaline peridotite aquifers and implications for microbial

habitability"' [Geochim. Cosmochim. Acta 179 (2016) 217–241]. *Geochim. Cosmochim. Acta* 197, 471 – 473. 10.1016/j.gca.2016.11.011 Miller_ea_2017_reply_to_Etiope

Miller, H. M., Matter, J. M., Kelemen, P., Ellison, E. T., Conrad, M. E., Fierer, N., et al. (2016). Modern water/rock reactions in Oman hyperalkaline peridotite aquifers and implications for microbial habitability. *Geochim. Cosmochim. Acta* 179, 217 – 241. 10.1016/j.gca.2016.01.033 Miller_ea_2016_WR_rxns

Miller, H. M., Mayhew, L. E., Ellison, E. T., Kelemen, P., Kubo, M., and Templeton, A. S. (2017b). Low temperature hydrogen production during experimental hydration of partially-serpentinized dunite. *Geochim. Cosmochim. Acta* 209, 161 – 183. 10.1016/j.gca.2017.04.022 Miller_ea_2017_experimental_H2

Mitchell, P. (2011). Chemiosmotic coupling in oxidative and photosynthetic phosphorylation. *Biochim. Biophys. Acta - Bioenerg.* 1807, 1507 – 1538. 10.1016/j.bbabio.2011.09.018. Special Section: Peter Mitchell - 50th anniversary of the chemiosmotic theory Mitchell_2011

Miura, M., Arai, S., and Mizukami, T. (2011). Raman spectroscopy of hydrous inclusions in olivine and orthopyroxene in ophiolitic harzburgite: Implications for elementary processes in serpentinization. *J. Mineral. Petrol. Sci.* advpub, 1103030170–1103030170. 10.2465/jmps.101021d Miura_ea_2011_fluid_inclusions

Moser, D. P., Gihring, T. M., Brockman, F. J., Fredrickson, J. K., Balkwill, D. L., Dollhopf, M. E., et al. (2005). Desulfotomaculum and Methanobacterium spp. Dominate a 4- to 5-Kilometer-Deep Fault. *Appl. Environ. Microbiol.* 71, 8773–8783. 10.1128/AEM.71.12.8773-8783.2005 Moser_ea_2005

Mulkidjanian, A. Y., Dibrov, P., and Galperin, M. Y. (2008). The past and present of sodium energetics: May the sodium-motive force be with you. *Biochim. Biophys. Acta - Bioenerg.* 1777, 985 – 992. 10.1016/j.bbabio.2008.04.028. 15th European Bioenergetics Conference 2008 Mulkidjanian_ea_2008

Mumma, M. J., Villanueva, G. L., Novak, R. E., Hewagama, T., Bonev, B. P., Disanti,

M. A., et al. (2009). Strong release of methane on Mars in northern summer 2003. *Science* 323, 1041–1045. 10.1126/science.1165243 Mumma_ea_2009

Murad, A. A. and Krishnamurthy, R. (2004). Factors controlling groundwater quality in Eastern United Arab Emirates: a chemical and isotopic approach. *J. Hydro.* 286, 227 – 235. 10.1016/j.jhydrol.2003.09.020 Murad_ea_2004_UAE_hydro

Myhre, G., Shindell, D., Bréon, F.-M., Collins, W., Fuglestvedt, J., Huang, J., et al. (2013). *Anthropogenic and Natural Radiative Forcing* (Cambridge, United Kingdom and New York, NY, USA: Cambridge University Press), book section 8. 659–740. 10.1017/CBO9781107415324.018 Myhre_ea_2013_IPCC_AR5_ch8

National Academies (2019). *Negative Emissions Technologies and Reliable Sequestration: A Research Agenda* (Washington, DC: National Academies Press). 10.17226/25259 National_Academies_2019_Negative_Emissions

Neal, C. and Stanger, G. (1983). Hydrogen generation from mantle source rocks in Oman. *Earth Planet. Sci. Lett.* 66, 315 – 320. 10.1016/0012-821X(83)90144-9 Neal_Stanger_1983_Oman_H2

Neal, C. and Stanger, G. (1985). Past and present serpentinisation of ultramafic rocks; an example from the Semail Ophiolite Nappe of Northern Oman. In *The Chemistry of Weathering* (Springer). 249–275. 10.1007/978-94-009-5333-8_15 Neal_Stanger_1985_Oman

Nealson, K. H., Inagaki, F., and Takai, K. (2005). Hydrogen-driven subsurface lithoautotrophic microbial ecosystems (SLiMEs): do they exist and why should we care? *Trends Microbiol.* 13, 405–410. 10.1016/j.tim.2005.07.010 Nealson_ea_2005_SLiMEs

Neubeck, A., Duc, N. T., Bastviken, D., Crill, P., and Holm, N. G. (2011). Formation of H_2 and CH_4 by weathering of olivine at temperatures between 30 and 70°C. *Geochem. Trans.* 12, 6. 10.1186/1467-4866-12-6 Neubeck_ea_2011

Nicolas, A. (1989). *Structures of Ophiolites and Dynamics of Oceanic Lithosphere | SpringerLink* (Springer, Dordrecht). 10.1007/978-94-009-2374-4 Nicolas_1989_book

Nicolas, A., Boudier, F., Ildefonse, B., and Ball, E. (2000). Accretion of Oman and United Arab Emirates ophiolite–discussion of a new structural map. *Marine Geophysical Researches* 21, 147–180. 10.1023/A:1026769727917 Nicolas_ea_2000_Oman_map

Noël, J., Godard, M., Oliot, E., Martinez, I., Williams, M., Boudier, F., et al. (2018). Evidence of polygenetic carbon trapping in the Oman Ophiolite: Petro-structural, geochemical, and carbon and oxygen isotope study of the Wadi Dima harzburgite-hosted carbonates (Wadi Tayin massif, Sultanate of Oman). *Lithos* 323, 218 – 237. 10.1016/j.lithos.2018.08.020. ABYSS Noel_ea_2018_carbonation_wadi_dima

Nolan, S. C., Skelton, P. W., Clissold, B. P., and Smewing, J. D. (1990). Maastrichtian to early Tertiary stratigraphy and palaeogeography of the Central and Northern Oman Mountains. *Geological Society, London, Special Publications* 49, 495–519. 10.1144/GSL.SP.1992.049.01.31 Nolan_ea_1990_Oman_Maastrichtian_limestone

Nothaft, D. B., Templeton, A. S., Rhim, J. H., Wang, D. T., Labidi, J., Miller, H. M., et al. (2020). Geochemical, biological and clumped isotopologue evidence for substantial microbial methane production under carbon limitation in serpentinites of the Samail Ophiolite, Oman. *Earth and Space Sci. Open Archive* 10.1002/essoar.10504124.1 Nothaft_ea_2020_CH4_stable_temp

Okland, I., Huang, S., Thorseth, I., and Pedersen, R. (2014). Formation of H_2, CH_4 and N-species during low-temperature experimental alteration of ultramafic rocks. *Chem. Geol.* 387, 22 – 34. 10.1016/j.chemgeo.2014.08.003 Okland_ea_2014

Ono, S., Wang, D. T., Gruen, D. S., Sherwood Lollar, B., Zahniser, M. S., McManus, B. J., et al. (2014). Measurement of a Doubly Substituted Methane Isotopologue, $^{13}CH_3D$, by Tunable Infrared Laser Direct Absorption Spectroscopy. *Anal. Chem.* 86, 6487–6494. 10.1021/ac5010579. PMID: 24895840 Ono_ea_2014

Op den Camp, H. J. M., Islam, T., Stott, M. B., Harhangi, H. R., Hynes, A., Schouten, S., et al. (2009). Environmental, genomic and taxonomic perspectives on methanotrophic

Verrucomicrobia. *Environ. Microbiol. Rep.* 1, 293–306. 10.1111/j.1758-2229.2009.00022.x Op_den_Camp_ea_2009_methanotroph_verrucomicrobia

Ortiz, E., Tominaga, M., Cardace, D., Schrenk, M. O., Hoehler, T. M., Kubo, M. D., et al. (2018). Geophysical Characterization of Serpentinite Hosted Hydrogeology at the McLaughlin Natural Reserve, Coast Range Ophiolite. *Geochem., Geophys., Geosyst.* 19, 114–131. 10.1002/2017GC007001 Ortiz_ea_2018_CRO_ERT

Oze, C., Jones, L. C., Goldsmith, J. I., and Rosenbauer, R. J. (2012). Differentiating biotic from abiotic methane genesis in hydrothermally active planetary surfaces. *Proc. Natl. Acad. Sci. U. S. A.* 109, 9750–9754. 10.1073/pnas.1205223109 Oze_ea_2012

Page, N. J., Pallister, J. S., Brown, M. A., Smewing, J. D., and Haffty, J. (1982). Palladium, platinum, rhodium, iridium and ruthenium in chromite- rich rocks from the Samail ophiolite, Oman. *Canad. Mineral.* 20, 537–548 Page_ea_1982_chromitite_Oman

Parsons International & Co., L. (2005). *Report on Findings of Exploration Program of Deep Groundwater in Northern Sharqiyah.* Tech. rep., Ministry of Regional Municipalities, Environment and Water Resources, PO Box 162, Postal Code 117, Wadi Al Kabir, Sultanate of Oman NSHQ_drilling_report

Paukert, A. (2014). *Mineral Carbonation in Mantle Peridotite of the Samail Ophiolite, Oman: Implications for permanent geological carbon dioxide capture and storage*. Ph.D. thesis, Columbia University. 10.7916/D85M63WZ Paukert_Thesis

Paukert, A. N., Matter, J. M., Kelemen, P. B., Shock, E. L., and Havig, J. R. (2012). Reaction path modeling of enhanced in situ CO_2 mineralization for carbon sequestration in the peridotite of the Samail Ophiolite, Sultanate of Oman. *Chem. Geol.* 330, 86–100. 10.1016/j.chemgeo.2012.08.013 Paukert_ea_2012_rxn_path_Oman

Peters, J. W., Schut, G. J., Boyd, E. S., Mulder, D. W., Shepard, E. M., Broderick, J. B., et al. (2015). [FeFe]- and [NiFe]-hydrogenase diversity, mechanism, and maturation.

Biochim. Biophys. Acta, Mol. Cell Res. 1853, 1350 – 1369. 10.1016/j.bbamcr.2014.11.021. SI: Fe/S proteins Peters_ea_2015

Petrenko, V. V., Smith, A. M., Brailsford, G., Riedel, K., Hua, Q., Lowe, D., et al. (2008). A New Method for Analyzing ^{14}C of Methane in Ancient Air Extracted from Glacial Ice. *Radiocarbon* 50. 10.1017/S0033822200043368 Petrenko_ea_2008_14CH4

Postec, A., Quéméneur, M., Bes, M., Mei, N., Benaïssa, F., Payri, C., et al. (2015). Microbial diversity in a submarine carbonate edifice from the serpentinizing hydrothermal system of the Prony Bay (New Caledonia) over a 6-year period. *Front. Microb.* 6, 857. 10.3389/fmicb.2015.00857 Postec_ea_2015

Prichard, H. M. and Brough, C. P. (2009). *Potential of ophiolite complexes to host PGE deposits* (Geological Publishing House), chap. 10. 277–290 Prichard_Brough_2009_PGE_ophiolites

Prinzhofer, A. A. and Huc, A. Y. (1995). Genetic and post-genetic molecular and isotopic fractionations in natural gases. *Chem. Geol.* 126, 281 – 290. 10.1016/0009-2541(95)00123-9. Processes of Natural Gas Formation Prinzhofer_Huc_1995

Proskurowski, G., Lilley, M. D., Seewald, J. S., Früh-Green, G. L., Olson, E. J., Lupton, J. E., et al. (2008). Abiogenic hydrocarbon production at Lost City hydrothermal field. *Science* 319, 604–607. 10.1126/science.1151194 Proskurowski_ea_2008_abiogenic_HCs_LCHF

Quast, C., Pruesse, E., Gerken, J., Peplies, J., Yarza, P., Yilmaz, P., et al. (2012). The SILVA ribosomal RNA gene database project: improved data processing and web-based tools. *Nucleic Acids Res.* 41, D590–D596. 10.1093/nar/gks1219 Quast_ea_2012_Silva

R Core Team (2019). R: A Language and Environment for Statistical Computing R_language

Rabu, D., Nehlig, P., and Roger, J. (1993). Stratigraphy and structure of the Oman Mountains. *Documents- B. R. G. M.* Rabu_ea_1993_Oman_stratigraphy

Raposo, P., Viver, T., Albuquerque, L., Froufe, H., Barroso, C., Egas, C., et al. (2019). Transfer of meiothermus chliarophilus (tenreiro et al.1995) nobre et al. 1996, meiothermus roseus ming et al. 2016, meiothermus terrae yu et al. 2014 and meiothermus timidus pires et al. 2005, to calidithermus gen. nov., as calidithermus chliarophilus comb. nov., calidithermus roseus comb. nov., calidithermus terrae comb. nov. and calidithermus timidus comb. nov., respectively, and emended description of the genus meiothermus. *International Journal of Systematic and Evolutionary Microbiology* 69, 1060–1069. https://doi.org/10.1099/ijsem.0.003270 Raposo_ea_2019_Meiothermus

Reeves, E. P., Seewald, J. S., and Sylva, S. P. (2012). Hydrogen isotope exchange between n-alkanes and water under hydrothermal conditions. *Geochim. Cosmochim. Acta* 77, 582 – 599. 10.1016/j.gca.2011.10.008 Reeves_ea_2012

Reimer, P. J., Brown, T. A., and Reimer, R. W. (2004). Discussion: Reporting and Calibration of Post-Bomb ^{14}C Data. *Radiocarbon* 46, 1299–1304. 10.1017/S0033822200033154 Reimer_ea_2004_F14C

Rempfert, K. R., Kraus, E. A., Nothaft, D. B., Spear, J. R., Sepúlveda, J., and Templeton, A. S. (in prep.). Intact Polar Lipid Membrane Adaptations in Communities Inhabiting Serpentinized Fluids. *J. Geophys. Res.: Biogeosci.* Rempfert_ea_in_prep_IPLs

Rempfert, K. R., Miller, H. M., Bompard, N., Nothaft, D., Matter, J. M., Kelemen, P., et al. (2017). Geological and geochemical controls on subsurface microbial life in the Samail Ophiolite, Oman. *Front. Microb.* 8, 1–21. 10.3389/fmicb.2017.00056 Rempfert_ea_2017_Oman

Richoz, S., Krystyn, L., Baud, A., Brandner, R., Horacek, M., and Mohtat-Aghai, P. (2010). Permian–Triassic boundary interval in the Middle East (Iran and N. Oman): Progressive environmental change from detailed carbonate carbon isotope marine curve and sedimentary evolution. *J. Asian Earth Sci.* 39, 236 – 253. 10.1016/j.jseaes.2009.12.014 Richoz_ea_2010

Rioux, M., Garber, J., Bauer, A., Bowring, S., Searle, M., Kelemen, P., et al. (2016). Synchronous formation of the metamorphic sole and igneous crust of the Semail ophiolite:

New constraints on the tectonic evolution during ophiolite formation from high-precision U–Pb zircon geochronology. *Earth Planet. Sci. Lett.* 451, 185 – 195. 10.1016/j.epsl.2016.06.051 Rioux_ea_2016_Oman_sole_geochron

Ritterbusch, F., Ebser, S., Welte, J., Reichel, T., Kersting, A., Purtschert, R., et al. (2014). Groundwater dating with Atom Trap Trace Analysis of ^{39}Ar. *Geophys. Res. Lett.* 41, 6758–6764. 10.1002/2014GL061120 Ritterbusch_ea_2014_39Ar

Rollinson, H. (2005). Chromite in the mantle section of the Oman ophiolite: A new genetic model. *Island Arc* 14, 542–550. 10.1111/j.1440-1738.2005.00482.x Rollinson_2005

Sabuda, M. C., Brazelton, W. J., Putman, L. I., McCollom, T. M., Hoehler, T. M., Kubo, M. D. Y., et al. (2020). A dynamic microbial sulfur cycle in a serpentinizing continental ophiolite. *Environ. Microbiol.* 22, 2329–2345. 10.1111/1462-2920.15006 Sabuda_ea_2020

Sachan, H. K., Mukherjee, B. K., and Bodnar, R. J. (2007). Preservation of methane generated during serpentinization of upper mantle rocks: Evidence from fluid inclusions in the Nidar ophiolite, Indus Suture Zone, Ladakh (India). *Earth Planet. Sci. Lett.* 257, 47 – 59. 10.1016/j.epsl.2007.02.023 Sachan_ea_2007

Sander, R. (2015). Compilation of Henry's law constants (version 4.0) for water as solvent. *Atmos. Chem. Phys.* 15. 10.5194/ACP-15-4399-2015 Sander_2015_Henry_Law

Satish-Kumar, M. (2005). Graphite-bearing CO_2-fluid inclusions in granulites: Insights on graphite precipitation and carbon isotope evolution. *Geochim. Cosmochim. Acta* 69, 3841 – 3856. 10.1016/j.gca.2005.02.007 Satish-Kumar_2005

Saunois, M., Stavert, A. R., Poulter, B., Bousquet, P., Canadell, J. G., Jackson, R. B., et al. (2020). The Global Methane Budget 2000–2017. *Earth Syst. Sci. Data* 12, 1561–1623. 10.5194/essd-12-1561-2020 Saunois_ea_2020_CH4_budget

Schidlowski, M. (2001). Carbon isotopes as biogeochemical recorders of life over 3.8 Ga of Earth history: evolution of a concept. *Precambrian Res.* 106, 117 – 134. 10.1016/S0301-9268(00)00128-5 Schidlowski_2001_C_isotopes

Schleheck, D., Weiss, M., Pitluck, S., Bruce, D., Land, M. L., Han, S., et al. (2011). Complete genome sequence of Parvibaculum lavamentivorans type strain (DS-1(T)). *Standards in genomic sci.* 5, 298–310. 10.4056/sigs.2215005 Schleheck_ea_2011

Sekiguchi, Y., Muramatsu, M., Imachi, H., Narihiro, T., Ohashi, A., Harada, H., et al. (2008). Thermodesulfovibrio aggregans sp. nov. and Thermodesulfovibrio thiophilus sp. nov., anaerobic, thermophilic, sulfate-reducing bacteria isolated from thermophilic methanogenic sludge, and emended description of the genus Thermodesulfovibrio. *Int. J. Syst. Evol. Microbiol.* 58, 2541–2548. 10.1099/ijs.0.2008/000893-0 Sekiguchi_ea_2008

Shennan, J. L. (2006). Utilisation of C2–C4 gaseous hydrocarbons and isoprene by microorganisms. *J. Appl. Chem. Biotechnol.* 81, 237–256. 10.1002/jctb.1388 Shennan_2006_aerobic_SCA_utilisation

Sherwood Lollar, B., Lacrampe-Couloume, G., Voglesonger, K., Onstott, T., Pratt, L., and Slater, G. (2008). Isotopic signatures of CH_4 and higher hydrocarbon gases from Precambrian Shield sites: A model for abiogenic polymerization of hydrocarbons. *Geochim. Cosmochim. Acta* 72, 4778 – 4795. 10.1016/j.gca.2008.07.004 SherwoodLollar_ea_2008_abiotic_polymerization_model

Sherwood Lollar, B., Westgate, T. D., Ward, J. A., Slater, G. F., and Lacrampe-Couloume, G. (2002). Abiogenic formation of alkanes in the Earth's crust as a minor source for global hydrocarbon reservoirs. *Nature* 416, 522–524. 10.1038/416522a SherwoodLollar_ea_2002

Shock, E. L. (1992). *Chemical Environments of Submarine Hydrothermal Systems* (Springer, Dordrecht). 67–107. 10.1007/978-94-011-2741-7_5 Shock_1992

Singh, R., Guzman, M. S., and Bose, A. (2017). Anaerobic Oxidation of Ethane, Propane, and Butane by Marine Microbes: A Mini Review. *Front. Microb.* 8, 2056. 10.3389/fmicb.2017.02056 Singh_ea_2017_anaerobic_ox_SCA

Skelton, P. W., Nolan, S. C., and Scott, R. W. (1990). The Maastrichtian transgression onto the northwestern flank of the Proto-Oman Mountains: sequences of rudist-bearing

beach to open shelf facies. *Geological Society, London, Special Publications* 49, 521–547. 10.1144/GSL.SP.1992.049.01.32 Skelton_ea_1990_Oman_Maastrichtia_fauna

Sleep, N., Meibom, A., Fridriksson, T., Coleman, R., and Bird, D. (2004). H_2-rich fluids from serpentinization: geochemical and biotic implications. *Proc. Natl. Acad. Sci. U. S. A.* 101, 12818–12823. 10.1073/pnas.0405289101 Sleep_ea_2004_H2_serp

Soret, M., Bonnet, G., Larson, K., Agard, P., Cottle, J., Dubacq, B., et al. (2020). Slow subduction initiation forces fast ophiolite formation Soret. In *International Conference on Ophiolites and the Oceanic Lithosphere: Results of the Oman Drilling Project and Related Research* (Sultan Qaboos University, Muscat, Sultanate of Oman), 232 Soret_ea_2020

Stanger, G. (1986). *The hydrogeology of the Oman Mountains*. Ph.D. thesis, Open University Stanger_1986_thesis

Stolper, D., Martini, A., Clog, M., Douglas, P., Shusta, S., Valentine, D., et al. (2015). Distinguishing and understanding thermogenic and biogenic sources of methane using multiply substituted isotopologues. *Geochim. Cosmochim. Acta* 161, 219 – 247. 10.1016/j.gca.2015.04.015 Stolper_ea_2015_CH4_clumps

Streit, E., Kelemen, P., and Eiler, J. (2012). Coexisting serpentine and quartz from carbonate-bearing serpentinized peridotite in the Samail Ophiolite, Oman. *Contrib. Mineral. Petrol.* 164, 821–837. 10.1007/s00410-012-0775-z Streit_ea_2012_serp_qtz_clumps

Stuiver, M. and Polach, H. A. (1977). Discussion Reporting of ^{14}C Data. *Radiocarbon* 19, 355–363. 10.1017/S0033822200003672 Stuiver_Polach_1977_14C

Suzuki, S., Ishii, S., Wu, A., Cheung, A., Tenney, A., Wanger, G., et al. (2013). Microbial diversity in The Cedars, an ultrabasic, ultrareducing, and low salinity serpentinizing ecosystem. *Proc. Natl. Acad. Sci. U. S. A.* 110, 15336–15341. 10.1073/pnas.1302426110 Suzuki_ea_2013

Suzuki, S., Kuenen, J. G., Schipper, K., van der Velde, S., Ishii, S., Wu, A., et al. (2014). Physiological and genomic features of highly alkaliphilic hydrogen-utilizing Betaproteobac-

teria from a continental serpentinizing site. *Nat. Commun.* 5, 3900. 10.1038/ncomms4900 Suzuki_ea_2014_serpentinomonas

Takai, K., Nakamura, K., Toki, T., Tsunogai, U., Miyazaki, M., Miyazaki, J., et al. (2008). Cell proliferation at 122°C and isotopically heavy CH_4 production by a hyperthermophilic methanogen under high-pressure cultivation. *Proc. Natl. Acad. Sci. U. S. A.* 105, 10949–10954. 10.1073/pnas.0712334105 Takai_ea_2008_122C_methanogen

Takami, H., Noguchi, H., Takaki, Y., Uchiyama, I., Toyoda, A., Nishi, S., et al. (2012). A deeply branching thermophilic bacterium with an ancient acetyl-CoA pathway dominates a subsurface ecosystem. *PloS one* 7, e30559–e30559. 10.1371/journal.pone.0030559 Takami_ea_2012

Templeton, A. S. and Ellison, E. T. (2020). Formation and loss of metastable brucite: does Fe(II)-bearing brucite support microbial activity in serpentinizing ecosystems? *Philos. Trans. R. Soc., A* 378, 20180423. 10.1098/rsta.2018.0423 Templeton_Ellison_2020_brucite

Templeton, A. S., Ellison, E. T., Glombitza, C., Morono, Y., Rempfert, K. R., Zeigler, S., et al. (in prep.). Accessing the subsurface biosphere within rocks undergoing active low-temperature serpentinization in the Samail Ophiolite (Oman Drilling Project). *J. Geophys. Res.: Biogeosci.* Templeton_ea_2020_in_prep_JGR

Terken, J. M. J. (1999). The Natih Petroleum System of North Oman. *GeoArabia* 4, 157–180 Terken_1999_petroleum_North_Oman

Terzer, S., Wassenaar, L. I., Araguás-Araguás, L. J., and Aggarwal, P. K. (2013). Global isoscapes for $\delta^{18}O$ and $\delta^{2}H$ in precipitation: improved prediction using regionalized climatic regression models. *Hydrol. Earth Syst. Sci.* 17, 4713–4728. 10.5194/hess-17-4713-2013 Terzer_ea_2013_GMWL

Thampi, K. R., Kiwi, J., and Graetzel, M. (1987). Methanation and photo-methanation of carbon dioxide at room temperature and atmospheric pressure. *Nature* 327, 506 Thampi_ea_1987_Ru_methanation

Timmers, P. H., Welte, C. U., Koehorst, J. J., Plugge, C. M., Jetten, M. S., and Stams, A. J. (2017). Reverse methanogenesis and respiration in methanotrophic archaea. *Archaea* 2017. 10.1155/2017/1654237 Timmers_ea_2017

Trias, R., Ménez, B., le Campion, P., Zivanovic, Y., Lecourt, L., Lecoeuvre, A., et al. (2017). High reactivity of deep biota under anthropogenic CO_2 injection into basalt. *Nat. Commun.* 8, 1063. 10.1038/s41467-017-01288-8 Trias_ea_2017_carbfix_biota

Turnbull, J. C., Lehman, S. J., Miller, J. B., Sparks, R. J., Southon, J. R., and Tans, P. P. (2007). A new high precision $^{14}CO_2$ time series for North American continental air. *J. Geophys. Res.: Atmos.* 112. 10.1029/2006JD008184 Turnbull_ea_2007_14CO2

USGS (2010). Digital Elevation - Global Multi-resolution Terrain Elevation Data 2010 (GMTED2010). /10.5066/F7J38R2N GMTED2010

Vacquand, C., Deville, E., Beaumont, V., Guyot, F., Sissmann, O., Pillot, D., et al. (2018). Reduced gas seepages in ophiolitic complexes: evidences for multiple origins of the H_2-CH_4-N_2 gas mixtures. *Geochim. Cosmochim. Acta* 223, 437–461. 10.1016/j.gca.2017.12.018 Vacquand_ea_2018_ophiolite_gas

Vankeuren, A. N. P., Matter, J. M., Stute, M., and Kelemen, P. B. (2019). Multitracer determination of apparent groundwater ages in peridotite aquifers within the Samail ophiolite, Sultanate of Oman. *Earth Planet. Sci. Lett.* 516, 37–48. 10.1016/j.epsl.2019.03.007 Vankeuren_ea_2019_groundwater_age_Oman

Waite, J. H., Glein, C. R., Perryman, R. S., Teolis, B. D., Magee, B. A., Miller, G., et al. (2017). Cassini finds molecular hydrogen in the Enceladus plume: Evidence for hydrothermal processes. *Science* 356, 155–159. 10.1126/science.aai8703 Waite_ea_2017

Waldron, S., Scott, E. M., and Soulsby, C. (2007). Stable Isotope Analysis Reveals Lower-Order River Dissolved Inorganic Carbon Pools Are Highly Dynamic. *Environ. Sci. Technol.* 41, 6156–6162. 10.1021/es0706089. PMID: 17937296 Waldron_ea_2007

Wang, D. T., Gruen, D. S., Lollar, B. S., Hinrichs, K.-U., Stewart, L. C., Holden, J. F., et al. (2015). Nonequilibrium clumped isotope signals in microbial methane. *Science* 348, 428–431. 10.1126/science.aaa4326 Wang_ea_2015_nonequilibrium_methane

Wang, D. T., Reeves, E. P., McDermott, J. M., Seewald, J. S., and Ono, S. (2018). Clumped isotopologue constraints on the origin of methane at seafloor hot springs. *Geochim. Cosmochim. Acta* 223, 141–158. 10.1016/j.gca.2017.11.030 Wang_ea_2018_seafloor_hydrothermal_CH4

Wang, D. T., Welander, P. V., and Ono, S. (2016). Fractionation of the methane isotopologues $^{13}CH_4$, $^{12}CH_3D$, and $^{13}CH_3D$ during aerobic oxidation of methane by Methylococcus capsulatus (Bath). *Geochim. Cosmochim. Acta* 192, 186–202. 10.1016/j.gca.2016.07.031 Wang_ea_2016_aerobic_methanotrophy

Wang, Q., Garrity, G. M., Tiedje, J. M., and Cole, J. R. (2007). Naïve Bayesian Classifier for Rapid Assignment of rRNA Sequences into the New Bacterial Taxonomy. *Appl. Environ. Microbiol.* 73, 5261–5267. 10.1128/AEM.00062-07 Wang_ea_2007_RDP

Welhan, J. A. and Craig, H. (1983). *Methane, Hydrogen and Helium in Hydrothermal Fluids at 21°N on the East Pacific Rise* (Boston, MA: Springer US). 391–409. 10.1007/978-1-4899-0402-7_17 Welhan_Craig_1983

Welte, C. U., Rasigraf, O., Vaksmaa, A., Versantvoort, W., Arshad, A., Op den Camp, H. J., et al. (2016). Nitrate- and nitrite-dependent anaerobic oxidation of methane. *Environ. Microbiol. Rep.* 8, 941–955. 10.1111/1758-2229.12487 Welte_ea_2016_NO3_NO2_AOM_review

Weyhenmeyer, C. E., Burns, S. J., Waber, H. N., Macumber, P. G., and Matter, A. (2002). Isotope study of moisture sources, recharge areas, and groundwater flow paths within the eastern Batinah coastal plain, Sultanate of Oman. *Water Resources Research* 38. 10.1029/2000WR000149 Weyhenmeyer_ea_2002_Oman_water_isotopes

Wheat, C. G., Becker, K., Villinger, H., Orcutt, B. N., Fournier, T., Hartwell, A.,

et al. (2020). Subseafloor Cross-Hole Tracer Experiment Reveals Hydrologic Properties, Heterogeneities, and Reactions in Slow-Spreading Oceanic Crust. *Geochem., Geophys., Geosyst.* 21, e2019GC008804. 10.1029/2019GC008804. E2019GC008804 2019GC008804 Wheat_ea_2020_North_Pond

Whiticar, M. J. (1999). Carbon and hydrogen isotope systematics of bacterial formation and oxidation of methane. *Chem. Geol.* 161, 291 – 314. 10.1016/S0009-2541(99)00092-3 Whiticar_1999_CH4

Woycheese, K. M., Meyer-Dombard, D. R., Cardace, D., Argayosa, A. M., and Arcilla, C. A. (2015). Out of the dark: transitional subsurface-to-surface microbial diversity in a terrestrial serpentinizing seep (Manleluag, Pangasinan, the Philippines). *Front. Microb.* 6, 44. 10.3389/fmicb.2015.00044 Woycheese_ea_2015_philippines

Yoshinaga, M. Y., Holler, T., Goldhammer, T., Wegener, G., Pohlman, J. W., Brunner, B., et al. (2014). Carbon isotope equilibration during sulphate-limited anaerobic oxidation of methane. *Nat. Geosci.* 7, 190–194. 10.1038/ngeo2069 Yoshinaga_ea_2014_ANME_C_isotope_eq

Young, E., Kohl, I., Lollar, B. S., Etiope, G., Rumble Iii, D., Li, S., et al. (2017). The relative abundances of resolved $^{12}CH_2D_2$ and $^{13}CH_3D$ and mechanisms controlling isotopic bond ordering in abiotic and biotic methane gases. *Geochim. Cosmochim. Acta* 203, 235–264. 10.1016/j.gca.2016.12.041 Young_ea_2017_12CH2D2

Young, E. D. (2020). *A Two-Dimensional Perspective on CH_4 Isotope Clumping : Distinguishing Process from Source* (Cambridge University Press), chap. 13. 388–414. 10.1017/9781108677950 Young_2020_DCO

Young, E. D., Rumble, D., Freedman, P., and Mills, M. (2016). A large-radius high-mass-resolution multiple-collector isotope ratio mass spectrometer for analysis of rare isotopologues of O_2, N_2, CH_4 and other gases. *Int. J. Mass Spectrom.* 401, 1 – 10. 10.1016/j.ijms.2016.01.006 Young_ea_2016_panorama

Zeebe, R. E. and Wolf-Gladrow, D. (2001). *CO_2 in seawater: equilibrium, kinetics, isotopes.* 65 (Elsevier) Zeebe_Wolf-Gladrow_2001_CO2_seawater

Zgonnik, V., Beaumont, V., Larin, N., Pillot, D., and Deville, E. (2019). Diffused flow of molecular hydrogen through the Western Hajar mountains, Northern Oman. *Arabian J. Geosci.* 12, 71. 10.1007/s12517-019-4242-2 Zgonnik_ea_2019

Zwicker, J., Birgel, D., Bach, W., Richoz, S., Smrzka, D., Grasemann, B., et al. (2018). Evidence for archaeal methanogenesis within veins at the onshore serpentinite-hosted Chimaera seeps, Turkey. *Chem. Geol.* 483, 567–580. 10.1016/j.chemgeo.2018.03.027 Zwicker_ea_2018_methanogen_biomarker

Appendix A

Supporting information for Chapter 2

A.1 Overview of CH_4 dynamics in other states of the system: wells WAB56, WAB71, and CM2A

Here, we briefly discuss three more wells to provide a broader perspective on CH_4 dynamics in the Samail ophiolite. The first of these wells is WAB56, which is situated in a catchment dominated by harzburgite (Main Text Figure 1; Figure A.1; Main Text Table 1; also, WAB56 is pictured in Figure 1b of Rempfert et al. (2017)). Thus, the hydrogeologic setting of WAB56 is similar to that of NSHQ14. Yet, in comparison to fluids from NSHQ14, fluids sampled from WAB56 in 2015, 2016, and 2017 had lower pH, $c_{\sum \mathrm{Ca}}$, $c_{\mathrm{H_2}}$, $c_{\mathrm{CH_4}}$, and $\delta^{13}\mathrm{C}_{\mathrm{CH_4}}$ (Main Text Table 1, Main Text Table 3, Main Text Table 4; Rempfert et al., 2017). For example, fluids sampled from WAB56 in 2015 had a pH of 10.6, $c_{\sum \mathrm{Ca}}$ of 430 $\mu\mathrm{mol} \cdot \mathrm{L}^{-1}$, and $c_{\mathrm{H_2}}$ below quantitatable levels (Rempfert et al., 2017). Differences in fluid chemistry between WAB56 and NSHQ14 could be related to well construction. While NSHQ14 was drilled to 304 m depth and is cased only to 5.8 m, WAB56 was drilled to 106 m depth and is fully cased with a screened interval from 7 mbgl to 27 mbgl (Main Text Table 1). Thus, the fluids sampled from WAB56 may have derived from a shallow aquifer containing fluids of relatively short residence time, or a mixture of deep and shallow peridotite-reacted waters. Fluids sampled from WAB56

in 2015 had $\delta^{13}C_{CH_4}$ of $-83.2\,‰$ VPDB and 4 % of 16S rRNA gene reads of subsurface biomass affiliated with *Methanobacterium*, which is remarkably similar to fluids sampled from WAB188 in the same year ($\delta^{13}C_{CH_4}$ of $-71.3\,‰$ VPDB and 8 % of 16S rRNA gene reads of subsurface biomass assigned to *Methanobacterium*) (Main Text Table 4; Rempfert et al., 2017). Thus, it seems that the casing construction at WAB56 has restricted sampling to shallow waters of relatively low pH, $c_{Ca^{2+}}$, and c_{H_2}, where conditions of H_2 limitation and excess $\sum CO_2$ allow the classic isotope effect of hydrogenotrophic methanogenesis to be expressed, as at WAB188.

Well WAB71 is located 2.4 km north of NSHQ04, and is set in dunite, 30 m east of a faulted contact with harzburgite (Main Text Figure 1; Figure A.1; Main Text Table 1). It is similar to NSHQ04 in aqueous chemical composition ($Ca^{2+}-OH^-$ water; Main Text Table 2), dissolved gas composition (high CH_4/H_2 and $C_1/(C_2+C_3)$ ratios; Main Text Figure 2, Main Text Table 3), $\delta^{13}C_{CH_4}$ (interannual mean of $+3.3\,‰$ VPDB, $s = 0.5\,‰$, $n = 4$; Main Text Figure 3a; Main Text Table 4), and CH_4-cycling microbial community composition. The dominant CH_4-cycling taxon at WAB71 appears to be *Methylococcus*, which accounted for 1 % of 16S rRNA gene reads of DNA extracted from subsurface biomass obtained in 2018 from WAB71 (Figure A.3), which is consistent with prior sampling at this well (mean 2015 through 2018 of 1 %; Rempfert et al., 2017; Kraus et al., 2018). 16S rRNA gene reads affiliated with *Methanobacterium* were not detected at WAB71 in this study of samples obtained in 2018, but were found in low relative abundance (< 1 % of reads) in samples from 2015 and 2017 (Rempfert et al., 2017; Kraus et al., 2018). The chemical and microbial similarities between WAB71 and NSHQ04 suggest that CH_4 cycle processes at WAB71 may be similar to those at NSHQ04, where a dominantly microbial source of CH_4 and an important role of aerobic CH_4 oxidation were inferred. However, this conclusion is more speculative at WAB71, since it was not feasible to measure clumped isotopologue relative abundances in CH_4 from WAB71 by the methods of this study due to the relatively lower c_{CH_4} at WAB71 ($7.76\,\mu mol \cdot L^{-1}$ in 2018, $14.8\,\mu mol \cdot L^{-1}$ in 2017; Main Text Table 3). In addition, some aspects of WAB71

differ from NSHQ04. These include that WAB71 fluids have higher pH by 0.7 and lower δD_{CH_4} (interannual mean of $-310\,‰$ VSMOW, $s = 4\,‰$, $n = 2$; Main Text Figure 3a; Main Text Table 4). In addition, WAB71 had the lowest Eh ($-229\,mV$; main text Table 1) and $c_{SO_4^{2-}}$ ($60.8\,\mu mol \cdot L^{-1}$) measured in groundwaters sampled in 2018. The reduced character and low $c_{SO_4^{2-}}$ of groundwaters sampled from WAB71 may be indicative of microbial SO_4^{2-} reduction at this well. Indeed, DNA extracted from subsurface samples from WAB71 had the highest 16S rRNA gene relative abundance of class Thermodesulfovibriona among wells sampled in 2018 (20 %; Figure A.3; also mean of 19 % from 2015 to 2018; Rempfert et al., 2017; Kraus et al., 2018). Cultured representatives of Thermodesulfovibrionia are capable of SO_4^{2-} reduction coupled to H_2 oxidation and may additionally/alternatively oxidize C_1-C_3 acids and use thiosulfate, sulfite, Fe^{3+} or NO_3^- as terminal electron acceptors for anaerobic respiration (Henry et al., 1994; Sekiguchi et al., 2008). Further, 16S rRNA gene sequences affiliated with ANME-1b have been detected in DNA from WAB71, albeit in low relative gene abundance ($< 1\,\%$ of reads in 2018; Main Text Figure 5; the same is true of samples from 2017 and 2015, but ANME-1b was not detected in 2016; Rempfert et al., 2017; Kraus et al., 2018). These data suggest that SO_4^{2-}-reducing bacteria may have contributed to the low c_{H_2} at WAB71, which may have allowed SO_4^{2-}-driven CH_4 oxidation by ANME-1b to be energetically competitive at this well, whereas it is apparently not in other sampled wells. The lower δD_{CH_4} at WAB71 relative to NSHQ04 could be due to a combination of aerobic and anaerobic methanotrophy at WAB71, which may have different C and H isotope effects than aerobic methanotrophy alone.

Well CM2A was drilled in the crust-mantle transition zone of the ophiolite by the Oman Drilling Project in late 2017 (Main Text Figure 1; Figure A.1). Drill cuttings from the rotary-drilled well, CM2A, and cores from the adjacent diamond-wireline drilled well, CM2B, contain mostly dunite, with occasional gabbro and harzburgite (Main Text Table 1). Of the 300 m of core retrieved from CM2B, chromitite was noted only in one 30 cm-thick layer at 115 m depth. The water level in CM2A was 13.4 m, so these deep chromitites should be water-

saturated and therefore not catalytic for CO_2 reduction to CH_4. CM2A contains $Ca^{2+} - OH^-$ waters with pH and major ion chemistry similar to NSHQ14 (Main Text Table 1; Main Text Table 2). Fluids sampled from CM2A had a c_{CH_4} of $152\,\mu\text{mol} \cdot \text{L}^{-1}$, which is almost double that of NSHQ14, concentrations of $C_2 - C_4$ *n*-alkanes up to $4.11 \cdot 10^{-2}\,\mu\text{mol}\cdot\text{L}^{-1}$, which is similar to or somewhat lower than those of NSHQ14, and a c_{H_2} of $3.38\,\mu\text{mol}\cdot\text{L}^{-1}$, which is 50 times lower than NSHQ14, although still higher than all other wells sampled in 2018 (Main Text Figure 2; Main Text Table 3). In comparison to NSHQ14 and NSHQ04, CH_4 in fluids sampled from CM2A had lower $\delta^{13}C$ (inter-laboratory mean of $-4.3\,‰$ VPDB; Main Text Table 4; Main Text Figure 3a). CH_4 from CM2A had the highest δD of all studied wells (inter-laboratory mean of $-198\,‰$ VSMOW; Main Text Table 4; Main Text Figure 3a). Values of $\varepsilon_{\text{methane/water}}$, $\Delta^{13}CH_3D$, and $\Delta^{12}CH_2D_2$ indicate that CH_4 from CM2A is not in isotopic equilibrium with water, nor intramolecular equilibrium (Main Text Figure 3b and d; Main Text Table 4). 16S rRNA gene sequences affiliated with *Methanobacterium* were detected in DNA extracted from biomass in waters pumped from CM2A at low relative abundances ($< 1\,\%$ of reads; Figure A.3). No sequences affiliated with methanotrophs were detected in DNA extracted from CM2A fluids (Main Text Figure 5). CM2A and NSHQ14 fluids share several relevant characteristics including isotopic disequilibrium in CH_4, detection of *Methanobacterium*, similar concentrations of major ionic species, and apparent scarcity of potentially catalytic, water-unsaturated chromitites. These similarities suggest that CH_4 in CM2A, like NSHQ14, is dominantly a mixture of abiotic CH_4 being released from fluid inclusions and microbial CH_4.

A.2 Supplementary figures

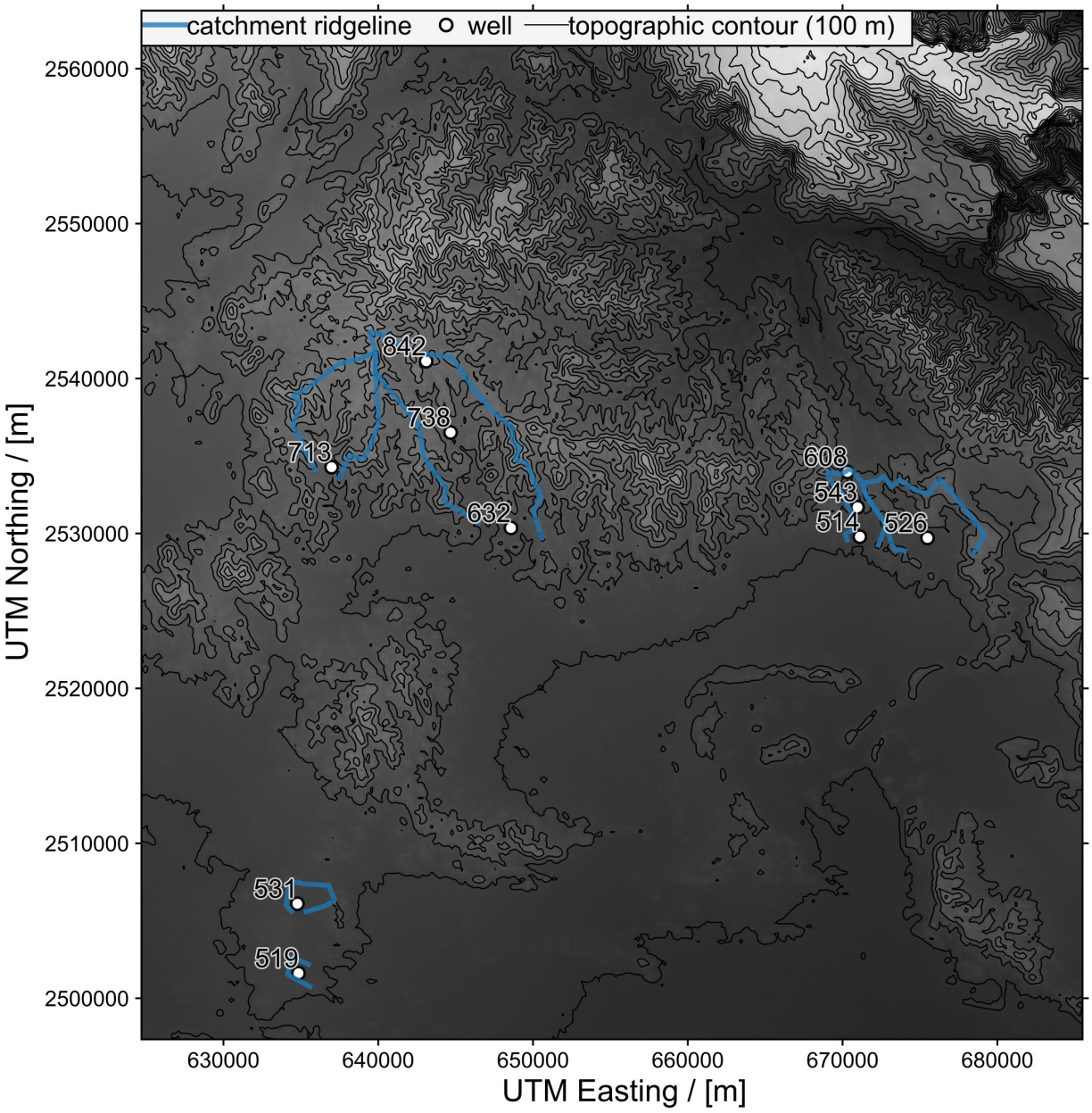

Figure A.1: Study area in Samail ophiolite, Sultanate of Oman. Digital elevation model from USGS (2010). Elevations in meters above sea level are listed on the upper left of well location markers. Colors are scaled by elevation from low (dark) to high (light). Ridgelines of hydrologic catchments were estimated from the topography. If multiple wells shared catchment area, one catchment is depicted for visual clarity (i.e. WAB71, NSHQ04, and WAB188 share catchment area that is separate from NSHQ14; see Main Text Figure 1 for well names).

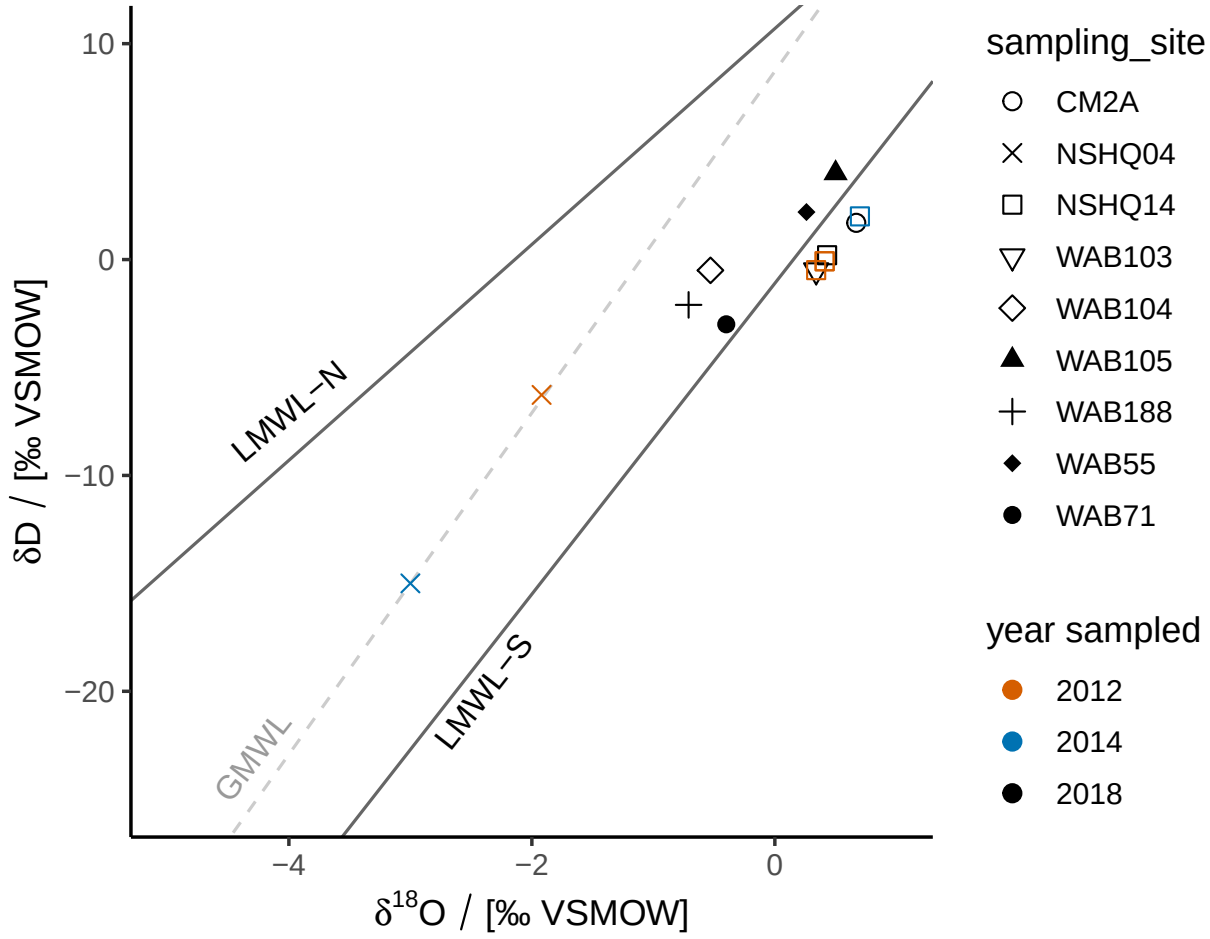

Figure A.2: Plot of Oman groundwater stable isotopic compositions. Samples from 2012 were reported in Vankeuren et al. (2019). Samples from 2014 reported in Miller et al. (2016). *Abbreviations:* LMWL-N and LMWL-S, Oman local meteoric water lines derived from northern and southern sources, respectively (Weyhenmeyer et al., 2002); GMWL, global meteoric water line (Terzer et al., 2013).

Figure A.3: Heat map of the top 50 16S rRNA gene taxonomic assignments in samples obtained in 2018, arranged in descending order of abundance. Read relative abundances are reported as percentages rounded to the ones place. Cases when a taxon was detected in a sample and was $< 1\,\%$ read relative abundance after rounding are labeled "< 1". Cases when no reads of a taxon were detected in a sample are labeled "n.r."

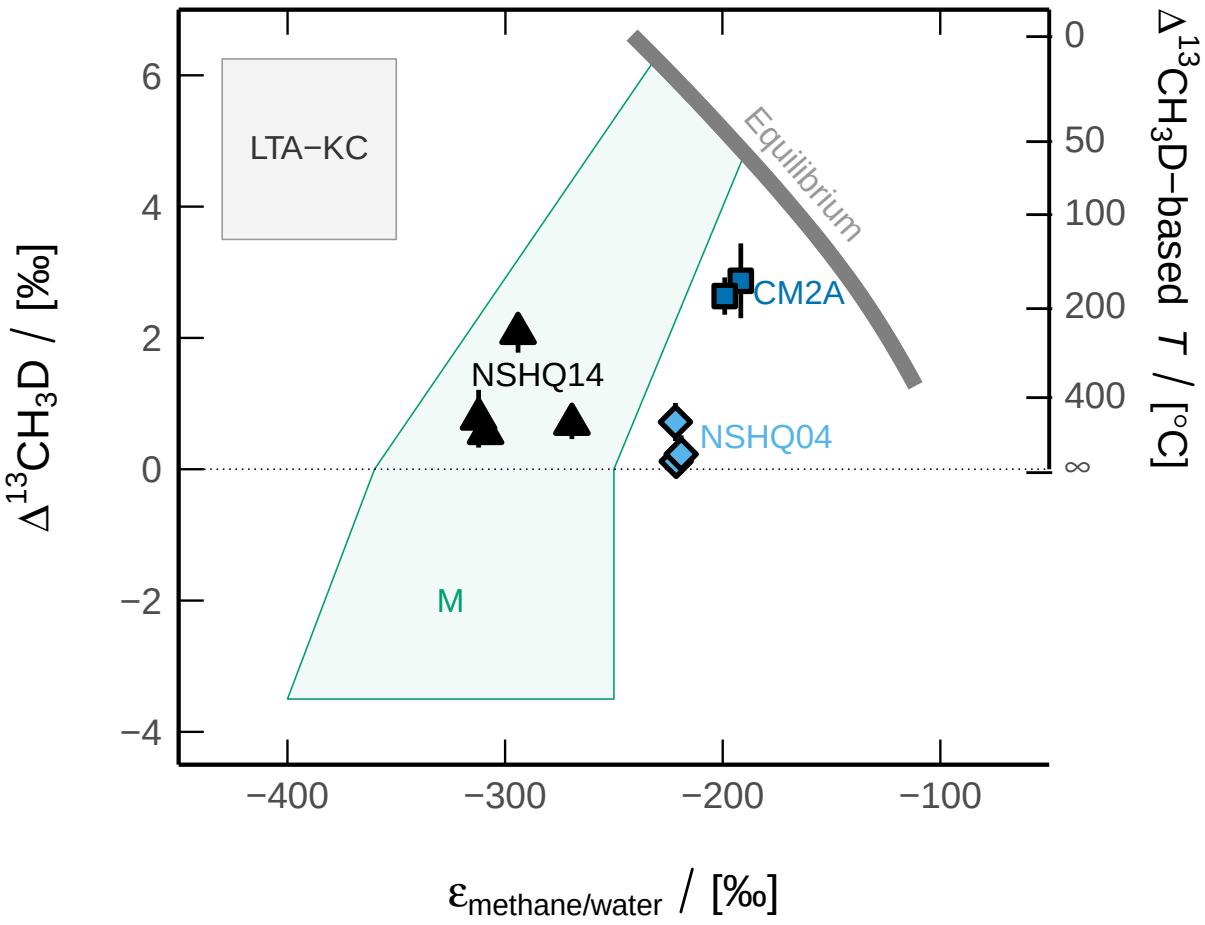

Figure A.4: $\varepsilon_{methane/water}$ and $\Delta^{13}CH_3D$ plot of methane from Oman well waters, after Wang et al. (2015). Equilibrium (thick, light gray line) from Horibe and Craig (1995) and Young et al. (2017). *Abbreviations:* LTA-KC, low-temperature abiotic (Kidd Creek-type); M, microbial.

Appendix B

Supporting information for Chapter 3

B.1 Data processing

Data (in Excel format) and source code (in R Markdown format) used to produce the figures, data tables and analyses for this paper (as well as additional data on analytical uncertainties and trace element concentrations) are available online at `https://github.com/danote/Oman-14CH4`. Additional DNA sequence data processing codes are available at `https://github.com/danote/Samail_16S_compilation`.

B.2 Supplementary figures

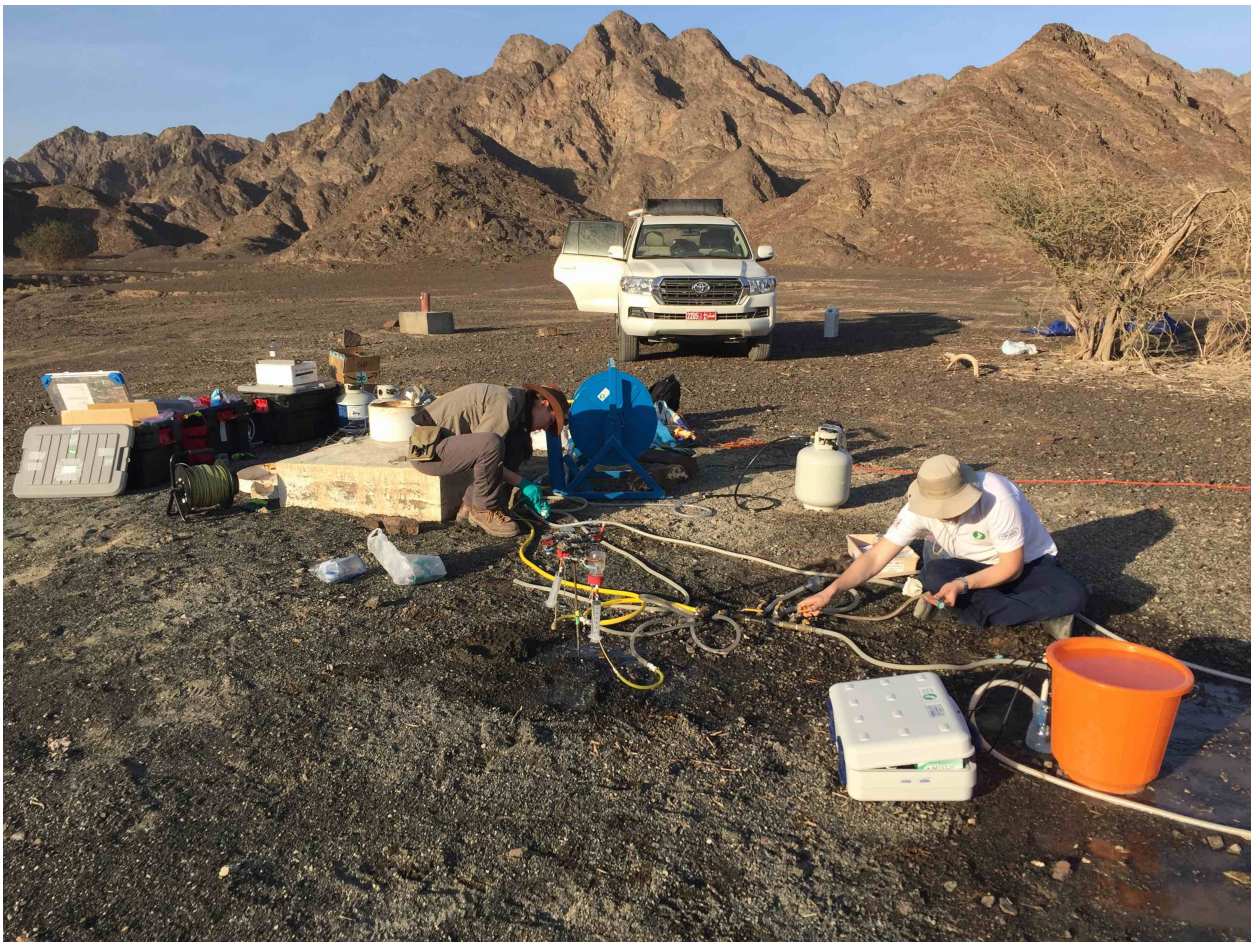

Figure B.1: Fluid pumping and sampling at well NSHQ14 (white casing in foreground), January, 2019. Well BA3A is in the background of the photo, with red-orange casing, 10 m from NSHQ14.

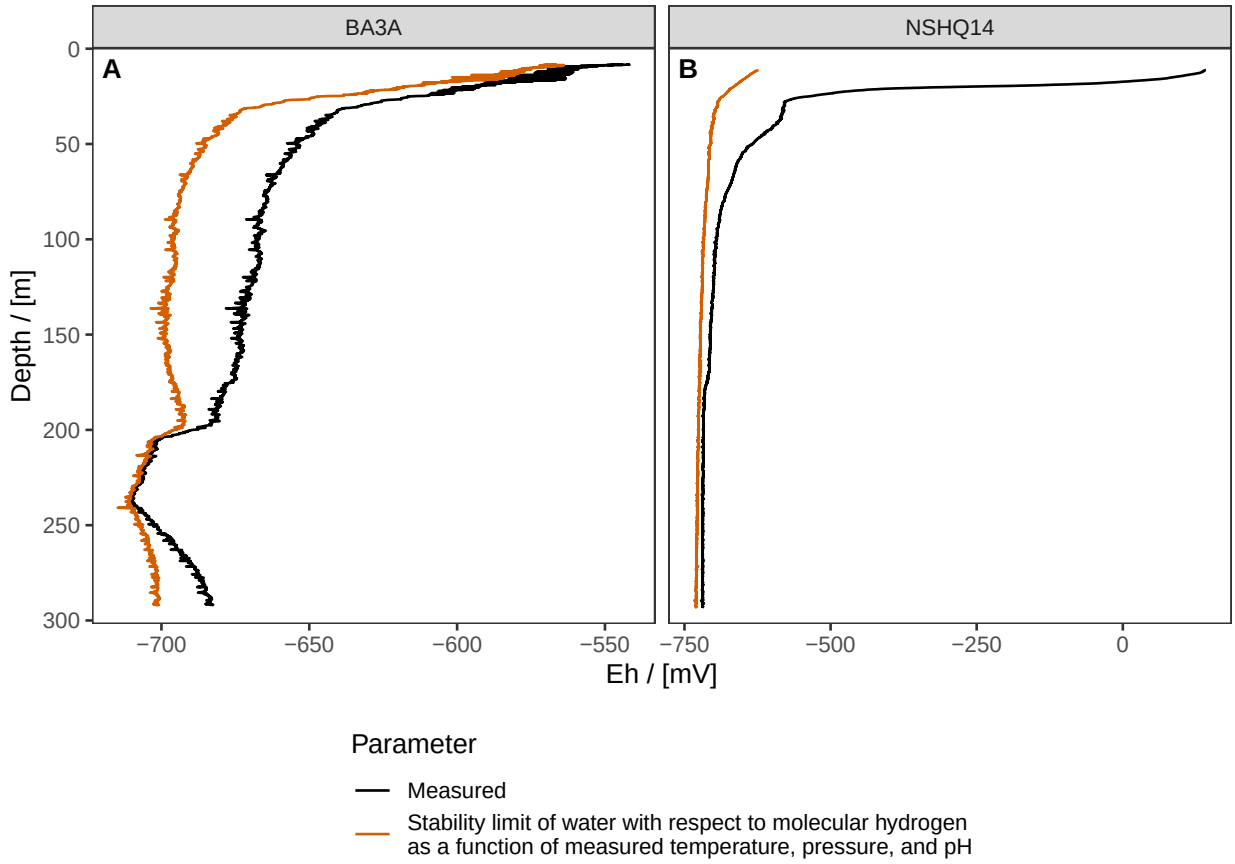

Figure B.2: *Eh* profiles of BA3A (A) and NSHQ14 (B) logged in March, 2018. Note the different X-axis scales in panels A and B. Measured *Eh* values are shown in black. Calculated *Eh* values at the stability limit of water with respect to molecular hydrogen (H_2) are shown in orange. Groundwaters in both wells closely approach this stability limit, especially in the 200 m to 250 m depth interval of BA3A. The differences in this calculated stability limit between the wells are mostly driven by pH differences. See Section B.1 for calculations.

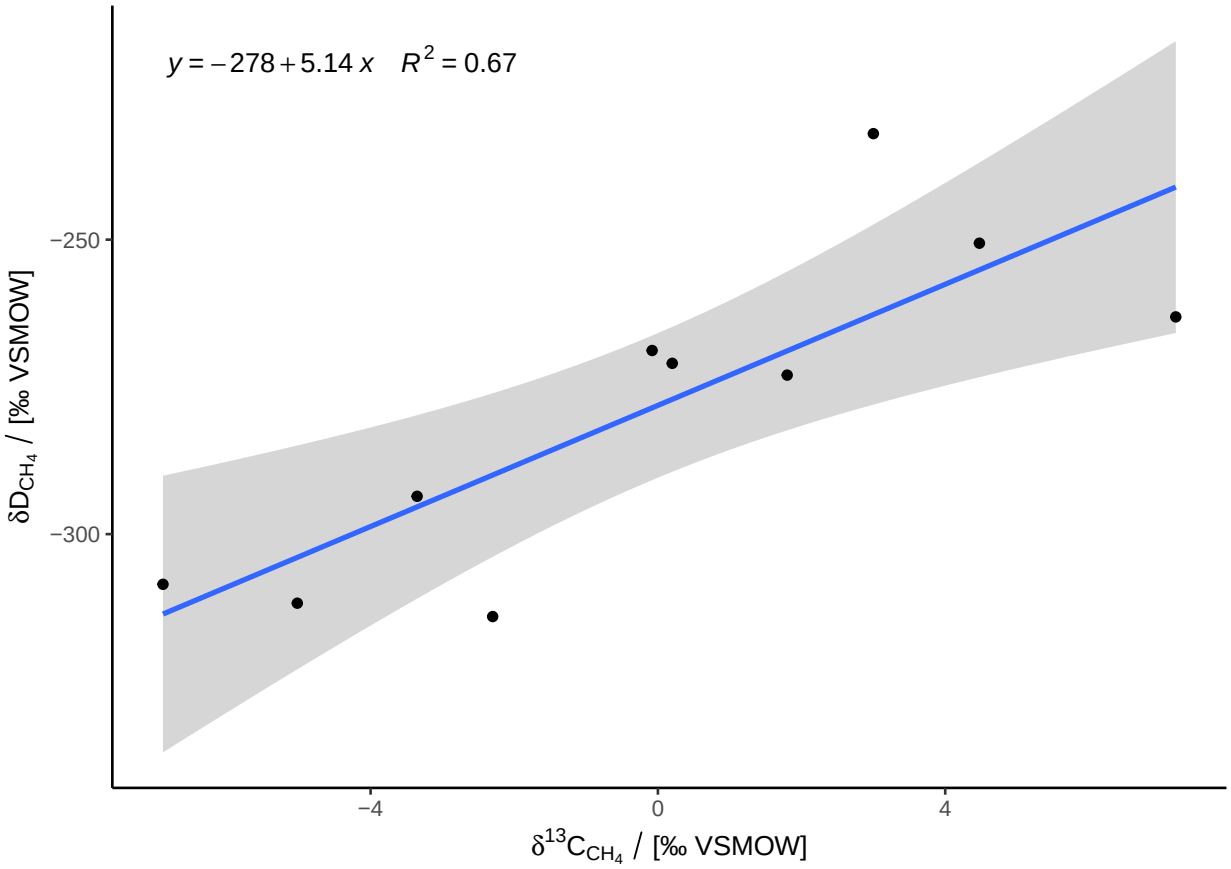

Figure B.3: All paired δ^{13}C and δD analyses of CH_4 sampled from well NSHQ14 in 2014 through 2019, including data from refs. Nothaft et al., 2020 and Miller et al., 2016. Shaded area in plot represents the 95 % confidence interval of a least-squares linear regression (Section B.1).

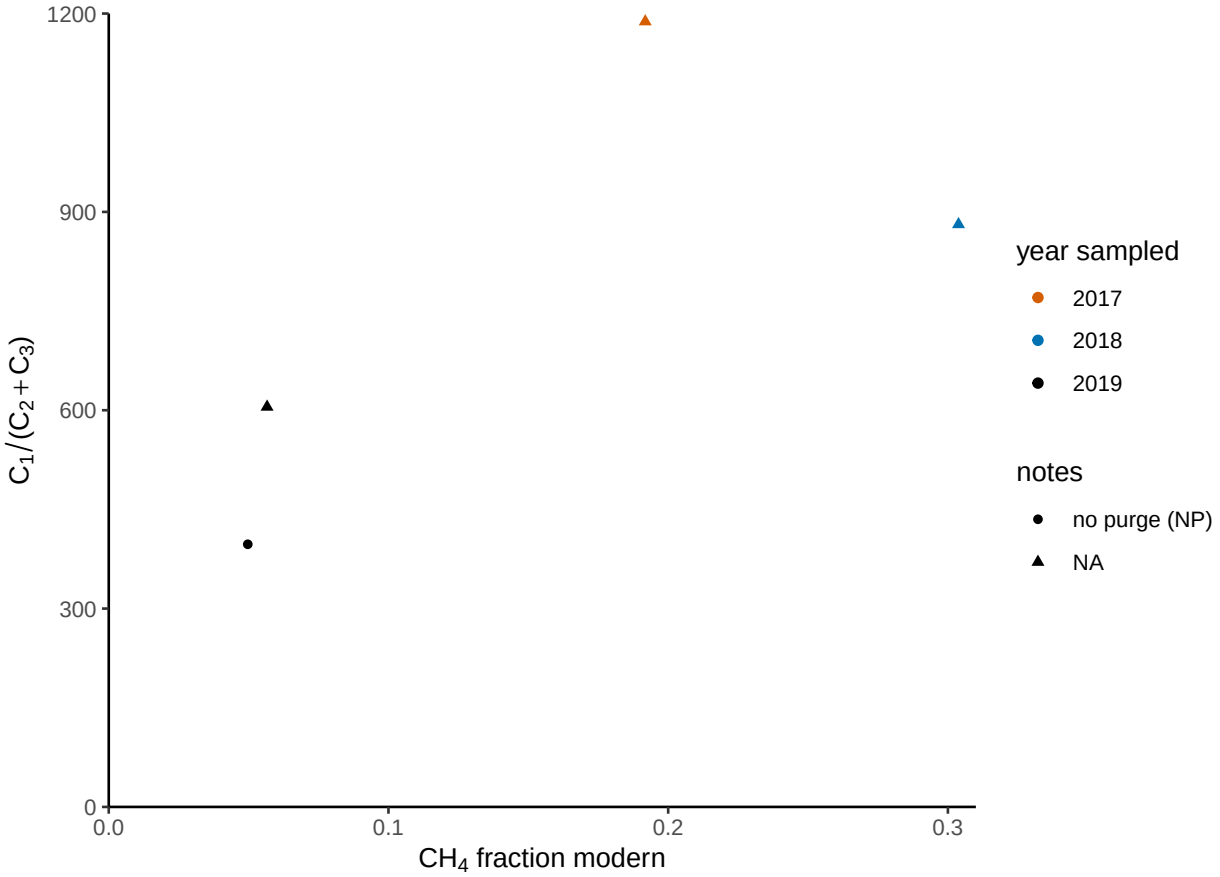

Figure B.4: $F^{14}C_{CH_4}$ and $C_1/(C_2 + C_3)$ at NSHQ14.

Appendix C

Supporting information for Chapter 4

C.1 Supplementary 16S rRNA gene sequencing

Two 1 L autoclaved glass bottles were filled with drill foam/fluid that had surfaced after subsurface circulation during drilling of BA1A in 2017. The drilling foam and fluid was filtered through 0.22 μm polycarbonate filters at Colorado School of Mines. The drill foam/fluid samples totaled 1.5 L in volume and were split into two replicates, resulting in 0.75 L of foam/fluid filtered for each replicate. Nucleic acids concentrated onto the filters were extracted, amplified, and sequenced as described by Kraus et al. (2018). The drill foam/fluid samples (Figure C.8) show very little taxonomic overlap with the fluids samples with packers (Main Text Figure 5).

In addition, a cell size fractionation experiment was performed for biomass filtering of BA1A in 2018. The sequential in-line filter housings described in the main text correspond to the three white cylinders near the bottom of Figure C.2. Main Text Figure 5 shows the results of sequencing 0.22 μm pore-diameter filters only. Results of sequencing filters of all pore diameters are reported in (Figure C.7).

C.2 Supplementary tables

Table C.1: Mixing extents based on Si, after Leong et al. (2020).

Sample ID	$\sum \mathrm{Si} / \left[\mu\mathrm{mol} \cdot \mathrm{L}^{-1}\right]$	Mixing extent / [% of $Mg^{2+} - HCO_3^-$ water]
BA1A_2018_55-66	1.97×10^2	65
BA1A_2018_100-400	4.49×10^1	15
BA1A_2019_0-30	3.33×10^2	110[a]
BA1A_2019_41-65	1.56×10^2	51
BA1A_2019_108-132	2.13×10^1	7.0
BA1D_2019_45-75	8.51	2.8
BA1D_2019_102-132	5.88	1.9

[a]BA1A_2019_0-30 has a calculated mixing extent $> 100\,\%$ we performed these calculations using the same $Mg^{2+} - HCO_3^-$ end member as Leong et al. (2020), which had a $c_{\sum \mathrm{Si}}$ of $303\,\mu\mathrm{mol} \cdot \mathrm{kg}$. This sample should be considered representative of a typical $Mg^{2+} - HCO_3^-$ water.

C.3 Supplementary figures

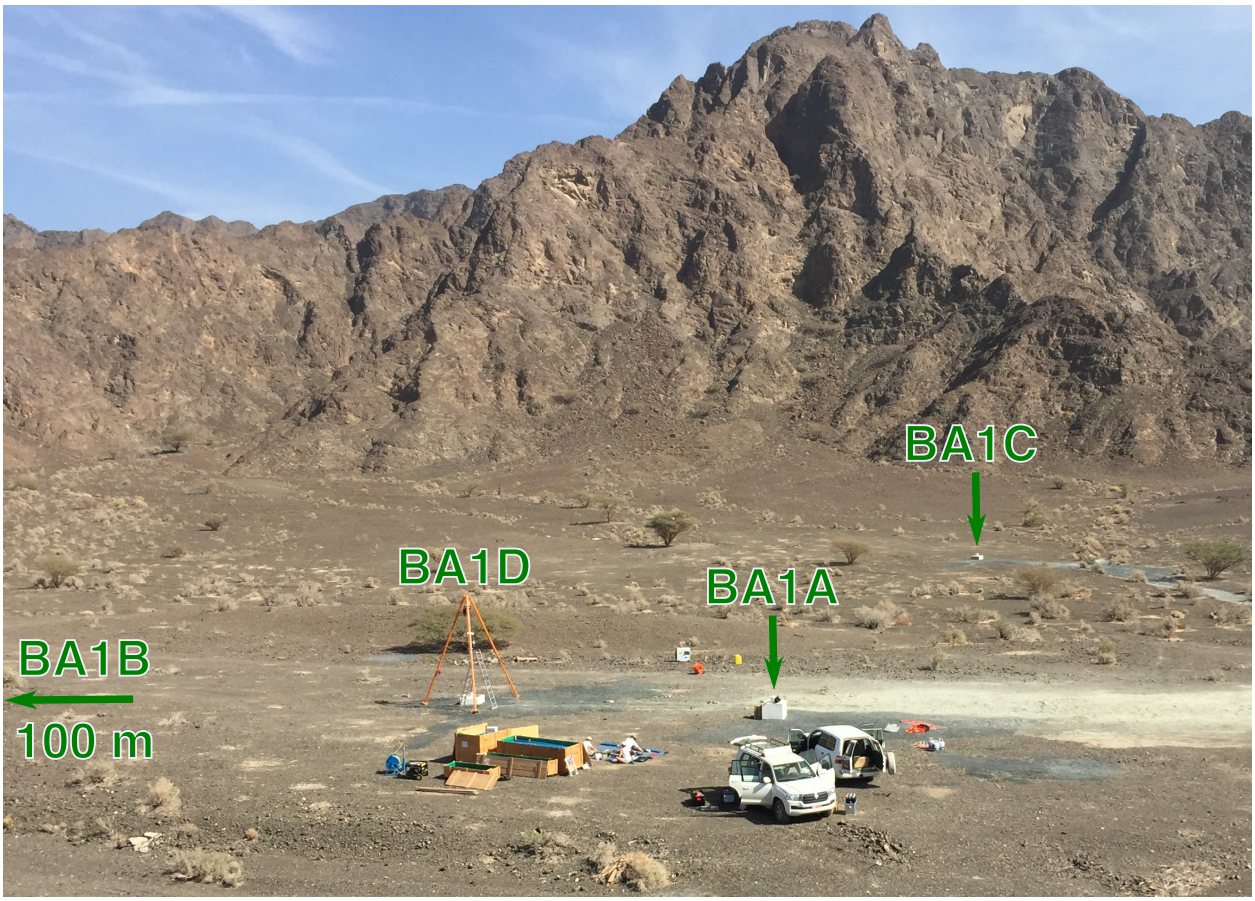

Figure C.1: Packer installation at BA1D, January, 2019. The orange tripod, installed at BA1D in the photo, was used to suspend the packer assembly down hole. The wellhead of BA1A can be seen 15 m to the right of BA1D in the photo. The third rotary well at the BA1 site, BA1C, which collapsed shortly after drilling, is pictured in the background. The cored borehole, BA1B, is 100 m to the left of the frame. Photo credit: Prof. Martin Stute.

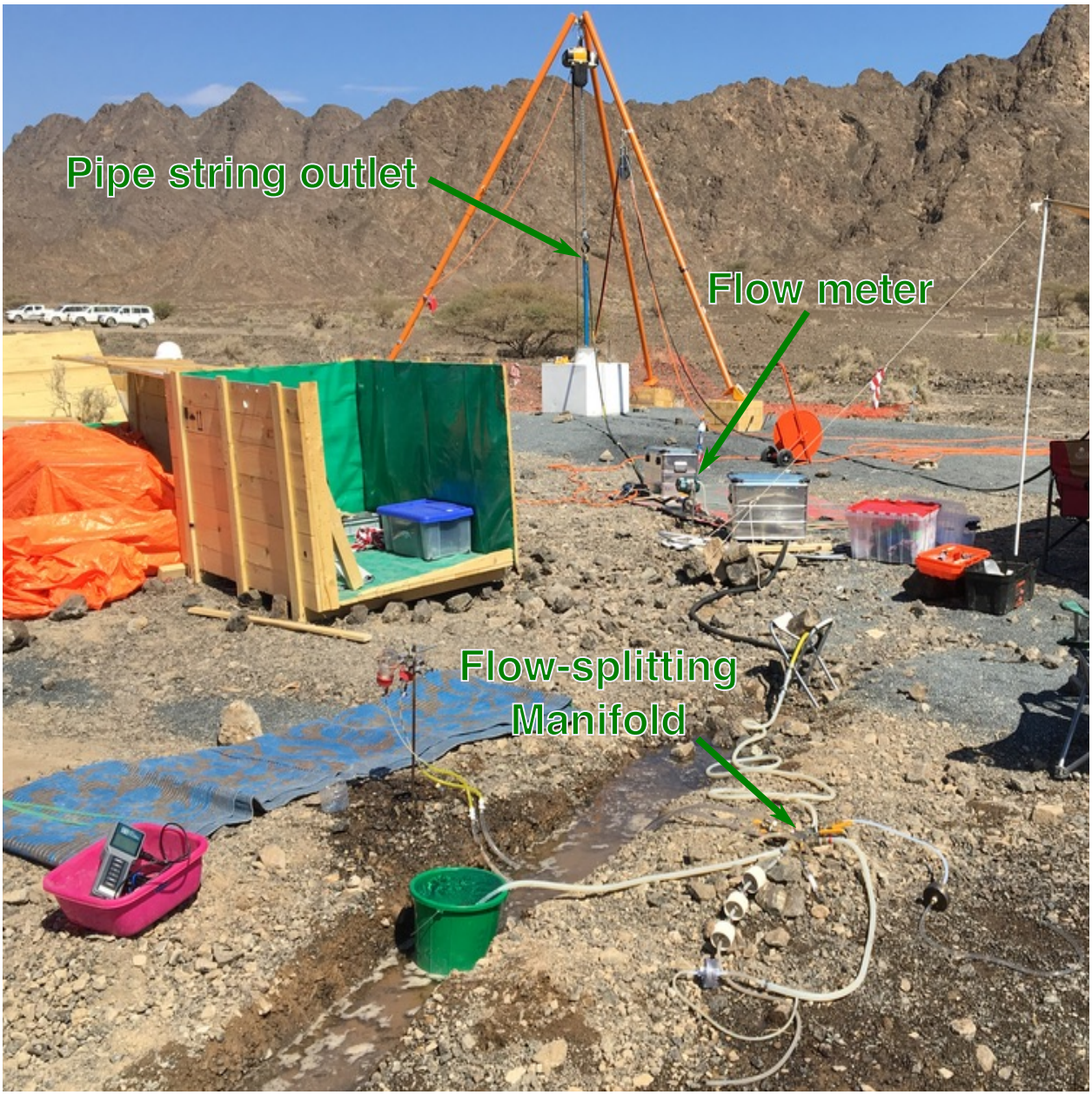

Figure C.2: Fluid pumping and sampling at BA1A, February, 2019. Labeled arrows indicate the top of the pipe string, from which the pumped water flowed, the flow meter used for hydrologic pump tests, and the flow-splitting manifold used for fluid and biomass sampling.

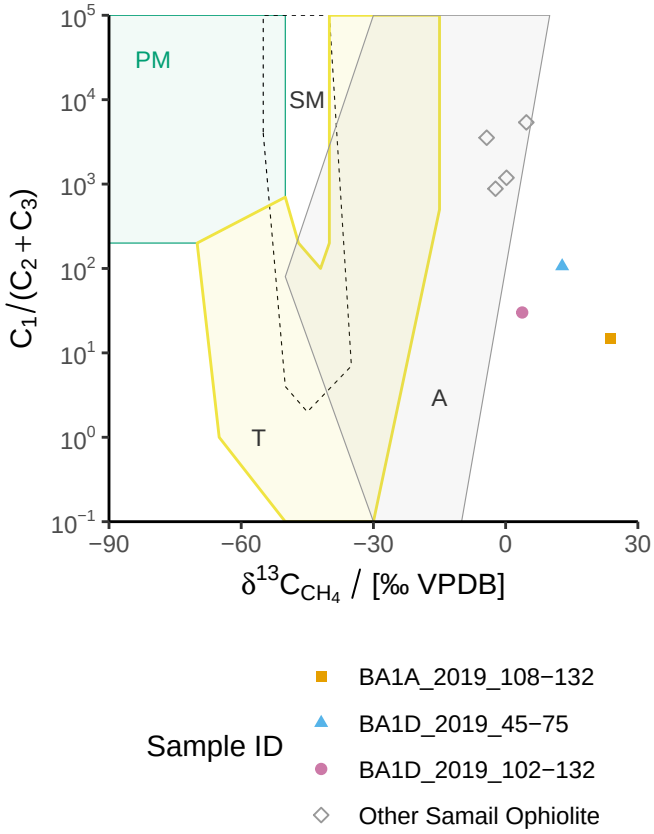

Figure C.3: Plot of ratio of methane (C_1) to the sum of ethane (C_2) and propane (C_3) vs. $\delta^{13}C_{CH_4}$. Only analyses for which C_2 was above limit of quantitation are plotted. If C_3 was below limit of quantitation, its contribution to $C_1/(C_2 + C_3)$ was assumed to be negligible, and therefore C_1/C_2 is plotted. Shaded fields of typical gas origin after Milkov and Etiope (2018). Contextual data from Samail Ophiolite from Nothaft et al., 2020; Etiope et al., 2015; Vacquand et al., 2018. *Abbreviations:* PM, primary microbial; SM, secondary microbial; T, thermogenic; A, abiotic.

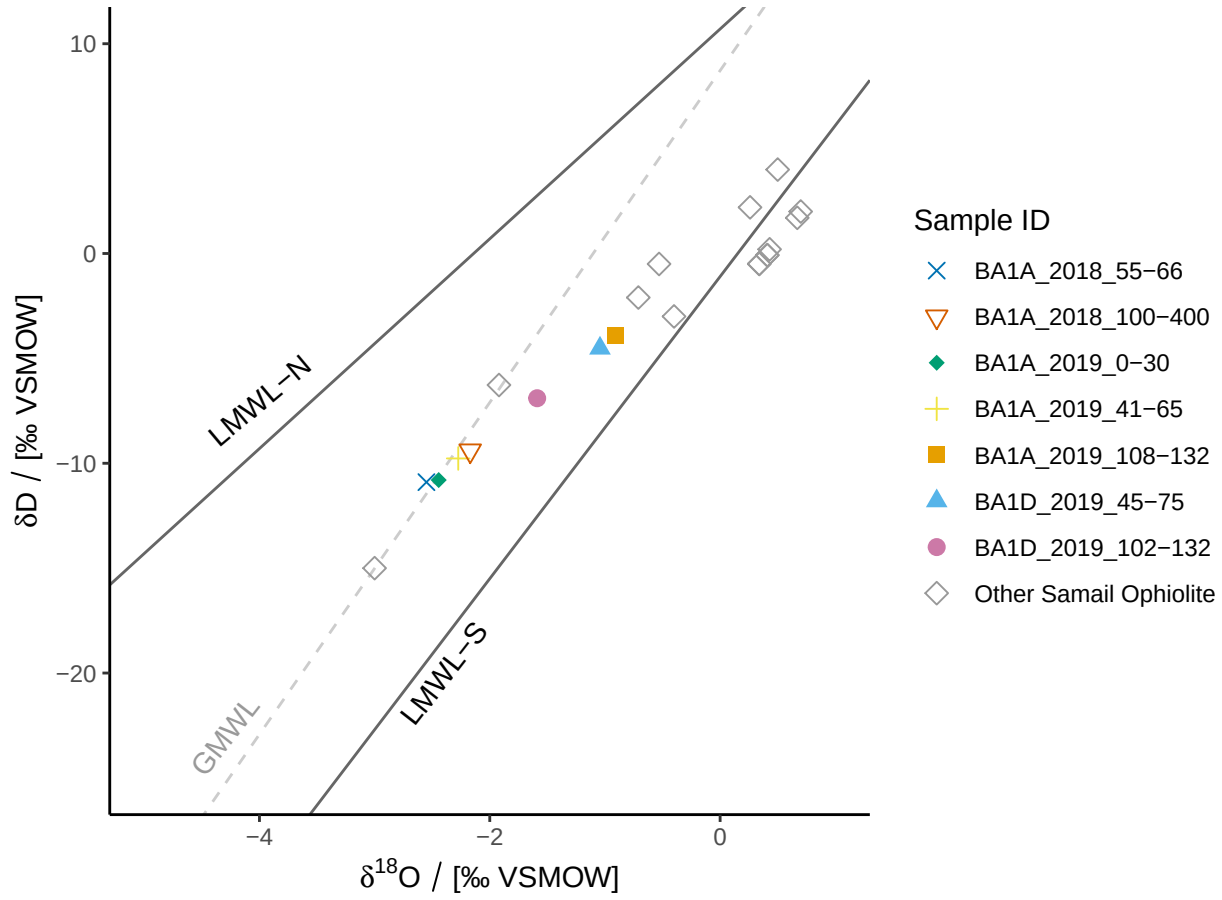

Figure C.4: Plot of Oman groundwater stable isotopic compositions. Samples from 2012 were reported in Vankeuren et al. (2019). Samples from 2014 reported in Miller et al. (2016). Samples from 2018 (apart from BA1A) reported in Nothaft et al. (2020) *Abbreviations:* LMWL-N and LMWL-S, Oman local meteoric water lines derived from northern and southern sources, respectively (Weyhenmeyer et al., 2002); GMWL, global meteoric water line (Terzer et al., 2013).

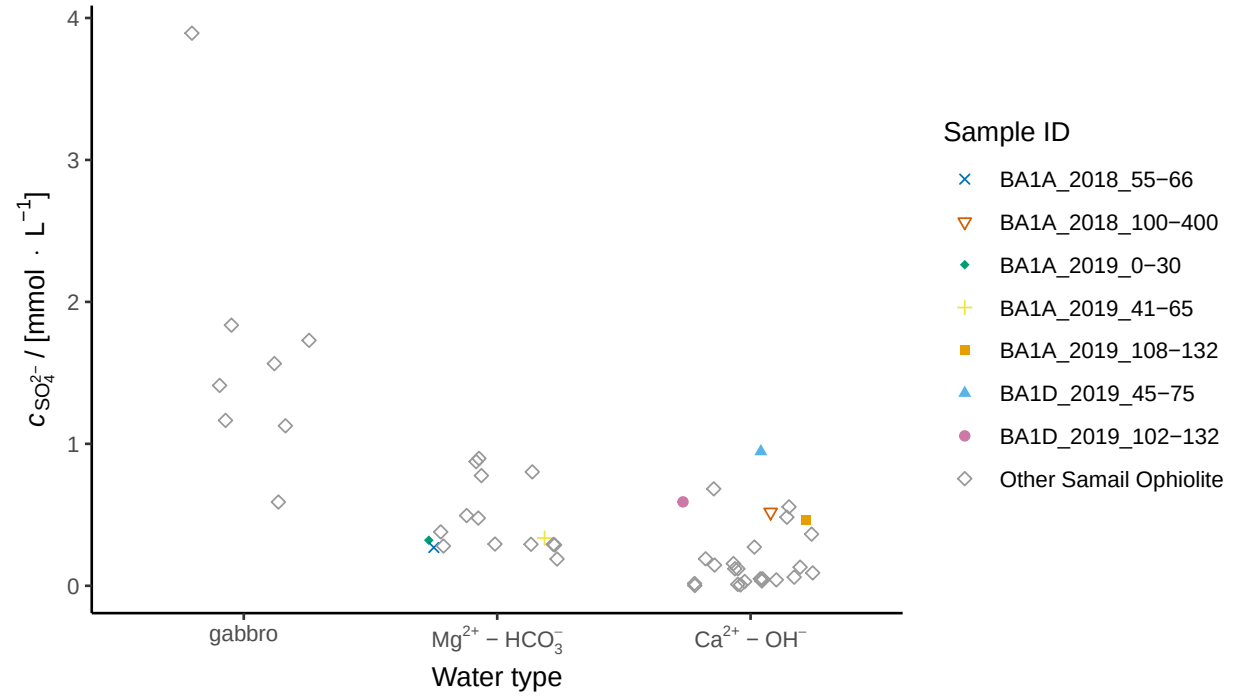

Figure C.5: SO_4^{2-} concentrations in Samail Ophiolite wells. Data from Miller et al., 2016; Rempfert et al., 2017; Kraus et al., 2018; Nothaft et al., 2020.

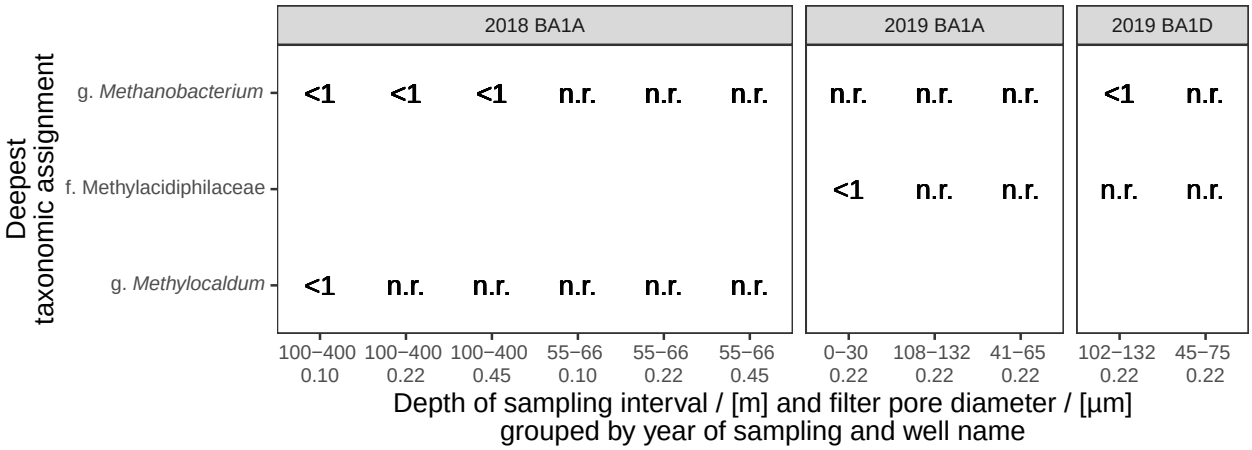

Figure C.6: 16S rRNA gene read relative abundances of DNA extracted from filter-concentrated groundwaters from BA1A and BA1D affiliated with CH_4-cycling taxa. Read relative abundances are reported as percentages rounded to the ones place. Cases when a taxon was detected in a sample and was $< 1\,\%$ read relative abundance after rounding are labeled "< 1". Cases when no reads of a taxon were detected in a sample, but when that taxon was detected in 16S gene reads of other Oman samples obtained during the same sampling year, are labeled "n.r." Cases when no reads were detected in any Oman sample within the data set of a given year are blank."

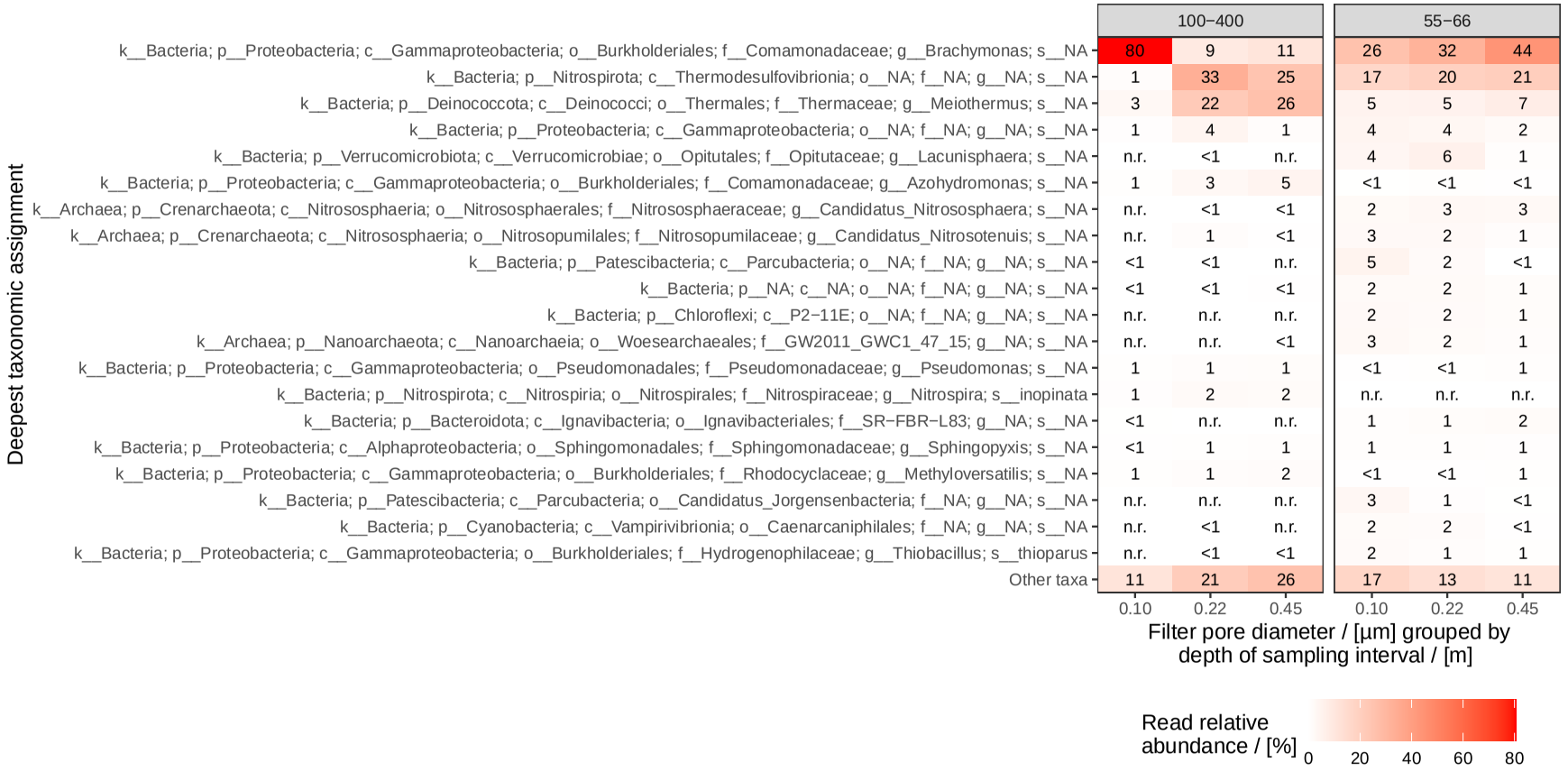

Figure C.7: 16S rRNA gene read relative abundances of 20 most abundant taxonomic assignments in DNA extracted from groundwaters from which biomass was concentrated using inline filters of sequentially decreasing pore diameters from well BA1A in 2018. Read relative abundances are reported as percentages rounded to the ones place. Cases when a taxon was detected in a sample and was $< 1\,\%$ read relative abundance after rounding are labeled "< 1". Cases when no reads of a taxon were detected in a sample, but when that taxon was detected in 16S gene reads of other Oman samples obtained during the same sampling year, are labeled "n.r." Cases when no reads were detected in any Oman sample within the data set of a given year are blank."

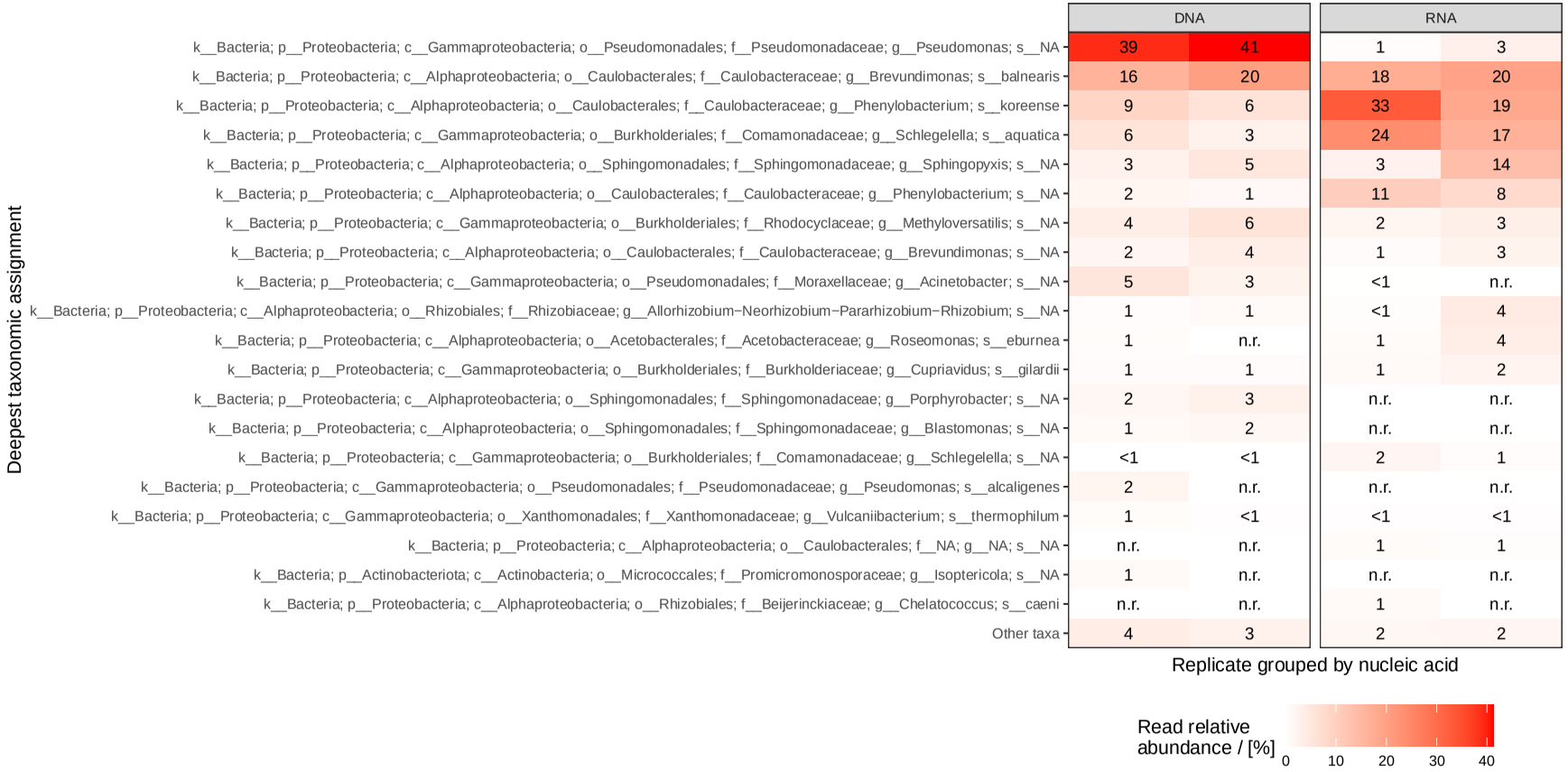

Figure C.8: 16S rRNA gene read relative abundances in of 20 most abundant taxonomic assignments in DNA and cDNA (from RNA) (Kraus et al., 2018) extracted from drill foam / fluid effluent from BA1A, acquired during drilling in 2017. Read relative abundances are reported as percentages rounded to the ones place. Cases when a taxon was detected in a sample and was $< 1\,\%$ read relative abundance after rounding are labeled "< 1". Cases when no reads of a taxon were detected in a sample, but when that taxon was detected in 16S gene reads of other Oman samples obtained during the same sampling year, are labeled "n.r." Cases when no reads were detected in any Oman sample within the data set of a given year are blank.

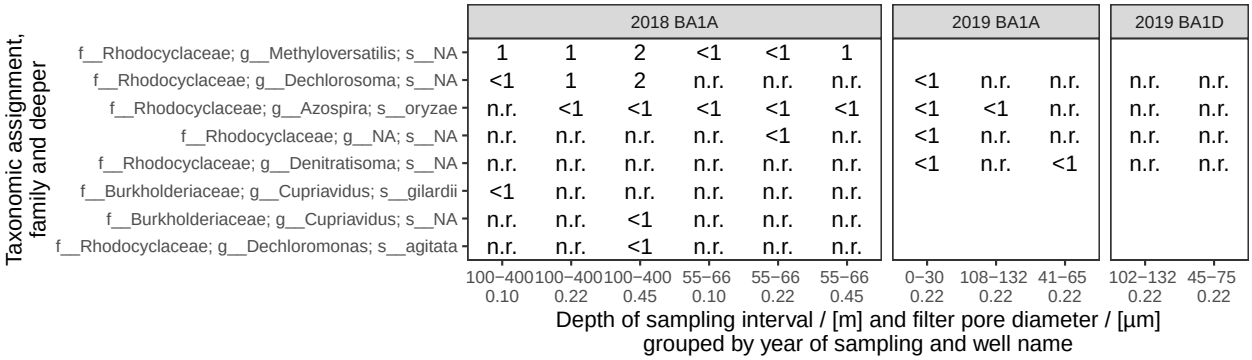

Figure C.9: 16S rRNA gene read relative abundances of DNA extracted from filter-concentrated groundwaters from BA1A and BA1D affiliated with S-oxidizing taxa noted by Rempfert et al. (2017) (presented at family level and deeper). Read relative abundances are reported as percentages rounded to the ones place. Cases when a taxon was detected in a sample and was $< 1\,\%$ read relative abundance after rounding are labeled "< 1". Cases when no reads of a taxon were detected in a sample, but when that taxon was detected in 16S gene reads of other Oman samples obtained during the same sampling year, are labeled "n.r." Cases when no reads were detected in any Oman sample within the data set of a given year are blank."

Appendix D

Advances in data acquisition, analysis, and curation at CU-Boulder

D.1 Overview of method development activities

To accomplish my analytical goals set out in Section 1.2.2, I had to expand the natural gas analytical capabilities of Templeton laboratory, which, as of 2015, consisted only of GC-FID analysis of CH_4. The formulation of my analytical ambitions coincided with new faculty appointments in the Department of Geological Sciences at CU-Boulder, notably Prof. Sebastian Kopf and Prof. Katie Snell. Thus, I started my Ph.D. at a time when several brand new mass spectrometers were coming online in the department and while few analytical methods had been established on these instruments. Due to these circumstances and the generosity of these professors and their laboratory managers, I was granted instrument time to establish several mass spectrometric methods.

My method development work started at the source: fluid sampling in the field. I also wish to note that I have gone to great lengths to document methodological details to have more transparent and reproducible science. Part of these efforts include making `protocols.io` documents of some of my most important methods, which can be accessed

at the DOI links referenced where applicable in this appendix. To increase the capability for advanced alkane gas isotopic analyses ($^{13}CH_3D$, $^{12}CH_3D_2$, $^{14}CH_4$, $\delta^{13}C_{C_{2+}}$, and $\delta^{13}C$ and $\delta^{13}D$ of low-c_{CH_4} samples), larger and more concentrated gas samples were required. I achieved these sampling objectives by employing the bubble strip method. I note that while bubble strip and evacuated vial gas sampling techniques are generally in decent agreement, the evacuated vial samples appear to be more accurate, possibly due to more complex phase and pressure changes involved with the bubble strip method. Therefore, evacuated vial gas sampling may be better suited to applications where quantitative accuracy in gas concentration measurements is a higher priority than lowering limits of quantitation, e.g. for isotopic analyses requiring a lot of gas. I describe this in greater detail in Section D.3, and I implemented this knowledge in the reporting of gas concentrations from samples taken in Oman in 2019 in Chapters 3 and 4. Also on a fundamental level, I observed some discrepancies in GC-FID quantitation of CH_4 and yields from conversion of CH_4 to CO_2 in preparation for ^{14}C analysis (which is a quantitative extraction of sample). This led to me revise methods for transferring gas via syringe from stoppered sampled to the GC. While task may seem mundane, it was crucial to accuracy improvements in the gas concentration data, which I applied to the data presented in Chapters 2, 3, and 4. For posterity, information on the syringe dilution corrections is supplied in Section D.4. On the topic of GC measurements, I also set up methods to quantitate $C_2 - C_6$ alkanes by GC-FID.

My efforts to increase isotopic measurement capabilities included setting up methods to measure $\delta^{13}C$ of $C_1 - C_6$ alkanes by GC-IRMS, and δD of CH_4. These efforts included a cross-comparison of CH_4 isotope standards obtained from USGS (courtesy of Mark Dreier) and Airgas. These method development tasks are thoroughly recorded in internal laboratory documents, which are stored on Google Drive at "OGL Shared Folder/Instruments CAREFUL EDITING/boba-fett/documents/Nothaft_C1-C6_alkane_d13C_dD_development_reports". These method optimization tasks enabled me to push limits of quantitation and obtain isotopic data that would not have been

possible working with most commercial laboratories. Further, I optimized methods to extract CH_4 from my butyl-stoppered glass vial gas samples to prepare the CH_4 for ^{14}C analysis. This is summarized in Section 3.5.2 and detailed in Section D.5. Preparing these samples in-house lowered costs of analysis and decreased sample turnaround time, enabling me to collect the largest set of $^{14}CH_4$ analyses from a serpentinizing environment ever. In addition, I established methods for quantitating concentration and $\delta^{13}C$ of $\sum CO_2$ (`http://dx.doi.org/10.17504/protocols.io.zduf26w`), which is not trivial because of the low $c_{\sum CO_2}$ in hyperalkaline waters in serpentinites. Through my method development on the GasBench, I worked with Brett Davidheiser-Kroll to establish a peak-fitting method that is capable of checking for faulty gas injections and may also decrease analytical uncertainties for concentration and $\delta^{13}C$ of $\sum CO_2$. The code for the peak-fitting method is available at `https://github.com/danote/Oman_CH4_stable_isotopes`. Further, I contributed $\delta^{13}C_{\sum CO_2}$ measurements to an inter-laboratory round-robin study where a reference material for $\delta^{13}C_{\sum CO_2}$ was proposed (Cheng et al., 2019). In this study, my measurements were found to be on-par with the top chemical oceanography laboratories in the field, which validated my methods.

D.2 Data analysis and curation

I also made several contributions to analysis and curation of data from the Samail Ophiolite. For example, I created a Github repository for 16S rRNA gene amplicon sequencing data analysis for samples from the Samail Ophiolite (`https://github.com/danote/Samail_16S_compilation`). Here, data from samples obtained from 2014 through 2019 was gathered and [re]processed in a consistent and reproducible manner. This was an important task because the processing of 16S rRNA gene amplicon data has considerably advanced since our group started doing such work (e.g. Miller et al., 2016). Differences in data processing made it difficult to compare data across years of sampling. One of the aspects of this data

processing that changes most rapidly is updates to the reference database used for taxonomic inferences, i.e. Silva. I set up my compilation repository so that a user can download a new reference database, change one line of code, and reprocess multiple years of data at once. Further, I wrote some custom code to visualize these data in heat maps that I find to be better than plots from standard packages commonly used for these tasks. I might turn this code into a small R package at some point if I find the time, but for now, the raw scripts are available at "ampliverse.R" on my Github (`https://github.com/danote/Oman_CH4_stable_isotopes`). All of the heat maps in this dissertation were made with that code.

In addition, I curated and compiled aqueous geochemical data from the Samail Ophiolite obtained by our group and made it publicly available in forms that can be directly imported into R and/or Python and that have limits of quantitation and analytical uncertainties saved alongside the primary data, where feasible. Bits and pieces of this can be found as "Oman_Geochem_2012-2018.xlsx" (or similar) in the Github supplements of Chapters 2, 3, and 4. This has facilitated the comparative and longitudinal aspect of my dissertation and has improved data quality (e.g., it has led to the identification and correction of some data entry/compilation errors from before I started collecting samples from Oman). I recommend that this data structure be used by future researchers studying fluid chemistry in the ophiolite.

I also digitized the geologic map of my study area within the Samail Ophiolite from Nicolas et al. (2000) to work with it in the free and open-source software, QGIS. This Nicolas et al. (2000) map is used by most researchers studying the ophiolite and is found in many publications. However, to my surprise, it apparently only existed as a non-georeferenced PDF / Adobe Illustrator file. I suppose most researchers using this map roughly estimated locations of samples and manually sketched them onto this map in Illustrator (or other vector graphics software), which is not very accurate. My version of the map can be seen in Figures 2.1 and A.1. I also contributed a version of this map to Kraus et al. (in press). I hope this digital map continues to serve as a resource for the community of researchers studying the

ophiolite.

D.3 Oman 2019 CH_4, CO_2, and H_2 sampling method comparison

D.3.1 Presentation of gas data

Concentrations of CH_4, CO_2, and H_2 from GC analyses on gas samples taken in Oman during January 2019 are shown in D.1. Limits of quantitation, in terms of aqueous concentration, are shown for the bubble strip, headspace (evacuated vial), and copper tube gas sampling methods in D.2.

Table D.1: Oman 2019 gas data. All concentrations in $\mu\text{mol} \cdot \text{L}^{-1}$, aqueous phase. NA indicates below limit of quantitation. *Abbreviations:* BS: bubble strip, HS: headspace gas (evacuated vial), Cu: copper tube.

site	replicate	c_{CH_4}	c_{CO_2}	c_{H_2}
WAB71	BS1A	1.59E+01	NA	NA
WAB71	BS1B	1.57E+01	NA	NA
WAB71	BS2A	1.41E+01	NA	1.33E-01
WAB71	BS2B	1.48E+01	NA	NA
NSHQ14	BS1A	5.09E+01	NA	1.55E+02
NSHQ14	BS1B	7.10E+01	NA	2.11E+02
NSHQ14	BS2A	4.84E+01	NA	1.41E+02
NSHQ14	BS2B	4.82E+01	NA	1.40E+02

site	replicate	c_{CH_4}	c_{CO_2}	c_{H_2}
WAB105	BS1A	1.49E-01	NA	2.49E-01
WAB105	BS2A	1.12E-01	NA	1.55E-01
BA1D4575	BS1A	9.75E-01	NA	NA
BA1D4575	BS1B	1.51E+00	NA	NA
BA1D4575	BS2A	9.43E-01	NA	NA
BA1D4575	BS2B	1.72E+00	NA	NA
WAB56	BS1A	7.45E+00	NA	1.46E+02
BA1D102132	BS1A	1.84E+00	NA	7.51E-01
BA1D102132	BS1B	1.98E+00	NA	9.31E-01
BA1D102132	BS2A	2.12E+00	NA	1.12E+00
BA1D102132	BS2B	2.04E+00	NA	1.13E+00
BA1A<30	BS1A	NA	NA	NA
BA1A<30	BS1B	NA	3.02E+01	NA
BA1A<30	BS2A	NA	2.41E+01	NA
BA1A<30	BS2B	NA	NA	NA
BA1A4165	BS1A	5.89E-02	3.70E-01	NA
BA1A4165	BS1B	5.89E-02	2.24E+01	NA
BA1A4165	BS2A	9.29E-02	NA	NA
BA1A4165	BS2B	9.39E-02	NA	NA
BA1A108132	BS1A	7.47E-01	NA	NA

site	replicate	c_{CH_4}	c_{CO_2}	c_{H_2}
BA1A108132	BS1B	8.04E-01	NA	2.06E+00
BA1A108132	BS2A	9.39E-01	NA	8.40E+00
BA1A108132	BS2B	9.32E-01	NA	1.03E+00
NSHQ14NP	BS1A	5.22E+01	NA	1.89E+02
NSHQ14NP	BS1B	4.21E+01	NA	1.47E+02
NSHQ14NP	Cu	1.33E+02	NA	5.04E+02
WAB71	HS	2.35E+01	NA	NA
NSHQ14	HS	6.77E+01	NA	2.27E+02
WAB105	HS	NA	4.67E+01	NA
BA1D4575	HS	2.13E+00	NA	NA
WAB56	HS	1.57E+01	NA	3.10E+02
BA1D102132	HS	3.53E+00	NA	3.29E+00
BA1A<30	HS	NA	8.75E+01	NA
WAB84	HS	1.34E+00	NA	NA
BA1A4165	HS	NA	2.12E+01	NA
BA1A108132	HS	9.70E-01	NA	NA
NSHQ14NP	HS1	1.16E+02	NA	4.21E+02
NSHQ14NP	HS2	1.21E+02	NA	4.43E+02

Table D.2: Limits of quantitation in aqueous phase and total sample size of various gas sampling methods. The differences in scale of limit of quantitation reduction between the various gases is due to their different Henry's Law constants.

method	limit of quantitation / μmol $\cdot$ L^{-1}, aqueous phase			total μmol CH_4 sampled, NSHQ14NP
	CH_4	CO_2	H_2	
bubble strip	2.05E-02	9.24E-01	6.43E-02	46
headspace	6.70E-01	2.48E+00	3.29E+00	7
Cu tube	1.22E+00	3.59E+00	6.05E+00	2

D.3.2 Explanation of sampling methods

D.3.2.1 Copper tube

The low permeability, high malleability, and affordability of Cu tubes have made Cu tube gas sampling the standard method for dissolved gas sampling in the noble gas community, and it has been shown to be suitable for dissolved H_2 gas sampling (Paukert, 2014). In this method, the Cu tube is connected to the pumped water stream, as demonstrated by Prof. Martin Stute in Figure D.1. Back-pressure is applied by tightening the outflow ball valve, until no bubbles are observed in the glass section of the tube sampling apparatus. This ensures that gas exsolution is not occurring. The Cu tube is crimped by ratcheting down on the sampling apparatus.

The Cu tube containing water at *in situ* pressure must then be equilibrated with a gas headspace for GC analysis. To do this, tubings and fittings were attached and connected to an evacuated glass line as shown in Figure D.2. The key components here are a Swagelok ball valve, which can isolate the headspace from the vacuum line. Also, a 1/4 in. Ultra-Torr fitting, with a rubber septum (606MSLB-9.5, J.G. Finneran) and washer inside were used to access the headspace via syringe and needle. Brett Davidheiser-Kroll and I tested this setup and found that it held a vacuum quite well.

Next, I had to determine the headspace volume. First, the Cu tube apparatus was

Figure D.1: Copper tube sampling method.

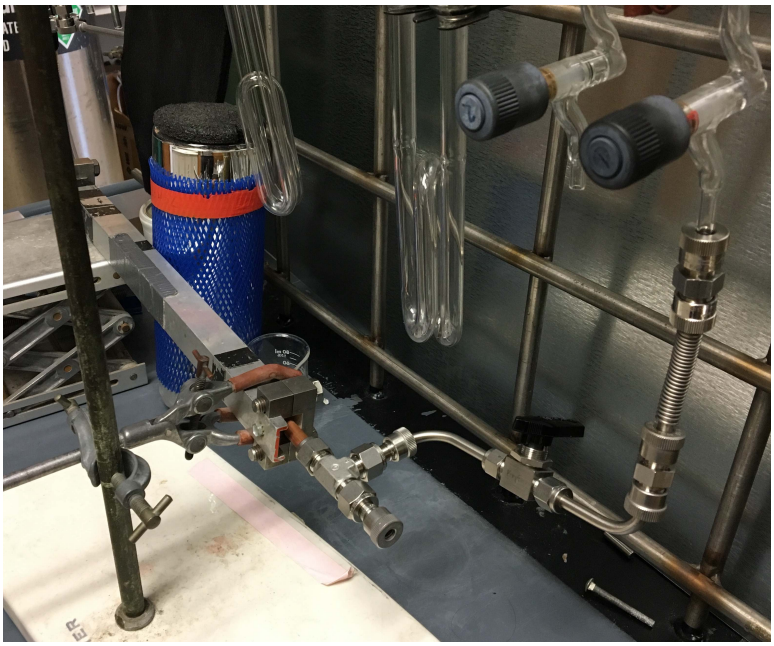

Figure D.2: Connecting copper tube to an evacuated glass line.

evacuated, and the ball valve was closed, and the apparatus was removed from the vacuum line. Then, I filled a 60 mL syringe with water, attached a 23G needle, and punctured the septum. The plunger was pulled in slowly by the vacuum. I applied some additional pressure until the syringe stopped. 6 mL of water was introduced to the apparatus in this manner. I then opened the ball valve and drained the tubing. I refilled the headspace through the septum with the same 60 mL syringe until I saw water coming out of the ball valve. I obtained 5 mL volume through this method. I supposed that some water may have not been drained from the apparatus, so I took 6 mL as the headspace volume. To dry the headspace area, I reconnected the apparatus to the vacuum line and evacuated it for 72 hr.

After the headspace was re-evacuated, the ball valve closed, and the Cu tube removed from the vacuum line, the Cu tube was un-crimped using the big vice in BESC 445. I lightly shook the tube to increase gas exsolution rates. I then brought the un-crimped Cu tube to the little vice by the GC and let the tube sit for 1 min, as shown in Figure D.3. I had calculated that the headspace would still be lower than atmospheric pressure, so I injected 6 mL of N_2 at Boulder atmospheric pressure via syringe to bring the headspace up to atmospheric pressure. I let the tube sit for 3 additional minutes, and then took a 0.2 mL sample with with a 1 mL gas-tight syringe and injected it on the GC. A replicate (0.4 mL) sample 15 min later yielded the same (volume corrected) result within error, which suggests that the gases had sufficiently equilibrated with the headspace and that the septum had a good seal. After gas extraction, the water in the Cu tube was drained into a glass vial, whose mass had been measured. The vial was re-weighed, and a volume of 17 mL water was calculated.

D.3.2.2 Headspace gas (evacuated vial)

Blue butyl stoppers were inserted into 117 mL borosilicate glass vials. In 2019, Prof. Stute evacuated these vials at Lamont-Doherty Earth Observatory. In the field, a 60 mL syringe was connected to the luer-lock port on the pump manifold. The syringe was flushed and a

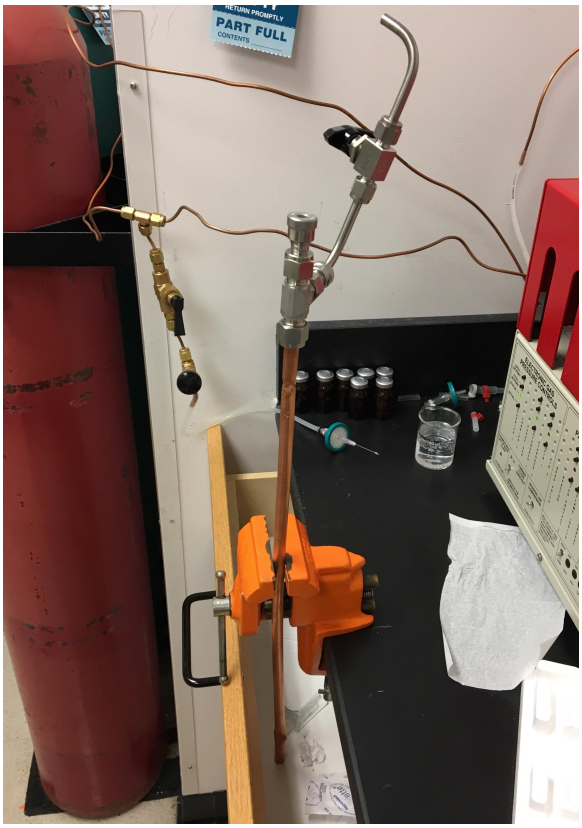

Figure D.3: Equilibrating copper tube water with headspace for GC analysis.

sample of water was taken. A 0.2 μm syringe filter and needle were attached to the syringe. The needle and filter were flushed with site water. A 60 mL water sample was injected from the syringe into the evacuated vial. Vials were stored upside down (water in contact with septum facing groundwards). A strong vacuum remained on these samples at the time of GC analysis, indicating a good seal with the blue butyl stopper. Therefore, 60 mL of high-purity N_2 at Boulder atmospheric pressure were added to the vials with a 60 mL syringe in order to bring the headspace gas to atmospheric pressure to facilitate extraction of gases for injection on the GC.

D.3.2.3 Bubble strip

Details on bubble strip gas sampling are available at `http://dx.doi.org/10.17504/protocols.io.2x5gfq6`. In 2019, equilibrated gases were sampled into 37 mL borosilicate glass vials that had been autoclaved, capped with NaOH-leached and autoclaved blue butyl rubber stoppers and filled with autoclaved saturated NaCl solution. 30 mL of equilibrated gas sample were injected into these vials by displacement. Vials were stored upside down (water in contact with septum facing groundwards).

D.3.3 Comparison of gas data obtained through various sampling methods

Gas concentrations determined from samples obtained through the various methods described in Section D.3.2 were compared for NSHQ14NP. These were replicate samples of well NSHQ14 8 days after our first sampling at this well in 2019. NP stands for "no purge." The first time we sampled NSHQ14 in 2019, we purged the well for 237 min at 21.7 L·min^{-1} prior to sampling. The second time we sampled, we immediately started sampling when the pump started. We were testing the degree to which purging the well affected well chemistry.

Aqueous H_2 and CH_4 concentrations determined at this site for each sampling method are shown in Figure D.4. All samples had the same H_2/CH_4 ratio (3.4), which suggests that

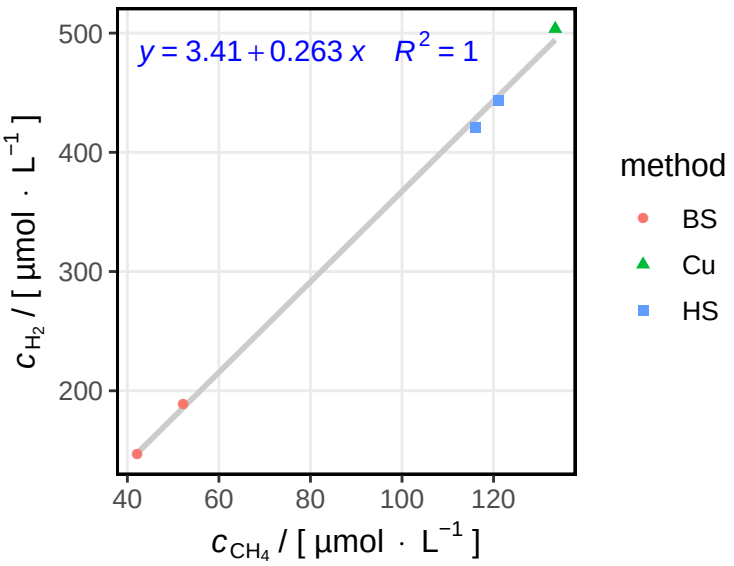

Figure D.4: Plot of aqueous concentrations of CH_4 and H_2 determined through bubble strip "bubble strip", copper tube "Cu", and headspace "HS" gas sampling methods from NSHQ14NP (no-purge).

the same gas was sampled by all methods and that diffusion / exsolution kinetic differences between H_2 and CH_4, as well as potential microbial alteration of these gases post-sampling, was probably minimal. The reproducibility among sample types (bubble strip and headspace gas replicates) seems good. However, there are considerable discrepancies between sampling methods. The headspace gas and Cu tube methods yielded similar results, with the Cu tube yielding slightly higher concentrations. This could be interpreted as loss of gas in the headspace gas samples from exsolution due to the pressure drop and/or permeable silicone tubing involved with our sampling technique. However, I think that concentrations obtained from the headspace gas and Cu tube samples are indistinguishable within error due to uncertainties in the volume of the various sampling containers and/or headspace. Thus, if we accept the copper tube sample as accurate, it would appear that the headspace sample performed well, but the bubble strip sample considerably underestimated the aqueous gas concentration (bubble strip sample aqueous gas concentrations were $\sim 40\,\%$ of those from headspace gas samples at NSHQ14NP).

Comparisons of aqueous gas concentrations through multiple years of sampling with

headspace gas and bubble strip methods are shown in Figures D.5, D.6, and D.7 for H_2, CH_4, and CO_2, respectively. In Figure D.5, we can see that bubble strip samples generally yield lower dissolved H_2 concentrations than the headspace gas samples. The discrepancy is particularly large in the higher concentration samples. Bubble strip samples could underestimate headspace gas samples if the bubble strip headspace does not fully equilibrate with the water. However, at least for the high H_2 samples, this is not consistent with field observations. For example, in well NSHQ14, which is has the highest H_2 among the sampled wells, the bubble strip headspace volume expands during sampling. In fact, at NSHQ14, it is not even necessary to add a headspace. H_2 will spontaneously come out of solution and collect in the overturned bubble strip vial. Thus, gas phase / aqueous phase exchange kinetics seem sufficiently rapid for equilibrium to be readily achieved during sampling. Rather, bubble expansion appears to be the problem. Prof. Stute noted this in the field. The premise of the bubble strip method is that the gases in the headspace "bubble" obtain partial pressures in equilibrium with the water. If the sum of the partial pressures of gases dissolved in the water is greater than atmospheric pressure, then there will be a pressure differential between the bubble and the atmosphere, which will cause the bubble to expand until it fills up the entire bubble strip vial. If there was some way to force the bubble to maintain constant volume, the bubble could have a pressure different from atmospheric pressure, and then could truly equilibrate with waters whose gases are at any pressure. It is not clear to me whether some bubble strip apparatus designs are capable of maintaining constant bubble volume, or whether the method is typically applied to waters in which the dissolved gases collectively have partial pressures near atmospheric pressure, and therefore do not have substantial inaccuracies. I cannot think of an easy way to ensure that the inflow and outflow of a bubble strip apparatus are equal. Therefore, I think my inaccurate bubble strip measurements are a result of sampling waters with unusually high dissolved gas pressures. The bubble strip technique is usually billed as a way to measure $\mathrm{nmol \cdot L^{-1}}$ aqueous H_2 concentrations because it up-concentrates the gas. Perhaps it just has not been used at $> 100\,\mu\mathrm{mol \cdot L^{-1}}$ H_2 waters

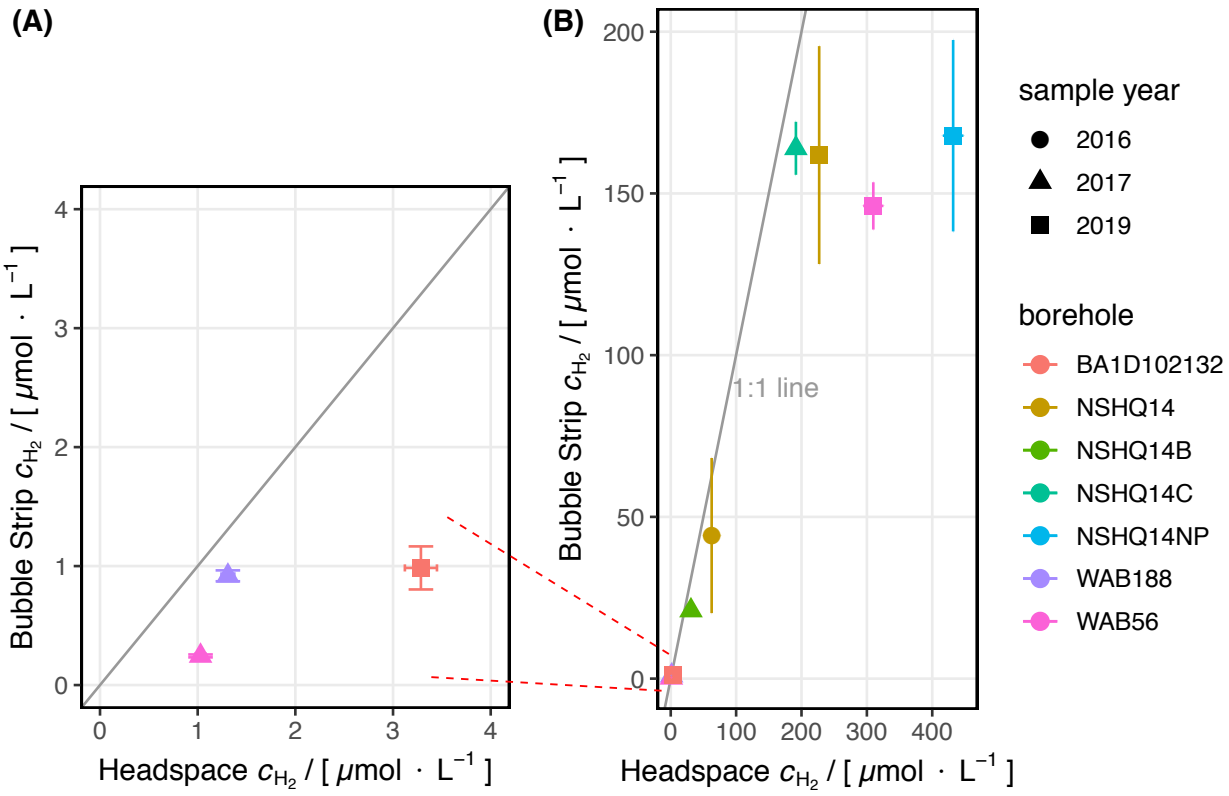

Figure D.5: Comparison of aqueous H_2 concentrations between bubble strip and headspace gas methods. **(A)** lower concentrations. **(B)** full dataset. Error bars are 1 sample standard deviation where replicates are available; otherwise error bars are 5 % of the measured value.

like the ones we deal with in Oman.

Dissolved CH_4 concentrations (Figure D.6) were for the most part also lower for bubble strip samples than headspace gas samples, particularly for samples in the 100 μmol · L^{-1} range. A notable exception is NSHQ04. That particular sample has somewhat larger uncertainty than is represented in the error bars because its concentration was corrected from an initial low volume measurement to the yield obtained on the INSTAAR CH_4 radiocarbon preparation line (see Sections D.4 and D.5). However, I do think the corrected CH_4 concentration from NSHQ04 is fairly accurate. If so, why is it that the bubble strip sample is in better agreement with the headspace gas sample in this high CH_4 well compared to the high H_2 well, NSHQ14? I think this mostly has to do with our pumping methods. Due to well collapse at NSHQ04, we sample quite close to the water table. In 2017, we sampled at

5.8 meters below top of casing (mbtc) at NSHQ04. In contrast, at NSHQ14, we typically sample from 85 mbtc. I think the shallow samples of NSHQ04 interact with the atmosphere and therefore the sum of partial pressures of gases dissolved in our NSHQ04 samples are likely much closer to atmospheric pressure. Additionally, we use a much lower flow pump at NSHQ04, so it is possible that this also contributes to lower water/gas pressure in these samples. I do not recall observing volume expansion of the bubble strip bubble at NSHQ04. This suggests that the NSHQ4 bubble was close to atmospheric pressure. For this reason, perhaps the bubble strip samples are more accurate for shallow groundwater samples like at NSHQ04.

For completeness, I also include data on dissolved CO_2 concentrations (D.7), but I do not think these data are very accurate due to higher risk of atmospheric contamination during sampling and the higher CO_2 background on our GC. Thus, I only use the dissolved inorganic carbon samples for pCO_2 calculations.

In summary, it appears that the bubble strip method as I have been using it can be somewhat inaccurate, particularly when the sum of partial pressures of gases dissolved in the groundwater are much higher than atmospheric pressure. Thus, it seems to me that 2019 aqueous gas concentrations should be reported only from headspace gas samples. What is the value, then, of the bubble strip method? The bubble strip method is good for up-concentrating gases and allowing the gas sample to be separate from the water sample. This is highlighted in Table D.2, which compares limits of quantitation in terms of aqueous concentration for the various sampling methods used in 2019. This comparison shows that the limits of quantitation are generally 10 to 100 times lower for bubble strip samples. In 2019, this has enabled quantitation of CH_4 in WAB105 and BA1A4165 and H_2 in WAB71, WAB105, and BA1A108132 in bubble strip samples, whereas these gases were not quantitatable in headspace gas samples (Table D.1).

Table D.2 also shows the total μmol of CH_4 contained in each sampling vessel for samples from well NSHQ14NP. This shows that at least 10 times more gas can be obtained through

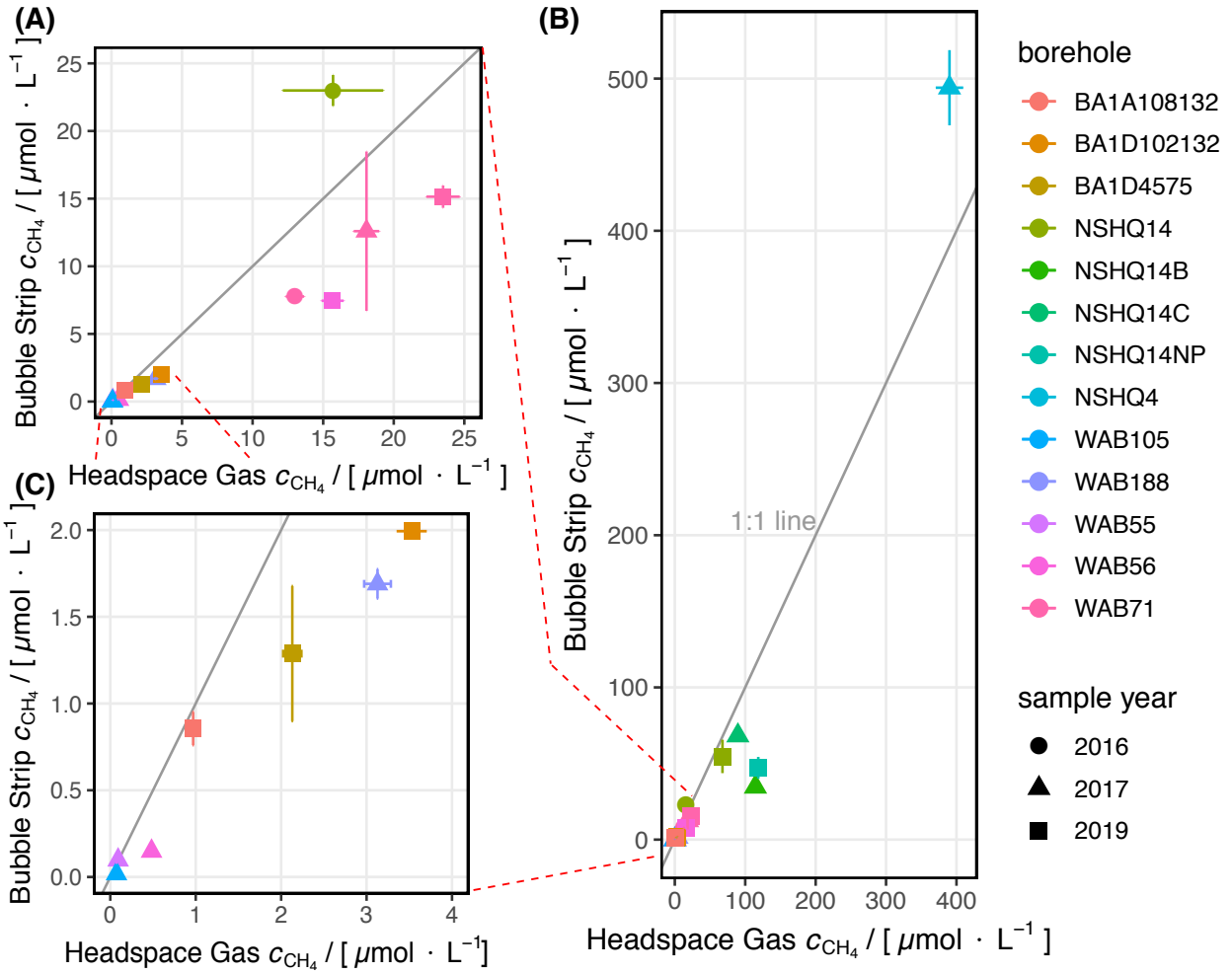

Figure D.6: Comparison of aqueous CH_4 concentrations between bubble strip and headspace gas methods. **(A)** and **(C)** lower concentrations. **(B)** full dataset. Error bars are 1 sample standard deviation where replicates are available; otherwise error bars are 5 % of the measured value.

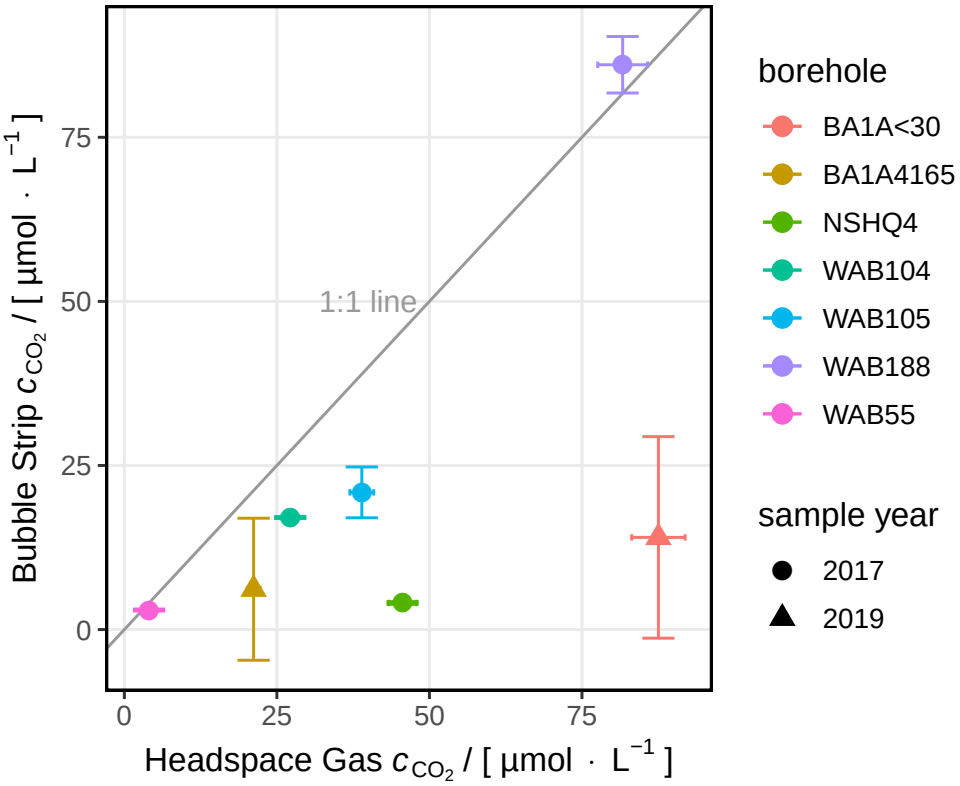

Figure D.7: Comparison of aqueous CO_2 concentrations between bubble strip and headspace gas methods. **(A)** lower concentrations. **(B)** full dataset. Error bars are 1 sample standard deviation where replicates are available; otherwise error bars are 5 % of the measured value.

bubble strip samples, despite these samples having just a fraction of the mass of the other sample types (because water need not be transported for bubble strip samples). Bubble strip samples are also scalable, such that an essentially unlimited amount of gas can be obtained from a water sample through this method. This is very important for advanced isotopic analyses. For example, of the samples obtained in 2019, only those for which the bubble strip method was used had sufficient CH_4 for precise ^{14}C analysis.

In conclusion, it seems to me that future gas sampling in Oman projects may benefit from a multi-sample approach. Cu tubes or headspace gas / evacuated vial samples could be used for concentration determinations, while bubble strip samples could be used for isotopic analyses.

D.4 Effects of syringe aliquoting volume and method on gas concentration measurements

D.4.1 Results of GC injection volume experiment

On January 28, 2020, I conducted an experiment to test the effect of the method of aliquoting from a rubber-stoppered glass vial on measured gas concentrations on a gas chromatograph (GC). The experimental setup was as follows. 5.00 mL aliquots of the Templeton lab 10.0 % CH_4 in N_2 tank (at lab P and T) were added to each of two 37 mL blue butyl rubber-stoppered glass serum vials. From vial #1, aliquots for GC injection were obtained by directly uptaking the gas in the vial without any additional pumping of the syringe barrel. From vial #2, aliquots for GC injection were obtained by pumping the syringe barrel 5 times while the syringe was connected via needle to the vial. By "pump", I mean withdrawing the syringe barrel to nearly its full extent and then pushing the syringe barrel inward as far as it can go. GC injections were alternated between aliquots from vial #1 and vial #2 over a range of injection volumes from 0.10 mL and 1.00 mL. To avoid biasing the experimental

results due to potential systematic errors in corrections for repeated aliquots as a function of inject volume, I alternated the sequence of injections from low to high volume.

The results from the experiment are shown in Figure D.8. All results are corrected for repeated aliquoting from one fixed-volume container. The dashed line in Figure D.8 represents the CH_4 concentration that I expected in the vial based on the vial volume, my aliquot volume, and the concentration of the tank reported by Airgas. The shapes of data points reflect the amount of times the syringe barrel was pumped during aliquoting.

In agreement with my previous findings (data not shown), measurements from aliquots directly taken from the vial without pumping the syringe barrel had measured concentrations well below the expected concentration, and this underestimation increased in magnitude with lower inject volumes. The new element of this dataset is the data series in which aliquots were taken with repeated pumping of the syringe barrel. The data from aliquots taken with syringe barrel pumping were relatively closer to the expected concentration in the vial than aliquots without syringe barrel pumping (Figure D.8), but were still lower than expected. The underestimation in this data series also increased in magnitude with lower inject volumes.

D.4.2 Discussion

The results shown in Figure D.8 strongly support my previous conclusion that gas concentrations measured on the GC can be considerably underestimated depending on the injection volume and method of aliquoting a sample from a stoppered glass vial. In my previous report on the subject, I was at a loss to describe how such a large amount of dilution could occur based on the volume of the needle I calculated from its length and diameter. However, in Templeton Laboratory group meeting, Eric Ellison pointed out that the stopcock and needle do not fully interlock. Rather, there is a volume of air between the stopcock and needle, which is referred to here as "deadspace" (highlighted in Figure D.9). Eric proposed, as is his normal procedure, to pump the syringe barrel during aliquoting to replace the GC carrier gas in the deadspace with sample gas to get around this dilution problem. Testing

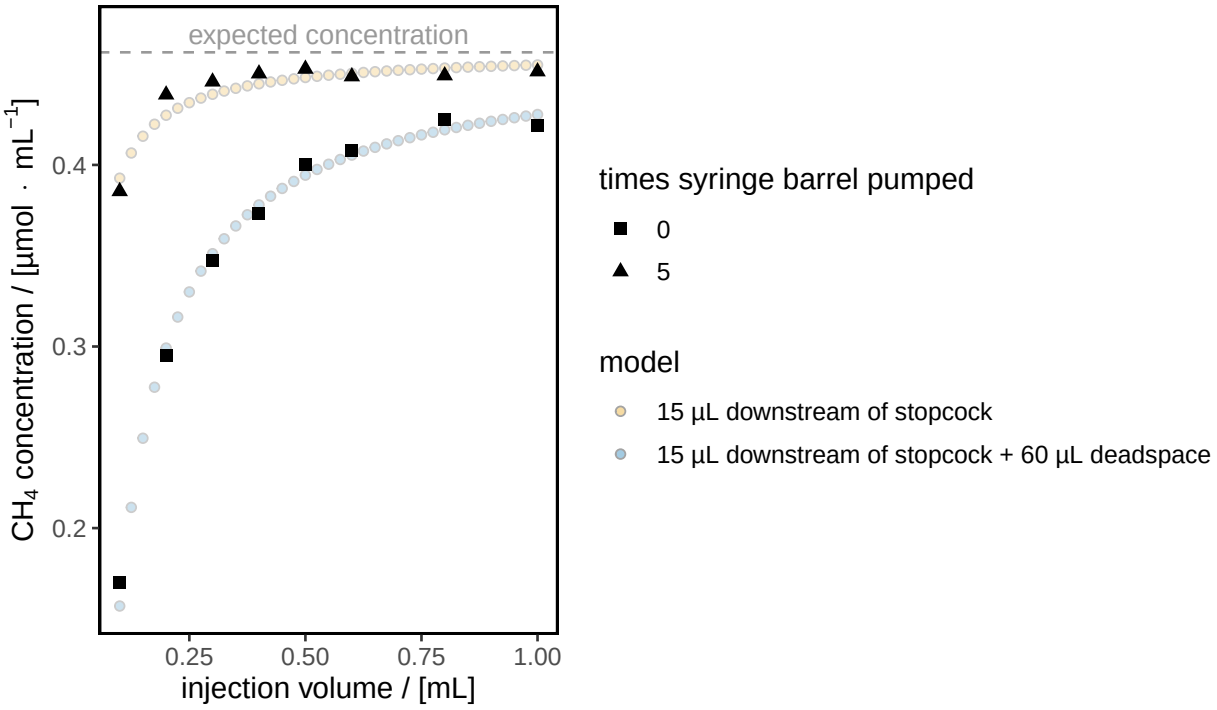

Figure D.8: Plot of CH_4 concentrations of GC analyses of 5.00 ml Templeton 10.0 % CH_4, 90.0 % N_2 tank (Boulder atm. P) in 37 ml air-filled vials versus GC injection volume. The dashed line represents the CH_4 concentration that I calculated based on the vial volume, my aliquot volume, and the concentration of the tank reported by Airgas. Data are shown corrected dilution by repeat aliquoting of a fixed volume container. See text for descriptions of dilution models.

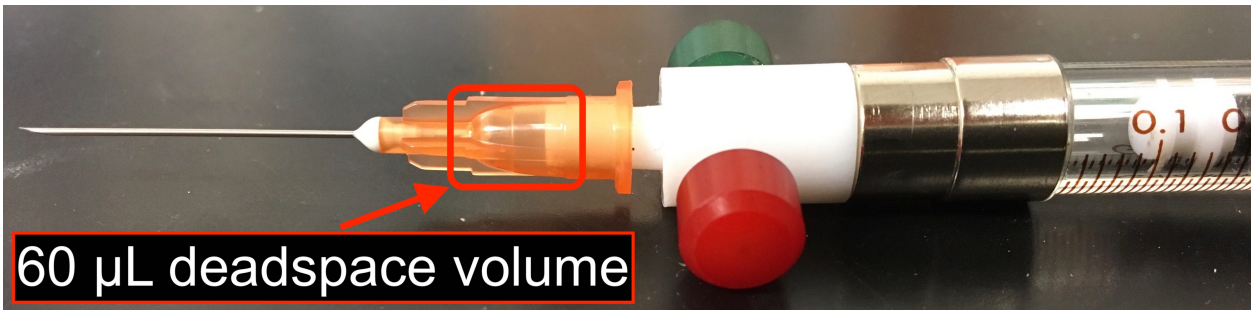

Figure D.9: Photo of syringe with stopcock and sampling needle attached. A volume of air between the stopcock and needle, which is referred to here as "deadspace" is highlighted. Note syringe volume marker of 0.1 mL to the right of photo for a volumetric scale.

the differences between these two methods of aliquoting was the impetus for this new round of experiments.

As shown in Figure D.8, pumping the syringe barrel before aliquoting does yield more accurate concentrations, but these are still underestimates, especially at lower injection volumes. Why could this be? I think it has to do with the loss of sample downstream of the stopcock (Figure D.10), which occurs as the sampling needle is replaced with the GC needle. As discussed in group meeting, this is a way in which the sampling methods and the calibration standard injections differ.

The simple dilution model I propose for the loss of sample downstream of the stopcock is:

$$\text{measured concentration} = (\text{true concentration}) \cdot \left(\frac{\text{apparent inject volume} - \text{volume downstream of stopcock}}{\text{apparent inject volume}} \right). \tag{D.1}$$

This model fits well to the data series in which aliquots were taken after pumping the syringe barrel 5 times, as shown in Figure D.8. 15 μL of volume downstream of stopcock provided a good fit to the data.

The aliquots taken without pumping the syringe barrel still have the issue of loss of volume downstream of the stopcock and additionally have the issue of dilution from the deadspace volume. The deadspace dilution multiplies the following factor to the right side

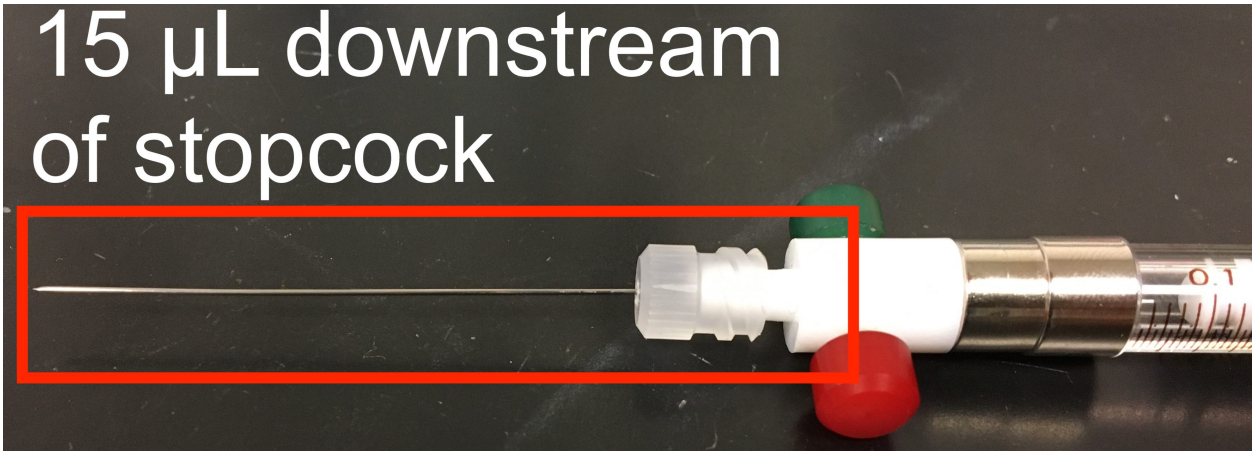

Figure D.10: Photo of syringe with stopcock and GC needle attached. Note syringe volume marker of 0.1 mL to the right of photo for a volumetric scale.

of the dilution model in Equation D.1:

$$\left(\frac{\text{apparent inject volume} - \text{deadspace volume}}{\text{apparent inject volume}}\right). \tag{D.2}$$

Conceptually, Equation D.2 describes a situation in which the deadspace volume takes up a finite amount of the injected volume, with the remainder of the injected volume being the sample gas. This model fits well to the data series in which aliquots were taken without pumping the syringe barrel, as shown in Figure D.8. 60 μL of deadspace provided a good fit to the data. This is also true of my previous round of experiments, despite the switch to a different vendor for 25 G, 1 inch needles, indicating that the blue and orange needles share a similar geometry.

D.4.3 Closing considerations

- Since this injection volume / aliquoting method bias has now been repeatedly demonstrated, I plan to apply these corrections to my data from Oman samples taken in 2017 through 2019. Fortunately, the model equations shown here seem to match the data quite well and consistently and can be easily re-arranged to solve for the "true concentration."

- Although the corrections I describe here seem sufficient for the types of samples used in

this experiment, I recommend that people consider the effect of deadspace volume when aliquoting from small gas headspaces. When the headspace is small, the additional 60 μL of volume from the deadspace may need to be considered in corrections (i.e. imagine a 10 mL headspace, in which the deadspace would be 6 % of the headspace.)

D.5 Methods for CH_4 extraction and conversion to CO_2 for graphitization and ^{14}C analysis

To introduce gas from our blue chlorobutyl rubber-stoppered serum vials onto the INSTAAR conversion line, Steve Morgan and I first tried a syringe actuator approach. This approach entails using a syringe to take an aliquot of gas from the sample vial, then slowly injecting it into a stream of C-free air using a syringe actuator machine. In a first test, after connecting the sample-filled syringe to sample introduction line (but with the valve to the full conversion line closed), we evacuated the introduction line, then commenced flow of C-free and syringe actuation, and connected the sample introduction line to the full conversion line. Yield on this test sample was very low ($< 2\,\%$). After some more quick testing, we figured that our "gas-tight" valve on the syringe was probably not suitable for the level of vacuum that we applied, and that we may have evacuated away our sample. Thus, rather than evacuating the sample introduction line, we tried flushing it with C-free air. Unfortunately, we still had poor yields. We reasoned that there may have been issues with the syringe. Firstly, we were trying to take 25 ml aliquots from vials that were only 37 ml, which may have created a vacuum and leaks in syringe connections, which could have resulted in poor sample transfer. Alternatively, there may have been slow leaks in the syringe fittings that lost sample over the period of syringe actuation.

Therefore, we tried a flow-through method of sample introduction, which is pictured in Figure D.11. In the flow-through method, C-free air flows through the sample vial and into the conversion line. A potential disadvantage of this method is that it is difficult to purge or

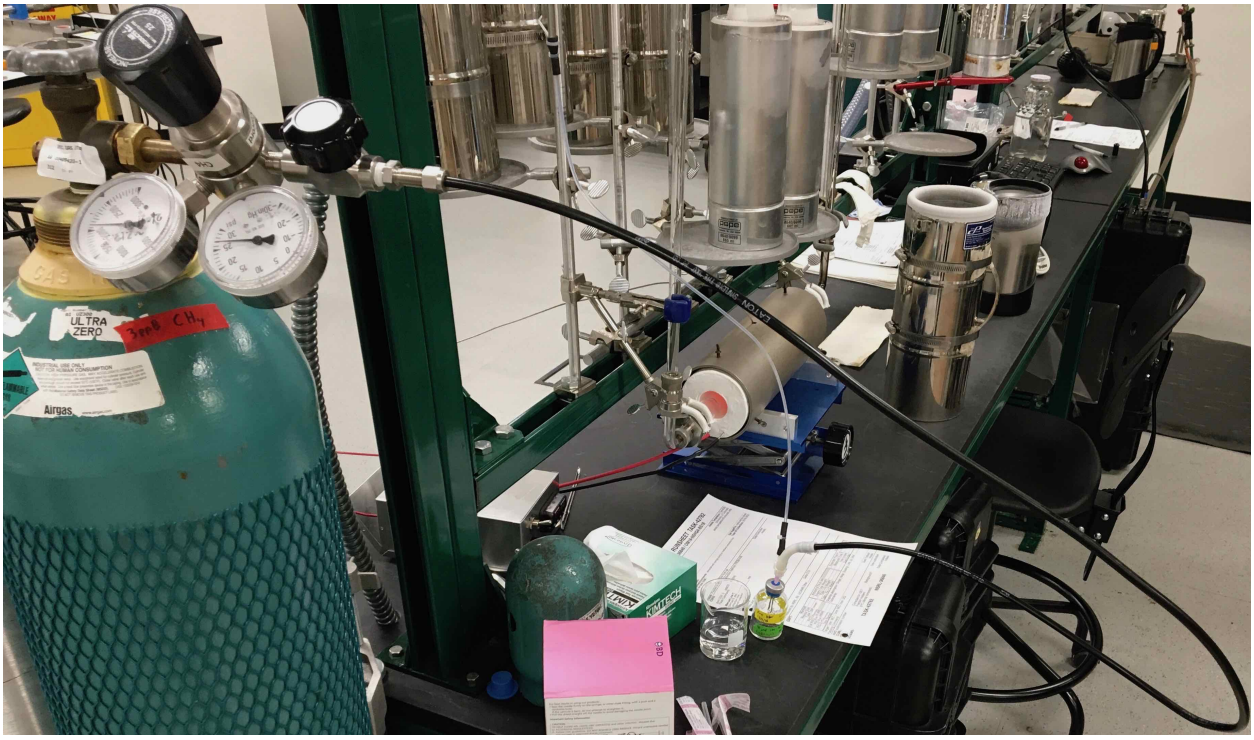

Figure D.11: Extraction of CH_4 from blue-butyl stoppered serum vial and introduction onto INSTAAR conversion line for removal of water, CO_2, and CO, and combustion of residual gas to CO_2.

evacuate all parts of the sample introduction line, which could result in higher blanks due to air contamination. A major advantage of this method is that it allows for the complete extraction of a gas sample, and does not involve any aliquots by syringe. This simplifies the procedure and also enables the measurement of lower concentration samples.

The results of tests of the flow-through method are shown in Table D.3. The yields were 85 % to 89 %, which was far superior than what we were able to achieve with the syringe actuator method. Additionally, the method blank was very low (Table D.3). The flow rates and extraction times we used allowed the vial to be flushed with C-free air at least 40 times, which seemed like plenty for complete extraction of CH_4 from the vial. Our observation of growth of the frozen CO_2 ring after combustion shortly after the start of flow with very little subsequent growth indicates that the majority of the CH_4 was immediately extracted, and supports our hypothesis that this extraction time is sufficient. If there is a "wave" of CH_4 that comes all at once, it may significantly increase the CH_4 : O_2 ratio in the combustion

reactor, and possibly decrease combustion efficiency somewhat, which could account for the remaining 10 % to 15 % of CH_4 that apparently was not converted to CO_2 in these tests, although further testing would be needed to confirm this. Overall, we deemed these test results to be satisfactory, and proceeded to extract my field samples by the same methods, at $300\,\mathrm{ml} \cdot \mathrm{min}^{-1}$ for 15 min. I checked all connections on the sample introduction line for leaks using Snoop solution at this flow rate, and did not find any leaks, indicating that there were no conspicuous points of failure in the line.

Table D.3: Summary of test CH_4 extractions and conversions to CO_2 using flow-through method.

sample	mass C expected / [mg]	mass C converted / [mg]	yield	C-free air flow rate / $[\mathrm{ml} \cdot \mathrm{min}^{-1}]$	extraction time / [min]
13.5 ml 10% CH_4 : 90% N_2 at Boulder atmospheric P injected into 36.6 ml air-filled stoppered glass vial.	0.60	0.510	85%	100.	15
Blank. Same vial as above, but purged with C-free air for 10 min at vigorous flow rate.	0	<0.005	NA	100.	15
22.5 ml 10% CH_4 : 90% N_2 at Boulder atmospheric P injected into 36.6 ml air-filled stoppered glass vial.	1.0	0.890	89%	300.	15